Journal of Cardiovascular Magnetic Resonance (2005) **1,** 3–90

ISSN: 1097-6647 print / 1532-429X online
DOI: 10.1081/JCMR-200048619

Taylor & Francis
Taylor & Francis Group

Oral Abstracts

101. Serial Quantification of Targeted Fumagillin Therapy Using $\alpha_v\beta_3$-Targeted Paramagnetic Nanoparticles in Early Atherosclerosis at 1.5 T

Patrick M. Winter, PhD,[1] Anne M. Morawski, BS,[1] Shelton D. Caruthers, PhD,[2] Thomas D. Harris, PhD,[3] Grace Hu, PhD,[1] Ralph W. Fuhrhop,[1] Huiying Zhang, MD,[1] John S. Allen, BS,[1] Elizabeth K. Lacy, BS,[1] Todd A. Williams, BS,[1] Samuel A. Wickline, MD,[1] Gregory M. Lanza, MD, PhD.[1]
[1]*Cardiology, Washington University, St. Louis, MO, USA,* [2]*Philips Medical Systems, Cleveland, OH, USA,* [3]*Bristol-Myers Squibb Medical Imaging, Billerica, MA, USA.*

Introduction: The severity or propensity of atherosclerosis in asymptomatic patients may be indirectly estimated by the circulating concentrations of inflammatory markers or lipoproteins. However, circulating biomarkers are confounded by many factors and cannot accurately delineate the spatial distribution or total burden of atherosclerosis within the vasculature. Angiogenesis is an integral feature in the progression of atherosclerosis and the development of vulnerable plaques. The $\alpha_v\beta_3$-integrin is a selective signature of angiogenic endothelium, which can be used to characterize the neovascular demand of expanding intramural plaques. In the present study, we utilized $\alpha_v\beta_3$-targeted perfluorocarbon nanoparticles to deliver fumagillin, an anti-angiogenic therapy, and to quantify its effectiveness with serial, noninvasive molecular imaging.

Methods: Male New Zealand White rabbits were fed a 0.25% cholesterol diet for 75 days. Transverse black-blood MRI (TR/TE = 380/11 ms) of the thoracic aorta was performed with a clinical 1.5 T magnet (NT Intera with Master Gradients, Philips Medical Systems, Best, Netherlands) using a quadrature birdcage coil (250 by 250 μm in-plane resolution and 5 mm slice thickness). Images were collected before and four hours after peripheral injection of $\alpha_v\beta_3$-targeted paramagnetic nanoparticles (1 ml/kg) incorporating 0 (n = 18) or 0.2 mole% (n = 18) fumagillin, 30 mole% Gd-DTPA-bisoleate, and 0.1 mole% vitronectin peptidomimetic antagonist covalently coupled to phospholipids in the outer surfactant layer. Following baseline treatment, half the rabbits within each treatment group remained on the high-cholesterol diet while the remainder was switched to normal rabbit chow. All animals were imaged weekly with $\alpha_v\beta_3$-targeted paramagnetic nanoparticles (no drug) over the next four weeks to quantify neovascular $\alpha_v\beta_3$-integrin expression in the aorta. MRI signal enhancement was calculated from T1w intensities measured before and after paramagnetic nanoparticle injection using a semi-automated image segmentation program.

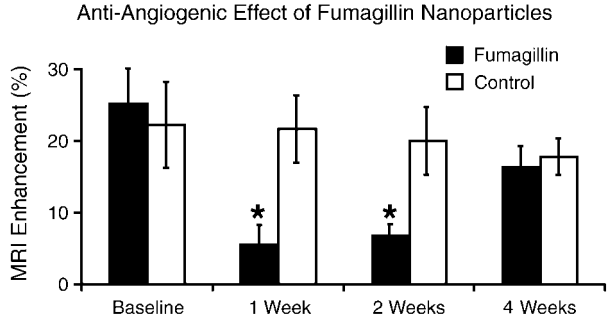

Results: At baseline, MRI signal enhancement among all fat-fed rabbits across the entire descending thoracic aorta was 23.9 ± 3.7% and did not differ ($p > 0.05$) between fumagillin-treated (25.2 ± 4.9%) and no drug (22.2 ± 6.0%) groups. Discontinuation of the hyperlipidemic diet did not impact ($p > 0.05$) neovascular contrast levels in the fumagillin-treated or control rabbits. Preinjection MR scans revealed no week-to-week carry-over of contrast enhancement from the $\alpha_v\beta_3$-targeted paramagnetic nanoparticles. Moreover, weekly administration of $\alpha_v\beta_3$-targeted nanoparticles elicited no anti-angiogenic effect. One week after fumagillin treatment, MRI enhancement was significantly lower, 5.5 ± 2.7%, in fumagillin treated animals versus control rabbits, 21.7 ± 4.7% (*$p < 0.05$), independent of diet. By four weeks, complete recrudescence of the neovasculature was noted among animals injected with the single dosage of fumagillin 16.3 ± 3.0% in reference to the no drug control rabbits (17.8 ± 2.5%, $p > 0.05$).

Conclusions: Molecular imaging with MRI provided a non-invasive means to detect early atherosclerosis and serially monitor anti-angiogenic therapy using a clinical 1.5 T scanner. A single-dose of fumagillin-bearing nanoparticles induced an acute anti-neovascular response regardless of the post-treatment diet (high-cholesterol versus normal rabbit chow) that recrudesced after one month. $\alpha_v\beta_3$-targeted paramagnetic nanoparticles had no week-to-week residual T1w contrast and repeated injections elicited no therapeutic effect. These results suggest that $\alpha_v\beta_3$-targeted nanoparticles can provide repeated assessment of angiogenesis without impacting the underlying pathophysiology and without cumulative enhancement effects.

102. In Vivo Magnetic Resonance Imaging of Atherosclerotic Plaque Inflammation in Apolipoprotein E Deficient Mice

David E. Sosnovik, MD,[1] Matthias Nahrendorf, MD,[2] George Dai, PhD,[2] Farouc Jaffer, MD, PhD,[1] Chris Farrar,

PhD,[2] Ralph Weissleder, MD, PhD.[2] [1]*Cardiology, Massachusetts General Hospital, Charlestown, MA, USA,* [2]*Radiology, Massachusetts General Hospital, Charlestown, MA, USA.*

Introduction: Apolipoprotein E deficient ($ApoE^{-/-}$) mice are a biologically important model of atherosclerosis, and are frequently used to identify new therapeutic targets and to assess the efficacy of novel anti-atherosclerosis therapies. The role of inflammation in the development of atherosclerotic plaques, strokes and acute coronary syndromes is now well recognized. However, studies of plaque inflammation in $ApoE^{-/-}$ mice have been hampered by the inability to image the inflammatory process in these mice in-vivo. The purpose of this study was thus to determine whether a dual-modality magneto-optical iron oxide agent (CLIO-Cy5.5) could be used to image atherosclerotic plaque inflammation in $ApoE^{-/-}$ mice, in vivo.

Methods: In-vivo MR imaging was performed on 4 $ApoE^{-/-}$ mice (ages 24–28 weeks, high cholesterol diet for 12–16 weeks) 24 hours after the injection CLIO-Cy5.5 (15 mg/kg) into their tail veins. ECG and respiratory-gated T2* weighted gradient echo cines were obtained on a 9.4 T horizontal bore scanner with the following parameters: FOV 30 mm, slice thickness 1 mm, matrix 200 × 200, NEX 4. Each cine consisted of 16 frames per RR interval resulting in a TR of 7–8 ms. Images at echo times of 2.7 ms and 4.7 ms were acquired in the long axis of the thoracic aorta, and in the short axis of the aortic arch. The mice were then euthanized, the aorta was dissected and embedded in agar for ex-vivo MRI in a vertical bore 14 T magnet (gradients 950 mT/m). T2* weighted gradient echo images where acquired with a slice thickness of 0.5 mm, in-plane reolution 100 × 100 um, a TR of 200 ms, 16 NEX, and TEs of 3 ms and 6 ms. Following MR imaging, the aorta was sectioned for near infrared fluorescence (NIRF) microscopy and immunofluorescence staining for the MAC3 macrophage antigen. The identical MR and optical imaging protocol was repeated in a control $ApoE^{-/-}$ mouse injected with normal saline, and in a wildtype mouse injected with the CLIO-Cy5.5 probe.

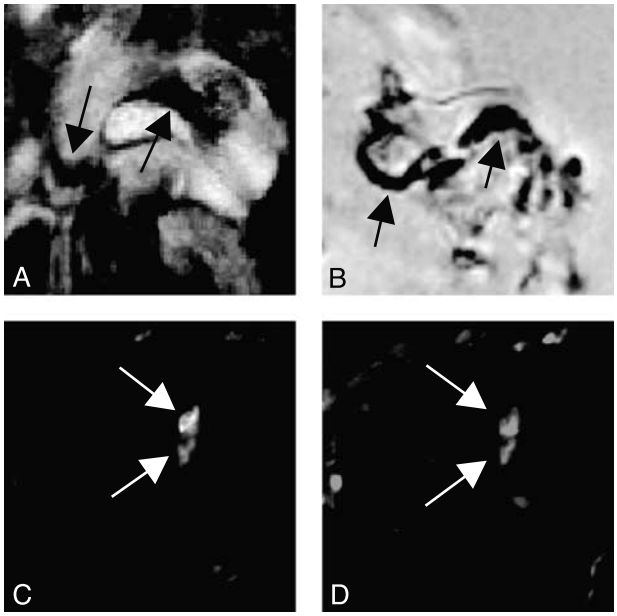

Figure 1. A: in vivo and B: ex vivo MRI. Arrows point at regions with negative signal enhancement caused by CLIO-Cy5.5 within plaques at the lesser curvature and the aortic root. C: fluorescent Cy5.5 signal and D: Texas red immunofluorescence staining of macrophage antigen MAC3 merged with dapi stain for nuclei at 400 × magnification. C and D were obtained from the same slide. Arrows point at 2 macrophages that took up CLIO-Cy5.5.

Results: Regions of negative signal enhancement were seen along the aortic root, the lesser curvature of the aortic arch and at the origins of the great vessels in the $ApoE^{-/-}$ mice that received the CLIO-Cy5.5 probe (Figure 1A and B) but not in the control mice. NIRF microscopy confirmed the presence of CLIO-Cy5.5 in the regions demonstrating negative MR signal enhancement, which are also known to be sites prone to the development of atherosclerosis in $ApoE^{-/-}$ mice. Co-localization of the NIRF signal from CLIO-Cy5.5 with the MAC3 immunofluorescence signal confirmed that the presence of CLIO-Cy5.5 in the atherosclerotic lesions was due to uptake by plaque macrophages (Figure 1C and D).

Discussion: The results of this study demonstrate that high resolution MRI following the administration of superparamagnetic nanoparticles can be used to image the degree of plaque inflammation in-vivo in a murine model of atherosclerosis. The fluorescent properties of the dual modality CLIO-Cy5.5 probe permit precise and specific localization of iron oxide using NIRF microscopy, and demonstrate colocalization of iron oxide and plaque macrophages. This approach should allow the degree of plaque inflammation in mice to be quantified serially and non-invasively, and could be used to assess the efficacy of new anti-inflammatory atherosclerotic therapies.

103. In Vivo Thrombus Detection with Magnetic Resonance Imaging: A Comparative Study Using a Fibrin-Targeted Contrast Agent and Gd-DTPA

Marc Sirol, MD, Juan J. Badimon, PhD, Valentin Fuster, MD, PhD, Zahi A. Fayad, PhD. *Cardiovascular Institute, Mount Sinai School of Medicine, New York, NY, USA.*

Introduction: Arterial thrombosis plays a critical role in clinical manifestation of cardiovascular diseases. Therefore, the ability of detecting the presence of thrombosis has a significant clinical implication for both, diagnostic and guidance of therapy. Feasibility of thrombus detection by MRI has been already demonstrated using non-contrast

enhanced MRI. Recent advances in the field of molecular imaging have led to the development of novel paramagnetic and superparamagnetic targeted MR contrast agents that bind exclusively to atherosclerotic plaque components.

Purpose: We sought to test a novel gadolinium labeled fibrin-targeted peptide, EP-2104R (EPIX Medical Inc.) for thrombus detection in a rabbit model of carotid thrombosis. Thereafter, we compared this thrombus-enhancing contrast agent to a conventional gadolinium chelate (Gd-DTPA) for its potential to enhance contrast between thrombus, blood, and surrounding tissues.

Methods: Carotid artery thrombus was induced by external injury and blood stasis in 12 New Zealand Whtie rabbits. MRI was performed in a 1.5 T MRI system, before and immediately after EP-2104R injection. T1-weighted MR images were acquired using both a 2D fast spin-echo and a 3D fast gradient-echo sequences. MR imaging parameters included: repetition time (TR) and echo time (TE) of 400/7 ms; receiver bandwidth (BW) = ± 42 KHz; echo-train length = 16; slice thickness = 2 mm; no slice gap; field-of-view (FOV) = 8 cm; acquisition matrix 256 × 256; number of signal average = 4; double-inversion preparatory pulses inversion time (TI) = 350 ms; and chemical fat suppression pulse. Gd-DTPA was injected (50 μmolGd/kg) the next day in the same animal, and images were acquired using the same sequences with a careful registration. Different thrombus age were assessed. From the day of thrombus induction (Acute), after a week, two weeks up to four weeks after thrombus formation. Histopathologic analyses of the thrombi were systematically performed.

Results: This model consistently produced an occlusive fibrin-rich thrombus in all animals (n = 12) according to pathology. Detection of arterial thrombi was achieved in all cases after EP-2104R injection. Thrombus contrast-to-noise ratio (CNR) was dramatically increased after EP-2104R injection compared to pre-contrast imaging ($P < 0.001$). Gd-DTPA was not usefull for thrombus detection. A decrease of thrombus CNR was observed after Gd-DTPA injection due to perivascular enhancement of the surrounding tissue (muscle). The bar graph depicts the trend of thrombus CNR before and after EP-2104R and Gd-DTPA injection respectively. A trend in decrease of thrombus CNR was observed with oldest thrombi (> 3 weeks), corresponding to a progressive thrombus organization, where fibrin was gradually replaced by colagen matrix ($P = .082$).

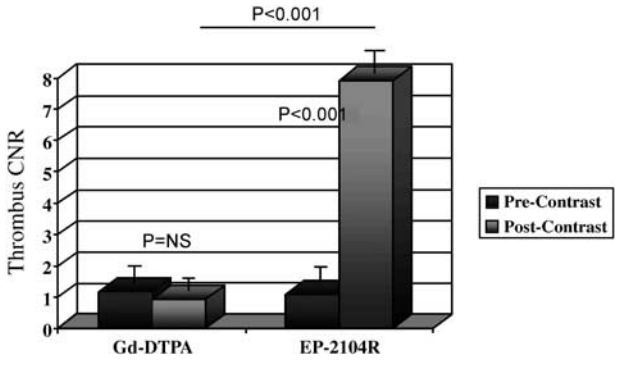

Conclusions: We demonstrated the feasibility of a fibrin-targeted MR contrast agent for detection of unorginized and orginized thrombi in vivo. We showed the superiority of EP-2104R for thrombus detection and assessement of thrombus composition compared to conventional gadolinium chelates (Gd-DTPA). Potential application includes thrombus detection in patients with unstable angina and stroke.

104. Spatial and Temporal Characterization of MRI Contrast Enhancement in Atherosclerotic Lesions with Gadolinium Texaphyrin Complexes

Henning Steen,[1] Matthias Stuber, PhD,[2] Subroto Chatterjee, PhD,[3] Joao A. C. Lima, MD,[4] Al Lardo, PhD.[5] [1]*Cardiology, Universität Heidelberg, Heidelberg, Germany,* [2]*Radiology, Johns Hopkins, Baltimore, MD, USA,* [3]*Pediatrics, Johns Hopkins, Baltimore, MD, USA,* [4]*Cardiology, Johns Hopkins, Baltimore, MD, USA,* [5]*Cardiology, Johns Hopkins, Baltimore, MD, USA.*

Introduction: Atherosclerosis lesions can be visualized non-invasively by high resolution magnetic resonance imaging (MRI). Further discrimination of plaque morphology may be possible using contrast agents that preferentially bind to specific plaque components and thereby improve MRI signal to noise and contrast to noise ratios (SNR, CNR). Gadolinium-based texaphyrin complexes (Gd Tex, Pharmacyclics, Inc.) that are water-soluble but significantly lipophilic may potentially be used as molecular imaging contrast agents that may selectively localize in atheromatous plaque.

Purpose: The purpose of this study was to characterize preferential and selective plaque uptake kinetics of a number of Gd Tex complexes in a rabbit model of severe atherosclerosis.

Methods: Aortic wall SNR-and CNR dynamics of three Gd Tex complexes with varying degrees of lipid binding affinity (PCI-0160,-0210,-0400, 2 mg/dl) were investigated in Watanabe rabbits (focal aortic injury and high-cholesterol diet for 8 weeks) on a 1.5T-MRI-System (Philips Medical). Multiple sub-renal ECG-gated fat-saturation aortic 3D-black-blood Fast-Spin-Echo vessel wall images (TR = 3 RR, TE = 10.5 ms, TI pre/post = 400/270 ms, FOV = 76 mm, in-plane resolution = 250 μm) were acquired pre and post administration of Gd Tex (10 mg/dl i.v. per animal) and every 10 minutes over 120 minutes. SNR and CNR over time were characterized using a semi-automated analysis algorithm.

Results: High quality vessel wall imaging was achieved in all animals. At 60 minutes post-contrast, T1-SNR increased for all three agents [PC-160 = 50 to 54 (8%), PC-210 = 54 to 64 (20%), PC400 = 36 to 62 (75%)] and CNR increased for two agents [PC-160 = 41 to 44 (6%), PC210 (unchanged), PC400 = 32 to 45 (43%)]. At 120 minutes

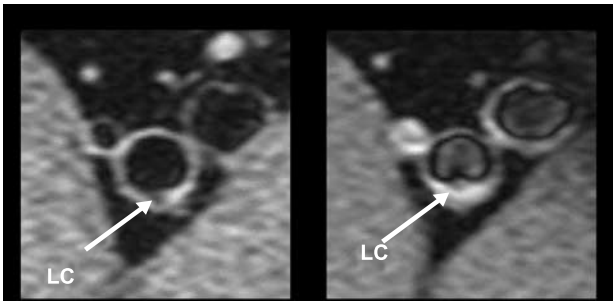

Figure 1.

post contrast, enhancement of the plaque and its lipid core (LC) is demonstrated with partial protrusion into the lumen (Fig. 1, arrow) that was not appreciable at baseline.

Conclusions: Gadolinium-containing texaphyrin molecular contrast agents preferentially enhance aortic atherosclerotic plaque and increase both T1 SNR and CNR in a rabbit model of severe atherosclerosis. The degree of lipid binding of these compounds can be modified to selectively target specific plaque constituents, which may have implications for improved plaque characterization and non-invasive disease screening of rupture prone plaque.

105. CMR Detection of VCAM-1 Expression in Activated Human Endothelial Cells with Targeted SPIO Nanoparticles

Szilard Voros,[1] Brett R. Blackman, PhD,[2] Dongfeng Pan, PhD,[3] Craig H. Meyer, PhD,[2] Ian J. Sarembock, MD,[1] Walter J. Rogers, PhD.[3] [1]*Cardiology, University of Virginia, Charlottesville, VA, USA,* [2]*Biomedical Engineering, University of Virginia, Charlottesville, VA, USA,* [3]*Radiology, University of Virginia, Charlottesville, VA, USA.*

Introduction: In-vivo visualization of molecular processes would have major implications in early diagnosis of atherosclerosis as well as in in-vivo testing of pharmacologic agents designed for prevention and treatment.

Purpose: We sought to develop and validate a targeted molecular magnetic resonance imaging platform using a monoclonal antibody as targeting ligand and small paramagnetic iron oxide (SPIO) as the reporter for the detection of vascular cell adhesion molecule 1 (VCAM-1) expression on activated human umbilical vein endothelial cells.

Methods: SPIO was chosen as the MR reporter probe given its high sensitivity due to susceptibility effects. Targeted SPIO (tSPIO) was prepared by conjugation of anti-VCAM-1 antibody to its dextran coating, using imine-bond chemistry. Human umbilical vein endothelial cells (HUVECs) were plated on plastic cover slips, were grown to confluence and were activated by 1000 IU of TNF-α. Cells were incubated with 3 different doses of SPIO or tSPIO (7.84 μg/ml [1 ×], 78.4 μg/ml [10 ×] and 156.8 μg/ml [20 ×]). MR imaging of cells was performed on a 1.5 T clinical imaging system (Siemens Sonata). Gradient recalled echo pulse sequences with 3 different weightings were used to create increasing sensitivity for the presence of iron (T1: TR/TE 100/5 ms, T2*: TR/TE 500/20 ms and 500/40 ms). Other imaging parameters included FoV 150 mm, matrix 320 × 320, slice thickness 4 mm, number-of-averages 6. For semiquantitative analysis, binary maps were created with signal intensity (SI) below 2 and 4 SD for each sequence and the area of SI below the threshold was computed. After imaging, the presence of VCAM-1 expression was confirmed on HUVECs by immunohistochemistry (O) and the presence of iron particles was confirmed by Luna's iron stain (B) and scanning electron microsopy (C).

Results: tSPIO (D-L) but not SPIO (A) bound to VCAM-1 expressing HUVECs. Area of signal loss on binary maps increased with increasing T2 weighting and with increasing concentration of tSPIO for each pulse sequence (D: T1, 1 × ;

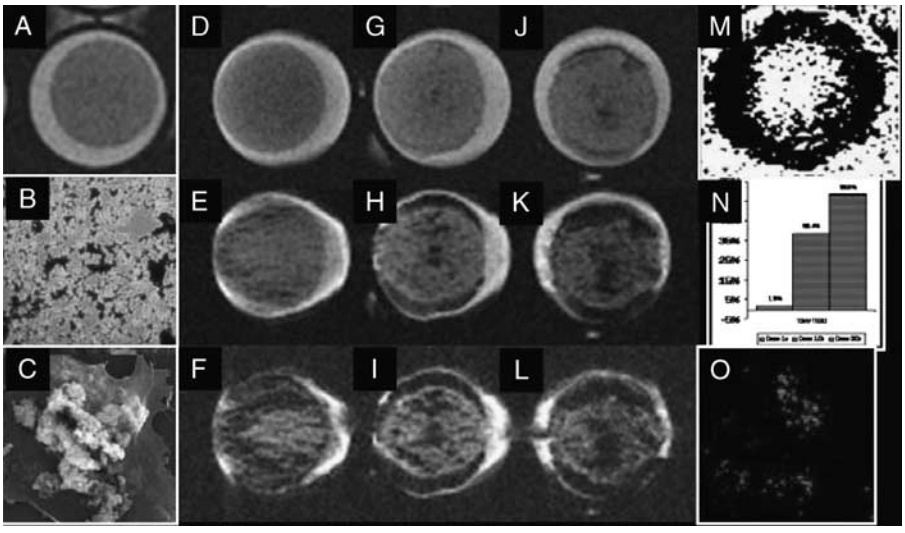

E: T2 TR20, 1 × , F: T2 TR 40, 1 × , G: T1, 10 × ; H: T2 TR20, 10 × ; I: T2 TR40, 10 × ; J: T1, 20 × ; K: T2 TR20, 20 × ; L: T2 TR40, 20 ×). Binary map of T2* images (TE = 20 ms) with 2 SD distinguished different doses best (M, N).

Conclusions: We demonstrate for the first time that our strategy of CMR visualization of VCAM-1 targeted SPIO is a robust technique for the detection of VCAM-1 expression on activated HUVECs. This approach is now ready to be applied for in-vivo detection of molecular imaging of atherosclerosis.

106. Molecular MRI of Left Atrial Thombi in a Swine Model Using EP-2104R

Elmar Spuentrup, MD,[1] Bernd Fausten, MD,[1] Sylvia Kinzel, VD,[1] Andrea J. Wiethoff, PhD,[2] Rene M. Botnar, PhD,[3] Edward C. Parsons Jr., PhD,[2] Philip B. Graham, PhD,[2] Stephan Haller, MD,[1] Marcus Katoh, MD,[1] Warren J. Manning, MD,[3] Thomas Busch, MD,[1] Rolf W. Gunther, MD,[1] Arno Buecker, MD.[1] [1]*RWTH-Aachen, Aachen, Germany,* [2]*EPIX Pharmaceuticals, Inc., Cambridge, MA, USA,* [3]*Beth Israel Deaconess Medical Center and Harvard Medical School, Boston, MA, USA.*

Introduction: The detection of left cardiac masses and especially thrombi is important in patients with thrombembolic diseases such as stroke, and potentially thrombogenic diseases, such as atrial fibrillation (AF) and heart failure. Since even small clots may be the origin of embolism, highly sensitive detection of clots would be advantageous. Further, accurate exclusion of clot is required prior to cardioversion in patients with atrial fibrillation.

Purpose: The aim of this study was to investigate a new MRI fibrin-specific contrast agent (EP-2104R, EPIX Pharmaceuticals, Cambridge, MA, USA) for molecularly targeted imaging of left atrial clots.

Methods: Chronic human thrombi were surgically implanted in the left atrial appendage in swine (n = 5). MRI was performed using a navigator-gated, free-breathing and cardiac triggered 3D inversion-recovery black-blood gradient-echo sequence before and after systemic administration of 4.0 μmol/kg EP-2104R. Images were analyzed by two investigators and contrast-to-noise ratio was calculated. Location of clots was proven by autopsy and Gadolinium (Gd) concentration in the clots was assessed post-mortem by ICP.

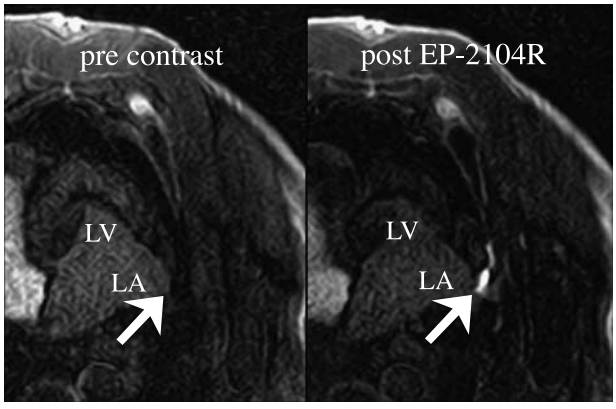

Figure 1.

Results: Prior to contrast administration thrombi were not visible on black-blood MR images. After EP-2104R administration, all atrial clots were selectively enhanced (Figure 1), with a high contrast-to-noise ratio (CNR clot/blood = 29.7 ± 8.0). Gd-concentration in the clots averaged 74 ± 45 μM. (Average clot size = 243 ± 133 mg).

Conclusion: The fibrin-specific MR contrast agent EP-2104R allows for selective, high contrast visualization of left atrial clots through molecular targeted MRI, even with relatively low concentration (< 100 μM) of fibrin. The agent is thus promising for the detection of small clots in the left atrial appendage, and may be helpful to differentiate among clot, neoplasm or appositional thrombi on masses when compared to conventional MR-imaging techniques or other imaging modalities.

107. Non-invasive In Vivo "Histology": Visualizing Single Immune Cells in Acute Allograft Rejection After Heterotopic Heart Transplantation with Micrometer-Sized Iron Oxide Containing Particles

Yijen L. Wu, PhD, Lesley Foley, BS, T. Kevin Hitchens, PhD, John B. Williams, PhD, Qing Ye, MD, Chien Ho, PhD. *Pittsburgh NMR Center for Biomedical Research, Carnegie Mellon University, Pittsburgh, PA, USA.*

Introduction: In vivo cell tracking with MRI provides means for observing biological processes and monitoring cell therapy in vivo. We have previously demonstrated that acute allograft rejection after heart transplantation can be non-invasively visualized by in vivo labeling of immune cells, primarily macrophages, with nanometer-sized ultrasmall dextran-coated iron-oxide (USPIO) particles. The extent of MR signal changes correlated well with the rejection grade. However, nanometer-sized USPIO is much smaller compared to the size of a cell. It requires loading many particles and it is unlikely to resolve individual cells in vivo.

Purpose: We explore the possibility of using the much bigger micrometer-sized (0.98 μm) iron oxide particle, Bangs particles, to track individual immune cells with in vivo labeling. Bangs particles are styrene/divinyl benzene polymer microspheres that contain magnetite core as well as a fluorescent dye.

Methods:

1. Animal model: We use an abdominal heterotopic working heart and lung transplantation model in rats with DA to BN transplantation pairs.

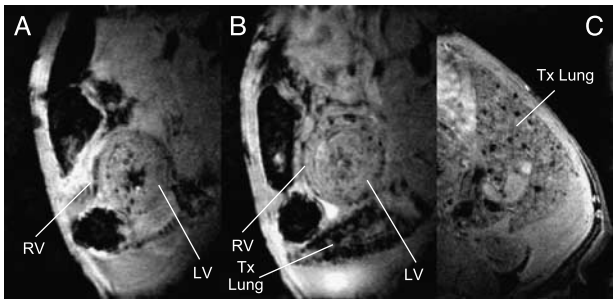

Figure 1. Allograft heart (A, B) and lung (C) 20 hours post-Bangs particle administration.

2. MRI methods: EKG and respiration gated T2*-weighted cine imaging on Bruker AVANCE 4.7-T system was used for in vivo imaging with the in-plane resolution of 156 μm. High-resolution 3D imaging is performed at 11.7 T with voxel size: 46.8 μm × 46.8 μm × 93.8 μm.
3. Iron oxide particle labeling: Immune cells, mostly macrophages, are labeled in vivo by direct intravenous injection of USPIO or Bangs particles 1 day prior to MRI scans.

Results: Distinct punctate areas of high contrast can be seen in the transplanted allograft heart (Fig. 1A and B) and lung (Fig. 1C) 1 day after Bangs particle administration at post-operational day (POD) 6. This dotted pattern can be seen as early as 2 hours after Bangs particle administration. With USPIO labeling, accumulation of immune cells, primarily macrophages, in the rejecting sites can be readily seen (Fig. 2C). However, although the darkening is regional, there is no punctate blackening contrast seen as with Bangs particles. The isografts show no detectable signal changes (Fig. 2B).

Each "dot" of high contrast with Bangs particle labeling could possibly represent a single cell, or even a single particle, for the background gradient generated by iron oxide particles can propagate as large as 50 times of the radius. This can be better depicted with high resolution MR microscopy at 11.7-Tesla (Fig. 3). With about 50 μm resolution, discrete black dots can be seen throughout the heart with Bangs particle labeling (Fig. 3A, D), and the size of the black dots ranges from 50 to 150 μm. On the other hand, even with this high resolution, the allograft labeled with USPIO (Fig. 3C and F) still show smeared, but not punctate, pattern. The punctate pattern with Bangs particle labeling is not due to random interstitial deposition of iron oxide particles, but uptake of the particles into cells. Electron micrograph reveals the uptake iron is within membrane bound vesicles.

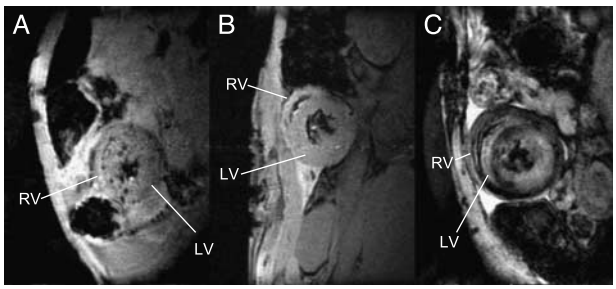

Figure 2. In vivo macrophage accumulation at POD 6 (A) Allograft with Bangs particle (B) Isograft with USPIO (C) Allograft with USPIO.

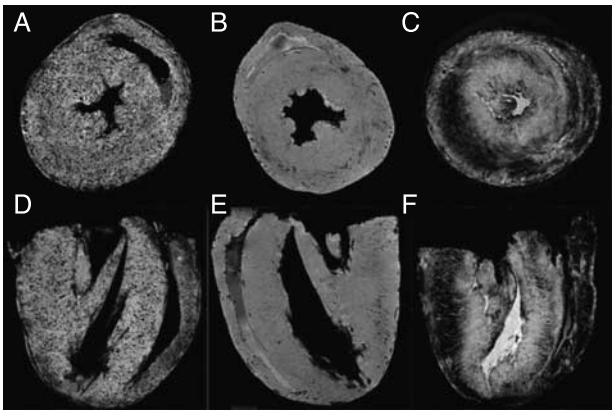

Figure 3. MR microscopy at 11.7 T(A, D) allograft with Bangs particles at POD 7 (B, E) isograft with USPIO at POD 7 (C, F) allograft with USPIO at POD 6. (A–C) short-axis view (D–F) long-axis view.

Conclusions: Our preliminary results indicate that more sensitive contrast agent, such as Bangs particles, provides potential for monitoring single cells in vivo. With better cell labeling strategies, much better methodologies can be developed that are not only important and useful for detecting organ rejection, but also for many other biological processed.

108. Recombinant HDL-like Nanoparticles, a Specific Contrast Agent for MRI of Atherosclerotic Plaques

Juan C. Frias, PhD,[1] Kevin Jon Williams, MD,[2] Edward A. Fisher, MD, PhD,[3] Zahi A. Fayad, PhD.[1] [1]*Cardiology, Mount Sinai School of Medicine, New York, NY, USA,* [2]*Thomas Jefferson University, Philadelphia, PA, USA,* [3]*Cardiology, New York University School of Medicine, New York, NY, USA.*

Atherosclerosis remains a major health problem in the US, with significant morbidity and mortality. The early detection of atherosclerosis may direct therapies to prevent this disease. The ability to image the presence or biological activity of specific molecules ("molecular imaging") in atherosclerotic plaques in vivo would be of considerable interest. Most of the available paramagnetic magnetic resonance (MR) contrast agents are not capable of delivering a large amount of gadolinium (Gd^{3+}) ions to induce a large MR signal. Here, we present a high-density lipoprotein HDL-like nanoparticle contrast agent that selectively targets atherosclerotic plaques. In order to match the results found by MRI with confocal fluorescent microscopy, a fluorecent phospholipid was also included in the formulation of the contrast agent.

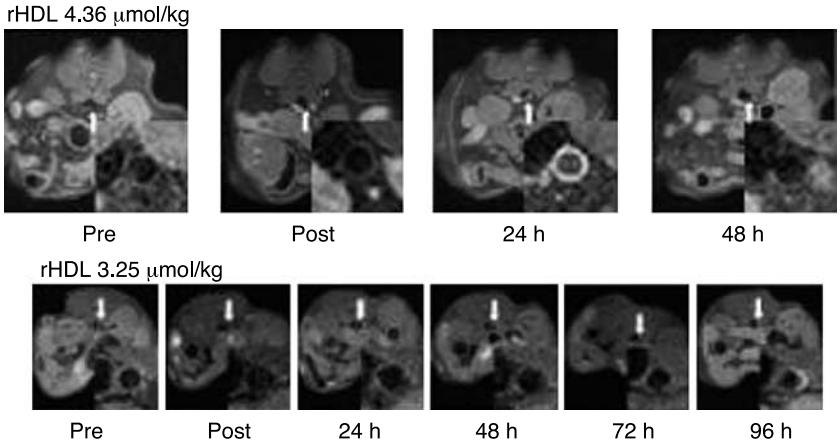

Figure 1.

Genetically engineered mice were used as models of human atherosclerosis and were in vivo imaged. The reconstituted HDL contrast agent (rHDL) was injected via a tail vein catheter. Sequential MRI showed that the contrast agent localized predominantly at the atherosclerotic plaque by 24 hours after injection. Furthermore, by 48 hours after injection, the intensity of the plaque decreased to a value similar to that observed for the plaque immediately after injection. Importantly, the enhancement was also related to plaque composition as in another group of animals the enhancement was found to be at its maximun at 72 hours post injection (Figure 1). Histopathological analysis of the plaque revealed that the animals that showed enhancement at 24 hours had a smaller content of lipids but a higher number of cells in the intima compared to those that showed enhancement at 72 hours.

After MRI, the aorta was isolated, frozen sections cut and stained for DAPI and antiCD68:RPE. The images reveal how a small number of cells (macrophages) retain the fluorescence (Figure 2).

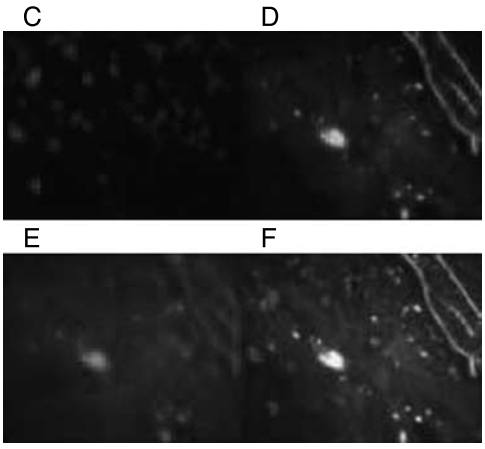

Figure 2.

In summary, we have demonstrated that Gd-loaded HDL-like nanoparticles localize to atherosclerotic plaques in vivo and substantially enhance the MRI image. Owing the flexibility of the HDL platform, targeting molecules can be easily incorporated into this contrast agent.

109. Detection of Early Atherosclerotic Plaque In Vivo by Gadofluorine M-Enhanced Magnetic Resonance Imaging

Marc Sirol,[1] Pedro Moreno, MD,[1] Valentin Fuster, MD, PhD,[1] K-Raman Purushothaman, MD,[1] Bernd Misselwitz, PhD,[2] Hanns Joachim Weinmann, PhD,[2] Zahi A. Fayad, PhD.[1] [1]*Cardiovascular Institute, Mount Sinai School of Medicine, New York, NY, USA,* [2]*Research Department, Schering, Berlin, Germany.*

Introduction: Atherosclerotic plaque detection and characterization with high-resolution and multicontrast MRI has been previously demonstrated. However, detection of subclinical atherosclerosis such as early lesions remains difficult with current methods and could be improved with contrast agents that assess plaque biological activity. Our group has recently reported the use of Gadofluorine M-enhanced MRI for detection of lipid-rich plaques.

Purpose: We sought to compare to non-contrast enhanced MRI the use of Gadofluorine M for the assessment of early and advanced atherosclerotic plaques.

Methods: Aortic denudation was performed in 12 New Zealand White rabbits fed with 0.2% cholesterol diet (HC) for either 2 months [early plaque group (Ea)] or for 8 months [advanced group (Ad)]. Six animals were used as control (no HC). MRI was performed on a 1.5 T MR machine before contrast injection using high-resolution T1w, T2w and PDw sequences. A T1-weighted 2D segmented gradient-echo sequence was used for plaque detection 24 hours after

50 μmol/kg Gadofluorine M (Schering AG) injection (i.v.). The sequence parameters were as follow: TR/TE = 300/4 ms; flip angle = 20°; BW = ± 230 Hz/pixel; Nex = 16; slice thickness = 2.0 mm; FOV = 12 cm; matrix 256 × 256; number of segments = 15. Histopathological analyses using hematoxylin and eosin (H&E) stain and Masson's trichrome elastin stain (CME) were systematically performed.

Results: Plaque enhancement was successful after injection in both Ea and Ad group. Contrast-to-noise ratio (CNR) 24 hours after Gadofluorine M injection was significantly higher in Ad group compared to Ea group ($P< 0.01$). No enhancement was seen in the control animals. AHA classification revealed type II and III plaque in Ea group, and type Va and Vc plaque in Ad group ($P< 0.001$). Precontrast MRI using multicontrast technique was not able to identify atherosclerotic plaques in the Ea group compared to the Ad group ($P< 0.001$).

Conclusions: We demonstrate the successful use of Gadofluorine M for early plaque detection compared to non-contrast enhanced MRI. Early lesions could be differentiated from advanced plaque according to CNR values after Gadofluorine injection. This approach may be useful in the assessment of atherosclerotic burden in patients at different stages of the disease.

110. Detection of Macrophage Infiltration Within Atherosclerotic Plaques as Positive and Negative Contrast by USPIO MRI: Ex Vivo Rabbit Study

Masahiro Terashima, MD, PhD,[1] Charles H. Cunningham, PhD,[2] Takayasu Arai, MD,[1] Paula M. Jacobs, PhD,[3] Phillip C. Yang, MD,[1] John M. Pauly, PhD,[2] Steven M. Conolly, PhD,[2] Michael V. McConnell, MD, MSEE.[1] [1]*Division of Cardiovascular Medicine, Stanford University, Stanford, CA, USA,* [2]*Department of Electrical Engineering, Stanford University, Stanford, CA, USA,* [3]*Advanced Magnetics, Inc., Cambridge, MA, USA.*

Introduction: Inflammation, including macrophage infiltration, is an important feature of vulnerable atherosclerotic plaques. The ultra-small superparamagnetic iron oxide (USPIO) agent ferumoxtran-10 has been shown to be taken up by macrophages in animal and human atherosclerosis, but detection by MR has relied on imaging areas of signal loss.

Purpose: 1) To study a novel off-resonance MRI sequence, which generates positive contrast of iron oxide contrast agents, and 2) to investigate the distribution of ferumoxtran-10 within the vessel wall, in a balloon-injured rabbit atherosclerosis model.

Methods: Seven New Zealand White rabbits underwent aortic balloon injury and high-fat diet for 14 or 26 weeks to induce atherosclerotic plaques and then were sacrificed. Five days prior to sacrifice, 25 mgFe/kg ferumoxtran-10 (Combidex®, Advanced Magnetics, Inc.) was given intravenously. The aorta was removed and underwent perfusion fixation, followed by ex vivo MRI and then histology. MRI was performed on a 1.5 T whole-body scanner (GE Signa CV/i) equipped with high-performance gradients (40 mT/m, 150 T/m/ms) using a standard 3-inch surface coil. The positive contrast off-resonance sequence utilized a spectrally selective RF pulse to null on-resonance water (by 120 dB) in order to detect the off-resonance water adjacent to the USPIO-laden cells (TR/TE = 800/14 ms, FOV = 8 cm, Matrix = 256 × 128, NEX = 1, offset of − 600 Hz, projection image). For comparison, a standard 3D fast gradient-echo sequence was performed to visualize the negative contrast T2* effect (TR/TE = 19.1/7.3 ms, NEX = 1, FOV = 8 cm, slice thickness = 2.0 mm, Flip angle = 30, Matrix = 512 × 512, in-plane spatial resolution = 156 um).

Results: In all rabbits, USPIO-laden areas of the rabbit aorta were seen on MRI as bright signal using the off-resonance sequence, which corresponded to areas of signal loss using the gradient-echo sequence (Figure 1). Histologically, plaque USPIO uptake was noted to be high in the smaller macrophages localized to the subendothelial area of the plaque. The larger lipid-laden foamy macrophages had more limited USPIO uptake, particularly in comparison to their plaque volume (Figure 2).

Conclusions: MRI in conjunction with USPIO can detect plaque macrophage infiltration using a novel positive contrast off-resonance sequence. Interestingly, there appear to be differences in the extent of iron uptake based on the type of plaque macrophage. These findings may help in further developing MR imaging approaches for the detection of plaque inflammation.

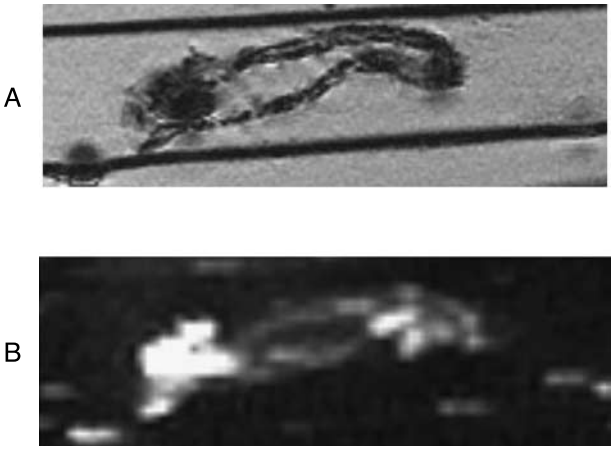

Figure 1. MR images of ex vivo rabbit aorta. A) Conventional gradient-echo image of an atherosclerotic aortic arch in rabbits with signal loss in areas of iron oxide uptake. B) Off-resonance image of the same specimen with a positive contrast effect seen.

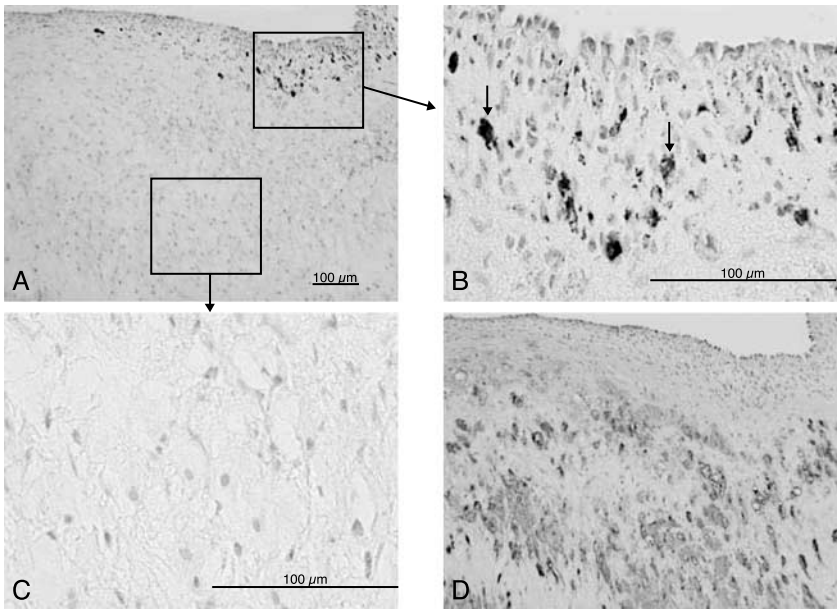

Figure 2. Histological examination. A) Perl's iron staining demonstrates iron-containing macrophages seen preferentially in the subendothelial area of the plaque (magnified in B), but not in the large lipid-laden foamy macrophages (magnified in C). D) RAM-11 immunohistochemistry confirms the abundant plaque macrophages.

111. 3-Dimensional Quantification of Atherosclerotic Injury with MRI Molecular Imaging

Tillmann Cyrus, MD, PhD, Shelton D. Caruthers, PhD, John S. Allen, BS, Todd Williams, BS, Ralph Fuhrhop, Thomas D. Harris, PhD, Veronica Glattauer, PhD, Jerome Werkmeister, PhD, John A. Ramshaw, PhD, Samuel A. Wickline, MD, Gregory M. Lanza, MD, PhD. *Cardiology, Washington University, Saint Louis, MO, USA.*

Background: Development of interventional MRI is a rapidly progressing field marked by the development of new catheters and stents. In contradistinction to classic x-ray angiography, MRI uniquely offers angiography in conjunction with high-resolution characterization of vascular atherosclerotic changes and wall morphology. In this study, targeted nanoparticles are used to define and quantify the spatial distribution of intramural biochemical signatures in extracellular matrix and on smooth muscle cells exposed by balloon overstretch injury.

Methods and Results: Carotid arteries of 12 domestic pigs were subjected to balloon stretch injury using a transcutaneous approach through the right femoral artery. Using the same femoral artery sheath, a double-balloon method was implemented to expose the injured arterial segments to paramagnetic nanoparticles targeted specifically to $\alpha_v\beta_3$-integrin or collagen III in the injured vessel wall. In each pig, one carotid received molecularly targeted nanoparticles and the contralateral vessel received either non-targeted nanoparticles or placebo. Carotid arteries underwent T1-weighted MRI at 1.5 T to define contrast enhancement of vascular injury. Routine time-of-flight MR angiograms were indistinguishable between control and targeted vessel segments and did not reveal evidence of the underlying stretch-induced microfractures. However, $\alpha_v\beta_3$-integrin targeted and collagen III targeted paramagnetic nanoparticles delivered locally penetrated the wall and followed along the microfractures of the injury. Both formulations provided significant contrast enhancement and allowed for determination not only of the volume but also the pattern of the vascular injury. The contrast-to-noise ratio of $\alpha_v\beta_3$-integrin targeted nanoparticles (13.8 ± 5.2) was 4-fold greater ($p < 0.05$) than the collagen III-targeted formulations (3.3 ± 0.3), suggesting a greater retention of the integrin-targeted agent. The estimated length and volume of mural

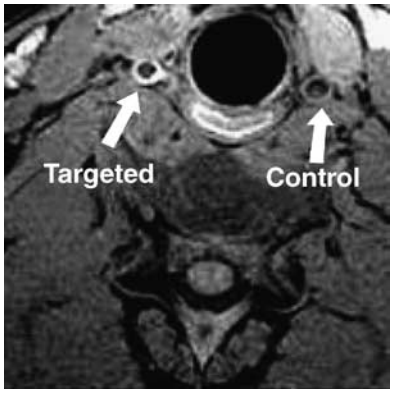

microvascular injuries did not differ between the collagen III- and integrin-targeted carotids, which averaged 31 ± 5 mm and 955 ± 234 mm^3, respectively. Interestingly, the average length of injury was greater than 50% longer than the balloon size (20 mm). Contrast enhancement was not appreciated in the control vessels.

Conclusions: Molecular imaging with $\alpha_v\beta_3$-integrin-targeted or collagen III-targeted nanoparticles enables the non-invasive 3-dimensional characterization of arterial lesions with MRI. These agents extend the diagnostic and therapeutic potential opportunities of interventional MR in the setting of advanced atherosclerotic disease.

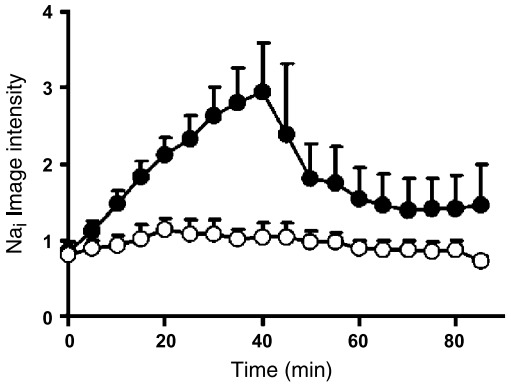

Figure 2. Intracellular Na^+ image intensities relative to the buffer intensity (%) of the area at risk (closed circles) and the right coronary perfusion bed (open circles) (n = 5 hearts).

112. Intracellular Sodium MRI During Acute Regional Myocardial Ischemia and Reperfusion

Maurits A. Jansen, PhD, Marcel G.J. Nederhoff, MSc, Cees J.A. van Echteld, PhD. *CardioNMR Laboratory, Heart Lung Center Utrecht, University Medical Center, Utrecht, The Netherlands.*

Introduction: Late enhancement MRI is rapidly becoming the new gold standard for assessment of myocardial viability. However, several false positives have been reported, most likely related to edema. As an alternative we have suggested ^{23}Na chemical shift imaging (CSI) because of the rapid changes of intracellular $[Na^+]$ ($[Na^+]_i$) during ischemia and reperfusion of viable myocardium. We have previously shown that imaging of intra- and extracellular sodium is superior to total sodium imaging in identifying the affected zone in chronic myocardial infarction (Jansen et al., 2004a). Furthermore, we found a very good correlation between Na^+_i-image intensity at the end of global low flow ischemia and recovery of rate pressure product at the end of reperfusion of isolated rat hearts (Jansen et al., 2004b). This shows that Na^+_i-image intensity can predict the ability of myocardial tissue to recover after ischemia.

Purpose: To investigate the potential of ^{23}Na CSI in acute regional ischemia and reperfusion in isolated rat hearts.

Methods: Data were acquired using a Bruker AVANCE 400 spectrometer. Rat hearts were perfused using a dual-perfusion cannula (Avkiran and Curtis, 1991), which allowed independent perfusion of both sides of the heart. To assess the area at risk, one side of the heart was perfused with a Gd-DTPA-BMA-containing perfusate and a T_1-weighted ^1H-image was acquired after 15 min. Next, the contrast agent was omitted and the shift reagent $TmDOTP^{5-}$ was included in the perfusate on both sides to separate the intra- and extracellular sodium resonance. Subsequently, acquisition-weighted ^{23}Na-CSI (16 × 16, FOV 20 × 20 mm, slice thickness 5 mm, voxel size 7.8 µl, 5 min/scan) was performed during control perfusion, ischemia of only the left side of the heart for 40 min (flow to the other side remained unaltered) and reperfusion. At the end of the experiment, the right side of the heart was perfused with methylene blue to determine the area at risk for histology. Thereafter, the whole heart was perfused with 1% triphenyltetrazolium chloride (TTC) to stain the viable tissue.

Results and Discussion: Figure 1 shows short axis $^{23}Na_i$ images of a heart subjected to acute regional ischemia and reperfusion and the corresponding ^1H- and TTC image. Na^+_i

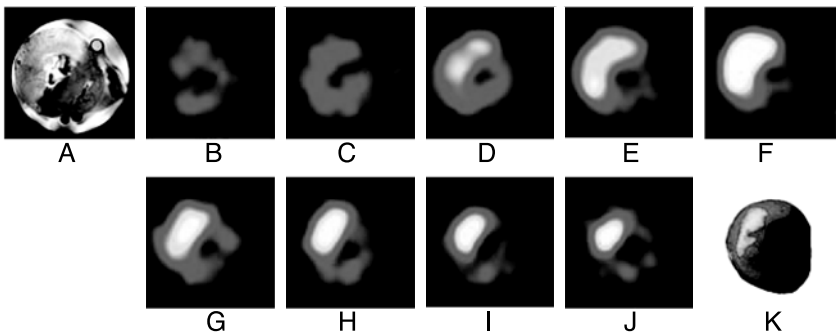

Figure 1. A: T_1-weighted ^1H-image of an isolated rat heart perfused with Gd-DTPA-BMA only on the left side, showing the area at risk, intracellular ^{23}Na-images during control perfusion (B), ischemia of the left side of the heart for 40 min (C–F) and reperfusion (G–J), and a TTC-image showing also the infarct (K, white).

was already visible during control perfusion. Na_i-image intensity increased significantly during ischemia of the left side to 345 ± 75% while that of the right side remained unaltered (Figure 2). During reperfusion, Na_i-image intensity returned to normal in 2 of the 5 hearts. **Total**^{23}Na image intensity remained unaltered during the entire protocol in both sides of the heart. The area on the Na_i-image at the end of ischemia with increased Na_i-intensity correlated well with the unstained area on the TTC-image (R = 0.73).

Conclusion: These data demonstrate that intracellular ^{23}Na-CS-imaging is a promising tool for assessment of myocardial viability.

REFERENCES

Avkiran, M., Curtis, M. J. (1991). *Am. J. Physiol.* 261:H2082–H2090.

Jansen, M. A., Nederhoff, M. G. J., van Echteld, C. J. A. (2004a). *J. Cardiovasc. Magn. Res.* 6(1):318.

Jansen, M. A., van Emous, J. G., Nederhoff, M. G. J., van Echteld, C. J. A. (2004b). *Circulation*. in press.

113. Prognostic Value of High-Dose Dobutamine Stress MRI in Coronary Artery Disease: Long-term Follow-Up of Cardiac Events in Patients Not Undergoing Revascularization

Peter Hunold, MD,[1] Markus Jochims, MD,[2] Oliver Bruder, MD,[2] Kai-Uwe Waltering, MD,[1] Walter O. Schüler, MD,[2] Thomas Schlosser, MD,[1] Jörg Barkhausen, MD.[1] [1]*Department of Diagnostic and Interventional Radiology, University Hospital, Essen, Germany,* [2]*Department of Cardiology, Elisabeth Hospital, Essen, Germany.*

Introduction: Cardiac Stress MRI using high-dose dobutamine (DS-MRI) has been established as a reliable technique for the assessment of myocardial ischemia in coronary artery disease (CAD). Beyond the detection of ischemia and the prediction of functional recovery in patients with ischemic global or regional dysfunction after revascularization, little is known about the prognosis of patients suffering from ischemic dysfunction.

Purpose: To evaluate the utility of high-dose dobutamine stress MRI for the assessment of cardiac prognosis in patients with suspected coronary artery disease.

Methods: High-dose DS-MRI was successfully performed in 384 patients (288 male, 96 female; mean age, 64) with clinically suspected CAD. All examinations were performed on a 1.5 T MR System (Magnetom Sonata; Siemens Medical Solutions; Erlangen, Germany) using a segmented steady-state free precession sequence (TrueFISP, TR, 3 ms; TE 1.5 ms; FA 60°). A dobutamine/atropine stress protocol (dobutamine: 10, 20, 30, and 40 μg/kg*min and up to 1 mg of atropine) was used until 85% of the age-predicted heart rate was achieved (220-age). The DS-MRI examinations were evaluated by an experienced radiologist and a cardiologist in consensus. Myocardial ischemia was defined by new or worsening wall motion abnormalities under stress in more than one myocardial segment. Clinical follow-up was performed for at least 12 months (mean 16 months), and the occurrence of major adverse cardiac events (cardiac death, myocardial infarction, unstable angina requiring hospitalization and coronary arterial revascularization) was determined.

Results: In 153 patients, coronary catheter angiography was performed, and DS-MRI yielded a sensitivity of 86% and specificity of 88% for the detection of coronary artery stenosis > 70%. 64 of these 153 patients were scheduled for immediate revascularization and, thus, excluded from the follow-up study. Therefore, a clinical long-term follow-up could be performed in 320 patients. In 49 patients, wall motion abnormalities were detected at DS-MRI. Of these 49 patients, 12 (24.5%) had major adverse cardiac events during the follow-up time frame, whereas only 23 of 271 patients (8.5%) without wall motion abnormalities had major adverse cardiac events within the follow-up period.

Conclusions: High-dose dobutamine stress MRI is a robust and accurate diagnostic test for the assessment of myocardial ischemia. Beyond the detection and quantification of myocardial ischemia, DS-MRI can be used to forecast major adverse cardiac events in patients with known or suspected coronary artery disease.

114. Abnormal Rest Cardiac MR Perfusion Identifies Hibernating Myocardium in a Porcine Model of Chronic Myocardial Ischemia

Evan Appelbaum, Kraig V. Kissinger, MS, RT, Audrey Rosinberg, MD, Pierre Voisine, MD, Thomas H. Hauser, MD, Roger J. Laham, MD, Warren J. Manning, MD, Susan B. Yeon, MD, JD. *Cardiology, BIDMC, Brookline, MA, USA.*

Background: The identification of chronically underperfused, hypocontractile (hibernating) myocardium is an important predictor of myocardial recovery following coronary revascularization. Resting first-pass cardiac MR perfusion (CMRP) imaging has been used to identify microvascular obstruction (MO) after acute myocardial infarction, however its value in the identification of hibernating myocardium is unknown.

Hypothesis: CMRP correlates with microspheres in detecting resting perfusion abnormalities in chronic myocardial ischemia.

Methods: 15 Yorkshire pigs underwent cardiac MR (CMR) and coronary angiography(XRA) 3 weeks after surgical placement of an ameroid constrictor on the proximal left circumflex artery (LCx). Ameroid closure was confirmed in all 15 pigs by XRA. Cine functional, first-pass rest

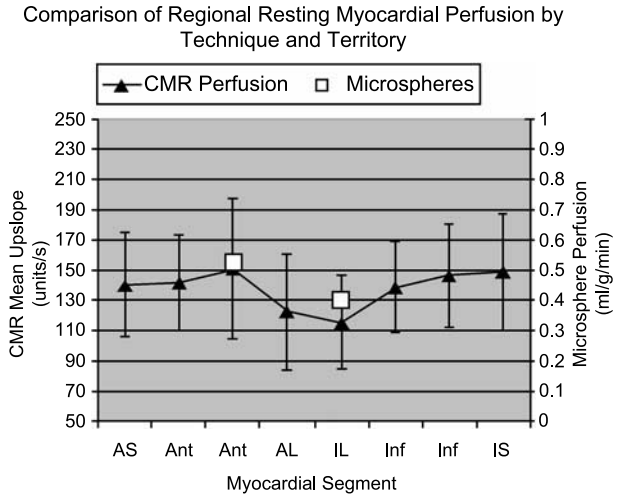

Figure 1.

perfusion, and delayed enhancement (DE-CMR) (scar) imaging (1.5 T, Philips ACS-NT, Best, NL) was performed in all animals. Isotope-labeled microspheres were injected into the left atrium. Animals were sacrificed and the whole hearts were explanted. Cardiac MR perfusion time-intensity analysis for 8 myocardial segments of a 10 mm thick midventricular slice was performed to obtain the mean upslope of myocardial enhancement for each segment. The cine functional and DE-CMR of the matched ventricular slice were examined for regional function and the presence of scar, respectively.

Results: In all animals, there was decreased radial thickening in the LCx as compared to the LAD territory. Microsphere analysis demonstrated reduced flow in the LCx territory [infero-lateral (IL)] as compared to the LAD territory [anterior (Ant)] ($p = 0.001$). By CMR, no animal had evidence of myocardial scar/infarction on DE-CMR. The CMRP demonstrated reduced mean upslope in the LCx territory as compared with the LAD ($p < 0.005$) (see Figure 1). There was a moderate correlation between microspheres and CMRP mean upslope (Spearman correlation 0.5, $p = 0.08$).

Conclusion: In this porcine model of hibernating myocardium, abnormal resting CMRP imaging reflects decreased myocardial perfusion. This novel application of CMRP may be ideally suited to define the extent of hibernating myocardium and to assess improvement in response to therapy.

115. Myocardial Blood Flow at Rest Is Impaired in Segments with Severe Coronary Artery Disease: an MR Study of Quantitative Perfusion Assessment

Joseph B. Selvanayagam,[1] Michael Jerosch-Herold,[2] Italo Porto,[3] Steffen E. Petersen,[1] Jane M. Francis,[1] Adrian Banning,[3] Stefan Neubauer.[1] [1]*University of Oxford, Oxford, UK,* [2]*Oregon Health and Science University, Portland, OR, USA,* [3]*John Radcliffe Hospital, Oxford, UK*

Background: Although impairment in perfusion reserve during vasodilator stress is well recognized in myocardial segments supplied by significantly diseased coronary arteries, it is unknown whether resting myocardial blood flow is abnormal in such segments. Quantitative first pass MR perfusion imaging allows absolute quantification of myocardial blood flow. We hypothesized that mean blood flow (MBF) assessed at rest by MR perfusion imaging would reliably identify myocardial segments affected by severe coronary stenosis.

Methods: 15 patients with one or two vessel coronary disease and normal global left ventricular function undergoing PCI were studied with pre-procedure and post-procedure (24 hours) first pass perfusion MR imaging at rest. 3 short axis images were acquired during every heart-beat using a T1-weighted turboFLASH sequence, with low-dosage Gd-DTPA bolus injection. The diagnostic coronary angiogram was used as the gold standard in defining affected myocardial segments. In each slice, MBF was determined for 8 myocardial sectors in ml/min/g by deconvolution of signal intensity curves with an arterial input function measured in the LV blood pool.

Results: Mean patient age was 60 ± 11 years. Coronary lesion severity was 80–100% stenosis by QCA. Mean MBF normalized by rate pressure product ('corrected MBF') was 1.1 ± 0.3 ml/min/g in segments without significant coronary stenosis and 0.7 ± 0.2 ml/min/g in segments with coronary stenosis pre PCI ($p < 0.0001$). Post procedure, the MBF was 1.0 ± 0.3 ml/min/g in revascularized segments, and 1.1 ± 0.3 ml/min/g in non-diseased segments ($p = 0.8$). There was a significant increase in the corrected MBF (0.4 ± 0.2 ml/min/g) in revascularized myocardial segments ($p < 0.001$). Binary logistic regression indicated that the odds ratio for the presence vs. absence of a coronary lesion decreased by 1:18 ($p < 0.001$) for every unit increase of resting MBF in the territory of the respective vessel.

Conclusion: MR perfusion imaging detects impairment of resting MBF pre-PCI in myocardial segments affected by severe coronary stenosis. Measurement of MBF may become clinically relevant for determining the territories affected by severe coronary stenosis.

116. Prediction of Event-Free Survival by Contrast Enhanced Cardiac Magnetic Resonance Imaging in Patients with Symptoms of Coronary Artery Disease

Carmen W. S. Chan, MD,[1] Edgar Kent Yucel, MD,[2] Glenn H. Reynolds, MSc,[3] Raymond Y. Kwong, MD.[1] [1]*Medicine, Brigham and Women's Hospital, Boston, MA, USA,* [2]*Radiology, Brigham and Women's Hospital, Boston, MA, USA,* [3]*General Electric Medical Systems, Boston, MA, USA.*

Table 1. Univariate analysis of prediction of adverse events

	Hazard ratio	Lower limit of 95% CI	Upper limit of 95% CI	p-Value
Age				
> 45 men	2.59	1.11	6.05	0.03
> 55 women				
Gender	1.08	0.61	1.92	NS
Hypertension	2.04	1.18	3.54	0.01
Diabetes	2.56	1.48	4.43	0.0008
Hypercholesterolemia	1.90	1.05	3.46	0.03
Global LV EF < 60% by CMRI	2.18	1.20	3.96	0.01
History of Prior MI	3.19	1.85	5.50	< 0.0001
CAD on ECG	1.38	1.09	1.74	0.008
Myocardial delayed enhancement on CMRI	5.75	2.81	10.59	< 0.0001

Introduction: Myocardial delayed enhancement (MDE) by contrast enhanced cardiac MRI (CMRI) characterizes abnormal myocardium from various diseases. Prognostication of serious cardiac events by MDE, relative to clinical predictors, in patients with symptoms of coronary artery disease (CAD) is not known.

Purpose: To determine the prediction of event-free survival by MDE in patients presented with symptoms of CAD.

Methods: Two hundred and eight-four patients (192 M, mean age 58) presented with symptoms of CAD were referred to undergo CMRI for assessment of myocardial viability or detection of myocardial infarction. Clinical history and ECG were obtained at the time of CMRI. Successful contact was achieved in 279 patients (98%). Adverse events were defined by death, acute myocardial infarction (MI), unstable angina, and decompensated heart failure requiring hospitalization. Three patients could not perform CMRI due to claustrophobia. Twenty-seven patients had a history of CAD and underwent successful coronary revascularization within 60 days prior to CMRI, were excluded from survival analysis. The remaining 257 patients formed the study cohort. Patients who underwent successful coronary revascularization subsequent to study entry at time of CMRI were censored on the day of coronary revascularization. Univariate hazard ratio analysis was used to identify significant clinical predictors of adverse events. Survival curves were performed by the Kaplan Meier method and were compared by log-rank tests for significance. A multivariable Cox proportional hazard regression model with a stepwise forward selection was used to include the strongest predictors into the model.

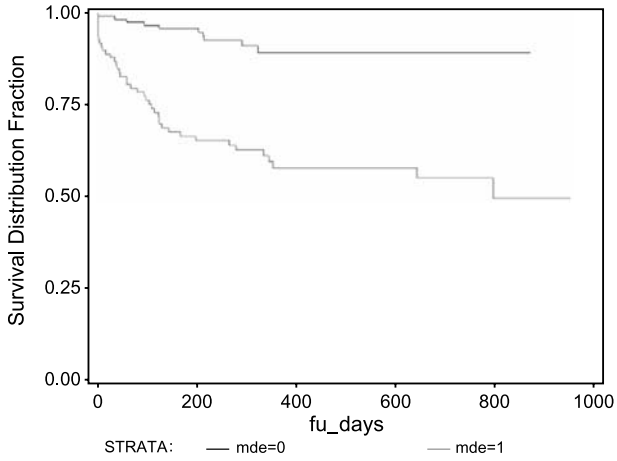

Figure 1.

Results: Over a mean follow-up of 13.8 months (range 6–33 months), 54 (21%) adverse events occurred including 30 deaths, 3 acute MI, and 21 unstable angina or decompensated congestive heart failure. Results of the univariate analysis are shown in Table 1. Kaplan Meier curves and results of the log-rank test were illustrated in Figure 1. Presence of MDE was associated with the highest hazard ratio of 5.75 (C.I. 2.88–11.5, $p < 0.0001$) to the development of adverse events. By the multivariable Cox regression model, MDE remained the strongest predictor after adjustment for age, global left ventricular function, prior MI, hypertension, diabetes, and abnormal ECG (Adjusted hazard ratio 3.99, CI 1.67–9.57, $p < 0.002$).

Conclusions: Myocardial characterization by CMRI strongly predicts adverse cardiac events in patients with symptoms of CAD. Prognostication by this technique extends beyond the risk prediction by the strongest known factors such as age, global left ventricular function, prior MI, hypertension, diabetes, and ECG findings.

117. Combined Use of Adenosine Stress Perfusion MRI and Multislice CT Coronary Angiography for Detecting Hemodynamically Significant Coronary Artery Disease

Okan Ekinci, MD,[1] Thorsten Dill, MD,[2] Ali Rad,[2] Jochen Hansel, MD,[2] Matthias Rau, MD,[2] Christian W. Hamm, MD, PhD.[2] [1]*Cardiology, German Clinic of Diagnostic, Wiesbaden, Germany,* [2]*Cardiology, Kerckhoff Heart Center, Bad Nauheim, Germany.*

Introduction: Contrast-enhanced angiography of coronary arteries using the newest generation of multi-detector computed tomography (CTA) allows detection of both calcified and non-calcified coronary artery lesions. On the other hand it is still difficult to assess the grade of stenosis, especially if calcified or mixed plaques are present. This makes ruling out hemodynamic significance of borderline stenoses by CTA impossible. The grade of stenosis is systematically overestimated, leading often to unnecessary x-ray angiographies.

Purpose: Adenosine stress perfusion MRI is a recently introduced method for myocardial perfusion imaging. We investigated the potential of this novel method as an additional diagnostic tool for assessing hemodynamic significance of coronary artery stenoses detected by CT angiography.

Methods: 200 consecutive patients (pts, 171 male, 59 ± 13 y) with no known coronary artery disease underwent calcium-scoring analysis and CT coronary angiography (Siemens Sensation Cardiac 16, rotation time 370 ms, collimation 0.75 mm, slice width 1 mm). ECG-triggered CT image acquisition was done after bolus injection of 1 mL/kg bw Iomerone (Imeron 400, Altana Pharma, Germany) at 4 mL/s and 20 mL saline flush.

68 (34%) pts with borderline stenosis or [moderate but diffuse] or [heavy but circumscript] calcification which made stenosis graduation difficult, underwent additionally adenosine stress MRI (Siemens Sonata, 1.5 T). After acquisition of functional cine images in standard orientations, 140 μg/kg body weight adenosine was applied for 6 min. After two minutes of infusion, contrast enhanced first-pass myocardial perfusion image acquisition was started using a ECG-gated breath-hold TrueFISP perfusion sequence with 3 slices (60 acquisitions) in short axis orientation and application of 0.1 mmol/kg body weight Gd-DTPA at 4 mL/s (Magnevist, Schering, Germany). Contrast bolus was chased with 20 mL of saline. Viability imaging for detecting areas of delayed hyperenhancement was done using a 3D-FLASH inversion recovery sequence with TI 270–300 ms, typically 10-15 min after perfusion imaging. Perfusion imaging at rest was performed finally, especially to rule out susceptebility artifacts.

Results: Out of 68 pts 49 (72%) had diffuse calcification of coronary vessels below or within the 75th percentile, 19 (28%) exceeded the age related threshold. Mean coronary calcium score according to Agatston was 280 ± 251.

Stress MRI revealed regional subendocardial perfusion deficit in 10 out of 68 pts. 2 of these patients showed subendocardial myocardial scar. All segments showing perfusion deficits could be assigned to CT-detected stenoses.

Additional X-ray coronary angiography was done in all patients with MR detected perfusion deficits. Among others—8 corresponding stenoses ranging from 60–85% (4 LAD, 2 CX, 2 RCA) were seen and could be treated by angioplasty. 1 occluded side branch (corresponding to a subendocardial infarction) was found and not interventionally treated.

58 out of 68 pts had no myocardial perfusion deficit or delayed hyperenhancement and could be treated conservatively.

Conclusions: Multislice CT only is not sufficient to diagnose hemodynamic significance of coronary artery stenoses. Adenosine stress MRI after CTA enables adequate clinical decision making in patients with borderline stenoses or diffuse or circumscript calcified coronary arteries by assessment of hemodynamic significance.

CT and stress MRI provide complementary data and combined use leads to less radiation exposure by preventing unnecessary X-ray angiographies.

118. Serial Magnetic Resonance Imaging for the Assessment of Myocardial Perfusion, Left Ventricular Function, and Infarct Size After Application of Blood-Derived Progenitor Cells in Recanalised Chronic Coronary Total Occlusions

Holger Thiele, Karsten Lenk, Sandra Erbs, Volker Adams, Stephan Gielen, Axel Linke, Gerhard Schuler, Rainer Hambrecht. *Cardiology, University of Leipzig-Heart Center, Leipzig, Germany.*

Introduction: Magnetic resonance imaging (MRI) is an excellent diagnostic tool for serial assessment of changes in left ventricular function, infarct size and myocardial perfusion. Circulating progenitor cells (CPC) injected intracoronary improve myocardial perfusion and function after acute myocardial infarction as shown by MRI. If similar effects can be achieved in chronic total occlusions (CTO), has not been studied.

Purpose: Aim of this randomised, placebo-controlled, double-blind study was to evaluate the impact of CPCs on myocardial perfusion, infarct size and left ventricular function assessed by MRI after successful recanalisation of a CTO.

Methods: So far 26 patients with reperfused CTO were randomised to either CPC's or inactive serum (control), which were infused into the target vessel. Patients underwent MR imaging on a 1.5 Tesla MR tomograph at baseline and at 3 months follow-up. For the assessment of left ventricular function cine loops of the complete heart in short and horizontal long-axis planes were acquired using a steady-state free precession technique (TR/TE/flip = 3.2/1.2/60). Additionally, delayed enhancement images covering the whole ventricle were acquired 10–20 min after a double-bolus of Gadolinium-BOPTA (Gadovist, Schering, Germany) using a 3 D inversion recovery gradient echo sequence (TR/TE/flip 2.8/1.1/15) with the inversion time adapted to null normal myocardium. Infarct size was determined as the percentage of the left ventricular mass. Furthermore, first-pass perfusion images were acquired with a hybrid TFE-EPI sequence at rest and stress using adenosine at standard dose.

Results: Serial MRI revealed a significant increase in left ventricular ejection fraction in the CPC group (from 51 ± 14

to 58 ± 13%; $p < 0.05$ versus baseline), a decrease in endsystolic volume (from 68 ± 33 to 60 ± 33 ml; $p < 0.05$ versus baseline) and unchanged enddiastolic volumes (136 ± 37 versus 133 ± 33, p = n.s. versus baseline). Infarct size in percent of left ventricular mass, measured as delayed enhancement MRI, decreased significantly from 10.3 ± 7.7 to 9.0 ± 7.2% ($p < 0.05$ versus baseline). First-pass myocardial perfusion MRI at rest and stress revealed a significant improvement of the myocardial perfusion reserve index in the affected segments by 1.1 ± 0.8 to 1.3 ± 0.9, $p < 0.05$. In the control group ejection fraction, left ventricular volumes, infarct size and myocardial perfusion reserve index remained unchanged.

Conclusions: Analysis of serial contrast-enhanced MRI suggests that intracoronary application of CPC post recanalisation of CTO is associated with an improved myocardial perfusion and subsequent improved recovery of left ventricular function as compared to a control group. Further investigations of the pathophysiological CPC effects on macro- and microvascular function are required.

119. Real-Time Myocardial Function During Arrythmia

Peter Kellman, PhD, Hiroshi Ashikaga, MD, Steven R. Mickelsen, Elliot R. McVeigh, PhD. *Nhlbi, NIH, Bethesda, MD, USA.*

Introduction: It has been previously shown with tagged MRI that mechanical asynchrony during ventricular contraction tracks with electrical asynchrony of activation. Unfortunately, to date, patients with non-periodic ventricular arrhythmia have not been studied with these techniques due to the need for reproducible heartbeats during the segmented data acquisition. In this study, we demonstrate the ability of real-time MRI SSFP acquisition with TSENSE to quantify regional function in the heart with non-periodic ventricular arrhythmia. This technique may provide a method to measure the spatial pattern of the underlying asynchrony of activation, where high resolution electrical mapping is unavailable.

Purpose: To demonstrate ability to quantify regional wall function by generating a time series of wall thickening during non-periodic ventricular arrhythmia.

Methods: Six dogs underwent MR studies 4 weeks after antero-septal myocardial infarction (MI) by proximal LAD occlusion. MI location and geometry were evaluated with a high-resolution late enhancement inversion recovery sequence. Polymorphic ventricular tachycardia (VT) was induced by a standard programmed stimulation protocol.

Real time imaging used a true-FISP sequence accelerated using the TSENSE (Kellman et al., 2001) parallel imaging method. During free-breathing without ECG triggering, a single short-axis slice containing the MI region was imaged during the first minute after inducing VT. Imaging was conducted using a 1.5 T Siemens Sonata. Imaging parameters were: BW 1395 Hz/pixel, TE/TR 1.2/2.4 ms, 55° readout flip angle, 128 × 52 image matrix. SENSE acceleration (rate R = 4) was used to obtain the full 52 line resolution using 13 phase encodes, corresponding to a temporal resolution of 31.5 ms (32 frames/s). The FOV was 250 × 172 mm^2 corresponding to an in-plane spatial resolution of 2 × 3.3mm^2, with a 6 mm slice thickness. The number of frames acquired was 480 corresponding to approx 15 s. A custom 8-element linear surface coil array from Nova Medical Inc. (Wilmington, MA) was used.

LV endocardial and epicardial contours were traced manually and a time series of regional wall thickening was computed at 32 equidistant angles. A respiratory signal was derived from the images by measuring the centroid of the signal intensity profile through the diaphragm.

Results: Results are shown for a case of polymorphic VT. A time series of 10 consecutive example images are shown in Fig. 1. The regional wall thickening versus time is displayed in Fig. 2(A) for 32 angles with wall thickness (intensity) displayed between 12 mm (dark) and 20 mm (bright). The MI region corresponds to the angle with thin and hypokinetic myocardium (dark horizontal band). A time series of the LV endocardial area (mm^2), is shown in Fig. 2(B) and respiratory signal in Fig. 2(C). The time window between the two arrows in Fig. 2(A) is magnified in Fig. 3. The ventricular contraction is highly irregular with cycle lengths of 180–450 ms. Figure 3 clearly shows short runs of reproducible activation (B3–B5). It is seen that at times (B1–B2) the LV is contracting sychronously (i.e., postero-lateral contracts with anterior wall), while at other times (B3–B7) regions become localized focii for independent mechanical activation.

Conclusions: We demonstrate that real-time MR imaging allows quantification of regional myocardial function during non-periodic ventricular arrhythmia. The time series of regional wall thickening provides not only a noninvasive method to quantify the myocardial function in each region but

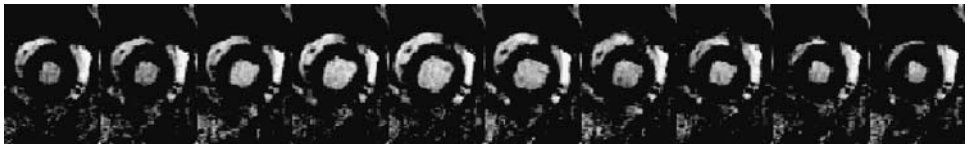

Figure 1. Example real-time images during ventricular tachycardia.

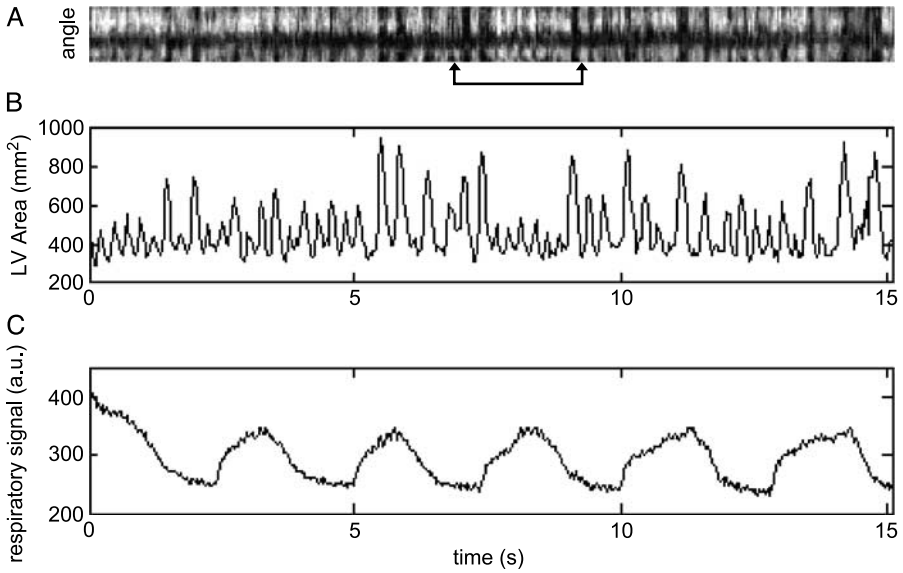

Figure 2. (A) Regional wall thickening vs. time, (B) LV area, (C) respiratory signal.

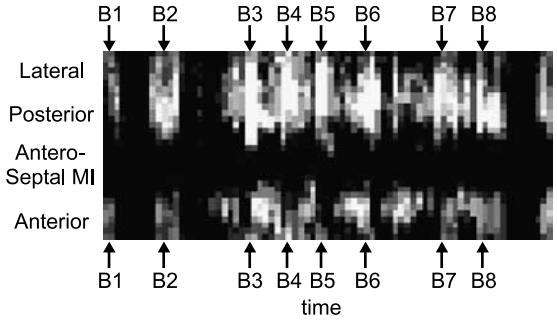

Figure 3. Regional wall thickening for several beats.

also the onset of wall thickening and thinning, which corresponds to the timing of mechanical activation and deactivation, respectively.

REFERENCE

Kellman, P., et al. (2001). *MRM* 45:846–852.

120. MR Phase Contrast Velocity Mapping for the Assessment of Regional Function of the Systemic Ventricle in Patients with Transposition of the Great Arteries

Oliver Wieben, PhD,[1] Bernd Jung, MS,[1] Petra Mehwald, MD,[2] Thorsten Bley, MD,[3] Deniz Kececioglu, MD,[2] Jürgen Hennig, PhD.[1] [1]*Department of Diagnostic Radiology-Medical Physics, University Hospital Freiburg, Freiburg, Germany,* [2]*Department of Congenital Heart Disease/Pediatric Cardiology, University Hospital Freiburg, Freiburg, Germany,* [3]*Department of Diagnostic Radiology, University Hospital Freiburg, Freiburg, Germany.*

Introduction: Although an actuarial survival of 75% after 25-years has been reported (Oechslin et al., 2000), the very long-term ability of the right ventricle to support the systemic circulation remains unknown. Several studies have described abnormalities in the RV function of such patients. However, functional parameters for assessing the need for surgical interventions such as conversion to arterial switch or transplantation or drug therapies have not been identified yet. MR Phase contrast (PC) velocity mapping (Markl et al., 2002) is an objective method to quantify segmental

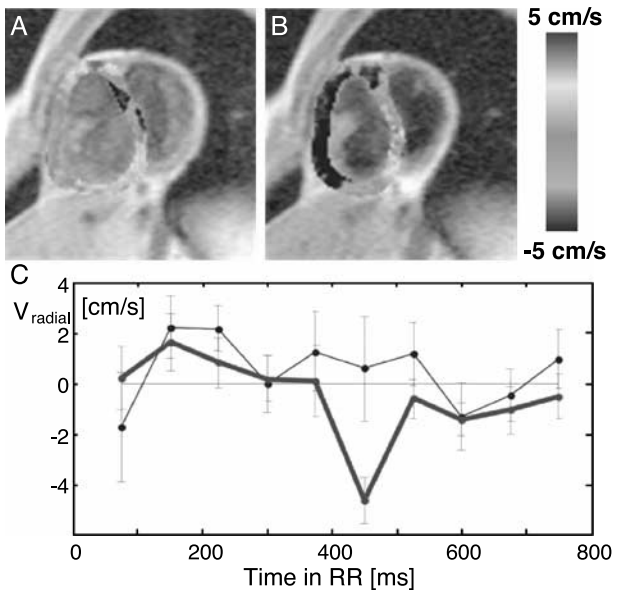

Figure 1.

myocardial wall motion and was used in this study to evaluate regional function of the systemic ventricle in patients that had undergone a Senning procedure.

Methods: PC measurements with in-plane velocity encoding were performed in short axis views of 5 patients (15–22 years) which had a Senning operation as newborns. A spoiled gradient echo sequence with black blood preparation and first-order flow compensation in read- and phase encoding direction for the reduction of flow artifacts was implemented on a 1.5 T Sonata system (Siemens Medical Solutions, Erlangen, Germany) Image acquisition parameters were as follow: TE/TR = 4.5/6.2 ms, flip angle = 15°, FOV = 300 mm × 400 mm, acquisition matrix = 256 × 96, venc = 20 cm/s. A temporal resolution of 49–87 ms was achieved with view sharing such that full in-plane velocity information of the beating heart was obtained in 13–22 heartbeats within a single breath-hold measurement. The right ventricular wall was manually segmented from the magnitude images and radial and tangential velocities were calculated for each of those pixels. The segmented RV was divided into 24 angular areas for which radial velocities were averaged and correlated to a reference time course based on the shape of the waveform (Markl et al., 2002). Positive correlation values correspond to similar or hypokinetic motion patterns, while values near zero describe akinetic motion and negative values express dyskinetic RV waveforms. The flow analysis and visualization was perfomed with a customized software tool written in Matlab (The Mathworks).

Results: All five patients showed a dyskinetic motion pattern of the ventricular wall. Figure 1 contains a representative example displaying the radial velocities of a mid-ventricular slice where red color represents contraction of the myocardium and blue color the expansion. The septum moves toward the LV wall while the RV free wall contracts during systole (A) and moves back during early diastole (B) while the RV free wall expands. Figure 1C shows the differences in the temporal evolutions of the radial velocities in the segments of the RV free wall (thick) and the septum (thin). This dyskinetic motion is also displayed in the color-coded correlation plots of radial velocities for various slice locations and the summarizing bullseye plot in Figure 2A and B, covering the heart from base to apex.

Conclusion: This pilot study demonstrated the feasibility of PC velocity mapping for the analysis of regional RV function in patients with transposition of the great arteries. It was shown, in agreement with Fogel et al. (1995), that the motion patterns of the systemic RV in Senning patients differ significantly from those of the normal human LV, where the contraction of the ventricular wall and the septum occur simultaneously. Further investigations with more patients in various stages of the remodeling process of the RV ventricle are warranted in order to understand the significance of these abnormalities and to assess potential benefits for therapeutic decisions.

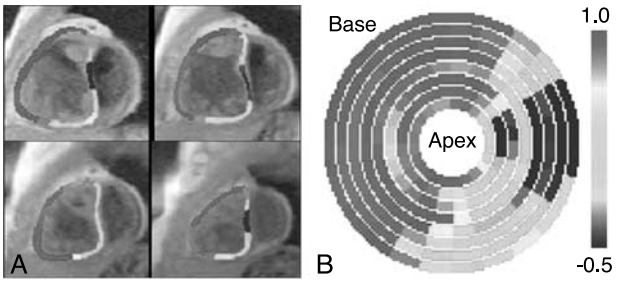

Figure 2.

REFERENCES

Fogel, M., et al. (1995). *Circulation* 92:219–230.
Markl, M., et al. (2002). *J. Magn. Reson. Imaging* 15:642–653.
Oechslin, E., et al. (2000). *Thorac. Cardiovasc. Surg.* 48:233–237.

121. Temporal Evolution of Myocardial Dysfunction in Mice After Reperfused Myocardial Infarction: A 3D Deformation Analysis Combined with Delayed Enhancement Infarct Imaging

Alistair A. Young, PhD,[1] Brent A. French, PhD,[2] Zequan Yang, PhD,[2] Brett R. Cowan, MbChB,[3] Wesley D. Gilson, PhD,[2] Stuart S. Berr, PhD,[2] Christopher M. Kramer, MD,[2] Frederick H. Epstein, PhD.[2] [1]*Anatomy with Radiology, University of Auckland, Auckland, New Zealand,* [2]*Radiology, University of Virginia, Charlottesville, VA, USA,* [3]*Medicine, University of Auckland, Auckland, New Zealand.*

Introduction: The mouse animal model is increasingly being used to investigate both the genetics and pharmacologic therapy of left ventricular (LV) remodeling after myocardial infarction (MI). Local changes in contractile function (strain) after MI can be quantified using 2D and 3D magnetic resonance (MR) tagging (Epstein et al., 2002; Young et al., 2004). However, to date, the 3D deformation pattern of the mouse heart has not been described with respect to the 3D extent of the region of infarction.

Purpose: 1) To extend a previously described method of 3D modeling of LV dysfunction (Young et al., 2004) to a regional analysis with regard to infarcted and noninfarcted areas of interest. 2) To develop tools to construct a 3D model of the infarcted area from multislice delayed enhancement (DE) infarct imaging. 3) To report 3D deformation parameters with respect to infarcted and noninfarcted areas over the first 28 days following MI.

Methods: Five C57BL/6 mice were used in this study, which was approved by the Institutional Animal Care and Use Committee. MI was surgically induced by 60 min occlusion of the left anterior descending coronary artery followed by reperfusion as described previously (Epstein et al., 2002). MRI was performed on a 4.7 T Varian scanner using a

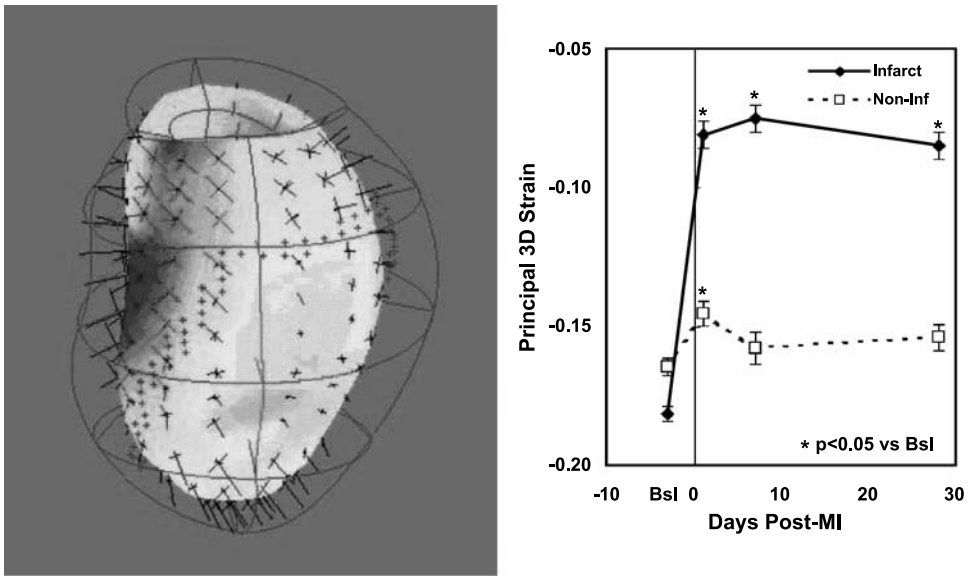

Figure 1.

custom-made birdcage RF coil. Mice were imaged at baseline, and at 1, 7 and 28 days after MI. The MR protocol included: 1) localizer scanning; 2) short-axis (8 slices) and long-axis (4 slices) imaging with black-blood myocardial tagging; 3) high flip-angle (60°) DE infarct imaging after IP injection of 0.4 mmol/kg Gd-DTPA. Three dimensional displacements of the tags were tracked in all images and a 3D finite element model of the LV was used to reconstruct the 3D deformation and strain, as described previously (Young et al., 2004). The finite element model was used to reconstruct 3D deformation and strain using 16 regional segments. Gd-enhanced areas were mapped onto the Day 1 heart models, and infarcted segments were defined as those with > 50% enhancement. In addition, areas of enhancement were outlined on multislice short axis DE images, and the infarcted region was indicated by a 3D bounding region on a polar bullseye projection map. The infarct zone was then mapped onto the FE model, so that the boundary points become material points which move with the deformation of the heart. The 3D material boundary was then used to calculate regional strains on the basis of infarcted region (within the boundary) or noninfarcted region (outside the infarct boundary).

Results: Figure 1 (left) shows the finite element model of the LV at end systole on Day 1, where + signs denote the edge of the infarct at end-diastole, crosses denote principal strains and color denotes maximal shortening (blue − 0.2, red 0.0). The graph (Figure 1, right) reports principal 3D strain in infarcted and non-infarcted segments over time after MI. MI caused a permanent loss of principal 3D strain in infarcted segments. In non-infarcted segments, 3D strain was significantly depressed on Day 1 post-MI, and then recovered to baseline levels at Days 7 and 28.

Conclusions: This study illustrates how 3D analyses of myocardial infarction from multislice DE imaging can be combined with strain information from multislice MR tagging, and applied in mice to study LV dysfunction post-MI. These quantitative tools will prove useful in determining the effects of genetic manipulation and/or pharmacologic therapy on LV remodeling.

REFERENCES

Epstein, F. H., et al. (2002). *Magn. Reson. Med.* 48:399–403.
Young, A. A., et al. (May 2004). Proc. ISMRM, 1792, Kyoto.

122. Matched Cine DENSE and Contrast-Enhanced CMR Identify Heterogeneity of Function in Noninfarcted Regions After Myocardial Infarction

Frederick H. Epstein,[1] Nicholas C. Nacey, BS,[2] Szilard Voros, MD,[2] Xiaodong Zhong, MS,[1] Elizabeth A. Cowart, MS,[1] Christopher M. Kramer, MD.[3] [1]*Radiology and Biomedical Engineering, University of Virginia, Charlottesville, VA, USA,* [2]*Medicine, University of Virginia, Charlottesville, VA, USA,* [3]*Radiology and Medicine, University of Virginia, Charlottesville, VA, USA.*

Introduction: Cine displacement-encoded imaging using stimulated echoes (cine DENSE) is a new technique for quantitation of intramyocardial displacement and strain with high spatial resolution and automated analysis after manual LV segmentation (Kim et al., 2004). While strain analysis of cine DENSE has been validated vs. myocardial tagging in normal volunteers (Kim et al., 2004), this technique has not yet been evaluated in patients with ischemic heart disease.

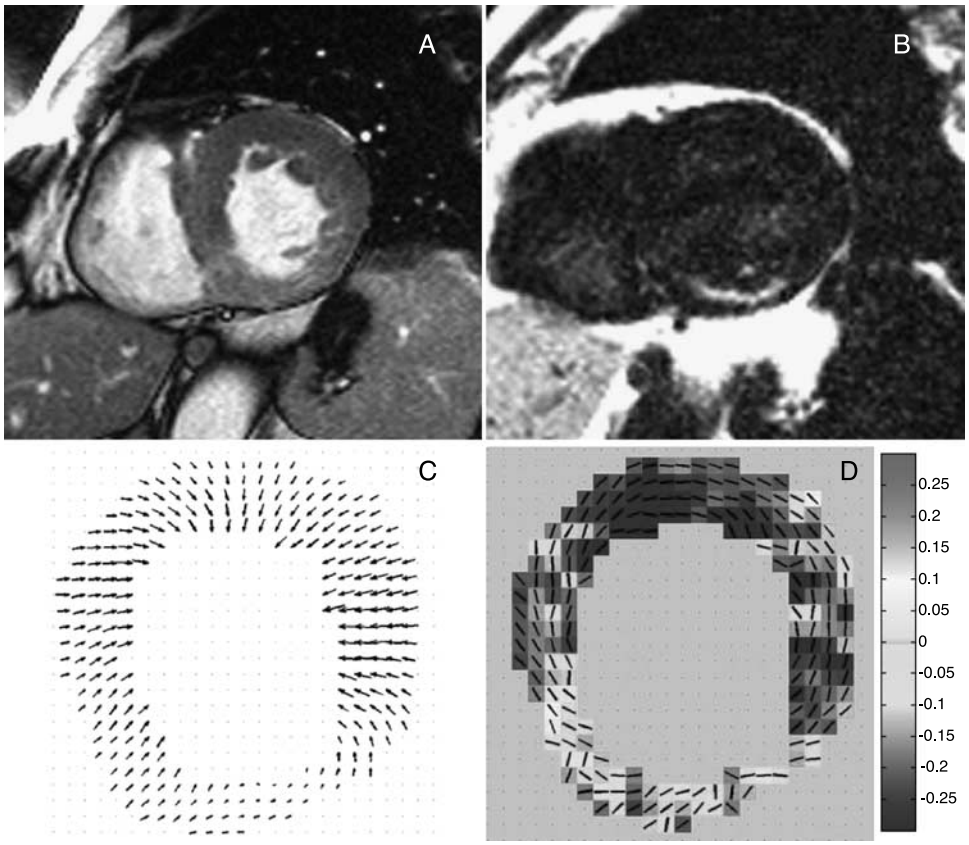

Figure 1. Matched images from a patient with inferior myocardial infarction. Cine SSFP is shown in (A), delayed contrast enhanced CMR is shown in (B), a DENSE displacement map is shown in (C), and a second principal strain map is shown in (D). The location of the wall motion defect agrees with and extends beyond the region of delayed hyperenhancement.

Purpose: To demonstrate the feasibility of applying cine DENSE in patients with myocardial infarction (MI) and subsequently test the hypothesis that matched cine DENSE and delayed contrast-enhanced CMR could identify heterogeneity of function within noninfarcted regions.

Methods: Thirteen patients (age 53 ± 9, 10 male) with reperfused first MI (5 anterior, 8 inferior, troponin 86 ± 136, week 6 ± 6 post-MI) underwent cine SSFP, cine DENSE, and contrast-enhanced inversion-recovery gradient echo CMR on a 1.5 T Siemens Sonata. In addition, 6 normal subjects underwent cine DENSE and cine SSFP imaging. The cine DENSE sequence used in this study employed single-echo SSFP for signal generation as described previously (Cowart et al., 2004), instead of using multishot EPI (Kim et al., 2004). Specific cine DENSE parameters included FOV = 360 mm, matrix = 128 × 96, slice thickness = 8 mm, TR = 3.8 ms, TE = 1.9 ms, flip angle = 25°, segments = 16, cardiac phases = 12–16, and displacement encoding frequency = 0.44 rad/mm. Matched cine DENSE, SSFP, and contrast-enhanced images were acquired in 2–3 short-axis planes. Multiphase DENSE images were analyzed offline using custom-written software developed in MATLAB. For each cardiac phase, a 2D displacement map and 2D myocardial strain maps were automatically computed from phase-reconstructed DENSE images after manual segmentation of the LV from a magnitude-reconstructed DENSE image. The 2D strain tensor was computed for each 4-pixel neighborhood of myocardium using finite element methods. Next, regions of hyperenhancement on matched contrast-enhanced images were used to define infarcted (hyperenhanced), adjacent (2 cm

Table 1. Regional circumferential strain (Ecc)

	Normal subjects	Patients infarct	Patients adjacent	Patients remote
Ecc	−0.19 ± 0.02	−0.03 ± 0.04*	−0.08 ± 0.04*,#	−0.17 ± 0.04#,†

*$p < 0.05$ vs. normal subjects.
#$p < 0.05$ vs. infarct.
†$p < 0.05$ vs. adjacent.

border zone), and remote zones. Mean circumferential strain (E_{cc}) was then computed for the three distinct zones by applying the zone classifications to the strain maps. Significant differences in strain between the three zones from MI patients and between normal volunteers was assessed by one-way analysis of variance.

Results: Example data demonstrating inferior wall MI with subendocardial hypenhancement is shown in Figure 1. Specifically, the end systolic phase from cine SSFP is shown in (A), subendocardial delayed hyperenhancement is shown in (B), an end-systolic DENSE displacement map is shown in (C), and an end-systolic DENSE second principal strain map is shown in (D). Cine DENSE displacement movies clearly depicted the temporal evolution of reduced intramyocardial motion within regions of delayed hyperenhancement and abnormal regional twist patterns around the border zones of the infarcts. Data summarizing circumferential strain in normal subjects and patients post-MI are provided in Table 1.

Conclusions: This is the first demonstration that cine DENSE can be used to quantify myocardial displacement and strain at high spatial resolution in patients with MI. Matched cine DENSE and contrast-enhanced CMR detect dysfunction within adjacent noninfarcted myocardium post-MI. Together, these techniques could prove useful in the testing of efficacy of novel therapies in patients with MI.

REFERENCES

Cowart, E. A., Gilson, W. D., Kramer, C. M., Epstein, F. H. (2004). Imaging 3D myocardial motion with cine SSFP DENSE. *Proc. Int. Soc. Magn. Reson.* 2660.

Kim, D., Gilson, W. D., Kramer, C. M., Epstein, F. H. (2004). Myocardial tissue tracking with two-dimensional cine displacement-encoded MR imaging: development and initial evaluation. *Radiology* 230:862–871.

123. Comparison of Peak Velocities in the Ascending Aorta Detected by k-t BLAST Accelerated MR-FVE and Echocardiography

Christof Baltes,[1] Michael Schacht Hansen,[2] Jeffrey Tsao, PhD,[3] Sebastian Kozerke, PhD,[1] Klaas P. Pruessmann, PhD,[1] Erik M. Pedersen, PhD,[2] Peter Boesiger, PhD.[1] [1]*Institute for Biomedical Engineering, University and ETH Zurich, Zurich, Switzerland,* [2]*MR-Centre, Skejby Hospital, Aarhus University Hospital, Aarhus, Denmark,* [3]*Novartis Institutes for BioMedical Research, Inc. (NIBRI), Cambridge, MA, USA.*

Introduction: For quantifying aortic valve stenosis, MR phase-contrast (PC) velocity measurements have been compared to echocardiography as the clinical standard routine (Caruthers et al., 2003). Although a good correlation between MR and echocardiography was found, PC measurements tended to underestimate the actual peak velocities. Fourier velocity encoding (FVE) (Moran, 1984) allows accurate peak velocity determination, but standard FVE scans are usually not applicable in cardiac applications due to their long acquisition times.

In this project, the FVE data collection was accelerated by up to 16-fold using the *k-t* BLAST framework. In phantom experiments, non-accelerated and accelerated FVE measurements were compared to ultrasound, to validate the accuracy of peak velocity detection. Initial in-vivo results were acquired in the ascending aorta of a healthy volunteer, for which data from single breath-hold FVE scans were compared to echocardiography.

Methods: Acquiring high resolution FVE data leads to long acquisition times due to the additional encoding along one or more velocity dimensions. For natural objects, the raw FVE data typically exhibit a significant correlation in time, space and velocity (Fig. 1A). This correlation can be exploited to accelerate the data collection using the *k-t* BLAST approach (Fig. 1B) (Hansen et al., 2004; Tsao et al., 2003).

In phantom experiments, the accuracy of the accelerated FVE scans was investigated by comparing the determined peak velocities with results from Doppler ultrasound. For this purpose, physiological, pulsatile flows were generated in tubes with inner diameters of 8 mm and 20 mm and varying degrees of area stenosis (0%, 25%, 50%, 75%, 90%) resulting in peak velocities from 30 to 550 cm/s. MR scans were performed on a Philips Intera 1.5 T system with the following parameters: FOV: 58 mm × 230 mm, resolution: 0.9 × 0.9 × 5 mm^3, TE/TR: 4.0–7.1/12.0 ms. Non-angulated,

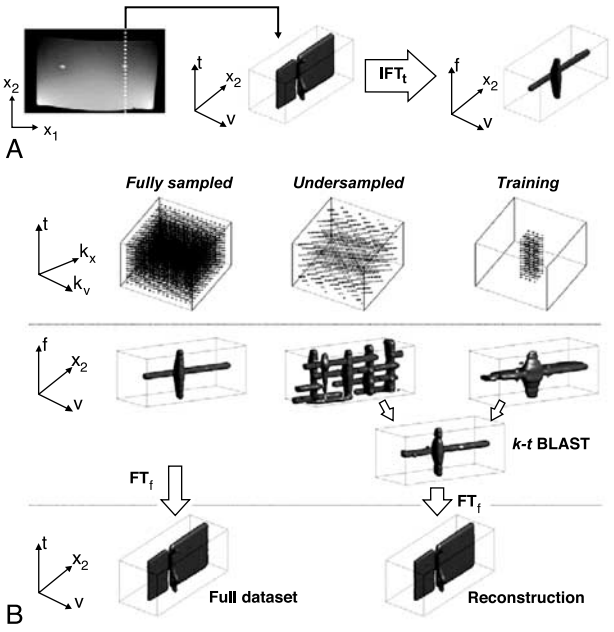

Figure 1. A) Sparse signal distribution in x-v-t space and in corresponding x-v-f space B) Non-accelerated and accelerated data acquisition and the corresponding reconstruction scheme according to the *k-t* BLAST framework.

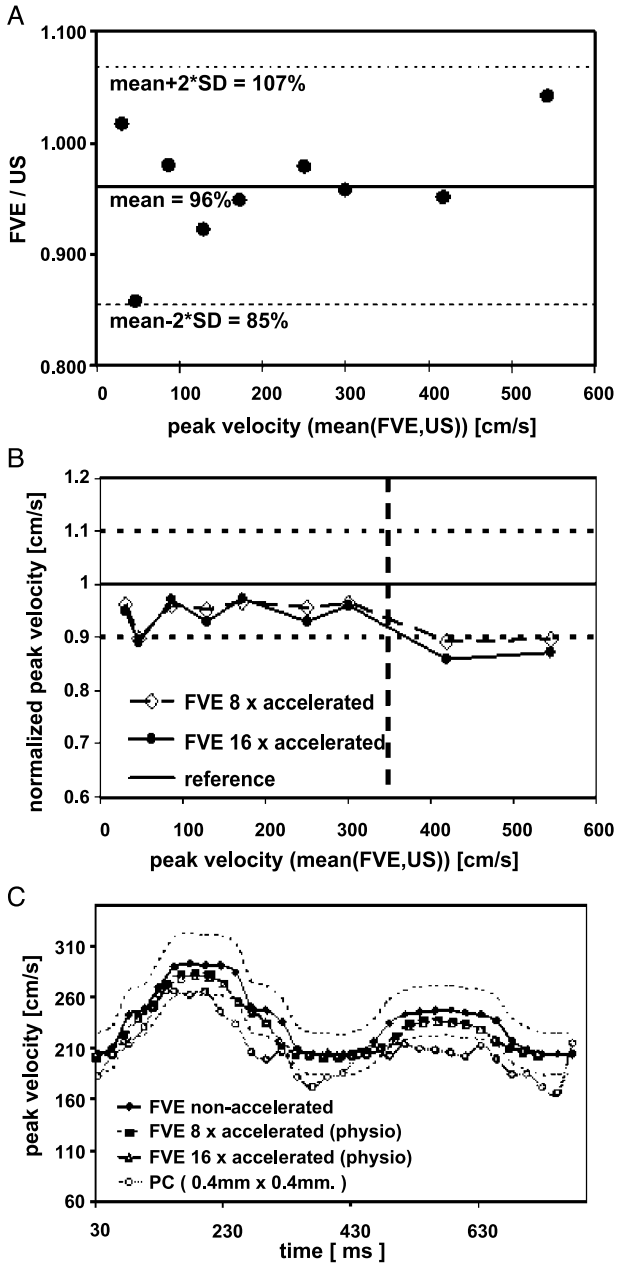

Figure 2. A) Bland-Altman graph comparing peak velocities detected by Doppler ultrasound (US) against non-accelerated MR-FVE (FVE). B) Comparison of normalized peak velocities at peak systole detected using accelerated MR-FVE against reference value (= mean of ultrasound and non-accelerated MR-FVE).

pulsed wave Doppler measurements were performed using a standard General Electric Vivid 7 system.

In order to enable single breath-hold acquisitions in the ascending aorta, the spatial in-plane resolution of the accelerated FVE scans was reduced. To evaluate the effect of the larger image voxel on the peak velocity detection, the experiments were repeated with the following settings: FOV: 227 × 330 mm, resolution: 2.6 × 2.6 × 5 mm^3, TE/TR: 3.0–6.0/5.2–7.3 ms. In addition, peak velocities were determined with MR-PC velocity mapping (FOV: 58 × 230 mm, resolution: 0.4 × 0.4 × 5 mm^3, TE/TR: 4.3–5.3/12.0 ms, 2 averages).

In-vivo FVE data were collected in the ascending aorta of a healthy volunteer using acceleration factors 8 and 16 and compared to echocardiography.

Results: A good agreement of the peak velocities detected with Doppler ultrasound and non-accelerated MR-FVE was found (Fig. 2A). Accelerated FVE (Fig. 2B) underestimated the peak velocities only slightly ($\leq$ 10%) in the range from 30 to 350 cm/s, while significant underestimation (> 10%) occurred over 350 cm/s. Figure 2C shows peak velocities over time measured in a 20 mm tube with 75% stenosis using low-resolution MR-FVE and conventional MR-PC. Even with larger voxel volumes, the peak velocities detected with accelerated MR-FVE stayed within 10% of the values from the high-resolution, non-accelerated scan, while standard MR-PC exceeds the 10% limit (Fig. 3).

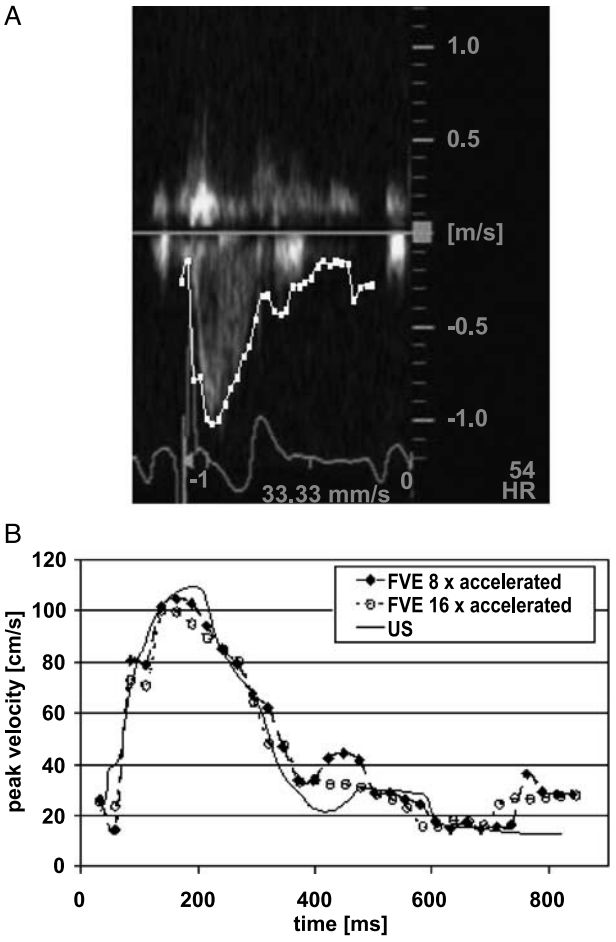

Figure 3. Peak velocity measurement in the ascending aorta of a healthy volunteer: A) Comparison of Doppler ultrasound (background) and 8-fold accelerated MR-FVE (white line). Detected peak velocity at peak systole: 104 cm/s using 8-fold accelerated MR-FVE and 108 cm/s using ultrasound. B) Ultrasound compared to 8-fold and 16-fold accelerated MR-FVE acquired in one single breath-hold of 21s and 17s, respectively.

In in-vivo measurements in the ascending aorta, Doppler ultrasound and 8-fold and 16-fold accelerated MR-FVE compared well resulting in peak velocities at peak systole of 104/100 cm/s [MR-FVE (8-/16-fold)] and 109 cm/s (ultrasound), respectively.

Discussion: In this work, the acquisition time of MR-FVE measurements was drastically reduced using the *k-t* BLAST framework.

Phantom experiments showed that peak velocities detected by accelerated FVE scans remained accurate (deviation: $\leq 10\%$) below 350 cm/s. Above 350 cm/s, significant deviations occur due to the temporal low-pass filtering resulting from the *k-t* BLAST reconstruction. Even low-resolution FVE scans deviated less than 10% and were superior to PC velocity mapping.

Initial in-vivo experiments showed promise for accurate detection of peak velocities within a clinically relevant timeframe using *k-t* BLAST accelerated MR-FVE.

REFERENCES

Caruthers, S. D., et al. (2003). *Circulation* 108:2236–2243.
Hansen, M. S., et al. (2004). *Proc. ESMRMB* (146).
Moran, P. R. (1984). *MRM* 1(4):197–203.
Tsao, J., et al. (2003). *MRM* 50(5):1031–1042.

124. Cardiac-Output Measurement in 5 Seconds Using Ungated Spiral Phase-Contrast

Jong B. Park,[1] Bob S. Hu,[2] Juan M. Santos,[1] Krishna S. Nayak,[3] Girish Narayan,[4] Dwight G. Nishimura.[1] [1]*Electrical Engineering, Stanford University, Stanford, CA, USA,* [2]*Cardiovascular Medicine, Palo Alto Medical Foundation, Stanford, CA, USA,* [3]*Electrical Engineering, University of Southern California, Los Angeles, CA, USA,* [4]*Cardiovascular Medicine, Stanford University, Stanford, CA, USA.*

Introduction: Cardiac output (CO) is a key indicator for assessing all cardiovascular diseases. However, no reliable non-invasive method exists for measuring CO dynamically. A technique called ungated spiral phase-contrast (USPC) has been shown to rapidly measure accurate volume flow rates without cardiac-synchronization in peripheral arteries. In this work, we modified USPC for successful CO application. Ten subjects including one patient with patent ductus arteriosus (PDA) were scanned.

Purpose: To show that USPC can be a fast and robust MRI method for measuring CO.

Methods: USPC uses spiral readouts and temporal averaging for calculating through-plane-direction time-averaged volume flow. To accurately measure CO at the ascending aorta (AA), following modifications were made to USPC: short 480us RF-pulse, 10 degree flip, axial imaging slice at the iso-center, 24 cm FOV, 2 mm spatial resolution, and short TR of 12 ms with N = 12 interleaved spiral readout trajectories. The short RF-pulse, low flip angle, and imaging-slice orientation were chosen to minimize possible errors from AA flow itself and from gradients. Compared to the original USPC, FOV, spatial resolution, TR, and N are tailored to AA (highly pulsatile flow and larger vessel size), while keeping the high temporal sampling rate of flow-encodings (i.e., using the short TR).

Triggered real-time steady-state-free-precession (RT-SSFP) imaging is used as the gold standard. RT-SSFP can measure left-ventricle (LV) stroke-volumes, which can be then used to indirectly compute CO in subjects without regurgitant flow at the aortic valve. With RT-SSFP, cardiac-gated movie loops of 10 slices covering LV are acquired in breath-holds of 10 R–R intervals.

For each subject, USPC and RT-SSFP are repeated 3 and 2 times, respectively. The total scan-times were 5 seconds with USPC and 10–20 heartbeats with RT-SSFP. With the PDA patient, the cardiac-catheterized Fick method was also used as a reference. In a 28-second continuous scan, the data is averaged with 5-second window to produce temporally resolved CO.

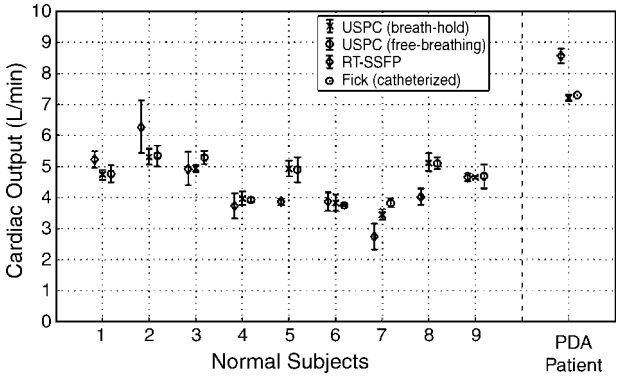

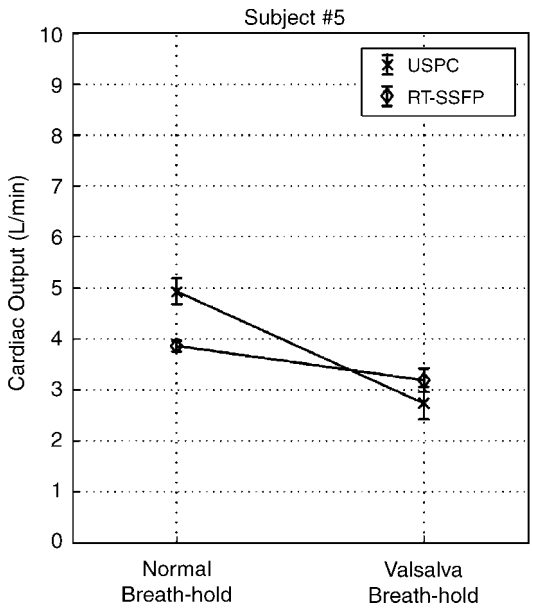

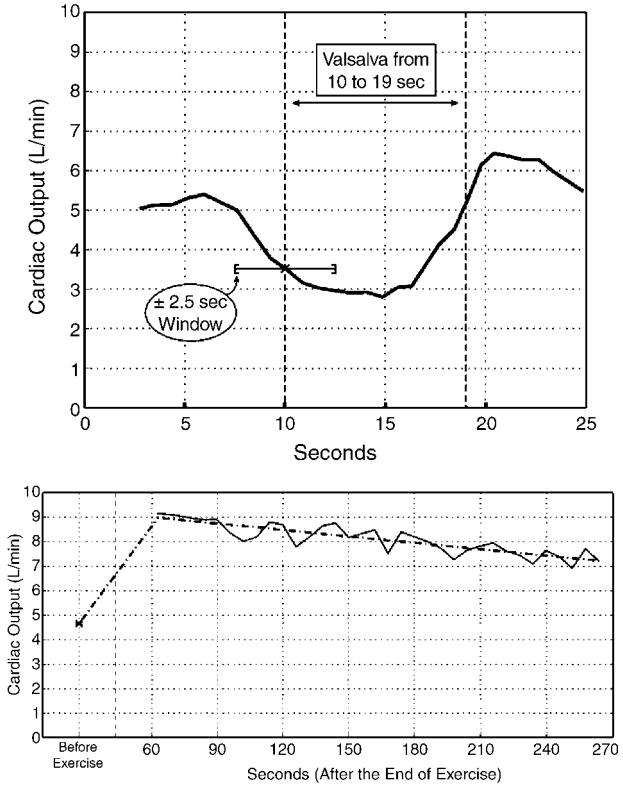

Results: USPC and RT-SSFP showed good agreement in all studies (mean difference: 0.1 + − 0.7 L/min). Higher COs were observed with the PDA patient, which also agreed with the Fick method. CO dropped about 20–40% with valsalva breath-hold. In the 28-second continuous scan, USPC temporally resolved the physiological changes accurately. In a stress study with a 5-minute exercise, CO increased about 100% and then gradually decreased.

Conclusions: USPC can be a rapid and accurate in-vivo CO measurement technique. The high temporal resolution and sensitivity to physiologic maneuvers can provide insights into the pathophysiology and response to therapy for a diverse set of patients.

125. Effect of Optimal Pharmacological Treatment on Left Ventricular Remodeling in Chronic Heart Failure Assessed by Cardiovascular Magnetic Resonance

Nikolay P. Nikitin, MD, PhD, Klaus K. A. Witte, MRCP, Ramesh de Silva, MRCP, Simon D. R. Thackray, MRCP, Poay Huan Loh, MRCP, Elena I. Lukaschuk, MSc, Andrew L. Clark, MA, MD, FRCP, John G. F. Cleland, MD, FRCP, FACC. *Academic Unit of Cardiology, University of Hull, Kingston Upon Hull, UK.*

Left ventricular (LV) remodeling is believed to be an important mechanism driving the progression of chronic heart failure (CHF). This prospective observational study was designed to investigate if optimal pharmacological treatment with beta-blockers and ACE inhibitors prevents further progression of LV remodeling in CHF patients due to LV systolic dysfunction. Cardiovascular magnetic resonance (CMR) was chosen as the method of serial investigation of cardiac anatomy and function due to its high accuracy and reproducibility.

Table 1.

	Baseline	6 months	12 months	*P*
LVEDV, ml	236 ± 78	233 ± 75	233 ± 77	NS
LVESV, ml	160 ± 65	156 ± 65	155 ± 69	NS
LVEF, %	33 ± 8	35 ± 9	36 ± 11	NS
LVEDMM, g	194 ± 51	191 ± 51	187 ± 48	NS

Methods and results: The study population initially included 102 patients with CHF aged 69 ± 8 years with LV systolic dysfunction (ejection fraction < 45% as assessed by CMR) who had been on established pharmacological therapy with beta-blockers and ACE inhibitors in optimal doses for at least 6 months. Serial cinematographic (FIESTA) ECG-triggered breath-hold CMR was performed at baseline, at 6 months and after 12 months of observation using a 1.5 Tesla scanner (Signa CV/i, GE Medical Systems). The multi-slice cine data sets covering the left ventricle from apex to base were analysed to calculate LV end-diastolic volume (LVEDV), LV end-systolic volume (LVESV), LV end-diastolic myocardial mass (LVEDMM) and LV ejection fraction (LVEF) with the use of MRI-MASS software system (MEDIS, Leiden, NL). Twenty patients who died and one patient who underwent heart transplantation during the follow-up were excluded from the analysis. Therefore, 81 patients completed the study. After 6 and 12 months of optimal treatment there were no increase in LVEDV or LVESV or decline in LVEF to suggest progressive adverse LV remodelling (Table 1). LVEDMM was slightly reduced, but this did not reach statistical significance.

Conclusions: Patients with CHF on established optimal pharmacological therapy with a beta-blocker and ACE inhibitor do not demonstrate progressive LV remodeling or deteriorating global LV systolic function. These results suggest that in the beta-blocker era, mechanisms other than maladaptive ventricular remodeling drive the progression of CHF.

126. Intermediate and Long-Term Remodeling of Remote Left Ventricular Myocardium Following Percutaneous Transcatheter Septal Myocardial Ablation in Hypertrophic Obstructive Cardiomyopathy Detected by Cine MRI

John M. Cahill, MB, Robert A. Quaife, MD, Cathleen Kenny, NP, Deb Singel, RT, Marianne Shanahan, RT, Tyler Miller, Bertron M. Groves, MD. *Cardiology, University of Colorado Hospital, Denver, CO, USA.*

Introduction: Percutaneous Transcatheter Septal Myocardial Ablation (PTSMA) has been shown to reduce left ventricular outflow (LVOT) gradient in patients with hypertrophic obstructive cardiomyopathy (HOCM) and leads to symptomatic improvement with reduction in NYHA class in many cases. Recent data suggest that geographical variations in infarct position within the interventricular septum (IVS) may affect LV remodeling and outcome, depending upon infarct location of the right, left or transmural septal regions.

Purpose: To establish the contribution of remote LV remodeling to reduction in LV mass in the intermediate and long term following successful (transmural or left-septal) PTSMA.

Methods: As part of an ongoing study, cardiac MRI studies were performed pre-PTSMA and at 3 and 12 months following the procedure. LV mass, ejection fraction (EF), end-diastolic (EDV) and end-systolic (ESV) volumes were calculated from True FISP gated, single breath-hold cine images in the short axis plane using a 1.5-T magnet. At follow-up studies, a bolus of 0.1 mmol/Kg of Gadolinium-DTPA was administered, with infarct size and position within the IV septum (transmural, left septal or right septal) assessed using a segmented inversion-recovery turboFLASH sequence in short and long axis views with delayed contrast enhancement at 10 minutes and appropriate TI correction.

Using *ARGUS* software (*Siemens Medical*), baseline short axis slices were mounted on a split-screen viewer beside the corresponding follow-up study and the corresponding contrast-enhanced infarct short-axis 8 mm slices.

Epicardial and endocardial borders were traced by manual planimetry. To correct for thinning in the region of the infracted target area, we reprocessed the post-PTSMA studies, this time following the pre-PTSMA endo- and epicardial border contours, using baseline septal thickness and visual prompts as a guide.

LV mass and volumes derived from this corrective technique were compared to the pre-PTSMA data, with any reduction from baseline in mass observed being attributed to remote LV remodeling. Baseline values were compared to 3-month (intermediate) and 12 month (long-term) data with and without correction for thinning and volume loss in the infarct zone.

Results: Of 51 PTSMA procedures in 44 patients, MRI data at baseline and follow-up were available in 20. Of these, 5 cases resulted in infarction of the right septum only, with 2 of these requiring repeat PTSMA for optimal symptomatic improvement. This group is not included in the results presented in this abstract. Successful PTSMA resulted in a significant reduction in LV outflow tract gradient in the other 15 cases (77 ± 42 to 17 ± 12 mmHg, $p < 0.001$), therefore intermediate data were available in 15 patients and long-term data in 8.

Absolute LV mass was significantly reduced (281 ± 96 to 225 ± 79 g, $p = 0.0003$) at 3 months, even after correction for infarct thinning (281 ± 96 to 251 ± 86 g, $n = 15$, $p = 0.008$), with further mass reduction from 3 to 12 months (245 ± 86 to 229 ± 70 g, $n = 8$, $p = 0.08$).

No significant changes were noted in LV volumes or LVEF at 3-month follow-up (LVEF 73 ± 7 to 70 ± 3%, p = ns; EDV 70 ± 15 to 72 ± 18 ml, p = ns; ESV 22 ± 7 to 22 ± 7 ml, p = ns) or at 1 year. Infarct volume was smaller as determined by delayed contrast enhancement between 3 and 12 month follow up studies (13.1 ± 6.1 ml to 8.7 ± 3 ml, $p = 0.02$).

Conclusions: Following successful PTSMA, reduction in LV mass is significantly more than could be accounted for by infarct thinning alone, suggesting remote LV remodeling which continues beyond 3 months.

127. Human Infarct Resorption Patterns and Long-Term Ventricular Remodeling Following Myocardial Infarctions of Varying Size

Paula Tejedor, MD, Edwin Wu, MD, Chiara Bucciarelli-Ducci, MD, Daniel C. Lee, MD, Preeti Kansal, MD, James C. Carr, MD, Thomas A. Holly, MD, Francis J. Klocke, MD, Robert O. Bonow, MD. *Northwestern University, Chicago, IL, USA.*

Introduction: Limitation of acute myocardial infarct size is the goal of all reperfusion therapies in order to improve long-term outcome. Accurately measuring acute infarct and non-infarct sizes is necessary to monitor the potential of future therapeutic interventions. Contrast enhanced MRI (ceMRI) has the ability to identify the extent of acute and chronic myocardial infarcts (MI). This long-term, clinical study describes the pattern of infarct healing and its effects on ventricular remodeling in humans after a MI.

Methods: We studied 56 subjects using cine and ceMRI within 7 days and 218 ± 174 days following an acute MI. 48 of the 56 subjects presented with an ST segment elevation MI. All subjects underwent emergent or urgent revascularization and had documented elevation in cardiac enzymes. Delayed, contrast-enhanced images were obtained using an inversion-recovery, segmented turboFlash sequence following gadolinium contrast. Images were obtained 15 to 20 minutes following hand-bolus injection. The inversion time (TI = 250–350 ms) was progressively optimized to null normal myocardium. Left ventricular ejection fraction (EF), left ventricular mass and thickness of remote, non-infarcted myocardium were measured. Infarct areas were analyzed for transmural thickness, endocardial length, and infarct mass as a percentage of total LV mass. The radial extent of the infarction was expressed as a fraction of the remote wall thickness, and the endocardial circumferential ratio was the length of the short-axis endocardial hyperenhancement over the full endocardial circumference.

Results: The mean initial EF was 42 ± 12% (range from 17% to 55%). The mean EF during the follow-up

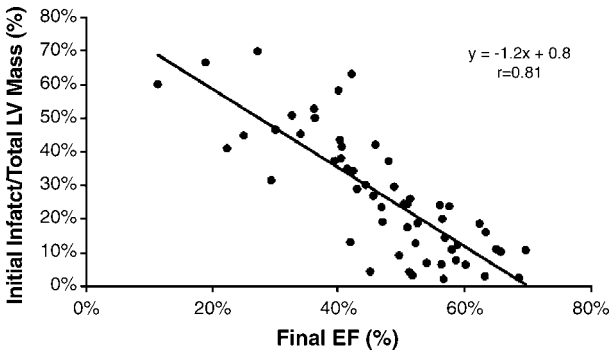

Figure 1.

examination improved to 47 ± 13% (p = 0.03). The initial infarct mass represented 27 ± 22% of the total LV mass, and it decreased to 21 ± 17% (p < 0.001) in the follow-up studies. Decreases in infarct size varied inversely with infarct size (y = 0.184 Ln(x) − 0.057, r = 0.6). The radial transmural extent also decreased by 26 ± 43% (from 90 ± 30% to 63 ± 32%; p < 0.001); however, the endocardial circumferential ratio did not significantly change (2.6 ± 7%; p = 0.3). Although the initial percent of infarct mass correlated with the initial EF (r = 0.73), there was a stronger correlation between the initial infarct percent and final EF (r = 0.81, see Fig. 1).

Conclusions: Over a wide range of infarct sizes, the size of the acute myocardial infarct predicts the follow-up EF after infarct healing has occurred. As the size of the initial infarct increases, the EF declines. The improvement of EF likely represents improvement in dysfunctional, but viable "stunned" myocardium. Additionally, infarct sizes systematically decrease following a reperfused acute MI. The degree of decrease is greater transmurally than circumferentially and varies inversely with the initial infarct size.

128. Left Ventricular Remodelling in Dilated Cardiomyopathy with and without Evidence of Late Gadolinium Enhancement

Ravi Assomull, Jonathan Lyne, Dudley Pennell, Sanjay Prasad. *CMR Unit, Royal Brompton Hospital, London, UK.*

Introduction: Late gadolinium enhancement cardiovascular magnetic resonance imaging (LGE-CMR) shows a patchy, midwall pattern in approximately 25% of patients with a clinical diagnosis of idiopathic dilated cardiomyopathy. The pattern of late enhancement in this group correlates well with the distribution of fibrosis seen in post-mortem specimens.

Purpose: In patients with non-ischaemic dilated cardiomyopathy, to assess whether there is adverse remodelling in those patients with late enhancement compared to those with no evidence of late enhancement.

Methods: The scans of 33 consecutive patients with dilated cardiomyopathy (DCM) were analysed. Patients who had clinical evidence of ischaemic heart disease or had coronary angiograms showing flow-limiting lesions were excluded. Overall, 22 patients (66%, 15 male, mean age 51 ± 19 years) showed no late enhancement whilst 11 (33%, 9 male, mean age 40 ± 11 years) displayed midwall late enhancement. Left ventricular dimensions (including LV mass and mass index) as well as left ventricular ejection fraction (LVEF) were compared between the two groups using a 2 sample independent t-test. Right ventricular parameters were similarly compared.

Results: DCM patients with late enhancement had a significantly higher LV end diastolic volume index (LVEDVI) when compared to patients without late enhancement (166 ± 50 ml/m^2 vs. 124 ± 36 ml/m^2 respectively, p = 0.009). The LV end systolic volume index (LVESVI) was also significantly higher in the late enhancement group (118 ± 56 ml/m^2 vs. 81 ± 39 ml/m^2 respectively, p = 0.04).

Mean LV mass in the late enhancement group was also significantly higher than in the non-enhancement group (251 ± 87 g vs. 198 ± 52 g, p = 0.03) as was LV mass index (123 ± 25.4 g/m^2 vs. 103 ± 26 g/m^2, p = 0.04). There was no difference in LVEF between the two groups (30.2 ± 13.5% vs. 36.1 ± 12.4%, p = 0.22). RV volumes and EF were comparable between the two groups.

Conclusions: Whilst the pattern of midwall late enhancement seen in DCM with LGE-CMR is now well documented, very little is know of its clinical significance. Our finding shows a significant difference in the LV dimensions between the enhancement and non-enhancement DCM groups. Patients with DCM and midwall late enhancement had significantly larger LV volumes and mass than patients with no enhancement, reflecting adverse remodelling. This did not result however in poorer function. Potential explanations are that mid-wall fibrosis is a feature of more severe left ventricular disease or conversely that this reflects a differing underlying aetiology and pathologic process that results in greater LV volumes. Further work is required to understand the temporal onset of late enhancement and its correlation with clinical outcome.

129. Bradykinin B2 Receptor Does Not Mediate the Anti-remodeling Effects of the Angiotensin II Type 2 Receptor Following Myocardial Infarction

David C. Isbell,[1] Szilard Voros, MD,[1] Zequan Yang, MD, PhD,[2] Mark Conaway, PhD,[3] Joseph M. Dimaria, BA,[4] Stuart S. Berr, PhD,[4] Brent A. French, PhD,[4] Frederick H. Epstein, PhD,[4] Rene Jack Roy,[4] Robert M. Carey, MD,[1] Christopher M. Kramer, MD.[1] [1]*Medicine, University of Virginia, Charlottesville, VA, USA,* [2]*Biomedical Engineering, University of Virginia, Charlottesville, VA, USA,* [3]*Health Evaluation Sciences, University of Virginia, Charlottesville, VA, USA,* [4]*Radiology, University of Virginia, Charlottesville, VA, USA.*

Table 1.

		AT2OX	AT2OX/BKO	Wild type	P value
EDVI	Day 0	1.46 ± 0.10	1.81 ± 0.10	1.77 ± 0.05	< 0.01
	Day 28	2.56 ± 0.23	2.51 ± 0.08	3.72 ± 0.17	< 0.01
LVMI	Day 0	2.92 ± 0.19	3.01 ± 0.05	2.68 ± 0.07	< 0.02
	Day 28	3.66 ± 0.25	3.48 ± 0.07	3.79 ± 0.10	NS

Introduction: Left ventricular (LV) remodeling following large anterior myocardial infarction (MI) often results in congestive heart failure. Angiotensin II (Ang II) has been recognized as an important mediator of LV remodeling, largely through its promotion of vascoconstriction, cellular hypertrophy, and interstitial fibrosis. While Ang II type 1 receptors (AT2-1) promote remodeling, type 2 receptors (AT2-R), which are upregulated following myocardial injury, appear to attenuate this process as demonstrated in murine models of AT2-R overexpression (AT2-R OX) after anterior MI. Furthermore, recent evidence suggests that the cardio-protective effects of AT1-R antagonism are in fact facilitated through the AT2-R. Mechanisms underlying the benefit of AT2-R OX in the heart have yet to be fully elucidated. We hypothesized that the beneficial effects of AT2-R OX are mediated by the bradykinin B2 receptor (B2-R).

Methods: Twenty seven transgenic (TG) AT2-R OX mice and 11 wild type mice all on a C57Bl/6 background were studied. Thirteen of the 27 AT2-R OX were also knockout for B2-R (B2-R KO) after several generations of crossbreeding (AT2-R OX/B2-R KO). All were studied by Cardiac MRI at baseline (day 0) and days 1 and 28 post-MI induced by 1 hour of occlusion of the left anterior descending artery followed by reperfusion. Short axis images from apex to base were used to compare LV mass index (LVMI), end-diastolic and end-systolic volume indices (EDVI, ESVI), and ejection fraction (EF). Imaging was performed on a Varian 200/400 Inova 4.7 T MRI system with Magnex gradients and a custom-built 2.5 cm birdcage receiver coil. A 2D fast, low-angle shot (FLASH) sequence was used to obtain orthogonal long-axis images. Six to 8 short-axis slices were acquired, each 1 mm thick. Prior to imaging on day 1, 0.3 mmol/L Gd-DTPA was infused intraperitoneally for the purpose of infarct sizing. Echo time was 3.9 ms and the TR adjusted continuously to obtain 14–16 equally spaced phases during each cardiac cycle. A 20 degree flip angle was used in all but the contrast-enhanced images where a 60 degree flip angle was used to improve T1 weighting. Three signal averages were used resulting in an acquisition time of approximately 4 minutes per slice and total imaging time of 30 to 45 minutes per mouse. All images were quantitatively analyzed by a blinded observer using the ARGUS (Siemens Medical Systems) image analysis program.

Results: At baseline prior to MI, EDVI and ESVI were lower and EF and LVMI higher in AT2-R OX compared to AT2-R OX/B2-R KO and WT mice respectively (Table 1, Figures 1 and 2). Infarct size was similar between the three groups (41.4 ± 3.1 in AT2-R OX, 35.8 ± 1.6 in AT2-R OX/B2-R KO, and 40.9 ± 1.5% in WT, P = NS). When controlled for baseline differences, no differences were observed at day 28 between AT2-R OX and AT2-R OX/B2-R KO mice in any measured parameter; however, EDVI and

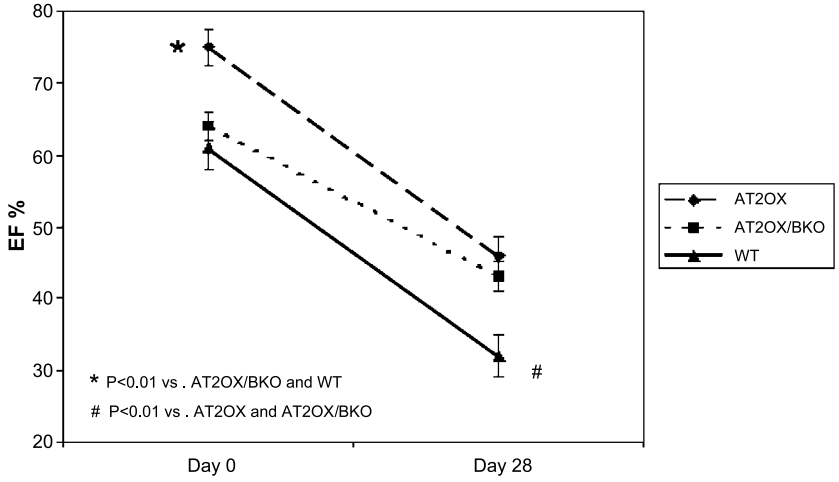

Figure 1.

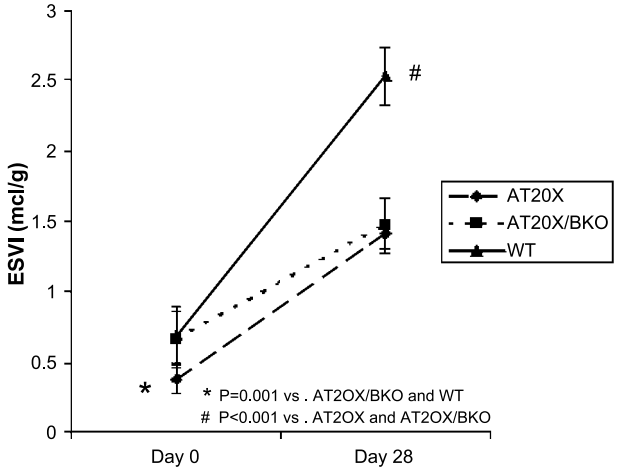

Figure 2.

ESVI were lower and EF higher in both transgenic goups than in WT mice (Table 1, Figures 1 and 2). LVMI did not differ between groups at day 28 (Table 1).

Conclusion: The bradykinin B2 receptor does appear to have a role in the smaller cavity size and supranormal function observed at baseline in AT2-R overexpressed animals. However, attenuation of post-infarct remodeling by overexpression of AT2-R is not directly mediated via the bradykinin B2 receptor.

130. CMR Demonstrates Reduced Post-infarct Left Ventricular Remodeling in Mice with iNOS Inhibition

Frederick H. Epstein, PhD,[1] Zequan Yang, MD, PhD,[2] R. Jack Roy,[3] Yaqin Xu, MD, PhD,[2] Stuart S. Berr, PhD,[1] Brent A. French, PhD.[2] [1]*Radiology and Biomedical Engineering, University of Virginia, Charlottesville, VA, USA,* [2]*Biomedical Engineering, University of Virginia, Charlottesville, VA, USA,* [3]*Radiology, University of Virginia, Charlottesville, VA, USA.*

Introduction: CMR of knockout mice has previously demonstrated the detrimental role of inducible nitric oxide synthase (iNOS) in post-infarct left ventricular (LV) remodeling (Gilson et al., 2003). Specifically, it was shown that iNOS knockout mice exhibit reduced end systolic volume (ESV) and wall thickness and increased ejection fraction (EF) at 7 and 28 days after a large anterior myocardial infarction (MI) compared to wild-type (WT) mice (Gilson et al., 2003).

Purpose: The purpose of the present study was to test the hypothesis that similar reductions in post-infarct LV remodeling could be pharmacologically conferred upon WT mouse hearts by selective iNOS inhibition.

Methods: Ten untreated WT mice and 5 WT mice treated with 1400W (Alexis Biochemicals, San Diego, CA), a highly selective iNOS inhibitor, were studied by CMR before and at 1, 7, and 28 days after experimental MI. MI was induced by a 1 hour occlusion of the LAD followed by reperfusion. 1400W was administered (1.25 mg/kg-hr) starting 1 hour post-reperfusion until day 14 post-MI using implanted Alzet micro osmotic pumps (Model 1002, Durect Corp, Cupertino CA). CMR studies included 1) localizer scanning, 2) 6–8 short-axis slices of black-blood cine imaging to cover the entire heart, and, 3) at day 1, 6–8 gadolinium-enhanced short-axis inversion recovery slices. Gd-DTPA was infused after cine imaging through an indwelling IP line. All imaging was performed on a 4.7 T scanner using custom-built birdcage or Litz RF coils. All images had a field of view of 2.56 cm, a matrix size of 128 × 128, and a zero-filled spatial resolution of 0.1 × 0.1 mm^2. Myocardial volumes, EF, and the circumferential extent of post-infarct wall thinning (wall thickness < 0.5 mm) were measured from the cine images. Day 1 infarct size was measured as percent of LV mass from the gadolinium-enhanced images.

Results: Gadolinium enhanced CMR demonstrated similar day 1 infarct sizes in treated and untreated WT mice (38.7 ± 9.4% vs. 36.8 ± 4.5%, p = NS). These infarct sizes were not different than those in the prior study (Gilson et al., 2003) using iNOS knockout mice (35.2 ± 4.2%, p = NS). Example mid-ventricular end-systolic images at day 28 are shown in Figure 1 illustrating the effect of iNOS. Specifically, LV cavity dilatation and circumferential wall thinning are seen in the untreated WT mouse (Figure 1A). In contrast, preservation of cavity size and confinement of wall thinning to the anterior segment are seen in the 1400W-treated mouse (Figure 1B). Figure 1C shows a day 28 iNOS knockout mouse from the prior study with an appearance similar to the

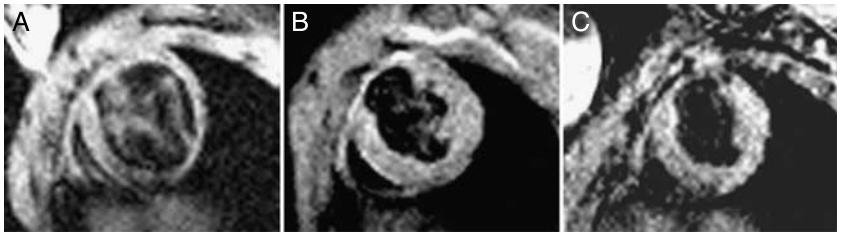

Figure 1. Mid-ventricular short axis images 28 days post-MI of (A) an untreated WT mouse, (B) a WT mouse treated with 1400W, and (C) an iNOS knockout mouse. Reduced cavity size and circumferential extent of wall thinning are evident in (B) and (C).

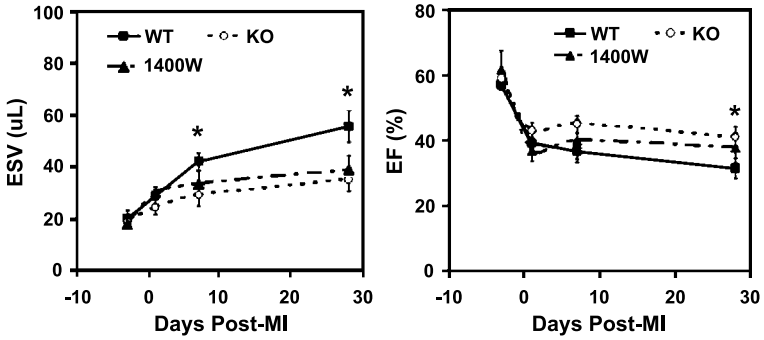

Figure 2. End systolic volume (ESV) and ejection fraction (EF) at baseline and during the first 28 days following MI. Inhibition of iNOS (1400W) reduces ESV and increases EF to a degree similar to that seen in iNOS knockout (KO) mice compared to untreated wild-type (WT) mice. *P < 0.05.

1400W treated mouse. Figure 2 shows ESV and EF data summarizing the present study and incorporating data from the previous iNOS knockout study. Specifically, iNOS inhibition led to reduced ESV at days 7 and 28 vs. untreated WT mice ($p < 0.05$) and increased EF at day 28 vs. untreated WT mice ($p < 0.05$). No significant differences in ESV or EF were found between treated WT and iNOS knockout mice. Reflecting reduced infarct expansion, the circumferential extent of wall thinning was reduced in treated vs. untreated mice in basal ($20 \pm 8°$ vs. $69 \pm 24°$, $p < 0.01$), mid-ventricular ($42 \pm 7°$ vs. $123 \pm 51°$, $p < 0.01$) and apical ($56 \pm 6°$ vs. $189 \pm 88°$, $p < 0.01$) slices.

Conclusions: Using CMR we have shown that selective inhibition of iNOS reduces post-infarct LV remodeling to an extent similar to previous findings in iNOS knockout mice. More generally, these results demonstrate the utility of serial CMR in mice for comprehensive genetic and pharmacological studies of the molecular mechanisms underlying the progression of ischemic heart disease.

REFERENCE

Gilson, W. D., Epstein, F. H., et al. (Oct. 28, 2003). Cardiac MRI reveals reduced left ventricular remodeling after myocardial infarction in iNOS knock-out mice. *Circulation* 108(17):3177. Suppl. S.

131. Prevalence of Cardiac Damage in Patients with Sarcoidosis: A Delayed Enhancement Cardiac MRI Study

Manesh R. Patel, MD, Peter J. Cawley, MD, John F. Heitner, MD, Igor Klem, MD, Michele Parker, M.Sc., Trip J. Meine, MD, Michael Elliott, MD, Robert Judd, PhD, Raymond J. Kim, MD. *Cardiology, Duke University, Durham, NC, USA.*

Background: In patients with sarcoidosis, cardiac involvement is clinically evident in < 5% of patients. However, cardiac fibrosis is found in 20–30% of patients at autopsy and likely plays a role in sudden death. Current diagnostic tools and myocardial biopsy are insensitive for detection of cardiac damage. Delayed-enhancement magnetic resonance imaging (DE-MRI) allows visualization of small amounts of scarring/fibrosis.

Methods: 70 consecutive patients with biopsy proven sarcoidosis but without clinically known cardiac involvement were prospectively identified from outpatient clinics. Each patient had a standard clinical evaluation, ECG, echocardiogram, and de-MRI performed. Patients with evidence of myocardial damage on DE-MRI had cardiac cath performed to exclude coronary artery disease. Blinded evaluation of DE-MRI was compared to Japanese Ministry of Health criteria for cardiac sarcoid. The pattern of damage was also identified, and logistic regression was used to identify clinical factors associated with cardiac damage.

Results: The mean age of the group was 46 years old, 63% were female, and 71% were black. The most common clinical sites were lung (94%) and skin (23%), with a mean of 9.4 years since diagnosis. The mean EF was 50% (± 4%). DE

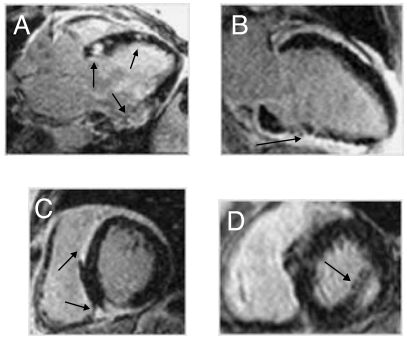

Figure 1. Delayed enhancement in sarcoid hearts. Delayed enhancement (DE) patterns in cardiac sarcoid: A shows mid-myocardial DE in the septum and transmural DE in basal lateral wall, B + C show epicardial and inferior septal DE in a patient

identified cardiac damage in 17 (24%) of patients, compared to 8 (14%) by the Japanese Ministry of Health criteria for cardiac sarcoid, p = 0.0005. A majority of the patients with DE 14/17 (88%) had a non-CAD pattern, mid-myocaridal and/or epicardial (Fig. 1).

Conclusion: DE-MRI identified cardiac damage in 24% of patients with sarcoidosis, a rate similar to autopsy studies and significantly higher than standard clinical criteria. The pattern of scarring on MRI was often found to be mid-myocardial and epicardial.

132. Myocardial Scarring in Beta Thalassemia Major by Late Gadolinium-Enhanced Magnetic Resonance Imaging: Correlation with Iron Overload and ECG-Changes

Alessia Pepe, MD,[1] Fortunato Sorrentino, MD,[2] Alessandro Pingitore, MD,[1] Vincenzo Positano, PhD,[1] Daniele De Marchi,[1] Paolo Rigano, MD,[3] Lorella Pitrolo, MD,[4] Liliana Cuccia, MD,[5] Massimo Midiri, MD,[6] Massimo Lombardi, MD.[1] [1]*MRI Lab, CNR, Clinical Physiology Institute, Pisa, Italy,* [2]*Department of Radiology, University of Palermo, Palermo, Italy,* [3]*Department of Haematology, V. Cervello Hospital, Palermo, Italy,* [4]*Department of Pediatrics, Villa Sofia Hospital, Palermo, Italy,* [5]*Department of Pediatrics, G. Di Cristina ARNAS Hospital, Palermo, Italy,* [6]*Department of Haematology, University of Palermo, Palermo, Italy.*

Introduction: In beta thalassemia major (TM) cardiac disorders are the most common cause of death. Myocardial fibrosis has been shown in autopsy.

Purpose: Aim of this study was 1) to determine in patients (pts) with beta TM whether myocardial scarring can be detected by late gadolinium-enhanced Magnetic Resonance Imaging (MRI); 2) to correlate the presence of myocardial scarring with iron overload and electrocardiographic changes.

Methods: 38 beta TM pts (12 male; 26 ± 8 yy) were enrolled. MRI studies were performed on a 1.5 T scanner (GE, USA). Myocardial fibrosis was determined by late gadolinium-enhanced MRI. Images were evaluated by a visual assessment of two independent observers and by a semi-automatic post-processing software tool for objective pixel quantification. Iron overload was determined by a gradient T2-star (T2*) multi-echo sequence on three parallel short axis views (basal-medium-apical) of left ventricle. Cine dynamic images in short axis of the left ventricle were also obtained to evaluate regional function by qualitative analysis. Twelve lead Electrocardiogram (ECG) was performed in 30 patients before the MRI study.

Results: Scarring was present in 15 patients (40%), contrast to noise ratio resulted 1.8. The scarring was predominantly patchy. Out of the 15 pts with scar, 11 (73%) had two or more foci of scarring. Out of the 36 areas of scarring, 19 (53%) involved the interventricular septum. Scarring did not followed coronary distribution. No asynergic segments were detectable. Myocardial fibrosis did not significantly affect the T2* value (fibrosis 27 ± 10 ms vs. no-fibrosis 26 ± 12, p = 0.2). A significant correlation was found between the presence of myocardial scarring and ECG changes (atrio-ventricular block, right bundle-branch block, ST segment depression, T wave inversion, abnormal Q-waves or decreased R waves) (chi-square 8,3; p = 0.007). The sensitivity, specificity, negative predictive value and positive predictive value of ECG in detecting myocardial scarring were 90%, 63%, 92% and 58%, respectively.

Conclusions: Myocardial scarring is detectable in a significant percentage of patients with beta TM. Myocardial scarring did not correlate with iron overload. ECG changes showed a significant accuracy to predict myocardial scarring.

133. Baseline Findings of a CMR Driven Randomized Controlled Trial of Iron Chelation Therapy in Thalassaemia Major

Mark A. Tanner, MBBS,[1] Mark A. Westwood, MBBS,[1] Renzo Galanello,[2] Dudley J. Pennell, MD.[1] [1]*Cardiac MR Unit, Royal Brompton Hospital, London, UK,* [2]*Haematology Department, Ospedale Microcitemico, Cagliari, Sardinia, Italy.*

Introduction: Beta thalassaemia major (TM) is a hereditary anaemia affecting 60,000 births worldwide each year. Survival is dependent upon lifelong blood transfusions resulting in iron overload. Cardiac siderosis can result in a progressive dilated cardiomyopathy which accounts for over 70% of all deaths in TM. Yet this cardiomyopathy is both treatable and potentially reversible. Conventional treatment with the parenteral iron chelator desferrioxamine (DSF) improves morbidity and mortality but prognosis remains poor and it has been reported that 66% of treated patients have cardiac iron loading. More recently, the oral iron chelator deferiprone (L1) has been demonstrated to remove cardiac iron and it has been proposed that in combination with DSF it may have an additive or synergistic effect. The validated CMR T2* technique allows rapid, non-invasive, and reproducible quantification of tissue iron and is therefore well suited to assess the response to new therapies which may improve outcome in TM.

Purpose: To report the baseline data from a randomised controlled trial comparing DSF and placebo (monotherapy) with DSF and the oral chelator, L1 (combination therapy), which has cardiac T2* as the primary outcome measure.

Methods: Mobile CMR scanner (1.5 T Siemens Sonata) was transported to Cagliari, Italy. The cardiac T2* was assessed in 167 patients with TM aged 18–42 (30 ± 5.3 years). Those patients with cardiac iron loading (T2* < 20 ms) were

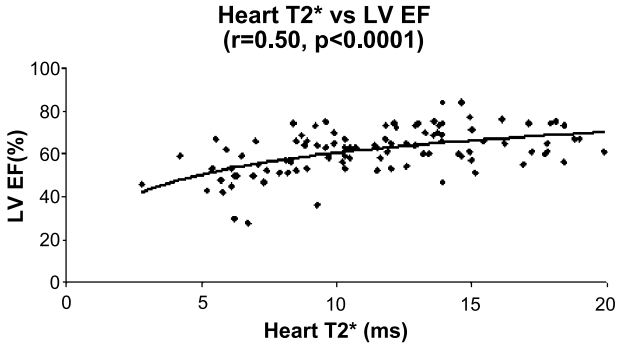

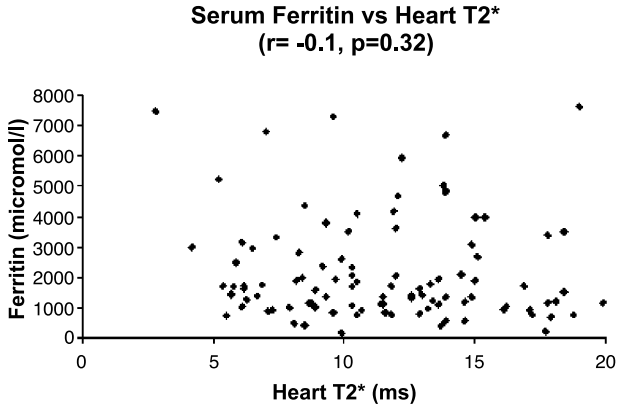

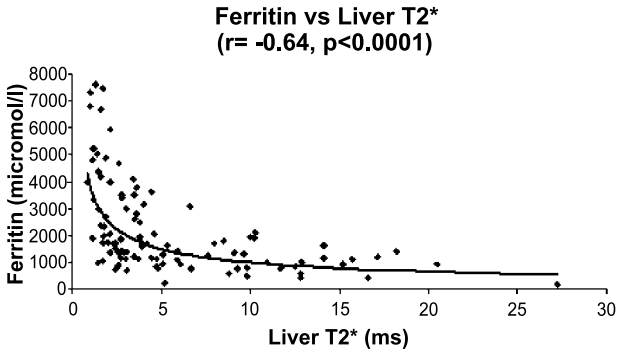

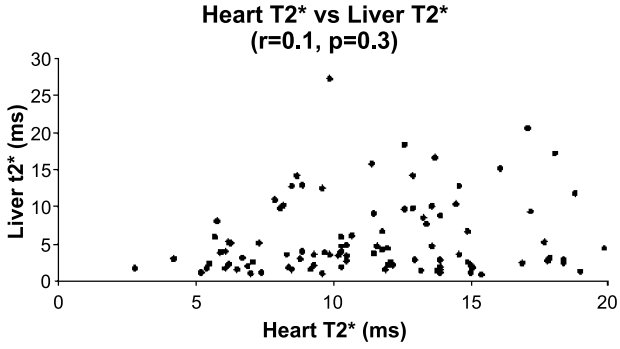

invited back for further CMR assessment including estimation of LV/RV volumes, and liver T2*. 65 patients who met the trial inclusion criteria were randomized (double blind) to receive either DSF and placebo or DSF and L1. Follow up assessments will take place at 6 and 12 months.

Table 1. Proportion of patients with LV dysfunction (EF < 56%)

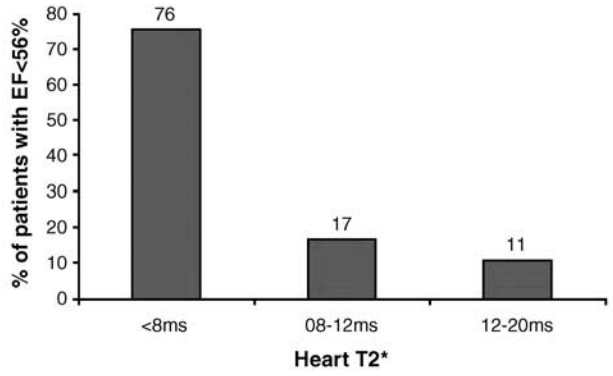

Results: Of the 167 subjects screened, 65% demonstrated cardiac iron loading (T2* < 20 ms), of whom 22 subjects had severe cardiac iron loading (T2* < 8 ms). There was a highly significant relationship between cardiac T2* and LVEF ($r = 0.5$, $p < 0.0001$). The risk of cardiac dysfunction (Table 1) was highest in subjects with severe cardiac iron loading [OR = 31.25 (7.4–125)]. Serum ferritin and liver T2* were negatively correlated ($r = -0.64$, $p < 0.0001$), but there was no significant relationship between ferritin and cardiac T2* ($r = -0.1$, $p = 0.32$). There was no significant relationship between heart and liver T2* ($r = 0.1$, $p = 0.3$).

Conclusions: 65% of the screened thalassaemic population demonstrated cardiac iron loading. This figure is comparable to prior reports and highlights the need for improved chelation regimes. The lack of correlation between serum ferritin and cardiac iron loading re-iterates the deficiency in using serum ferritin as a guide to cardiac management. However the relationship between T2*, LVEF and attendant risk of cardiac dysfunction is demonstrated clearly. These findings lend further support for the use of the T2* technique in the assessment of tissue iron loading and risk stratification. Through the application of this highly reproducible technique it is hoped that this trial could lead to the first randomized and placebo controlled evidence that myocardial iron can be reduced more effectively with combination treatment than by desferrioxamine alone. This will have major implications for treatment for thalassaemia patients in the future.

134. Improved R2* Measurements in Myocardial Iron Overload

Nilesh R. Ghugre, MS,[1] Cathleen M. Enriquez, BS,[1] Thomas D. Coates, MD,[2] Marvin D. Nelson, Jr., MD,[3] John C. Wood, MD, PhD.[1] [1]*Division of Cardiology, Childrens Hospital Los Angeles, Los Angeles, CA, USA,* [2]*Department of Hematology, Childrens Hospital Los Angeles, Los Angeles, CA, USA,* [3]*Department of Radiology, Childrens Hospital Los Angeles, Los Angeles, CA, USA.*

Introduction: Iron-induced arrhythmia and heart failure remain the leading cause of death in transfusion-dependent anemias. Conventional cardiac monitoring, including physical exam, ECG and echocardiogram, fail to predict iron induced cardiac disease prior to the onset of clinical symptoms. The MRI relaxation parameter R2* (1/T2*) lengthens in the presence of tissue iron and has demonstrated considerable promise for preclinical detection of cardiac iron. Unfortunately, R2* measurements can be confounded by magnetic susceptibility near the boundaries with cardiac veins, liver and lungs and by high spatial variation of cardiac iron deposition, as has been demonstrated in autopsy studies.

Purpose: The purpose of the study was to systematically evaluate R2* variability across the myocardium in sickle cell and thalassemia patients. The study would help indicate 1) regions of the heart most appropriate for R2* measurement 2) regions to be avoided due to neighboring magnetic susceptibility effects 3) appropriate R2* relaxation model, based on myocardial iron distribution.

Methods: We studied the spatial heterogeneity of cardiac R2* in 17 patients with transfusion-dependent sickle-cell disease (SCD) and 48 patients with thalassemia major (TM). Myocardial R2* was assessed in a single mid-papillary slice using a gated segmented gradient echo sequence and echo times of 2, 3, 4, 6, 9, 12, 15 and 18 ms, with one echo time per breath-hold. Image registration was performed using affine-transformation and mutual information criteria. Pixel-wise and region of interest (ROI) based R2* measurements were performed by fitting a monoexponential function (with and without offset correction). Average R2* calculated from pixel-wise maps were compared to R2* values estimated from ROI approach by Bland-Altman analysis. Circumferential and radial myocardial R2* were plotted for SCD, TM (T2* 20 ms) in order to observe nearby magnetic susceptibility effects. Based on patient data characteristics, R2* dependent synthetic maps of the interventricular septum were generated and processed to validate signal decay models.

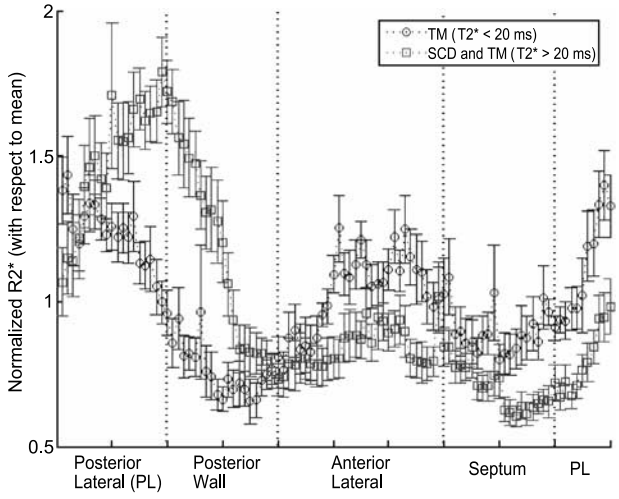

Figure 1. Myocardial circumferential variation.

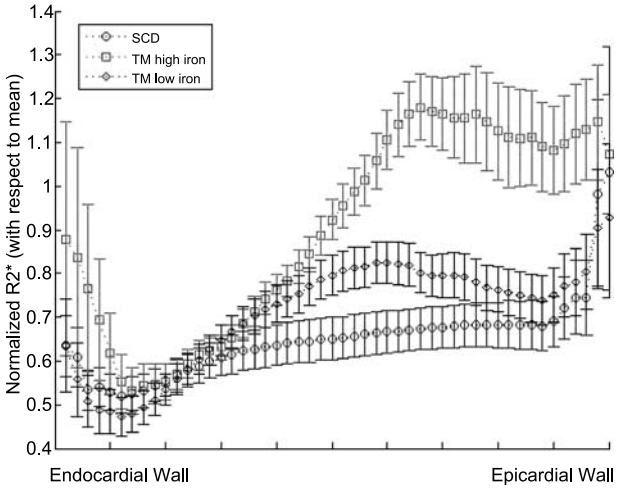

Figure 2. Septum radial variation.

Results: Mean cardiac R2* within septum was [24.94 Â ± 4.82] in SCD and [76.09 Â ± 80.13] in TM. R2* values were 70% higher in the posterior and anterior lateral regions relative to the interventricular septum in unloaded patients (T2*> 20) (Figure 1), suggesting susceptibility artifacts from adjacent cardiac veins, lung, and liver. Similar circumferential variation was also observed in iron-loaded patients (T2* < 20), however, septal R2* values were within 10% of the global mean. An endocardial to epicardial gradient in R2* values was noted at high R2*, consistent with pathologic studies (Figure 2). Pixel-wise R2* calculation and region of interest techniques were consistent with one another ($r = 0.99$, $p < 0.0001$) if offset correction was applied but disparate otherwise. Signal decay curves from patient examinations flattened at long echo time indicating the presence of a second long T2 component (above the predicted noise bias). Synthetic R2* maps, generated from these data, clearly demonstrate that monoexponential models badly underestimate true R2* values unless a offset or second exponential is included in the R2* fit.

Conclusion: Myocardial R2* mapping demonstrates that nonspecific R2* artifacts are large but can be minimized by restricting analysis to the interventricular septum. Circumferential R2* changes observed in iron-loaded hearts may represent true patterns of iron deposition or artificial R2* fluctuations imposed by cardiac/visceral geometric interactions. Postmortem analyses or R2 imaging may be helpful in addressing this question. The R2* gradient from endocardium to epicardium is consistent with patterns of iron deposition described in prior pathologic studies. In summary, clinical R2* measurements should be restricted to the interventricular septum. Region-of-interest analysis techniques are as accurate as pixel-wise mapping methods, however offset-correction or biexponential curve fitting is essential for accurate R2* measurements.

135. Impaired Aortic Properties in Patients with Chronic Heart Failure as Assessed by Cardiovascular Magnetic Resonance

Nikolay P. Nikitin, MD, PhD, Poay Huan Loh, MRCP, Ramesh de Silva, MRCP, Justin Ghosh, MRCP, Elena I. Lukaschuk, MSc, Andrew L. Clark, MA, MD, FRCP, John G. F. Cleland, MD, FRCP, FACC. *Academic Unit of Cardiology, University of Hull, Kingston Upon Hull, UK.*

Aortic properties change with age and in cardiac disease. In patients with chronic heart failure (CHF) it may contribute to patients' symptoms. In this study we used cardiovascular magnetic resonance (CMR) to assess the size and distensibility of the ascending and descending aorta in CHF patients with impaired and preserved left ventricular (LV) systolic function and compared it with younger and older normal subjects.

Methods: The study population included 209 patients with signs and symptoms of compensated CHF (NYHA functional class II or III). One hundred and forty patients (aged 69 ± 10 years) who had LV systolic dysfunction (LV ejection fraction < 45%) formed Group I, and 69 patients (aged 69 ± 11 years) with preserved LV systolic function (LV ejection fraction ≥ 45%) formed Group II. The control population included 14 older volunteers aged 66 ± 14 years (Group III) and 21 younger subjects aged 32 ± 4 years (Group IV) with no known cardiac disease. The subjects underwent cine CMR on a 1.5 T Signa CV/i GE Medical Systems scanner to characterise LV function and to assess cross-sectional areas and distensibility of the ascending aorta (AA) and the descending aorta (DA).

Results: There were no differences in age between groups I, II and III. Systolic blood pressure was significantly ($p < 0.05$) higher in group II (142 ± 30 mm Hg) and Group III (144 ± 29 mm Hg) as compared with Group IV (120 ± 8 mm Hg). Systolic blood pressure in Group I was 129 ± 22 mm Hg. Diastolic blood pressures were not significantly different between the groups (77 ± 13, 81 ± 17, 82 ± 13 and 75 ± 8 mm Hg respectively). The distensibility index (DI) of the AA and the DA was closely correlated with age ($r = -0.67$ and -0.68 respectively) in the entire study group. Maximal and minimal cross-sectional areas of the AA and the DA and corresponding DI indices in the 4 study groups are shown in Table 1. Aortic size increased and aortic distensibility declined with age. CHF patients (Groups I and II) demonstrated aortic dilatation and increased stiffness compared to both younger and older groups of normal volunteers. Aortic distensibility was slightly less reduced in the group of patients with preserved LV systolic function than in the group of patients with impaired LV function but this did not reach statistical significance.

Conclusions: Patients with CHF show impaired elastic properties of the ascending and the descending aorta. Diminished aortic distensibility is present in patients with both impaired and preserved LV systolic function.

136. Regional Differences in Systolic and Diastolic Function in Arrhythmogenic Right Ventricular Dysplasia/Cardiomyopathy Using Magnetic Resonance Imaging

Chandra S. Bomma, MD,[1] Darshan Dalal, MD, MPH,[1] Harikrishna Tandri, MD, MRCP,[1] Kalpana R. Prakasa, MD,[1] Khurram Nasir, MD, MPH,[1] Ariel Roguin, MD,[1] Crystal Tichnell, MGC,[1] Cynthia James, PhD,[1] Joao A.C. Lima, MD, MBA,[1] Hugh Calkins, MD,[1] David A. Bluemke, MD, PhD.[2]
[1]*Division of Cardiology (Department of Medicine), Johns Hopkins University School of Medicine, Baltimore, MD, USA,* [2]*Department of Radiology, Johns Hopkins University School of Medicine, Baltimore, MD, USA.*

Introduction: Arrhythmogenic right ventricular dysplasia/cardiomyopathy (ARVD/C) is characterized by abnormalities in right ventricular (RV) structure and function, as well as the development of ventricular arrhythmias. Histological evidence of left ventricle (LV) disease on autopsy has been reported to be as high as 70%. Early ARVD/C is a regional disorder and regional abnormalities of RV function have not been quantitatively evaluated in ARVD/C using MRI.

Table 1.

	AA area max (cm^2)	AA area min (cm^2)	DA area max (cm^2)	DA area min (cm^2)	DI (AA) (10^{-3} mm Hg^{-1})	DI (DA) (10^{-3} mm Hg^{-1})
Group I	8.61 ± 2.07†,‡	8.07 ± 1.99†,‡	5.16 ± 1.16‡	4.81 ± 1.11†,‡	1.36 ± 0.77†,‡	1.52 ± 0.8†,‡
Group II	8.91 ± 2.45†,‡	8.28 ± 2.36†,‡	5.21 ± 1.48‡	4.80 ± 1.40†,‡	1.52 ± 1.07†,‡	1.66 ± 1.17†,‡
Group III	7.10 ± 2.07$^{*,\#\ddagger}$	6.44 ± 1.95$^{*,\#,\ddagger}$	4.43 ± 1.12‡	4.00 ± 1.11$^{*,\#,\ddagger}$	2.15 ± 1.01‡	2.51 ± 1.4‡
Group IV	5.34 ± 1.15$^{*,\#,\dagger}$	4.35 ± 0.94$^{*,\#,\dagger}$	3.37 ± 1.03$^{*,\#,\dagger}$	2.72 ± 0.86$^{*,\#,\dagger}$	5.43 ± 1.97$^{*,\#,\dagger}$	5.55 ± 1.55$^{*,\#,\dagger}$

$^{\dagger}p < 0.05$ vs. group 3.
$^{\ddagger}p < 0.05$ vs. group 4.
$^{*}p < 0.05$ vs. group 1.
$^{\#}p < 0.05$ vs. group 2.

Purpose: The aim of this study was to quantitatively evaluate right and left global and regional function in patients with ARVD/C compared to control subjects using cine MRI.

Methods: The study included 14 patients with ARVD/C and 18 age-matched normal subjects. Cine gradient echo sequences were acquired using steady state free precession (SSFP) imaging. Right and left ventricle volumes were determined by contouring the endocardium on each slice, summing the slices and multiplying by the slice thickness (Simpson's rule) and interslice gap. Peak filling rates (PFR) and peak ejection rates (PER) of the RV and LV were assessed globally and regionally at basal, mid cavity, and apical regions.

Results: All global functional indices (PFR, PER and EF) of the RV were markedly reduced in ARVD/C patients compared to normal subjects. In the presence of normal systolic function, global LV diastolic dysfunction as evidenced by marked reduction in PFR was observed in ARVD/C patients vs. normal subjects [320 ml (264, 368) vs. 411 ml (359, 447) P = 0.001]. There was significant RV systolic and diastolic dysfunction at the basal region in the ARVD/C patients compared with normal subjects, with marked reduction in PER ($P < 0.001$) and PFR ($P < 0.001$). Regional diastolic dysfunction was present at the basal region of LV in ARVD/C patients, with reduced PFR [92 ml (85, 135) vs. 119 ml (98, 133) ARVD/C patients vs. controls respectively, P = 0.035] (Fig. 1).

Conclusions: The RV of patients with ARVD/C has global and regional systolic as well as diastolic dysfunction. Regional RV dysfunction is most severe at the RV base. Finally, LV diastolic dysfunction may also be present, in concordance with established reports of histological involvement of the LV in ARVD/C.

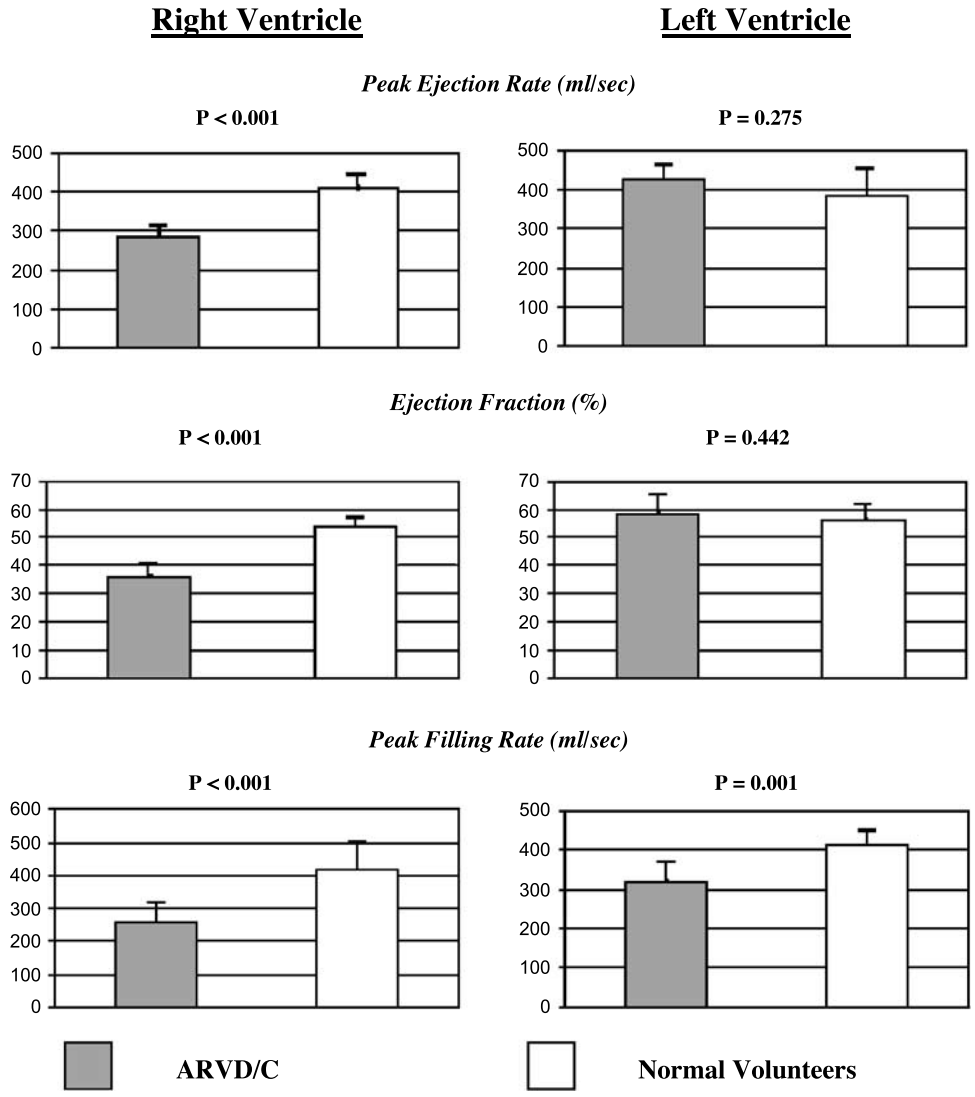

Figure 1. Global functional indices in ARVD/C patients and normal subjects.

137. CMR Follow Up of Patients with ARVC

Sven Plein, Deoraj Y. Zamvar, MD, Mohan U. Sivananthan, MD. *Cardiac MRI Unit, Leeds General Infirmary, Leeds, UK.*

Introduction: Cardiac Magnetic Resonance (CMR) Imaging can detect morphological and functional abnormalities of the right ventricle (RV) in patients with Arrhythmogenic Right Ventricular Cardiomyopathy (ARVC). ARVC is a progressive disease, but MRI follow up of patients with ARVC has not yet been reported.

Purpose: To assess morphologiacl and functional changes on CMR imaging on serial follow up of patients with ARVC.

Methods: 14 patients (mean age 42 years, 9 male) with ARVC fulfilling the Task Force of the Working Group on Cardiomyopathies were studied. All underwent CMR imaging annually for between 2 and 6 years. The MRI protocol consisted of axial T1 and T2 weighted and fat-suppressed spin echo images as well as axial gradient echo cines, axial cines with myocardial tissue tagging and velocity-encoded imaging of tricuspid flow. All data were analysed in a blinded fashion by two experienced observers. Morphologically, five criteria were evaluated: the presence of intramyocardial fat, wall thinning, aneurysms or outpouchings, dilatation and dyskinesia. Functional analysis included the calculation of RV volumes and ejection fraction and E/A ratios of tricuspid flow. Comparison was made between the first and the last MRI scan for each patient.

Results: One patient died during follow-up, two patients underwent implantation of a cardioverter-defibrillator. Mean follow-up was 41 months. On morphological criteria, 4 patients showed clear signs of deterioration between the first and the last MRI study. On the first study, patients showed a mean of 2.6 morphological abnormalities (7 fat, 8 thinning, 6 outpouching, 7 dilatation and 6 dyskinesia), increasing to a mean of 3.1 abnormalities on the last follow up study. In one patient an abnormal contraction of the left ventricle was reported. On functional analysis, EF was lower on follow-up in 9 patients. The mean EF reduced from 54% to 49% ($p < 0.05$). E/A ratios of tricuspid flow also reduced, but not significantly.

Conclusion: Serial CMR imaging can demonstrate progression of morphological and functional abnormalities in patients with ARVC.

138. Combined Contrast-Enhanced and T2-Weighted Cardiovascular Magnetic Resonance Accurately Detects Acute Myocarditis

Hassan Abdel-Aty,[1] Philipp Boyé,[1] Anja Zagrosek,[1] Ralf Wassmuth,[1] Andreas Kumar,[1] Daniel Messroghli,[1] Petra Bock,[1] Rainer Dietz,[1] Matthias G. Friedrich,[2] Jeanette Schulz-Menger.[1] [1]*Cardiology, Franz-Volhard-Klinik, Charité Campus Buch, Universitätsmedizin Berlin, Berlin, Germany,* [2]*Department of Cardiac Sciences, University of Calgary, Foothills Hospital, Calgary, AB, Canada.*

Background: Acute myocarditis is difficult to diagnose. CMR provides various means to visualize inflammatory changes of the myocardium. A comprehensive CMR approach that combines different pulse sequences and uses clear-cut diagnostic criteria would be desirable. We sought to identify the diagnostic performance of contrast-enhanced and T2-weighted cardiovascular magnetic resonance (CMR) in detecting acute myocarditis.

Methods: We investigated 25 patients hospitalized for acute myocarditis as defined by clinical criteria, ECG changes and serum markers of acute myocardial injury in the absence of significant coronary artery disease as defined by coronary angiography (18 males, 44 ± 17 years, time after myocarditis onset = 6 ± 4 days) and 23 healthy volunteers (13 males, 29 ± 10 years). CMR studies included the following sequences: 1) T2-weighted triple inversion recovery, 2) T1-weighted spin echo before and shortly after contrast injection and 3) Inversion recovery-gradient echo 10 minutes after contrast injection. Qualitative and quantitative image analysis was performed for: 1) Focal and global (in relation to skeletal muscle) T2 signal intensity, 2) Global myocardial relative enhancement (GRE) and 3) Areas of late gadolinium enhancement (LGE).

Results: Global myocardial T2 SI was significantly higher in patients than in volunteers (2.3 ± 0.4 vs. 1.7 ± 0.4; $p < 0.0001$). A cutoff value of 1.9 has a sensitivity of 84% and a specificity of 74% to identify the disease (area under the curve = 0.884, $p < 0.0001$). Moderate (Spearman correlation coefficient = 0.42) significant correlation was found between global T2 and troponin levels ($p = 0.035$). 8 patients had focal areas of high T2 signal as well and these patients had significantly higher peak CK levels (781.6 ± 695.4 vs. 254.5 ± 173.1; $p = 0.014$). GRE was significantly higher in patients compared to volunteers (6.8 ± 4.0 vs. 3.7 ± 2.3; $p < 0.001$). A cutoff value of 4.0 has a sensitivity of 80% and a specificity of 73% to identify myocarditis (area under the curve = 0.773, $p < 0.001$). The sensitivity and specificity of LGE were 44% and 100% respectively. LGE was always located in the epicardial or mid portion of the ventricular wall but never within the sub-endocardium. When data from the three sequences were combined together (considering cutoff values of 1.9 and 4.0 for T2 and GRE together with the presence of LGE), the sensitivity rose to 100%.

Conclusion: Combining the high sensitivity of T2-weighted and global (early) myocardial enhancement with the excellent specificity of focal (late) gadolinium enhancement provides an imaging approach with excellent overall diagnostic performance to detect acute myocarditis.

139. Influencing Factors Measuring Left Ventricular Function and Morphology by MRI-Is MRI the Golden Standard?

Henning Steen,[1] Dave Bluemke, MD, PhD,[2] Ellen Flynn,[3] Joao A. C. Lima, MD.[4] [1]*Cardiology, Universität Heidelberg,*

Heidelberg, Germany, [2]Radiology, Johns Hopkins, Baltimore, MD, USA, [3]Cardiology, Johns Hopkins, Baltimore, MD, USA, [4]Cardiology, Johns Hopkins, Baltimore, MD, USA.

Introduction: Cardiovascular reference parameters like LV mass (LVM), end-diastolic-/systolic volume (ED-/ESV) are strong predictors of cardiovascular morbidity and mortality. Accurate measurement is crucial for applied imaging techniques wherein MRI is considered golden standard.

Purpose: We hypothesized that although MRI-intra-observer variability is excellent, different contouring techniques lead to substantial measurement errors.

Methods: Using two different contouring techniques (CT-I = including papillary muscles and epicardial chemical shift artifact, CT-II = excluding aforementioned structures; Fig. 1) LV-short axes state-of-the-art MR-images (SSFP-sequence) of 10 Diabetes-II patients from an ongoing trial were randomly contoured by one observer for EDV-, ESV-, EF-, LVM measurement.

Intra-observer variability was analyzed using Pearson's Correlation Coefficient.

Results: For CT-1, ESV was significantly higher (66.37 ± 20.81 vs. 47.68 ± 19 ml, $p = 0.03$) and EF (54.61 ± 5.81 vs. 62.9 ± 7.7%), EDM (109.05 ± 16.44 vs. 130.53 ± 20.26 g) were significantly lower ($p < 0.01$) when compared to CT-2. EDV was insignificantly elevated (144.49 ± 35.4 vs. 124.52 ± 31.93). Intra-observer variability was low (2%).

Conclusions: According to its low intra-observer variability MRI is considered golden standard of cardiac function and morphology, however different contouring techniques potentially lead to considerable measurement errors on cardiovascular parameters especially for LVM but less pronounced for LV volumes.

140. MRI to Predict the Presence of Q Waves on the ECG

Theodorus A. M. Kaandorp,[1] Jeroen J. Bax, MD,[2] Hildo J. Lamb, MD,[1] Eric E. Viergever, MD,[2] Eric Boersma,[3] Don Poldermans, MD,[3] Ernst van der Wall, MD,[2] Albert de Roos, MD.[1] [1]*Radiology, Leiden University Medical Center, Leiden, The Netherlands,* [2]*Cardiology, Leiden University Medical Center, Leiden, The Netherlands,* [3]*Cardiology, Erasmus MC, Rotterdam, The Netherlands.*

Introduction: Studies have demonstrated that Q wave infarctions frequently have non-transmural scar formation, whereas non-Q wave infarctions may have transmural scars. The precise pathophysiological substrate underlying the Q waves remains unclear. MRI is the preferred technique to evaluate patients with infarction, since information can be

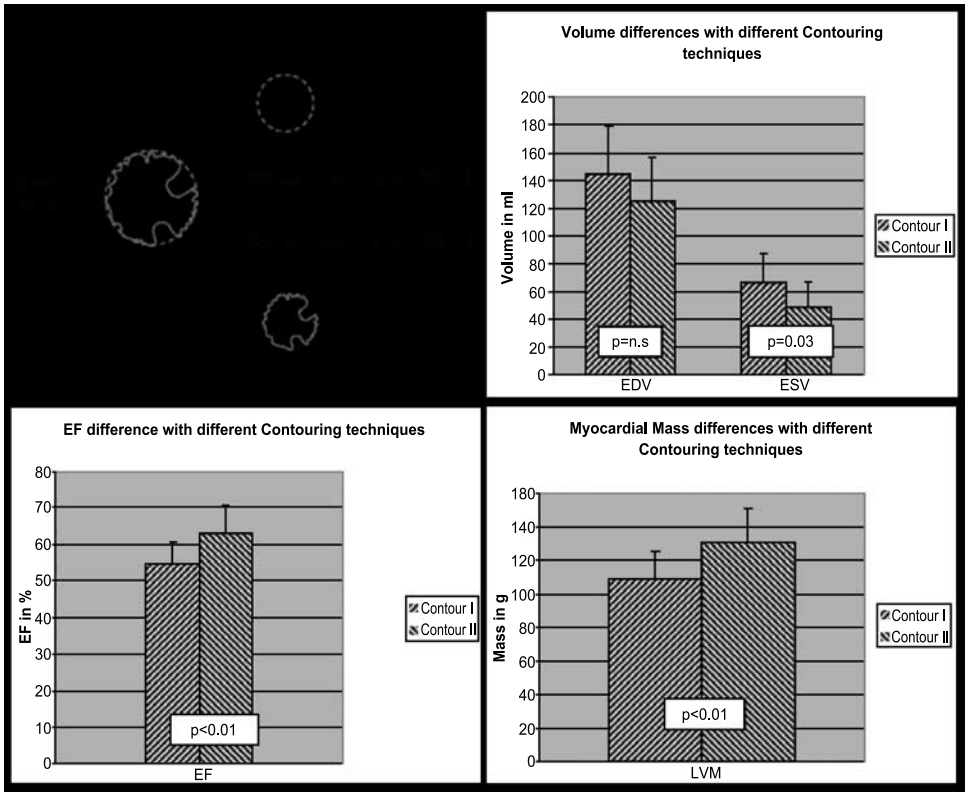

Figure 1.

obtained on function, contractile reserve (viability) and scar tissue.

Purpose: To predict the presence of Q waves on the ECG using MRI.

Methods: Consecutive patients (n = 69) with coronary artery disease and history of myocardial infarction underwent MRI; the protocol included resting MRI, low-dose dobutamine MRI and contrast-enhanced MRI. Parameters included: LVEF, LV volumes, end-diastolic wall thickness and contractile reserve in the infarct region, transmurality and spatial extent of scar tissue, total scar score and the quantified percentage of scar tissue of the LV. The MRI data were related to the presence/absence of Q waves on the ECG.

Results: Q waves were present in 39 (57%) patients. Univariate analysis identified the transmurality, the spatial extent, the total scar score and the quantified percentage scar tissue as predictors of Q waves. Multivariate analysis demonstrated that the quantified percentage scar tissue was the single best predictor. A cutoff value of 17% infarcted tissue of the LV yielded a sensitivity and specificity of 90% to predict the presence/absence of Q waves. When the quantified percentage scar tissue was removed from the model, the spatial extent of infarction was the best predictor.

Conclusions: Q waves on the ECG are best predicted by the quantified percentage scar tissue on contrast-enhanced MRI.

141. Contrast Enhanced Magnetic Resonance Imaging of Acute Myocardial Infarction: Optimization of Image Contrast

Kai-Uwe Waltering, MD,[1] Thomas Schlosser, MD,[1] Katja Gaida,[2] Oliver Bruder, MD,[3] Peter Hunold, MD,[1] Jörg Barkhausen, MD.[1] [1]*Department of Diagnostic and Interventional Radiology, University Hospital Essen, Essen, Germany,* [2]*Department of Radiology, Elisabeth Hospital Essen, Essen, Germany,* [3]*Department of Cardiology and Angiology, Elisabeth Hospital Essen, Essen, Germany.*

Introduction: Contrast-enhanced cardiac MR imaging (ceMRI) is well established for the assessment of myocardial viability and allows discriminating between reversible and irreversible ischemic injury. Image quality and the contrast between normal and infarcted myocardium depend on the tissue T1-times and the correct setting of the inversion time (TI). TI has to be adjusted individually and should be set to null the signal intensity of normal myocardium, which improves the contrast between viable and nonviable myocardium. The optimum TI depends on the T1 values of normal and infarcted myocardium. However, the time course of myocardial T1 times after contrast injection has not been investigated in patients with acute myocardial infarction yet.

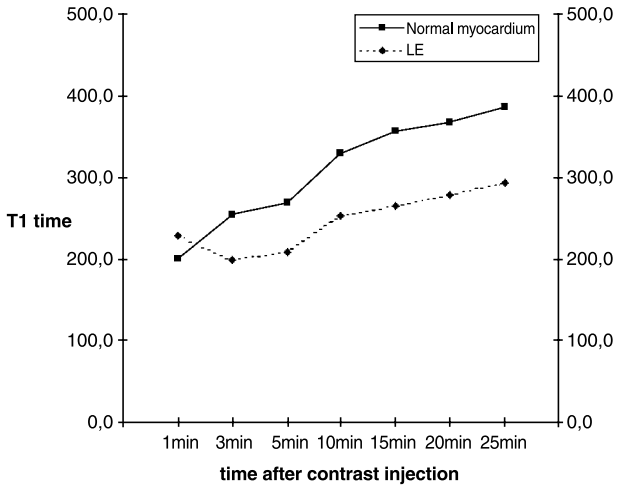

Figure 1. Normal myocardium and LE.

Purpose: Aim of our study was to measure T1 values of normal and infarcted myocardium after contrast injection using IR-SSFP sequences.

Methods: 38 patients (30 male, 8 female, mean age 56.0 ± 13.0 years) with first acute ST-elevation myocardial infarction (MI) were enrolled into the study. MR imaging was performed on a 1.5 T MR-system within 2.9 ± 1.9 days after MI. T1 values of non-infarcted myocardium and infarcted myocardium were estimated using an inversion recovery steady state free precession sequence (TR 2.5 ms, TE 1.1 ms, FA 50°) with incrementally increased inversion times acquired during a single breath-hold. Long axis views covering the area of the infarction were collected before and 1, 3, 5, 10, 15, 20 and 25 minutes after Gadodiamide injection (0.2 mmol/kg BW, Omniscan, Amersham). T1 values were obtained using the following equation: $T1 = TI_{(min)}/\ln 2$, where $TI_{(min)}$ is the inversion time of the image with the minimum signal intensity of the tissue. T1 values were calculated for normal myocardium, the area of late enhancement (LE) and the no-reflow zone.

Results: The T1 times of normal myocardium and LE showed no significant differences within the first three minutes after contrast injection. Thereafter, the area of LE showed significant shorter T1 values with a maximum difference 15 minutes after contrast (LE: 264 ± 38 ms; normal myocardium: 354 ± 33 ms); Fig. 1. The maximum difference between the no-reflow zone and the surrounding tissues was found immediately after contrast administration (no-reflow T1 = 347 ± 167 ms, normal myocardium T1 = 206 ± 41 ms, LE T1 = 211 ± 86 ms); Fig. 2.

Conclusions: Our data show, that the highest contrast between the no-reflow zone and the surrounding tissue can be obtained immediately after contrast administration, whereas the maximium contrast between normal and infarcted myocardium requires a delay of 15 minutes. Therefore, in patients with a acute myocardial infarction measurements of

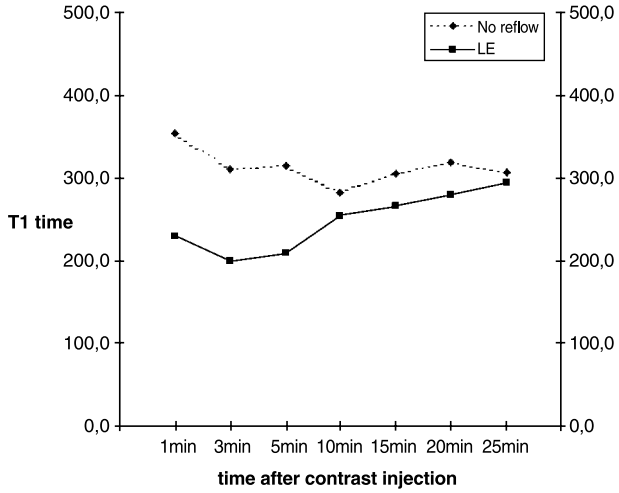

Figure 2. No reflow and LE.

the no-reflow zone should be performed immediately after contrast injection, whereas the area of LE should be assessed about 15 minutes after contrast injection.

142. Resolution of Microvascular Obstruction Occurs Within Days of an Acute Myocardial Infarction

Timothy S.E. Albert, MD, Manesh R. Patel, MD, Burkhard Sievers, MD, Michele A. Parker, MS, Michael D. Elliott, MD, Raymond J. Kim, MD, Robert M. Judd, PhD. *Medicine, Duke University Medical Center, Durham, NC, USA.*

Introduction: Microvascular obstruction (MO) can occur after acute myocardial infarction (AMI) and is felt to independently predict poor outcomes. Because of this there is currently an interest in developing devices and therapies that will decrease the size and extent of MO after AMI. Since infarct assessment by delayed-enhancement cardiac MRI (DE-CMR) is being considered as an endpoint in AMI clinical trials we felt it important to determine the predictors of MO in a large, well characterized cohort of AMI patients.

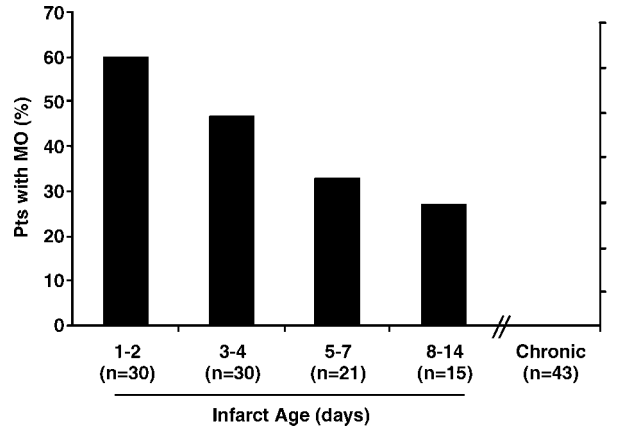

Figure 1.

Methods: AMI patients were eligible for inclusion if they had a clinically confirmed first time MI, no history of prior PCI or CABG, and were imaged using routine DE-CMR (10 min post injection of 0.1–0.2 mmol/kg of gadolinium) within 14 days of their infarct. A subset of patients had follow up DE-CMR at a chronic time point using a similar protocol in order to better evaluate the influence of infarct age on MO. All analyses of infarct size and MO were done by two blinded readers after combining and randomizing the acute and chronic scans. Infarct size and transmural extent were scored using a 17-segment model, while MO was identified by the presence of hypoenhancement surrounded by hyperenhancement (HE).

Results: 96 pts (age 56 ± 13 yrs, median peak CK-MB 142 ng/ml, 68% STEMI, 44% anterior MI) were imaged 4 ± 3 days (mean ± SD) after MI. MO was present in 43 pts (45%). On a per patient basis the prevalence of MO increased significantly with increasing infarct size and increasing number of segments with HE > 75% (TRANS) (both, $p < 0.0001$ for trend). There was an inverse relationship between the prevalence of MO and infarct age in days (d) in the AMI period: 60% at 1–2 d, 47% at 3–4 d, 33% at 5–7 d, and 27% at 8–14 d ($p < 0.02$) (see Figure 1). In the 43 pts with follow up DE-CMR (37% of which had MO in the AMI period, median infarct age 151 d, range 44 d–423 d) no MO was present. Multivariate analysis, which included infarct size as a variable, revealed that the number of segments with TRANS ($p < 0.0001$) and infarct age in the AMI period ($p = 0.013$) were the strongest predictors of the presence of MO.

Conclusion: Over half of all pts with AMI have MO within 1–2 days of infarct. This number decreases rapidly within the first 2 weeks, with complete disappearance of MO in chronic infarcts. The rapid time course of MO's resolution underscores the importance of considering infarct age in MRI studies of AMI.

143. Infarct Size Is an Independent Predictor of Mortality in Patients with Coronary Artery Disease

Rishi Kaushal,[1] David Fieno, MD,[2] Michael Radin, MD,[3] Emanuel Shaoulian, MD,[4] Jagat Narula, MD,[4] Jeffrey Goldberger, MD,[5] Alan Kadish, MD,[5] Kalyanam Shivkumar, MD, PhD,[1] David Bello, MD.[4] [1]*David Geffen School of Medicine at UCLA, Los Angeles, CA, USA,* [2]*Medicine, Cedars-Sinai Medical Center, Los Angeles, CA, USA,* [3]*Pacific Coast Imaging, Irvine, CA, USA,* [4]*Medicine, University of California at Irvine, Irvine, CA, USA,* [5]*Medicine, Northwestern University, Chicago, IL, USA.*

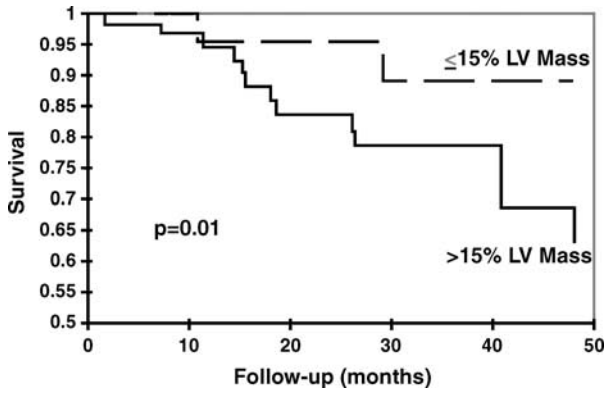

Figure 1. Survival curve for patients with infarct mass ≤ 15% and > 15% of LV mass.

Introduction: Cardiac magnetic resonance imaging (CMRI) can accurately determine infarct size. Prior studies using indirect methods to assess infarct size have shown that patients with larger myocardial infarctions (MI) have a worse prognosis than those with a smaller MI.

Purpose: This study sought to assess the prognostic significance of infarct size by CMRI.

Methods: Cine and contrast MRI were performed in patients with coronary artery disease (CAD) undergoing routine cardiac evaluation.

Results: 100 patients (mean age 66 ± 11 years, 87% male, diabetes 23%, hypertension 49%, prior MI 62%, mean ejection fraction (EF) 34 ± 13%) underwent CMRI. Mean follow-up was 25 ± 18 months after MRI, during which time 15 patients died. Cox regression was used to estimate the risk of death associated with traditional risk factors, heart failure symptoms, EF, angiographic severity of CAD, and extent of infarct size. Presence of MI based on CMRI was present in 91% of patients. The only two significant univariate predictors of death (all-cause) were evidence of infarct > 15% of LV mass and extent of LV dysfunction based on EF ($p < 0.05$); female gender, extent of CAD, prior history of MI, hypertension, and diabetes were not significant. On multivariate analysis, extent of MI (> 15% of LV mass) based on CMR was the best independent predictor of death ($p = 0.01$) with the adjusted relative risk for extent of MI being 9.9 (95% CI 1.6–63), Figure 1.

Conclusions: The extent of MI identified by CMRI is an independent predictor of death in patients with CAD.

144. Prognostic Value of Delayed Contrast-Enhanced Cardiovascular Magnetic Resonance in Patients After Reperfused Acute Myocardial Infarction

Matthias Regenfus, MD,[1] Christian Schlundt,[1] Carolin Stingl,[1] Johannes von Erffa,[1] Robert Krähner,[1] Michaela Schmidt,[2] Werner Adler,[1] Birgit Pucher,[1] Janice Hegewald,[1] Werner G. Daniel.[1] [1]*Medical Clinic II, FAU Erlangen-Nürnberg, Erlangen, Germany,* [2]*Siemens Medical Solutions, Erlangen, Germany.*

Introduction: Delayed contrast-enhanced cardiovascular magnetic resonance (DE-CMR) can be used to assess myocardial viability, its value for assessment of prognosis after reperfused acute myocardial infarction (MI) is not known.

Purpose: We investigated whether DE-CMR is able to determine cardiac prognosis in patients after reperfused acute MI.

Methods: 102 patients (pts) with left ventricular (LV) dysfunction (EF 42 ± 8%) were examined on a 1.5 T scanner within 6 ± 3 (4–10) days of an reperfused acute MI. Cine and DE-CMR (10 min after injection of 0.15 mmol/kg Gd-DTPA) was acquired and scored for regional wall thickening and contrast enhancement (HE) using a 17-segment model. Segments were considered to be viable if showing < 25% HE. LV ejection fraction (EF) was determined by planimetry. Serial clinical follow-up was obtained in all patients (mean follow-up 2.5 ± 1.3 years) regarding occurence of cardiac death, death attributable to any cause, MI, myocardial revascularization, and unstable angina or congestive heart failure requiring hospitalization. Patient-related and CMR data were analyzed in a multivariate Cox regression model.

Results: Among the 102 patients, there were 11 cardiac deaths and reinfarctions in the follow-up period, additionally there were 26 patients with myocardial revascularization or hospitalization due to unstable angina or congestive heart failure. Patients with events at follow-up showed significantly lower EF (45.3 ± 12.7 vs. 37.7 ± 14.3, $p = 0.006$) than patients without events. In patients with cardiac deaths or reinfarction, the dysfunctional area by CMR (0.65 vs. 0.48, $p = 0.08$) and the dysfunctional but viable area by CMR (0.16 vs. 0.27, $p = 0.008$) was significantly higher than in patients without such events. By multivariate analysis EF (hazard ratio 0.98, CI 0.95 to 1.0, $p = 0.03$) and the dysfunctional but viable area by CMR (hazard ratio 1.4, CI 0.9 to 3.0, $p = 0.04$) were related to occurence of future events independent of the presence of risk factors for coronary arterosclerosis.

Conclusions: In patients after reperfused acute MI, DE-CMR can be used to forecast major adverse cardiac events.

145. Delayed Enhancement Cardiac Magnetic Resonance Imaging Detects Acute Right Ventricular Myocardial Infarction

Andreas Kumar, MD,[1] Hassan Abdel-Aty, MD,[1] Ilka Kriedemann,[1] Jeanette Schulz-Menger, MD,[1] C. Michael Gross, MD,[1] Rainer Dietz, MD,[1] Matthias G. Friedrich,

MD, FESC.[2] [1]*Cardiology, Charite Franz-Volhard-Klinik, Humboldt University, Berlin, Germany,* [2]*Department of Cardiovascular Sciences, University of Calgary, Calgary, AB, Canada.*

Background: Right ventricular infarction (RVI) is a serious complication of acute inferior myocardial infarction. Delayed enhancement cardiac magnetic resonance imaging (CMR) accurately detects acute left ventricular infarction. We investigated the utility of delayed enhancement CMR for the detection of acute RVI.

Methods: We examined 41 consecutive patients (31 male, age 54 ± 11 years) with acute inferior myocardial infarction defined by ECG criteria. All underwent a physical examination for the presence of a triad of hypotension, clear lung sounds and jugular venous distension, an ECG for ST-elevation $\geq$ 0.1 mV in the V4r right precordial lead, an echocardiogram for right ventricular dilatation and wall motion abnormalities, and X-ray coronary angiography for the definition of the culprit lesion. After successful coronary reperfusion (reperfusion time 9.7 h ± 6.8 h, thrombolysis n = 3, percutaneous coronary intervention n = 38), all patients underwent a CMR examination 3.2 ± 2.2 days after onset of symptoms. We used a 1.5 T system (Signa CV/I, General Electric, USA), and the "delayed enhancement" sequence (inversion recovery gradient echo 10 min after application of 0.2 mmol/kg Gadolinium-DTPA, TR 7.1 ms, TE 3.1 ms, TI optimized to null remote myocardium 200–300 ms, matrix 256 × 192) was applied in short axis slices of the right and left ventricular myocardium. The studies were evaluated by two blinded observers for the presence of delayed enhancement in the right ventricular wall. In the absence of a single accepted gold standard for the detection of RVI in vivo, the results of the CMR study were compared to a score combining all non-CMR methods. That score rated the patient "positive" for RVI, when any one or more of the non-CMR methods were positive for RVI as described above. The results of the CMR study were also compared to each of the non-CMR methods alone.

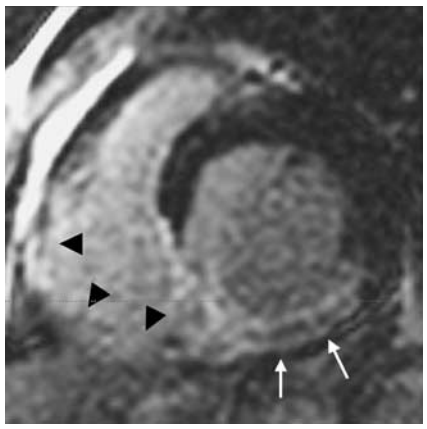

Figure 1.

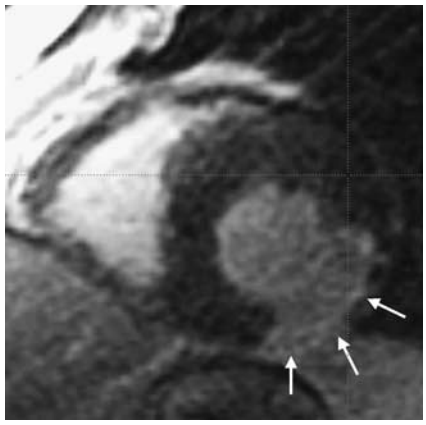

Figure 2.

Results: In our study population with acute inferior myocardial infarcts, delayed enhancement CMR showed RVI in 22 patients (example: Figure 1) and was negative for RVI in 19 patients (example: Figure 2).

When CMR was compared to the combined non-CMR methods for the detection of RVI, it reached a sensitivity of 85%, a specificity of 76%, a positive predictive value of 77% and a negative predictive value of 84% (standard of truth: $\geq$ 1 non-CMR methods as positive for RVI). CMR detected all but one patient, in whom at least two non-CMR methods were positive for RVI (sensitivity 88%).

Even when CMR was compared to each other technique (clinical triad, ECG V4r, and echocardiography) alone, the sensitivities for the detection of acute RVI were 88%, 83% and 88%, and the negative predictive values were 95%, 89% and 95%, respectively.

Furthermore, patients positive for RVI by CMR had significantly more proximal RCA lesions than patients negative for RVI by CMR (n = 12 vs. n = 4, $p < 0.05$), and they spent significantly more time on the Intensive Care Unit (3.9 ± 1,4 days vs. 2.9 ± 0.9 days, $p < 0.05$).

Conclusion: Delayed enhancement CMR yields high sensitivity and negative predictive values for the detection of RVI in acute inferior myocardial infarction and thus could be used to exclude RVI in these patients.

146. Detection of Right Ventricular Infarction by Cardiac Magnetic Resonance Imaging

D. Ian Paterson, MD, Alex Natanzon, MD, Breno Pessanha, MD, Andrew E. Arai, MD. *Laboratory of Cardiac Energetics, National Institutes of Health, Bethesda, MD, USA.*

Background: Right ventricular (RV) involvement in acute inferior wall myocardial infarction (IMI) is difficult to

diagnose with conventional techniques. However, clinically detected RV infarction has been shown to be associated with worse prognosis.

Hypothesis: We hypothesized that cardiac MRI (CMR) will detect clinically unsuspected right ventricular involvement in patients with acute IMI.

Methods: 45 consecutive patients (36 male, mean age 60) with first-time acute IMI underwent CMR in a community hospital. Imaging consisted of steady state free precession cine MRI (FIESTA) and contrast-enhanced inversion-recovery fast gradient-recalled echo for infarct detection. Left and right ventricular volumes, ejection fractions (EF) and regional wall motion abnormalities were specifically evaluated. Readers blinded to the CMR results performed chart reviews on all patients. Outcomes measured included in-hospital mortality and length of stay.

Results: Right ventricular involvement was detected by CMR (RV + /CMR) in 10 of 45 patients with acute IMI but was only clinically suspected in 2 ($p = 0.01$). RV delayed enhancement was present in 8 and RV wall motion abnormalities in an additional 2. 9 of these 10 patients underwent echocardiography however an RV abnormality was revealed in only 1 case. Older age ($p = 0.03$) and diabetes ($p = 0.054$) were more common in the RV + /CMR group than the RV-/CMR group. Mean blood pressure at presentation, peak cardiac enzyme rise and the presence of ST elevation were similar in both groups. At cardiac catheterization, the prevalence of significant stenoses of the proximal or mid right coronary artery as well as the rate of angioplasty and stent deployment were also similar between RV + /CMR and RV-/CMR patients. CMR revealed similar LVEF, left ventricular volume and right ventricular volume but RVEF was significantly decreased in the RV + /CMR group (52% vs. 60%, $p < 0.001$). Length of stay was similar in both groups, 2.6 days vs. 3 days, and all patients survived to discharge.

Conclusions: RV involvement associated with acute IMI was detected 5 times more often by CMR than was clinically suspected. However, outcome in these subclinical RV infarcts does not appear worse.

147. Differences of Late Gd-DTPA Kinetics and Partition Coefficient in Normal, Stunned and Necrotic Myocardium in Patients with Acute Myocardial Infarction

Christoph Klein, MD,[1] Thaiz Ruberti, MD,[1] Stephan G. Nekolla, PhD,[2] Bernhard Schnackenburg, PhD,[3] Eike Nagel, MD,[1] Eckart Fleck, MD.[1] [1]*Cardiology, German Heart Institute Berlin, Berlin, Germany,* [2]*Nuklearmedizin, Klinikum rechts der Isar der TU Muenchen, Muenchen, Germany,* [3]*Philips Medical Systems, Hamburg, Germany.*

Introduction: Contrast enhanced magnetic resonance can distinguish between stunned and infarcted myocardium.

Purpose: Aim of the study was to investigate the mechanism of enhancement by determining T1 relaxation kinetics of blood, normal, stunned and infarcted myocardium over time and calculate the partition coefficient (pc).

Methods: 22 patients with acute myocardial infarction were examined with a 1.5 Tesla scanner (Intera, Philips, Netherlands) 4 ± 3 days after the acute event and interventional revascularisation. Infarcted [with and without microvascular obstruction (MVO)], stunned and normal myocardium were defined in the inversion recovery (15–20 min post contrast) and cine technique (normal: normal wall motion + no enhancement; stunned: abnormal wall motion + no enhancement; infarcted: abnormal wall motion + enhancement; MVO: hypoenhancement within enhanced area). T1 values were calculated (Look-Locker) before and 5 to 40 minutes after 0.2 mmol/kg body weight Gd-DTPA for blood and myocardium. The pc was calculated by the equation $pc = deltaR1_{myocardium}/deltaR1_{blood}$.

Results: T1 was different ($p < 0.0001$) between normal, stunned and infarcted myocardium over the whole period after (Fig. 1), but not before contrast application. Significant differences between blood and infarcted myocardium did not exist at 20 min after contrast. Time course of the partition coefficient is shown in Fig. 2. There is steady state distribution of Gd-DTPA in normal and stunned myocardium, however pc in stunned mayocardium is significantly increased compared to normal ($p < 0.05$). Enhanced areas and areas with MVO show an altered pattern suggesting a reduced wash-in/wash-out kinetic.

Conclusions: In patients with acute infarction 1) stunned myocardium exhibits an higher pc than uneffected myocardium, possibly due to edema and/or partial necrosis, 2) infarcted and stunned myocardium can be distinguished by T1 weighted techniques between 5 and 40 minutes, 3) areas with MVO have a reduced contrast wash-in kinetic and 4) delayed enhancement is mainly due to an increased partition coefficient, but also shows an altered contrast wash-in and -out kinetic despite complete revascularisation.

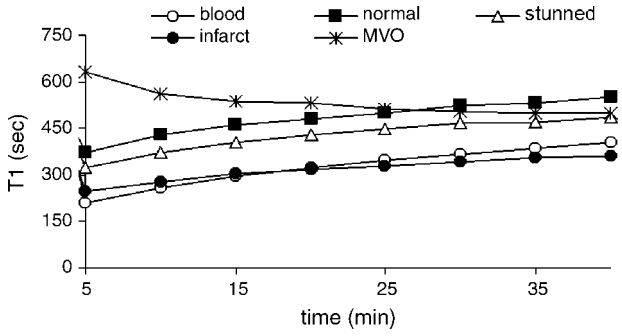

Figure 1.

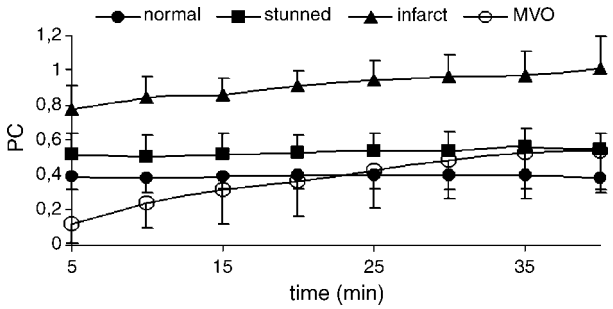

Figure 2.

148. Hypoenhancement on Delayed Contrast-Enhanced MRI Following ST-Segment Elevation Myocardial Infarction: an Alternate Approach for Evaluating No-Reflow

Chiara Bucciarelli-Ducci, MD, Edwin Wu, MD, Paula Tejedor, MD, Daniel C. Lee, MD, Preeti Kansal, MD, Thomas A. Holly, MD, James C. Carr, MD, Francis J. Klocke, MD, Robert O. Bonow, MD. *Northwestern University, Chicago, IL, USA.*

Background: "No-reflow" is defined as microvascular obstruction within an area of myocardial infarction, and it predicts worse functional recovery by negatively influencing left ventricular remodeling. Microvascular obstruction can be evaluated noninvasively by Gd-DTPA contrast-enhanced MRI (ce-MRI), and is usually identified as area of early hypoenhancement within 3 minutes of contrast injection. However, a similar phenomenon can sometimes also be seen on *delayed* viability images following an acute myocardial infarction, and limited data are available evaluating these delayed hypoenhanced areas.

Methods: Ce-MRI studies were performed in 32 patients within a week of successful percutaneously reperfused ST-elevation myocardial infarction. We utilized a multiple breath-hold, segmented inversion-recovery turbo FLASH pulse sequences using a 1.5-T system (Siemens). Images were acquired 15–20 minutes after 0.15–0.2-mmol/kg bolus injection of gadolinium. Multiple short-axis views were acquired to encompass the entire left ventricle from base to apex. Inversion-time (TI = 250–350 ms) was progressively optimized to null normal myocardium. A follow-up ce-MRI scan was performed more than three months later.

Results: Seventeen (34%) of the 32 patients showed "no-reflow" as an area of hypoenhancement on delayed contrast-enhanced images. A transmural infarct was observed in 10 patients in the "no-reflow" group and in 5 patients of the "absent no-reflow" group. Time to reperfusion was 9.1 ± 7.4 and 3.1 ± 2.3 hours in the "no-reflow" and "absent no-reflow" groups, respectively.

At baseline the "no-reflow" group showed larger mean infarct mass (54.8 ± 2.3 g), end-diastolic volume (EDV, 181.2 ± 31.6 cc), end-systolic volume (ESV, 121.8 ± 35.8 cc), and lower ejection fraction (EF, 35 ± 10%) when compared to the "absent no-reflow" group (25.8 ± 15.5 g, $p = 0.0002$; 141.8 ± 41.2 cc, $p = 0.004$; 81.8 ± 37.4 cc, $p = 0.004$; 44 ± 10%, $p = 0.01$). At follow-up, both in the "no-reflow" and "absent no-reflow" groups, infarct mass decreased significantly with respect to baseline (− 14 ± % and − 10 ± %, respectively), but this decrease was not different between the two ($p = 0.2$). However we observed a significant increase of EF in the "absent no-reflow" group (from 44 ± 10% to 52 ± 6%, $p = 0.0001$) but not in the "no-reflow" group (from 35 ± 10% to 36 ± 9%, $p = 0.4$). In the "no-reflow" group both EDV and ESV tended to increase (+ 15 ± 33.5 cc, $p = 0.07$ and + 3.5 ± 28.7 cc, $p = 0.6$), while in the "absent no-reflow" EDV tended to increase with a corresponding slight decrease of ESV (+ 12 ± 23 cc, $p = 0.04$ and − 7.8 ± 22.3 cc, $p = 0.2$) (Fig. 1).

Conclusions: Although "no-reflow" is commonly identified by ce-MRI as areas of early hypoenhancement, in our study we observed areas of persistent hypoenhancement on delayed contrast-enhanced images. The presence of "no-reflow" was observed in later reperfused myocardial

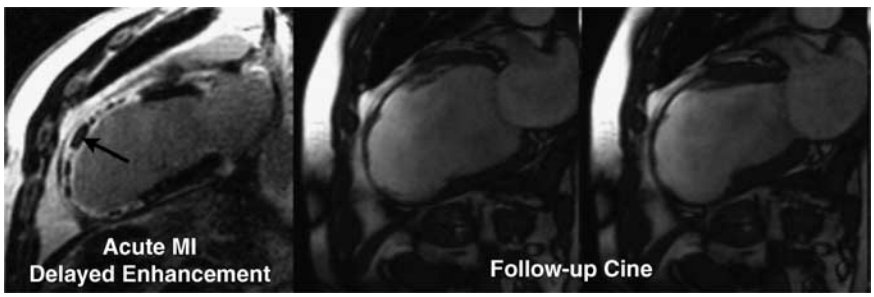

Figure 1. Two-chamber long-axis views of a patient following an acute ST-segment elevation myocardial infarction. Left panel shows multiple areas of hypoenhancement ("no-reflow") within a transmural hyperenhancement of the LAd region. The largest "no-reflow" area is indicated by a black arrow. The center (diastolic frame) and right (systolic frame) panels were taken 9 months later showing an enlarged EDV (230 cc) and ESV (200 cc) with an EF of 25%.

infarctions that were larger, more frequently transmural and had more compromised systolic function and increased volumes. We postulate that the presence of "no-reflow" on *delayed* contrast-enhanced images is related to absent penetration of contrast into the infarct core due to microvascular obstruction.

149. Risk Assessed by Framingham and Myocardial Perfusion Measured by MRI Selects Patients for Coronary Artery Angiography: the NHLBI-Sponsored Women's Ischemia Syndrome Evaluation (WISE) Study

Mark Doyle, PhD,[1] Gerald M. Pohost, MD,[2] Leslee J. Shaw,[3] Eduardo Kortright,[4] Diane A. Vido,[1] Sheryl F. Kelsey,[5] B. Delia Johnson,[5] William J. Rogers,[6] Steven E. Reis,[7] Marian B. Olson,[7] Barry L. Sharaf,[8] C. Noel Bairey-Merz,[9] Sunil Mankad, MD,[1] Robert W. W. Biederman, MD.[1] [1]*Allegheny General Hospital, Pittsburgh, PA, USA,* [2]*University of Southern California, Los Angeles, CA, USA,* [3]*ACRI, Atlanta, GA, USA,* [4]*University of New Orleans, New Orleans, LA, USA,* [5]*Graduate School of Public Health, Epidemiology Data Center, Pittsburgh, PA, USA,* [6]*University of Alabama at Birmingham, Birmingham, AL, USA,* [7]*University of Pittsburgh Medical Center, Pittsburgh, PA, USA,* [8]*Rhode Island Hospital, Providence, RI, USA,* [9]*Cedars-Sinai Research Institute, Los Angeles, CA, USA.*

Introduction: In women with suspected myocardial ischemia, most events occur above an intermediate Framingham score (Adult Treatment Panel III, ATP III). However, within this group, quantitative coronary angiography (QCA) identifies few women with severe disease. Thus, risk estimates based upon historical and risk factor measures are suboptimal guides in women, and improved testing criteria are required.

Hypothesis: We hypothesize that risk stratification combining ATP III and a global myocardial perfusion index (GMPi) calculated from magnetic resonance imaging (MRI) better identify patients at high risk of major adverse cardiovascular events (MACE) who would benefit from QCA testing.

Methods: Women (133), mean age 57.7 ± 11.3 yrs, with suspected myocardial ischemia and a mean ATP III score of 9.8 ± 10.0 underwent QCA. Resting MRI was performed and GMPi calculated. Follow-up was conducted (38 ± 14 months) to monitor MACE: death or myocardial infarction. Step-wise Cox regression modeling was used to determine independent predictors of MACE.

Results: There were 10 MACE (7%) and 21% of the population had a $\geq$ 50% lesion in one epicardial coronary artery. By Cox modeling, ATP III score and GMPi were independently predictive of MACE ($p < 0.005$). An ATP III score $\geq$ 10 (intermediate risk) identified 38% of patients and 80% of events (event rate not different between intermediate and high-risk groups). Combining ATP III $\geq$ 10 and GMPi in the lower two quartiles identified 20% of the population and 70% of MACE, risk ratio 9.2 and 95% confidence interval 2.54–33.11. The QCA severity score was not different between high and low-risk groups (14.50 ± 10.17 vs. 11.65 ± 10.01, $p = 0.3$). However, it was predictive of MACE in the high-risk but not low-risk group.

Conclusions: Women with suspected ischemia were risk stratified by the ATP III score and GMPi (by MRI). Patients with no risk variables (33%) remained event-free, those with one risk variable (47%) experienced low events, and those with both risk variables (20%) experienced 70% of events. Within the high-risk group, QCA severity score further stratified risk. The combined ATP III and GMPi risk variables identified patients who would potentially benefit from QCA and effectively would have excluded those who would not benefit from QCA.

150. Arrhythmic Risk Stratification in the MADIT-II Population

Sunil T. Mathew, MD, Nathaniel Reichek, MD, William Schapiro, BS, RT, David Hoch, MD, Stuart Schecter, MD, Joseph Levine, MD. *St. Francis Hospital, Roslyn, NY, USA.*

Introduction: In the MADIT-II study, patients with clinical left ventricular ejection fraction (LV EF) $\leq$ 30% and prior myocardial infarction had lower mortality with defibrillator therapy (ICD). However, the reliability of clinical EF has not been determined in this setting. Ventricular arrhythmia inducibility (+ EPS) is also a risk factor in this population and may relate to infarct size. We used CMR to evaluate clinical EF, CMR LV EF and volumes and infarct size in patients meeting MADIT II criteria.

Methods: CMR was performed in 43 patients (mean age = 66 ± 12 y, 3F) with clinical EF $\leq$ 30% and infarction > 1 month previously but no revascularization within < 3 months. Short axis TrueFISP cine imaging provided 3D LV volumes (MEDIS MASS) and infarcts were sized (n = 38) as percent LV mass using delayed hyperenhancement imaging after 0.2 mmol/kg gadolinium chelate. Clinical and CMR EF were compared with correlation and Bland-Altman limits of agreement techniques. Receiver operating characteristic (ROC) curves for a combined end-point of inducibility of ventricular tachycardia with programmed stimulation (+ EPS) plus early arrhythmic events in noninducibility with programmed stimulation (− EPS) and non-EPS patients were assessed for clinical and CMR EF, volume indices and infarct size.

Results: Inducibility was present in 28/34 EPS patients, while 4/9 non-EPS patients had events and ICD within < 5 months. Clinical EF derived from 2D echo (n = 31), radionuclide studies (n = 4) or invasive ventriculography (n = 7). Median interval from clinical EF to CMR was 17 days, but limits of agreement were similar in studies done the same day, < 14 days or > 14 days apart. Clinical EF correlated weakly with CMR EF (r = 0.37) and 13/43 (30%) subjects had CMR EF> 30% despite clinical EF $\leq$ 30%. Limits of agreement were wide: + 15 to − 30 EF %. Significant associations with the combined endpoint were found for CMR EF (AUC = 0.71, p < 0.04), end-systolic volume index (AUC 0.80, p < 0.0001) and LV mass/volume ratio (AUC 0.73 P < 0.005) but not clinical EF or infarct size (AUC = 0.67, AUC = 0.58, both p = NS).

Conclusions: In MADIT-II patients clinical EF is inaccurate. Lower CMR EF and mass/volume ratio and higher end-systolic volume index are associated with higher arrhythmic risk but clinical EF and infarct size are not. CMR may provide improved risk stratification among MADIT-II patients.

151. Pulmonary Vein Diameter Reduction in Early Magnetic Resonance Angiography After Radiofrequency Ablation: Prognostic Significance for Development of Severe Stenosis

Okan Ekinci,[1] Alexander Berkowitsch, PhD,[2] Thomas Neumann, MD,[3] Harald Greiss, MD,[2] Heinz-Friedrich Pitschner, MD,[2] Christian W. Hamm, MD, PhD,[2] Thorsten Dill, MD.[2]
[1]*Cardiology, German Clinic of Diagnostic, Wiesbaden, Germany,* [2]*Cardiology, Kerckhoff Heart Center, Bad Nauheim, Germany,* [3]*Cardiology, Justus Liebig University of Giessen, Giessen, Germany.*

Introduction: Arrhythmogenic myofibrills located at the orifice of pulmonary veins can trigger atrial fibrillation. Radiofrequency ablation (RFCA) around the ostia of pulmonary veins is done in patients with atrial fibrillation being refractory to medical treatment. Reduction of initial ostial PV diameter was found in patients directly after radiofrequency ablation. Furthermore, development of stenoses was reported in up to 10% of patients within a period of one year after ablation.

Purpose: Aim of this study was to investigate prognostic significance of the relative reduction of PV diameter (RRPVD) assessed by magnetic resonance imaging at next day after the procedure for development of severe PV stenosis during long term follow up.

Methods: Sixty four consecutive patients (mean age/SD = 53/10 years; 24 female) with highly symptomatic and drug refractory atrial fibrillation were enrolled in the study. The diameter of PV were evaluated using MR angiography one day prior to and one day after the ablation procedure. The further follow-up was by MR angiography every three months after the procedure. MR angiography was done using a non-gated contrast enhanced FISP-3D sequence and an i.v. bolus injection of 20 mL Gadolinium-DTPA. Using 3D reconstruction (MPR), the ostial PV diameter were measured.

Severe PV stenosis was defined as a diameter reduction > 70% of the initial ostial PV diameter. RRPVD was analyzed as dichotomized variable using cutoff determined by the method of maximizing the log-rank test statistic.

Results: A total of 228 PV were treated in study patients. The mean RRPVD at early control was 8% with SD = 14%. Severe stenosis was found in 13 PV within follow up (mean/SD = 6.5/4.6 months). The optimal cutoff point was found at RRPVD = 25%. The Kaplan-Meier analysis confirmed strong association of RRPVD $\geq$ 25% with long term development of PV stenosis (p < .0001; sensitivity = 42%; specificity = 90%). RRPVD was also tested in multivariate Cox regression model which revealed RRPVD to be strongest predictor for development of severe PV stenosis (p < .0001; HR = 4.97). The cumulative energy amount per PV was predictive as continuous variable (p < .001), but was not predictive after the dichotomization.

Conclusion: Relative reduction of the initial ostial PV diameter $\geq$ 25%, observed by MR angiography at the next day after the procedure is a strong independent predictor for development of severe PV stenosis. Patients should routinely undergo MR angiography for assessment of pulmonary vein diameters, early after RFCA of PV.

152. Myocardial Perfusion in Patients with Cardiac Syndrome X Assessed with Cardiovascular Magnetic Resonance and Positron Emission Tomography

Andrew G. Elkington,[1] Heiko Kindler (Joint first author),[2] Ornella E. Rimoldi, PhD,[2] Peter Collins, MD,[3] Paolo G. Camici, PhD,[2] Dudley J. Pennell, MD.[1] [1]*CMR Unit, Royal Brompton and Harefield NHS Trust, London, UK,* [2]*MRC Clinical Sciences Centre, Imperial College, London, UK,* [3]*Department of Cardiology, Royal Brompton and Harefield NHS Trust, London, UK.*

Introduction: Cardiac Syndrome X (CSX) patients have typical angina, abnormal exercise ECG, and normal coronary angiography.

Controversy exists on whether the chest pain results from microvascular dysfunction and ischaemia which might be subendocardial.We used cardiovascular magnetic resonance (CMR) and state-of-the-art positron emission tomography (PET) to measure transmural myocardial perfusion in CSX and controls (CON).

Methods: CSX patients were recruited from the Women's Heart Disease clinic at the Royal Brompton Hospital. Myocardial perfusion was assessed by both CMR and PET in 10 CSX (9 females, 57 ± 9 years) and 10 matched controls (9 females, 49 ± 9 years p = ns) at rest and during adenosine stress (140 μg/kg/min).

The mean time between CMR and PET studies was 10 ± 12 weeks. The CMR study was performed first in all cases.

Patients with hypertension, diabetes mellitus, left ventricular hypertrophy, left bundle branch block and minimal coronary artery disease were excluded.

CMR: All studies were performed on a 1.5T scanner (Siemens, Sonata). For each study, we used a bolus of gadolinium (Magnevist, Schering, 0.1 mmol/kg, 7 ml/s) and a hybrid EPI sequence, 2 (pixel size 2.1 × 2.1 mm, TR 6.2 ms, TE 1.3 ms, 196 ms image time) with 3 short axis slices.

All images were analysed off-line using dedicated software (CMRtools, London, UK). Myocardial perfusion reserve index (MPRi) was calculated in the subendocardium (ENDO) and subepicardium (EPI) as adenosine/resting perfusion by Fermi deconvolution.

PET: All studies were performed on an EXACT 3D (CTI PET Systems, Knoxville) with reconstructed spatial resolution of 4.5 × 4.5 × 4.2 mm FWHM using H215O. Absolute subendocardial and subepicardial perfusion (ml/min/g) and the ENDO- and EPI MPR were calculated.

Results: PET absolute perfusion and MPR: ENDO-perfusion was lower in CSX than in controls both at rest (0.98 ± 0.35 vs. 1.26 ± 0.50, p < 0.001) and during adenosine (2.79 ± 1.12 vs. 3.45 ± 1.55, p < 0.001) although MPR was comparable (3.05 ± 1.59 vs. 3.18 ± 1.0, p = 0.57).

EPI-perfusion at rest (0.92 ± 0.29 vs. 0.89 ± 0.34, p = 0.50), during adenosine (2.81 ± 1.16 vs. 2.61 ± 1.08, p = 0.22) and MPR (3.24 ± 1.39 vs. 3.24 ± 1.62 p = 0.9) were comparable in CSX and controls.

CMR Myocardial perfusion reserve index: MPRi was lower in CSX compared to controls in both ENDO (2.39 ± 0.79 vs. 2.69 ± 0.74, P = 0.009) and EPI (2.59 ± 0.89 vs. 2.96 ± 1.06, P = 0.01).

Conclusions: In CSX compared to controls, absolute ENDO perfusion measured by PET is lower (at rest and stress) although MPR is comparable to that in controls.

The MPRi measured by CMR is lower in both layers in CSX compared to controls. Whether these transmural differences of perfusion in CSX have a pathophysiological relevance remains to be determined.

153. The Relationship Between Myocardial Iron Deposition and Left Ventricular Dysfunction in Thalassemia Using Cardiovascular Magnetic Resonance

Mark A. Westwood, Lisa J. Anderson, Mark A. Tanner, Dudley J. Pennell. *CMR Unit, Royal Brompton Hospital, London, UK.*

Introduction: Beta thalassemia major (TM) is the commonest inherited genetic disorder worldwide, where the long term outlook is still poor. The majority of deaths are due to the sequelae of cardiac iron overload resulting from the multiple transfusions required from birth. The recent development of validated cardiovascular magnetic resonance (CMR) T2* imaging for the first time allows assessment of myocardial iron loading. However, the frequency of left ventricular (LV) dysfunction for a given myocardial T2* value is not known. This would be useful by allowing a better attribution of risk of significant LV dysfunction developing in a given patient, which is known to carry a mortality of 50%. By using a large cohort of T2* assessments it may be possible to evaluate this.

Purpose: To assess the relationship between LV dysfunction and myocardial iron loading in TM.

Methods: 972 CMR assessments on 470 patients with TM (and no other known pathology) were performed at the Royal Brompton Hospital in London between May 1999 and December 2003. In each case myocardial T2* and left ventricular ejection fraction (LVEF) were calculated. For myocardial T2* values < 20msec (rounded down to the nearest whole number) were taken to indicate significant myocardial iron loading. For LVEF, values < 56% were taken to indicate significant LV dysfunction. For each myocardial T2* value, the number of assessments where the LVEF < 56% was determined and hence the percentage of assessments were there was evidence of LV dysfunction could be calculated. These results were then plotted as graphs (Figures 1 and 2).

Results: In 586 assessments there was significant myocardial iron loading (i.e., myocardial T2* < 20msec) and in 99 of the cases there was evidence of LV dysfunction (i.e., LVEF < 56%.) The number of patients with LV dysfunction for each T2* value is shown in Figure 1, and the percentage of patients with LV dysfunction is shown in Figure 2. The majority of patients with an LV dysfunction had myocardial

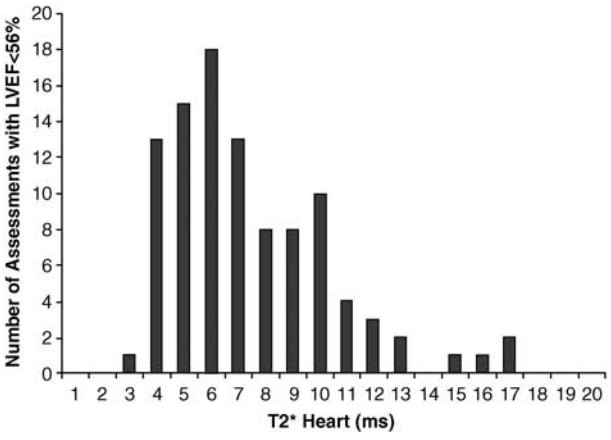

Figure 1.

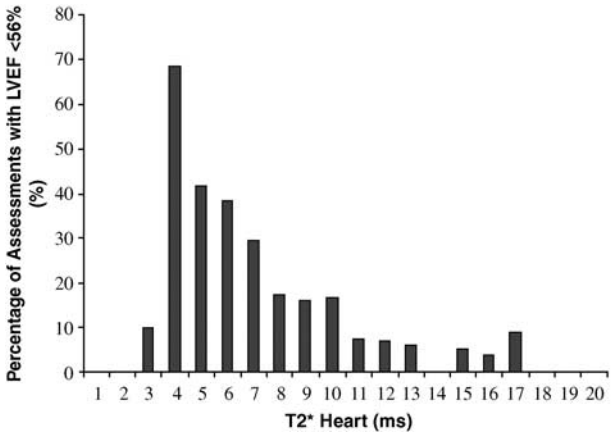

Figure 2.

T2* values < 8msec (60 out of 99 patients.) The frequency of LV dysfunction generally decreases as there is less myocardial iron loading (i.e., an increasing myocardial T2* value.) It is worth noting that no patient with a myocardial T2* > 20 msec had an LVEF < 56%.

Conclusions: That as myocardial iron loading increases (as assessed by a decreasing myocardial T2* value) the occurrence of LV dysfunction increases (as assessed by LVEF). In the most severely iron loaded (myocardial T2* 4msec) the risk of significant LV dysfunction is nearly 70%. This further validates the use of myocardial T2* imaging in the assessment of tissue iron loading and allows an estimation of the risk to a patient with a given myocardial T2* value.

154. Cardiac Magnetic Resonance Characterization of Patients with Pheochromocytoma

W. Patricia Ingkanisorn, MD, Sriram Padmanabhan, MD, Federico Mordini, MD, Andrew E. Arai, MD. *NHLBI, Laboratory of Cardiac Energetics, National Institutes of Health, Bethesda, MD, USA.*

Background: Pheochromocytoma is a tumor that releases excess catecholamines episodically. Thus, intermittent hypertension and increased heart rate are common physiologic changes associated with this diagnosis. Other cardiovascular manifestations of pheochromocytoma include myocardial infarction (MI), myocarditis, and dilated cardiomyopathy. Cardiac magnetic resonance (CMR) is a technique that has high accuracy and reproducibility of left ventricular structure and function. In addition, abnormal gadolinium delayed enhancement has been observed in MI, myocarditis, various cardiomyopathies, and other infiltrative processes.

We hypothesized that CMR imaging of pheochromocytoma patients would detect occult abnormal delayed enhancement patterns, as well as demonstrate differences in left ventricular structure and function when compared with CMR imaging of a group of healthy volunteers.

Methods: CMR was performed prospectively on 18 patients with known pheochromocytoma and a control group of 11 normal volunteers. Cine function, resting perfusion, and gadolinium delayed enhancement were performed. Resting heart rate and blood pressure were recorded prior to each study. All imaging was performed on a GE 1.5 T, CV/i scanner. Left ventricular (LV) indices such as stroke volume, ejection fraction, total mass, and maximal wall thickness were measured and compared between the two groups.

Results: Ten of the 18 pheochromocytoma patients had a history of hypertension. None of the normal volunteers had known hypertension. Multiple variables were compared between the 18 pheochromocytoma patients and the 11 normal volunteers. Two of the pheochromocytoma group had mildly decreased global LV systolic function; however, there were no statistically significant differences between the two groups when comparing age, LV ejection fraction (EF), LV end diastolic mass/BSA, maximal LV wall thickness, systolic blood pressure (BP), diastolic BP, or heart rate. Table 1 summarizes the findings.

Within the pheochromocytoma group, there were no findings of gadolinium delayed enhancement of the myocardium. Two of the pheochromocytoma patients were found to have extracardiac masses, both adjacent to the left atrium, and

Table 1.

	Pheochromocytoma	Normal	p value
Age	45 ± 14 yrs	46 ± 7 yrs	0.94
LV EF	64 ± 7	62 ± 3	0.37
LV end-diastolic mass/BSA	40 ± 9 g/m2	40 ± 17 g/m2	0.91
Maximal LV wall thickness	11 ± 2 mm	11 ± 2 mm	0.85
Systolic BP	123 ± 17 mm	135 ± 11 mm	0.26
Diastolic BP	77 ± 10 mm	89 ± 9 mm	0.07
Heart rate	68 ± 13 bpm	70 ± 13 bpm	0.74

Results reported as mean ± one standard deviation.

two patients had mediastinal masses. Of interest, 28% of the pheochromocytoma patients had prominent lipomatous hypertrophy of the interatrial septum.

In the normal volunteer group, one subject was found to have an atypical mid-wall delayed enhancement pattern. None of the normal volunteers had any cardiac or intrathoracic masses. Only 8% of the normal volunteer group had lipomatous hypertrophy of the interatrial septum.

Conclusion: Despite the known physiological effects of excess circulating catecholamine levels, this study found no statistically significant differences in left ventricular systolic structure and function between 18 consecutively enrolled pheochromocytoma patients and 11 normal volunteers. There also were no clinically silent myocardial infarctions. Thus, myocardial infarction associated with pheochromocytoma may represent late stage disease or the combined effects of excess catecholamines in patients with either vulnerable plaques or concomitant severe coronary artery disease. Of unknown significance was the finding of prominent lipomatous hypertrophy of the interatrial septum in almost 1/3 of the pheochromocytoma patients.

155. Prevalence and Structural Risk Factors for Left Ventricular Thrombus in Patients with Systolic Dysfunction as Assessed by Cardiac MRI

Han W. Kim, MD,[1] Jonathan W. Weinsaft, MD,[2] Igor Klem, MD,[2] Anna Lisa Crowley, MD,[2] Rhoda Brosnan, MD,[2] Thomas Todoran, MD,[2] John Heitner, MD,[2] Eric Velazquez, MD,[2] Michelle Parker, MS, RN,[2] Michael Elliott, MD,[2] Robert M. Judd, PhD,[2] Raymond J. Kim, MD.[2] [1]*Cardiology, Cornell University, New York, NY, USA,* [2]*Cardiology, Duke Cardovascular Magnetic Resonance Center, Durham, NC, USA.*

Background: Delayed enhancement MRI (DE-MRI) offers tissue characterization that accurately identifies the presence and extent of myocardial scarring and has the potential to be superior to cine MRI for detecting left ventricular thrombus (LVT). We used DE-MRI to evaluate the prevalence and structural risk factors for LVT and to compare LVT detection rate with cine MRI in a broad population of patients with systolic dysfunction.

Methods: We prospectively enrolled consecutive pts with systolic dysfunction (EF $\leq$ 45%) referred for cardiac MRI. Cine and DE-MRI were scored via a 17 segment model to quantify wall motion abnormalities (WMA), myocardial scar based on hyperenhancement (HE), and the presence of LVT. Studies were read by two independent observers blinded to patient history and clinical diagnosis.

Results: 535 pts were studied (age 60 ± 15, 66% M, 61% HTN, 30% DM). 65% had ischemic cardiomyopathy by clinical criteria. DE-MRI identified LVT in 42 pts (7.8%). The prevalence of LVT was 10.8% (n = 37) in pts with ischemic cardiomyopathy (n = 37) and 2.7% (n = 5) in patients with non-ischemic cardiomyopathy (p = 0.001). Cine MRI failed to identify LVT in 23% of cases detected by DE-MRI (p = 0.03). 98% of LVT identified by DE-MRI were adjacent to myocardium with scar. In multivariate analysis including several clinical and imaging parameters, only extent of scar (RR 1.4, CI 1.2–1.5, p < 0.0001) and severity of WMA (RR 1.1, CI 1.0–1.3, p = 0.02) were independent predictors of LVT. The figure demonstrates the additive effects of LV scar burden to severity of segmental wall motion abnormalities on the prevalence of LVT.

Conclusions: The prevalence of LVT by DE-MRI is dependent on the etiology of systolic dysfunction and includes a high proportion of pts missed by cine MRI. Myocardial scar burden predicts LVT independent of the severity of contractile dysfunction and may be a useful index for determination of thrombotic risk.

156. MR Imaging of Atherosclerosis in Aorta and Carotid Arteries of Patients with Acute Ischemic Stroke

Venkatesh Mani, PhD, Silvia H. Aguiar, MD, Karen B. Weinshelbaum, Katheleen E. Burger, David M. Brown, MD, Vitalii V. Itskovich, PhD, Juan Gilberto S. Aguinaldo, MD, Valentin Fuster, MD, PhD, Zahi A. Fayad, PhD. *Mount Sinai School of Medicine, New York, NY, USA.*

Introduction: The prevalence of Atherosclerosis in the arterial system may be different based on the risk of acute ischemic stroke (AIS).

Purpose: The aim of this study was to test the hypothesis that atherosclerotic profile in Acute Ischemic Stroke (AIS) Patients is different using black blood CMR.

Methods: 14 patients with AIS (aged 64.3 ± 8.6 years, range, 42.8% females) and age/gender-matched controls (n = 13) with similar cardiovascular risk distribution as determined by their 10-year risk profile using Framingham Score underwent high-resolution black-blood MRI of the aorta and carotid arteries using rapid extended coverage double inversion recovery turbo spin echo sequence [Mani et al., 2004) (Figure 1(A)]. For each subject, cross-sectional images of the aorta (n = 36 to 48) and carotids (n = 12 to 24) were analyzed. Total examination time was less than 1 hour. Average arterial wall area (AWA), a plaque index obtained by normalizing the AWA with respect to body surface area (PI) for both aorta (PIA) and carotids (PIC), average wall thickness (AWT), and maximal wall thickness (MWT) were measured for each resulting image.

Results: There was no significant difference between the patients with AIS and controls with respect to age, gender, mean cholesterol values, 10-year risk percentiles, BMI and traditional cardiovascular risk factors, AWA and PIC. AWT and MWT of both carotid and aorta were higher in AIS

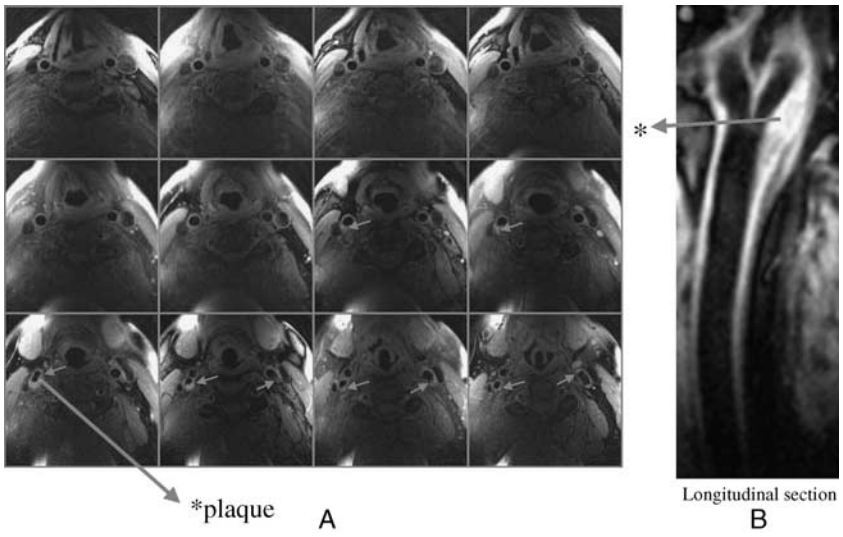

Figure 1.

subjects than in controls (2.3 ± 0.7 vs. 2.1 ± 0.6 mm, p = 0.0407). Aortic AWA was not significantly different between AIS subjects and controls (174.8 ± 42.9 vs. 160.0 ± 52.7, p = 0.22). However, normalized to body surface area, i.e. the PIA of AIS subjects was significantly higher than controls (8.64 ± 2.2 vs. 7.23 ± 1.78, p = 0.047).

Conclusions: This pilot study shows that MRI can be used to determine atherosclerotic profile in AIS patients and that AWT, MWT and PI is higher in patients with AIS. This method may establish a basis for future population studies on clinical screening and monitoring of patients at high risk for AIS.

REFERENCE

Mani, V., Itskovich, V. V., Szimtenings, M., Aguinaldo, J. G. S., Samber, D. D., Mizsei, G., Fayad, Z. A. (2004). Rapid extended coverage (REX) simultaneous multislice black blood vessel wall imaging. *Radiology* 23:281–288.

157. MR Delayed Enhancement Imaging in Post Cardiac Transplant Patients at Yearly Review

Richard E. Slaughter, MBBS, FRACR,[1] Wendy E. Strugnell, BSc,[1] Andrew John Galbraith, BMedSc, MBBS, FRACP,[2] Lora Medoro, MBBS.[1] [1]*Cardiovascular MRI Research Centre, Prince Charles Hospital, Brisbane, Australia,* [2]*Department of Cardiology, Prince Charles Hospital, Brisbane, Australia.*

Introduction: Coronary artery disease involves both large and small coronary vessels and is the main limitation to survival following cardiac transplantation. Cardiac damage at the time of transplantation, episodes of rejection and coronary artery disease may all result in myocardial fibrosis. Delayed enhancement imaging has the potential to demonstrate areas of myocardial fibrosis. This may be helpful in the understanding and management of this patent group.

Purpose: To determine the incidence and nature of delayed myocardial enhancement in post cardiac transplant patients.

Method: 42 post cardiac transplant patients referred for annual MRI assessment were reviewed. MR imaging was performed on a GE Medical Systems 1.5 Tesla Signa Twinspeed system with a 4-element cardiac phased array coil. Steady state free precession (SSFP) cine MR imaging series were acquired to provide functional assessment of the ventricles. Delayed enhancement imaging was performed in the vertical long axis, horizontal long axis and short axis orientations using a segmented inversion recovery fast gradient echo sequence. Images were acquired 8–15 minutes after administration of 0.2 mmol/kg of gadolinium-DTPA, using an inversion time of 200–250 ms.

Autopsy results were available in one case and were correlated with the MR findings.

Results: Areas of delayed myocardial enhancement were present in 16 of the 42 patients. Enhancement pattern fell into 3 groups:

1. Typical ischaemic type post infarct scarring (7 patients)
2. Patchy small areas of enhancement occurring at various locations in the myocardium and often not in a coronary artery distribution (6 patients)
3. Diffuse subendocardial enhancement (3 patients)

Typical ischaemic infarction in these patients most likely results from silent ischaemia due to transplant vasculopathy.

It is possible that some of the small areas of patchy enhancement may also be the result of small vessel diffuse coronary artery disease. In some patients, episodes of rejection were documented and this may be a causative factor.

Diffuse subendocardial fibrosis was present in 3 patients, all of whom were more than 10 years post transplantation. The nature of this process is not fully understood. Autopsy in one patient demonstrated extensive subendocardial fibrosis and fibrosis in the atrial septum which correlated well with the MR findings. Some epicardial fibrosis was also present.

Conclusion: Delayed myocardial enhancement imaging in post cardiac transplant patients may demonstrate areas of previous silent ischaemic infarction, patchy small areas of enhancement of unknown aetiology and diffuse subendocardial fibrosis in long standing post transplant hearts. Correlation with treatment, episodes of rejection and coronary artery anatomy may provide more understanding of the nature of these abnormalities.

158. Value of T2-Weighted-, First-Pass-Enhancement and Cine-MRI to Differentiate Between Acute and Chronic Myocardial Infarction

Gunnar K. Lund,[1] Alexander Stork,[2] Kai Müllerleile,[1] Martin Paul Bansmann,[2] Achim Barmeyer,[1] Gerhard Adam,[2] Thomas Meinertz.[1] [1]*Cardiology, Herzzentrum, Hamburg, Germany,* [2]*Diagnostic and Interventional Radiology, Hamburg, Germany.*

Delayed enhancement (DE) magnetic resonance imaging (MRI) is a validated tool to detect and to size myocardial infarction (MI). However, presence of DE does not differentiate between acute MI (AMI) and chronic MI (CMI), which is a clinically important question. Edema on T2w-MRI is usually found in AMI, whereas wall thinning on cine-MRI is typical for CMI. Furthermore, microvascular obstruction (MO) visualized on first-pass-enhancement (FPE)-MRI is mainly observed after AMI. The purpose of this study was to assess the diagnostic accuracy of myocardial edema on T2w-MRI, presence of MO on FPE-MRI, and wall thinning on cine-MRI to differentiate between AMI and CMI.

Material and Methods: 50 patients were imaged at 1.5 T 5.0 ± 3.3 days and 7.9 ± 2.7 months after AMI using T2w-, FPE-, DE- and cine-MRI. FPE- and DE-MRI were performed during and after injection of 0.1 mmol/kg Gd-DTPA. All images were acquired on identical short-axis planes. In a blinded consensus-reading edema on T2w-MRI, MO on FPE -MRI and wall-thinning on cine-MRI were graded as present or absent. Sensitivity and specificity of these imaging findings were calculated to differentiate between AMI and CMI.

Results: DE was present in all patients in the acute and chronic state. The sensitivity and specificity to differentiate between AMI and CMI were 96% and 98% for edema, 58% and 80% for MO, 92% and 40% for absence of wall-thinning, respectively. Edema was more sensitive to detect AMI than presence of MO ($P < 0.0001$) and edema on T2w-MRI was more specific for AMI than absence of wall-thinning ($p < 0.0001$).

Conclusion: Presence or absence of edema can reliably differentiate between AMI and CMI and is superior to presence of MO or absence of wall-thinning. In presence of delayed enhancement T2w-MRI may be helpful to estimate the age of the infarction.

159. Clinical Safety of Cardiac MRI Prior to Discharge in Patients with Acute Myocardial Infarction and Coronary Artery Stenting with Both Bare Metal and Drug-Eluting Stents

Manesh R. Patel, Timothy S. E. Albert, MD, Emily Honeycutt, MBI, Linda K. Shaw, PhD, Michael H. Sketch, MD, Michael Elliott, MD, Robert M. Judd, PhD, Raymond J. Kim, MD, David E. Kandzari, MD. *Cardiology, Duke University, Durham, NC, USA.*

Background: Magnetic resonance imaging (MRI) is generally felt to be safe in patients with coronary stents once endothelialization has occurred, approximately 6–8 weeks. There is limited data on the clinical safety of cardiac MRI (CMR) in acute myocardial infarction (AMI) patients early after coronary stent placement. With the introduction of drug-eluting stents (DES) into routine clinical care and increased interest in using cardiac MRI in AMI clinical trials, safety data are needed on early CMR after coronary stenting in AMI patients.

Methods: Patients with AMI and coronary stenting who underwent CMR prior to discharge and controls matched for age, sex, diabetes, and MI type (ST-segment elevation-STEMI vs. NSTEMI) were identified from the Duke Cardiovascular Disease Databank. Statistical analysis was performed on the rate of death and any revascularization within 30-days using logistic regression modeling.

Results: 66 patients with acute AMI had 97 stents (39% DES) placed. Cardiac MRI was performed prior to discharge, median 3 days post stenting. The median age was 56 years, 24% were diabetic, and 71% had STEMI. 124 control patients matched for these variables who were alive at day 4 after AMI were identified, see Table 1. Revascularization occurred in 5 (4%) control patients and 1 (1.5%) MRI patient at 30 days ($p = 0.35$). Death or revascularization occurred in 7 (5.6%) of control patients as compared to 1 (1.5%) MRI patient at 30-days ($p = 0.18$; 95% confidence interval 0 to 4.5%).

Table 1. AMI patients with stents and MRI vs. No-MRI

Baseline characteristics	Total N = 190	Control No-MRI N = 124	MRI performed N = 66	P-value ++
Age (median-yrs)	57	58	57	0.597
Diabetes mellitus	40 (21%)	24 (19.4%)	16 (24.2%)	0.431
Myocardial infarction characteristics				
ST-segment elevation MISTEMI	133 (70%)	86 (69.3%)	47 (71.2%)	0.790
Number of stents (% DES)	294	197 (10.2%)	97 (39.2%)	
Outcomes 30-days				
Revascularization	6 (3.2%)	5 (4.0%)	1 (1.5%)	0.344
Death	2 (1.1%)	2 (1.6%)	1 (1.5)	0.299
Death or revascularization	8 (4.2%)	7 (5.6%)	1 (0.1.5%)	0.177

Conclusion: Cardiac MRI appears to be safe when performed early after acute MI and coronary stenting. The risk of death or any revascularization is low and similar to patients who do not undergo cardiac MRI.

160. Contrast Enhanced Magnetic Resonance Imaging: A Novel Approach for Identifying the Infarct Related Artery in Patients with Non-ST Elevation Myocardial Infarction

John F. Heitner, Igor Klem, MD, Manesh Patel, MD, J Kevin Harrison, MD, Peter J. Cawley, MD, Jeffrey Washam, MD, Jonathan W. Weinsaft, MD, Anna Lisa Crowley, MD, Michele Parker, MD, Christopher K. Dyke, MD, Thomas M. Todoran, MD, Michael Elliott, MD, Robert M. Judd, PhD, Michael H. Sketch Jr., MD, Raymond J. Kim, MD. *Duke Univeristy, Durham, NC, USA.*

Background: Patients with non-ST elevation myocardial infarction (NSTEMI) often have multi-vessel disease and/or non-occlusive stenosis. Thus, determining the infarct related artery (IRA) using coronary angiography in NSTEMI patients can be difficult. Contrast enhanced magnetic resonance imaging (ce-MRI) has the ability to identify small areas of myocardial necrosis. The purpose of this study was to define whether ce-MRI improves the diagnostic ability of cardiac catheterization in identifying the IRA in patients with NSTEMI.

Methods: Patients with no prior history of coronary artery disease admitted to the coronary care unit with NSTEMI underwent ce-MRI prior to cardiac catheterization. Images were interpreted by readers blinded to patient care related decisions. The interventional cardiologists were blinded to results of the ce-MRI and documented each coronary vessel territory on a 17-segment model and assigned the IRA. The ce-MRI was interpreted blinded to angiography and also evaluated using this 17-segment model. The IRA was defined as the artery that supplied the territory with sub-endocardial infarction by ce-MRI. Ce-MRI was considered indeterminate if there was no evidence of infarction by ce-MRI or if there was > 1 coronary artery territory of infarction.

Results: Thirty patients, mean age 59.7 years, 53% female, were studied. Ten patients had insignificant coronary artery disease (< 50% epicardial stenosis) by cardiac catheterization, 4 had 1-vessel disease, 7 had 2-vessel disease, and 9 had 3-vessel disease. Fifteen patients underwent revascularization (PCI, n = 8; CABG, n = 7). Cardiac catheterization identified the IRA in 16 of the 30 (53%) patients. Ce-MRI identified the IRA in a significantly larger number of patients 26 of 30 (87%), $p < 0.0074$. Of the 4 patients that were ineterminate by ce-MRI, 3 were due to inability to visualize the infarct and 1 was due to infarct in more than one coronary vascular territory. The addition of infarct location by ce-MRI identified the IRA in 11 of the 14 patients in which the IRA could not be determined by cardiac catheterization alone. Two patients underwent PCI of an artery that was not the IRA by ce-MR.

Conclusion: Ce-MRI identified the IRA in significantly more patients than cardiac catheterization. Use of ce-MRI to identify IRA in NSTEMI patients may be a novel approach to help guide appropriate coronary revascularization strategies.

161. Changes in Left Atrial Geometry and Function After Left Atrial Ablation

Meyer M. Thomas, MD, Robert L. Eisner, PhD, Susan Eder, David B. Delurgio, MD, Fernando V. Mera, MD, Anita Bhandiwad, MD, Angel R. Leon, MD. *The Carlyle Fraser Heart Center, Emory Crawford Long Hospital, Atlanta, GA, USA.*

Background: Left atrial (LA) linear radiofrequency (RF) ablation has been shown to be effective in the elimination of atrial fibrillation (AF). While previous magnetic resonance imaging (MR) studies have investigated LA volume changes as a result of AF ablation, there is limited, if any, MR data on the effect of this procedure on LA function. Because of the extensive radiofrequency LA lesions produced during this procedure, there is a concern that AF ablation may adversely affect LA function. Therefore, we sought to

Table 1. Changes in LA volume, LA EF, and A-wave velocity before and after AF ablation

Patient	LA volume Pre, ml	LA volume Post, ml	Volume change (%)	LA EF Pre, %	LA EF Post, %	EF % change	A-wave velocity Pre (cm/s)	A-wave velocity Post (cm/s)	A-wave velocity % Change
1	116	101	−13%	40	43	+8	18	12	−20
2	72	95	+32%	54	40	−26	29	17	−41
3	99	76	−23%	48	34	−29	20	14	−30
4	83	104	+25%	46	35	−24	12	7	−42
5	94	92	−2%	45	40	−11	28	13	−54
6	92	63	−32%	46	37	−20	48	18	−63
7	71	53	−25%	N/A	N/A	–	N/A	N/A	–
8	115	89	−23%	N/A	N/A	–	N/A	N/A	–
9	72	67	−7%	N/A	N/A	–	N/A	N/A	–
10	81	73	−10%	N/A	N/A	–	N/A	N/A	–
11	136	124	−9%	N/A	N/A	–	N/A	N/A	–
MEAN	94 (+/− 21)	85 (+/− 21)	−8% (+/− 20) *(p = 0.13)*	52 (+/− 14)	38 (+/− 3)	−17% (+/− 14) *(p = 0.10)*	26 (+/− 13)	14 (+/− 4)	−37% (+/− 16) *(p = 0.03)*

Changes in LA volume before and after LA ablation. In patients in sinus rhythm during both exams (Patients 1–6), changes in LA EF and A-wave velocity was also calculated.

determine the effects of LA linear ablation on atrial function and remodeling by measuring changes in atrial ejection fraction (EF), peak atrial contraction velocity (A-wave) and LA volume changes.

Methods: Eleven patients with AF underwent LA ablation. Cardiac MR and contrast-enhanced MR angiography (CE-MRA) were performed at baseline and three months post ablation (Philips 1.5T Intera CV).

Sequences: 1) Cine-MR of the left atrium in the short axis (ECG-gated, Balanced Turbo Field Echo, TR 3.0, TE 3.1, 8–10 mm slice thickness) 2) Phase velocity mapping (ECG-gated, TR 5.4, TE 3.0, 8 mm slice thickness, 20 phases) in a short axis plane perpindicular to mitral valve in-flow in the left ventricle 3) CE-MRA (3D MRA, TR 4.6, TE 1.4).

Analysis: All analyses were performed using EasyVision software (Philips Medical Systems). LA volume was measured from the CE-MRA. In addition, for the six patients that were in sinus rhythm (SR) during both the pre- and post-MR scans, an atrial ejection fraction (EF) was calculated from the maximal atrial volume (after atrial filling) and the minimal atrial volume (after active atrial contraction) obtained on cine-MR images. For these patients in SR, we also measured the maximal A-wave velocity (representing active atrial contraction) from the phase velocity mapping.

Results: Changes in LA volumes and EF before and after ablation for individual patients are shown in Table 1. Most patients (9 of 11) had a significant decrease in LA volume after ablation. In the six patients in whom EF could be calculated, five of the six had a decrease in LA EF after AF ablation. However, all six patients had a decrease in atrial function as measured by A-wave velocity (mean velocity pre-ablation 26 cm/s (+ / − 13) and post-ablation 14 cm/s (+ / − 4), p = 0.03). A representative mitral inflow velocity curve for Patient 3 is shown in Figure 1.

Conclusions: 1) In most patients, LA linear RF ablation results in a reduction in LA volumes. However, this apparent

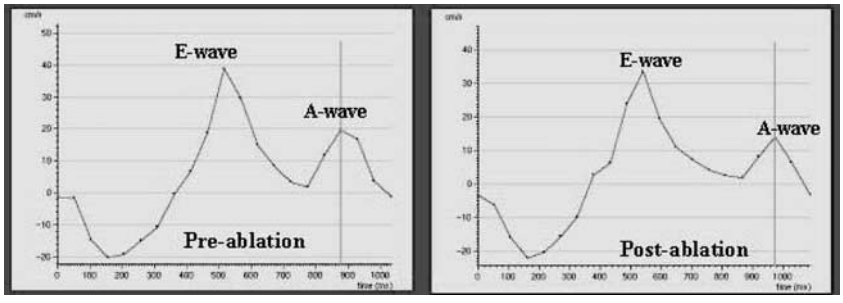

Figure 1. Mitral inflow velocity curves pre- and post-ablation for patient 3. A-wave velocity decreased from 20 cm/s to 14 cm/s.

positive remodeling did not translate into improved atrial function as measured by LA EF and active atrial contaction velocities (A-wave). In fact, our data indicates that atrial function may actually worsen as a result of the extensive lesions produced with LA ablation. 2) Using Cine-MR and phase velocity mapping of mitral inflow, MR imaging is a useful tool to measure left atrial function, especially before and after AF ablation.

162. Pulmonary Hypertension: Comparison Between Pulmonary-Aortic Transit Time Measured by Cardiac Magnetic Imaging and Right Heart Catheterization

Martin R. Goyenechea, MD,[1] Javier Sanz, MD,[1] Santo Dellegrottaglie, MD,[1] Roxana Sulica, MD,[1] Valentin Fuster, MD, PhD,[1] Sanjay Rajagopalan, MD,[1] Michael Poon, MD.[2] [1]*The Zena and Michael A. Wiener Cardiovascular Institute/ Mount Sinai Medical School, New York, NY, USA,* [2]*Cabrini Medical Center, New York, NY, USA.*

Introduction: Right heart catheterization (RHC) is the gold standard for diagnosis and assessment of therapeutic response in pulmonary hypertension (PH). However, it is an invasive procedure and is associated with significant risks. Non-invasive parameters that could serve as potential surrogates for pulmonary hemodynamics and outcome could be valuable in this disease.

Purpose: The aim of this study is to compare RHC hemodynamic measurements with pulmonary-aortic transit time (PATT) as determined by cardiac magnetic resonance (CMR) time-resolved pulmonary angiography in patients with PH.

Methods: 48 patients with suspected PH (43 women, 5 men; age range 24–88 years) underwent CMR including a left anterior oblique contrast enhanced time resolved 3D angiogram of the aorta and pulmonary arteries. RHC was performed within one week. Using a dedicated workstation for post-processing, circular regions of interest were drawn in the main pulmonary artery and the ascending aorta. Signal intensity-time curves were generated and the PATT was calculated measuring the time interval between the peak signal intensity in the pulmonary artery and in the aorta.

Results: Of the 48 patients, 41 were confirmed to have PH (mean pulmonary artery pressure > 25 mm Hg at rest or 30 mm Hg with exercise) by RHC. There was a strong negative correlation between pulmonary artery oxygen saturation (PAOS) and PATT ($r = -0.76$, $P < 0.0001$). There was a moderate correlation between PATT and pulmonary vascular resistance index ($r = 0.53$, $P < 0.0001$). No significant correlation was noted between PATT and mean or systolic pulmonary pressures.

Conclusion: PAOS is a reliable indicator of cardiac index and a strong predictor of clinical outcome in patients with PH. Our results demonstrated that PATT correlates negatively with PAOS and positively with pulmonary vascular resistance index. Thus PATT as determined by CMR time-resolved pulmonary angiography may be used as a noninvasive diagnostic technique for assessing and predicting outcome of this frequently undiagnosed disease.

163. Submillimeter Spatial-Resolution Contrast-Enhanced MRA of the Carotid Arteries Using Ferumoxytol in Humans

Vu M. Mai,[1] Sean Tutton, MD,[1] Wei Li, MD,[1] Linda Pierchala, BS,[2] Belinda S. Y. Li, PhD,[3] Ying Wu, MD,[1] Pottumarthi V. Prasad, PhD,[1] Joel Meyer, MD,[1] William J. Ankenbrandt, MD,[1] Robert R. Edelman, MD.[1] [1]*Radiology, Evanston Northwestern Healthcare and Feinberg School of Medicine, Northwestern University, Evanston, IL, USA,* [2]*Radiology, Evanston Northwestern Healthcare, Evanston, IL, USA,* [3]*Applied Science Laboratory Central, GE Healthcare, Evanston, IL, USA.*

Purpose: To study the feasibility of very high-resolution CE-3DMRA of the extracranial carotid artery (CA) using ferumoxytol.

Introduction: Current first-pass methods for CE-3DMRA of the CA suffer from limited spatial resolution. This problem can be overcome using nearly isotropic, very high-resolution MRA with ferumoxytol.

Methods and Subjects: Ferumoxytol (Advanced Magnetics Inc., Boston, MA), an iron oxide blood pool contrast agent with a plasma half-life of 14 hours, was used to obtain very high-resolution MRA of the extracranial CA. Studies were performed with IRB approval and informed, written consent. A dosage of 4 mg/kg diluted to 7.5 mg/ml was infused at 2 cc/sec. All studies were performed on a 1.5 T system (GE Medical Systems, Milwaukee, WI) equipped with TwinSpeed gradients and a 4-channel neurovascular coil and a 4-channel carotid coil. A series of 10 subjects (6 volunteers and 4 patients, 4 male/6 female, average age of 51.1) were studied. First-pass imaging was performed using a temporally-resolved TRICKS acquisition with the neurovascular coil. This was followed by an optimized very high-resolution 3DMRA sequence using the following parameters: TR/TE of 4.9 msec/1.4 msec, sampling BW of 83 kHz, FOV 26 cm, matrix size of 512 × 512, 1 NEX, and interpolated partition thickness of 0.8 mm. The in-plane spatial resolution was 0.5 mm × 0.5 mm. An axial 3D volume of 128 partitions covering the circle of Willis through the extracranial carotid bifurcation was acquired in approximately 5.5 min. In addition, a 3DMRA with lower in-plane resolution (1.0 mm × 1.0 mm, i.e. a matrix of 256 × 256) as well as a pre-contrast axial 2D TOF MRA with an in-plane resolution of 1.0 mm × 2.0 mm were acquired. We then changed to the

Figure 1. Shown are the right carotid arteries at isotropic resolution of 0.4 mm × 0.4 mm × 0.4 mm from a normal volunteer (left) and a patient with partially stenosed carotid artery (right).

carotid coil, and repeated the 3DMRA acquisitions at the aforementioned spatial resolutions. The volume location was centered on the bifurcation of the CA. In addition, we also acquired 3DMRA at isotropic voxel resolution of 0.4 mm × 0.4 mm × 0.4 mm from 5 of the 10 subjects (3 volunteers and 2 patients).

Multiplanar and maximum intensity reconstructions were performed. SNR of blood, muscle, and fat and CNR of blood relative to muscle and fat were measured in the source image of multiplanar reconstructions. Each source image was selected at level immediately before the carotid arteries bifurcated.

Results: No adverse events occurred. Very high-resolution MR angiograms showed improved delineation of the CA compared with first-pass images, steady-state images acquired at 256 × 256, and 2D TOF MRA. Oblique multiplanar reconstructions eliminated venous overlap and provided excellent delineation of the carotid bifurcations from a healthy and a patient volunteer with confirmed partial stenoses (Fig. 1). The average SNR and CNR from all subjects listed in Table 1 show that very high-resolution CE-3DMRA of the extracranial CA using ferumoxytol is feasible and can be useful in measuring the degree of stenosis.

Conclusion: Limitation of spatial resolution of current first-pass methods for CE-3DMRA of the CA can be overcome using nearly isotropic, very high-resolution MRA with ferumoxytol. The method has the potential to improve the accuracy and precision of measurements of carotid artery disease compared with current MRA methods.

164. Real-Time Guidance Strategy for Pulmonary Vein Ablations: Is XMR A Feasible Approach?

Sanjeet Hegde, MBBS, MRCPCH,[1] Kawal Rhode, PhD,[2] P. Lambiase, MBBS, MRCP,[3] M. Sermesant, PhD,[2] D. Hill, PhD,[2] J. Gill, MBBS, MRCP,[3] Reza Razavi, MBBS, MRCP, MD.[1] [1]*Imaging Sciences/Pediatric Cardiology, King's College London, London, UK,* [2]*Imaging Sciences, King's College London, London, UK,* [3]*Cardiology, St. Thomas' Hospital, London, UK.*

Introduction: Hybrid XMR interventional suites with X-ray and Magnetic Resonance (MR) imaging facilities offer the potential to carry out catheter interventions using a combination of the imaging techniques.

Hypothesis: XMR guided intervention combining MR three-dimensional anatomical images with conventional x-ray fluoroscopic images facilitates interventional cardiac catheterisation and radio-frequency ablation.

Methods: Imaging: Two MR scans were performed, one was a multislice volume (typically 512 × 512 matrix, 40 slices, resolution = .68 × . 68 × 1.4 mm^3, TR = 4.3 ms, TE = 1.4 ms, flip angle = 40°) to localise a skin marker and the other was a Gadolinium enhanced magnetic resonance angiography (typically 512 × 512 matrix, 50 slices, resolution = .84 × .84 × 1.8 mm^3, TR = 3.8 ms, TE = 1.2 ms, flip angle = 40°) of the relevant anatomy was performed in all patients and volume rendering of the pulmonary veins obtained.

Procedure: Following MR acquisition patients were moved to the x-ray end of the suite were optical tracking was used to determine the transformation matrices relating MR and x-ray image coordinates thus allowing real-time image fusion.

We applied the XMR technique to guide pulmonary vein ablation in ten patients (n = 10) with atrial fibrillation. During the procedure, the guidance system displayed the MR derived anatomical surface overlaid onto the x-ray images of the

Table 1. The average snr and cnr and their standard deviations from all volunteers of 3dmra data acquired with neurovascular and carotid coils at different in-plane spatial resolutions (b-blood, m-muscle, f-fat)

		SNR			CNR	
Coil	Matrix	B	M	F	B-M	B-F
Neurovascular	256 × 256	55.5 ± 26.7	7.9 ± 2.7	24.6 ± 11.0	47.7 ± 24.4	30.9 ± 20.1
	512 × 512	15.2 ± 3.7	3.4 ± 0.8	8.6 ± 2.8	11.8 ± 3.0	6.6 ± 2.6
Carotid	256 × 256	211.3 ± 85.7	22.1 ± 7.1	121.4 ± 55.9	189.2 ± 86.9	89.9 ± 43.8
	512 × 512	69.2 ± 24.2	9.0 ± 3.1	47.3 ± 24.3	60.1 ± 25.4	21.9 ± 13.2

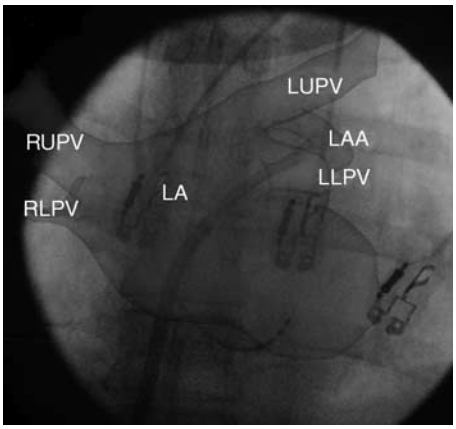

Figure 1.

catheters being used. The view selection mode of the guidance system was also used at times to orientate the c-arm to gain the appropriate x-ray view. Registration errors were shown to be clinically acceptable for alignment of images of the heart and the great vessels.

Results: The interventionalists were able to employ the XMR technique to guide a 16 electrode helical ablation catheter (Revelation Helix, Cardima, CA, USA) into three pulmonary veins (right upper, left upper and left lower) to carry out electrical isolation in all cases. Figure 1 shows the guidance system overlay when the delivery catheter was placed in the left lower pulmonary vein.

Conclusion: This technique offers a distinct advantage over conventional approach by way of superior anatomical visualisation of the left heart allowing easier guidance of catheters into the pulmonary veins. We were also able to choose working x-ray views without the administration of any additional x-ray dose by moving the c-arm until the anatomical overlay was suitably positioned. We have demonstrated that our technique can be successfully used to guide cardiac electrophysiology procedures.

165. Cartesian Self-Gated Cine MRI: Initial Clinical Experience

David N. Sandman, MD,[1] James C. Carr, MD,[1] John Salanitri, MD,[1] Mark E. Crowe, MS,[1] Randall R. Kroeker, PhD,[2] Andrew C. Larson, PhD,[1] F. Scott Pereles, MD,[1] Orlando P. Simonetti, PhD.[2] [1]*Department of Radiology, Feinberg School of Medicine, Northwestern University, Chicago, IL, USA,* [2]*Siemens Medical Solutions, Chicago, IL, USA.*

Introduction: ECG-gating requires additional patient preparation time, is susceptible to RF and magnetic interference, and is ineffective in a significant percentage of patients (Wozney et al., 1990). More recently, self-gating techniques have been described using either radial (Larson et al., 2004) or conventional Cartesian (Crowe et al., 2004) k-space sampling to potentially eliminate the need for external physiological signal monitoring. Self-gated cine with Cartesian sampling avoids the streak artifacts of radial imaging, and was recently shown to have equivalent image quality to ECG gated cine in a sample of healthy volunteers (Crowe et al., 2004). The purpose of this study is to demonstrate the clinical effectiveness of the self-gated cine sequence in a sample of patients referred for clinical cardiac MRI exams.

Table 1. Results of data analysis

	Mean single-plane ejection fraction	Mean overall image quality score	Mean artifact score
ECG-gating	55.35 (n = 19)	3.67 (n = 40)	0.55 (n = 40)
Self-gating	56.11 (n = 19)	3.56 (n = 40)	0.72 (n = 40)
P-value	**0.13**	**0.07**	**< 0.001**

The differences in ejection fractions and overall image quality were not statistically significant ($p > 0.05$). Artifact differences were significant though both mean scores were less than 1, signifying a less than "minimal" artifact score.

Methods: The sequence: This technique is a modified retrospectively gated TrueFISP cine sequence that acquires a short second echo after the readout and phase gradients have rewound. The peak amplitude of the second echo varies in proportion to the average signal in the image, which is expected to change in synchrony with the cardiac cycle. A band-pass filter (0.2 Hz–3 Hz pass-band) is applied to the echo-peak information to remove noise, and a peak-detection algorithm determines the trigger times.

Experimental Setup: Three to five slices, including short and long-axis views, were obtained in 9 patients (6 female, 3 male, 21–92 years [mean 56 years]) for a total of 40 measurements. ECG and self-gated image series were

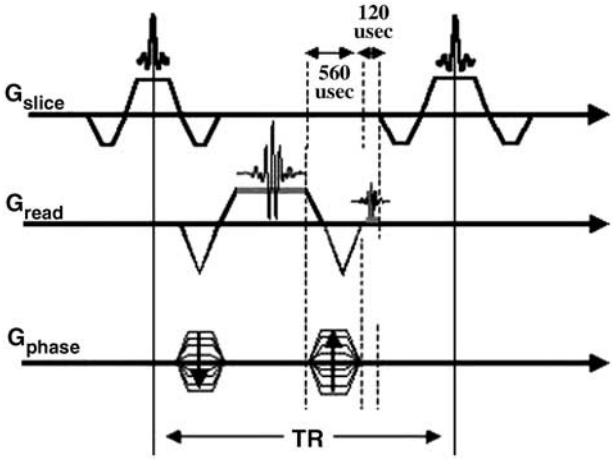

Figure 1. This self-gated, Cartesian True FISP sequence uses a short second echo to acquire the central k-space information necessary to derive a gating signal.

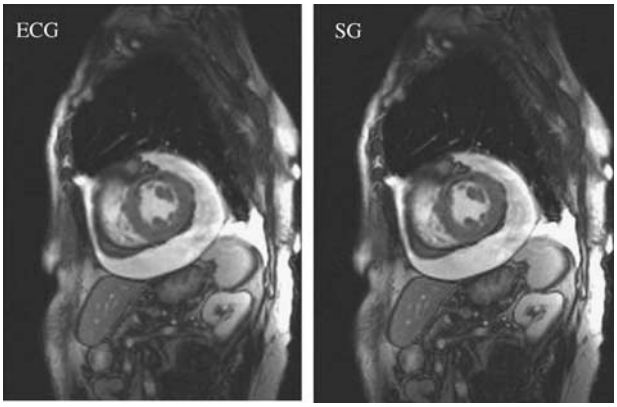

Figure 2. End-diastolic, short axis images comparing ECG-gating and self-gating sequences in a patient with a pericardial effusion.

retrospectively reconstructed from each measurement, resulting in 80 series. Indications for cardiac MR were variable, ranging from pulmonary vein mapping to viability studies. Imaging was performed using a Siemens 1.5 T Avanto with a 12-element body array coil. Breath-held acquisitions were performed using the following parameters: 263 mm * 350 mm FOV, 135 phase-encoding lines, 16 phases, 3.42 ms TR, 59.7 ms temporal resolution, 6 mm slice thickness, and a 1000 Hz/pixel bandwidth. Short axis series (n = 42) were evaluated to quantify left ventricular single-plane ejection fractions in a blinded fashion. All 80 series were evaluated for overall image quality (1–5 scale) and degree of artifact (0–3 scale) by two independent, blinded reviewers. All data were analyzed using a two-tailed paired t-test with statistical significance set at the 5% level.

Results: Quantitative results showed that there was no statistically significant difference between the calculated ejection fractions of the ECG-gated and self-gated acquisitions (p-value = 0.13). Qualitative evaluations were analyzed by pooling the data of the two reviewers. For overall image quality, there was no statistically significant difference between the two techniques (p-value = 0.07). There was a slightly higher rated level of artifact for the self-gated images which was statistically significant (p-value < 0.001) (Table 1).

Conclusion: Self-gated cine TrueFISP sequences, using a conventional Cartesian sampling scheme, showed no difference from ECG-gated sequences in quantifying single-plane ejection fractions and evaluating overall image quality in a sample of patients referred for clinical cardiac MR. There was a slight difference in qualitative assessment of artifact, with the average score indicating less than ''minimal'' artifact for both techniques, though quantitative results and overall quality of the images were unaffected. This self-gating technique has many advantages to ECG-gating and needs to be assessed in a larger population of patients with significantly depressed cardiac function (Figs. 1–3).

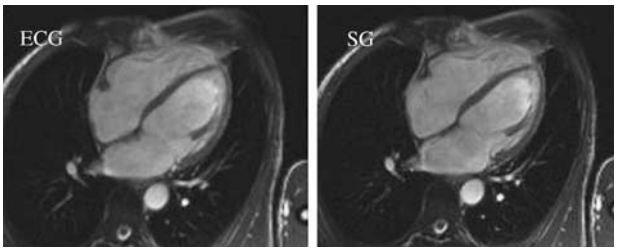

Figure 3. End-diastolic, long axis images comparing ECG-gating and self-gating sequences in a patient referred for pulmonary vein mapping prior to radiofrequency ablation of atrial fibrillation.

REFERENCES

Crowe, M. E., Larson, A. C., Zhang, Q., Carr, J. C., White, R. D., Li, D., Simonetti, O. P. (2004). Automated rectilinear self-gated cardiac cine imaging. *Magn. Reson. Med.* 52. in press.

Larson, A., White, R., Laub, G., McVeigh, E., Li, D., Simonetti, O. (2004). Self-gated cardiac cine MRI. *Magn. Reson. Med.* 51:93–102.

Wozney, P., Prorok, R., Petchney, R. (1990). Optimizing MR image quality: artifact causes and cures. In: Marcus, M. L., et al., eds. Cardiac Imaging. Philadelphia: Saunders, 776–793.

166. Free-Breathing Whole-Heart MRI with 3D-Radial SSFP and Self-Navigated Image Reconstruction

Christian Stehning,[1] Peter Boernert, PhD,[2] Kay Nehrke, PhD,[2] Holger Eggers,[2] Matthias Stuber, PhD[3] [1]*Institute of Biomedical Engineering, University of Karlsruhe, Karlsruhe, Germany,* [2]*Philips Research Laboratories, Hamburg, Germany,* [3]*Radiology, Johns Hopkins University, Baltimore, MD, USA.*

Introduction: In free-breathing, navigator-gated coronary MRA, the correlation between the measured navigator position and the actual position of the heart may be adversely affected by hysteretic effects, navigator location, and time delays between navigators and image acquisition. In addition, irregular breathing patterns during navigator-gated scanning may result in low scan efficiency and prolonged scan time. The purpose of this study was to implement a self-navigated, free-breathing, whole-heart 3D coronary MRA technique that is independent of navigator location and that minimizes time-delays between navigator and image acquisition. A signal synchronous to respiration was extracted directly from the echoes acquired for imaging, and the resolved motion information was used for retrospective rigid body through-plane motion correction.

Purpose: To develop a self-navigated, free-breathing whole-heart acquisition without the need for additional pencil-beam navigators.

Methods: A 3D-radial sampling pattern (Barger et al., 2002) was subdivided into interleaves, where one interleaf as shown in Fig. 1(A) is acquired in every cardiac cycle. The first echo was acquired in superior-inferior (SI) orientation to

sense respiratory motion using a center-of-mass approach (Larson et al., 2004) [“navigator projection”, Fig. 1(B)]. The sequence was implemented on a commercial 1.5 Tesla MR system (Philips Intera) equipped with a 5-element cardiac phased array coil. A bright-blood sequence (steady state free precession, SSFP) was used. To suppress signal from the static anterior chest wall, a regional saturation (REST) slab was applied prior to sampling. The following sequence parameters were used: $\alpha/2$-TR/2 start-up pulse; 20 dummy cycles; 32 readouts per RR-interval; $\alpha = 60°$; matrix: 256^3; FOV: $(300\ \text{mm})^3$; voxel size: $(1.17\ \text{mm})^3$; TR/TE: 4.2/2.1 ms; 16384 readouts, receiver bandwidth 781 Hz/pixel. For motion-corrected image reconstruction, the echoes measured in each cardiac cycle were modulated with a linear phase in k-space, which is determined by the SI-shift measured using the navigator projections and the azimuthal angle of the current readout.

To visualize the coronary vessels, the isotropic image data set was reformatted off-line. The images obtained with the self-navigated image reconstruction were compared to the results obtained using conventional prospective pencil-beam navigator tracking.

Results: A motion-corrected image using the conventional pencil-beam navigator for respiratory tracking is shown in Fig. 2(A), while a motion-corrected image using the self-navigated image reconstruction is displayed in Fig. 2(B). On both images, the proximal right coronary artery (RCA) is visualized. However, the vessel appears with better delineation and contrast when self-navigation is used. Some residual motion artifacts (blurring and streaking) are present in both images.

Discussion: This preliminary in-vivo study has shown that using the proposed 3D-radial acquisition scheme with navigator projections, a signal synchronous to respiration can directly be extracted from the image data, and can be used for retrospective respiratory motion correction. The motion information is obtained from a projection through the heart instead of the diaphragmatic position, which may eliminate potential hysteretic effects, and a minimal delay between the measurement of respiratory motion and the image acquisition is obtained. With this technique, the image quality was improved when compared to images obtained using a pencil-beam navigator for tracking. Residual motion artifacts primarily originate from static structures (e.g. anterior chest wall) in the imaged volume. However, this is a limitation of navigator tracking using pencil beams as well.

Conclusion: A fast, free-breathing whole-heart 3D coronary MRI technique with isotropic spatial resolution and intrinsic suppression of respiratory motion artifacts was implemented on a commercial MRI system. No additional pencil-beam navigators were neccessary, and the method permits the use of magnetization preparation pulses without compromising the performance of respiratory motion detection and -correction.

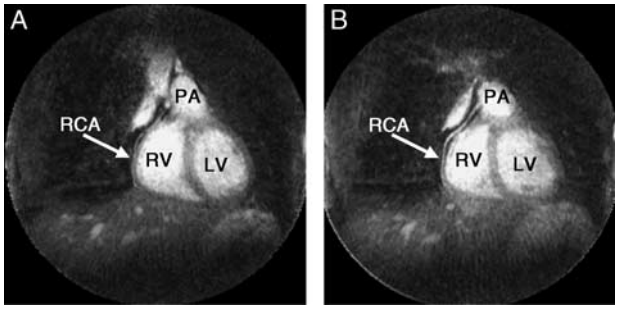

Figure 2. In vivo experiment. A reformatted view of the RCA from a volumetric acquisition obtained with navigator tracking (A) and with self-navigated image reconstruction (B). LV = left ventricle, RV = right ventricle, PA = pulmonary artery, RCA = right coronary artery.

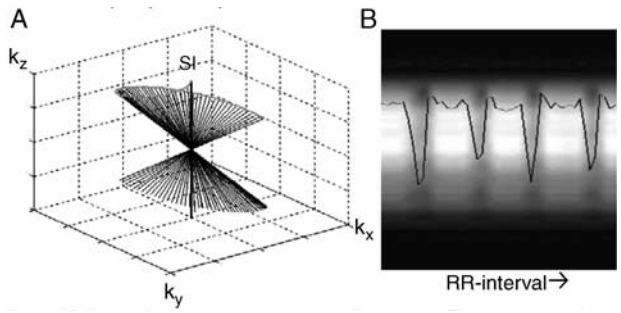

Figure 1. 3D Radial sampling with navigator projection. The acquisition of k-space is divided into interleaves, of which one is shown (A). The black solid line is the first echo, which is oriented in SI-direction. The respiration-induced bulk cardiac motion was extracted in-vivo from the 1D-FT of this echo [navigator projection, (B)] using a center-of-mass approach. The measured respiration-induced SI-shift of the heart is plotted as a solid curve in (B).

REFERENCES

Barger, A. V., et al. (2002). *MRM* 48:. 297–305.
Larson, A. C., et al. (2004). *MRM* 51:. 93–102.

167. Intraindividual Comparison of Coronary MR Angiography and Coronary CT Angiography in Calcified Coronary Segments

Murat Ozgun,[1] Michael Rink,[1] Andreas Hoffmeier, MD,[2] René M. Botnar, PhD,[3] Walter Heindel, MD,[1] Roman Fischbach, MD,[1] David Maintz, MD.[1] [1]*Department of Diagnostic Radiology, University of Muenster, Muenster, Germany,* [2]*Department of Cardiothoracic Surgery, University of Muenster, Muenster, Germany,* [3]*Beth Israel Deaconess Medical Center, Cardiovascular Division, Boston, MA, USA.*

Introduction: Coronary MR Angiography (CMRA) and Coronary CT Angiography (CTA) are alternative modalities for noninvasive coronary angiography.

Purpose: To investigate the effect of calcifications on the interpretability of luminal stenosis using Turbo-Field-Echo (TFE) and Steady-State-Free-Precession (SSFP) coronary MRA sequences in comparison to multidetector-row CTA.

Methods: 21 patients with known CAD were examined with a navigator (NAV) gated and corrected free-breathing 3D-segmented-gradient-echo (TFE) CMRA sequence (in-plane resolution 0.7 × 0.7 mm), a 3D-SSFP-CMRA sequence (inplane resolution 1 × 1 mm) and 16-slice coronary CTA (in-plane resolution ca. 0.3 × 0.3 mm). CMRA was performed either in transverse orientation for the left (5 segments: LM, LAD prox., LAD mid., CX prox., Cx mid.) or in a double oblique plane along the right coronary artery system (prox., mid. and distal segment). Segment-based analysis for the detection stenoses larger than 50% was performed and compared to results of the goldstandard conventional x-ray coronary angiography (XA). For calcification grading, each calcified plaque's mass was measured using a standard calcium scoring tool. Segments with relevant artery stenoses in XA were divided into four groups (A–D) according to their mass of calcification: group A was not evaluable in CTA because of severe calcification, group B high-grade calcification (> 25 mg CaHA), group C with a mass of 10–24.99 mg CaHA and group D with low mass (0–9.99 mgCaHA) (Fig. 1).

Results: Of 168 possible segments, 26 were calcified, had a relevant stenosis and were imaged by all three modalities. 9 segments were not evaluable because of severe calcification in CTA (group A, mean calcification 41.24 ± 28 mg CaHA).

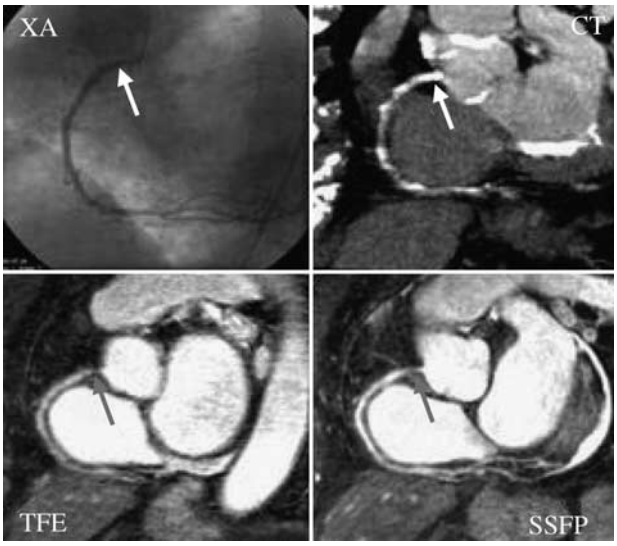

Figure 1. High-grade stenosis of proximal right coronary artery as proven in XA. CTA shows severe calcification, degree of stenosis not assessable. Both MRA sequences (TFE, SSFP) nicely depict the stenosis.

Of these, 4/6 were accurately diagnosed by SSFP, 3 segments were not evaluable due to poor image quality. With the TFE sequence accuracy was 2/4 with 5 segments not evaluable. For the other groups the accuracy for the detection of relevant artery stenoses in calcified segments were: group B included 7 segments (mean calcification 44.24 ± 18.85 mg CaHA): CTA accuracy 6/7, SSFP: 5/7, TFE: 2/3 with 4 excluded segments because of insufficient image quality. Group C included 10 segments (mean calcification 17.42 mg CaHA ± 4.38 mg): CTA accuracy 8/10, SSFP: 6/9, 1 segment not evaluable, TFE: 5/9, 1 segment not evaluable. Group D included 9 segments (mean calcification 1.49 ± 2.9 mg CaHA): CTA accuracy 7/9, SSFP: 8/9, TFE: 5/7, 2 excluded segments.

Conclusions: In segments with severe calcifications not interpretable with CTA, MRA might provide additional information. SSFP seemed to be superior for the detection or exclusion of coronary stenosis in comparison to TFE. For all three groups with segments interpretable by CTA, CTA offered superior accuracy compared to both CMRA sequences.

168. Feasibility of Single Breath-Hold Whole Heart Coverage Coronary MRA Using Highly Accelerated Parallel Imaging with a 32-Channel MR System

Thoralf Niendorf, PhD,[1] Christopher J. Hardy, PhD,[2] Randy O. Giaquinto,[2] Patrick Gross, PhD,[2] Harvey Cline, PhD,[2] Robert D. Darrow,[2] Shmuel Cohen, MAB,[3] Sanjay Joshi,[4] Gontran Kenwood, PhD,[2] Neil M. Rofsky, MD,[3] Daniel K. Sodickson, PhD, MD.[3] [1]*GE Healthcare Technologies, Applied Science Laboratory, Department of Radiology, Beth Israel Deaconess Medical Center, Harvard Medical School, Boston, MA, USA,* [2]*GE Global Research Center, Niskayuna, NY, USA,* [3]*Department of Radiology, Beth Israel Deaconess Medical Center, Harvard Medical School, Boston, MA, USA,* [4]*GE Healthcare Technologies, Waukesha, WI, USA.*

Introduction: Clinical 3D MRA applications are generally restricted to thin targeted slabs due to the competing constraints of acquisition time, signal-to-noise ratio (SNR) and spatial resolution. Alternatively, the use of large imaging volumes supports the visualization of tortuous segments of the coronary arteries using free breathing techniques (Weber et al., 2003). The use of many element coil arrays in conjunction with order-of-magnitude accelerated parallel imaging offers the potential for baseline SNR improvements, enhancements in the immunity to physiological motion and fundamental scan time reductions. It also affords the use of heretofore inaccessible comprehensive imaging volumes for single breath-hold whole heart coverage CMRA.

Purpose: This study demonstrates the feasibility of whole heart coverage CMRA using parallel imaging with two-dimensional accelerations (net acceleration as high as 16-fold)

with a 32-channel coil array/receiver system without exceeding clinically acceptable breath-hold times. This approach may render localizer scans obsolete and enhance patient comfort by substantially reducing otherwise prohibitive examination times.

Methods: Our 32-channel parallel array consisted of two 4×4 arrays on separated clamshell formers measuring approximately 40 cm (Hardy et al., 2003; Zhu et al., 2004). A 32-channel acquisition system including multiple sets of system electronics (GE Medical Systems, Waukesha, WI, USA) was employed for signal transmission/reception. A 3D SSFP pulse sequence was customized to synchronize the prospectively ECG gated data acquisition for all 32 channels. CMRA was conducted on normal volunteers. 3D SSFP was performed using: FOV = 40 cm, data matrix = 256×256, TE = 1.9 ms, TR = 3.7 ms. Data acquisition is completed in a single heartbeat for each acquired slice partition (Niendorf et al., 2004). Net acceleration factors of 8 (4×2) to 16 (4×4) were applied for 2D acceleration distributed to both phase encoding directions. For single breath-hold whole heart coverage CMRA large 3D axial slabs consisting of up to 120 slice partitions covering a S-I volume of 12 cm were acquired (interpolated voxel size of $(0.8 \times 0.8 \times 1.0)$ mm^3). Images were reconstructed using the generalized encoding matrix approach (Sodickson et al., 2001).

Results: Highly accelerated large-volume CMRA is compared with traditional thin-slab CMRA in Figure 1. The application of 8-fold (4×2) accelerated parallel imaging in conjunction with 3D SSFP revealed high image quality as demonstrated in Fig. 1A. The origin, proximal and more distal segments of the RCA are clearly visible for the highly accelerated large volume approach (Fig. 1A). For comparison Fig. 1B depicts the image quality derived with the unaccelerated conventional approach using restricted targeted slab acquisition. As shown in Fig. 2 clear delineation of the proximal segment of the RCA is still preserved for large-volume scans at acceleration factors as high as 16 (4×4), though available SNR becomes progressively challenging as acceleration increases. Note, the 16-fold accelerated dataset (Fig. 2B) also used a reduced slice thickness compared with the 8-fold accelerated data set (Fig. 2A), which also contributed to the SNR degradation.

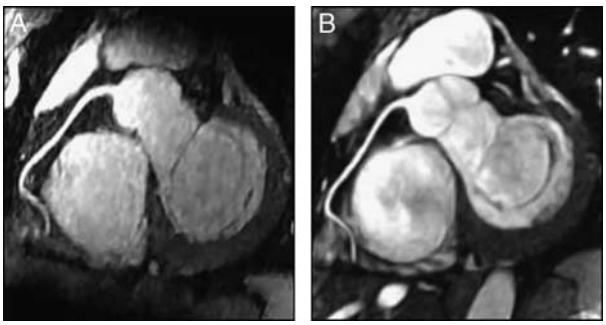

Figure 1. RCA images (MIP, 3 mm slice thickness) obtained from single breath-hold scans of the same subject using (A) a comprehensive volume acquisition (12 cm S-I coverage) together with 8-fold (4×2) accelerated parallel imaging and (B) an unaccelerated small targeted slab acquisition. Images were acquired using a 32 element RF-coil array. The origin, proximal and distal portion of the RCA are visualized in the raw data sets obtained for both large volume and the targeted slab acquisition.

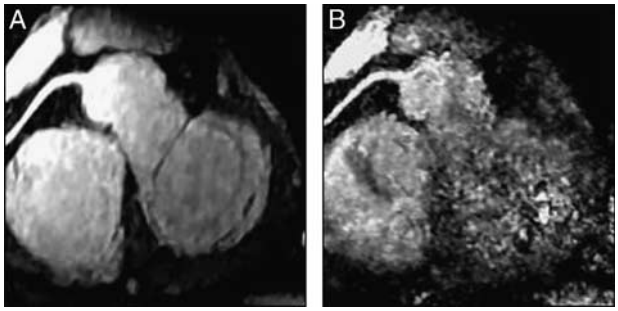

Figure 2. Zoomed RCA images (MIP, 3 mm slice thickness) obtained from 25 sec. breath-hold scans using (A) 8-fold accelerated (4×2, 60 slices, slice thickness = 2 mm) and (B) 16-fold accelerated (4×4, 120 slices, slice thickness = 1 mm) parallel imaging. Note the clear delineation of the proximal segment of the RCA for both scans (A, B) but also the increase in the noise amplification when advancing towards very high acceleration factors of much as 16 (4×4) (B).

Conclusions: Our initial experience suggests that single breath-hold CMRA with a 32-channel system is feasible and may provide benefits for clinical coronary MRA. The reported highly accelerated parallel imaging acquisition strategies enable whole heart coverage CMRA acquisitions with otherwise unattainable scan times. This holds the promise to extend the capabilities of breath-hold CMRA from multiple targeted slabs to single large volumes allowing comprehensive coverage. Highly accelerated robust single breath-hold whole heart coverage CMRA also promises further scan time reduction compared to free-breathing techniques. This, in turn, may enable integration of CMRA into a comprehensive cardiac examination for the detection of heart disease while improving both operator convenience and patient comfort. In conclusion, significant improvements in SNR may be expected with the use of many-element arrays tailored to fields of view generally used in cardiac MRI. Consequently, future studies including clinical comparisons are planned with prototype 32-element cardiac arrays.

REFERENCES

Hardy, C. J., et al. (2003). *ISMRM Proc.* 471.
Niendorf, T., et al. (2004). *ISMRM Proc.* 1876.
Sodickson, D. K., et al. (2001). *Med. Phys.* 28:. 1629.
Weber, O., et al. (2003). *MRM* 50:. 1223.
Zhu, Y., et al. (2004). *MRM.* in press.

169. Diagnostic Accuracy of Whole Heart Coronary Magnetic Resonance Angiography for the Detection of Significant Coronary Stenoses in Patients with Suspected Coronary Artery Disease

Yasutaka Ichikawa, MD,[1] Hajime Sakuma, MD,[2] Katsutoshi Makino, MD,[3] Shoko Okano, MD,[3] Shuji Chino, MD,[1] Tadanori Hirano, MD,[1] Kan Takeda, MD.[2] [1]*Radiology, Matsusaka Central Hospital, Matsusaka, Mie, Japan,* [2]*Radiology, Mie University Hospital, Tsu, Mie, Japan,* [3]*Cardiology, Matsusaka Central Hospital, Matsusaka, Mie, Japan.*

Introduction: Free breathing whole heart coronary MR angiography (MRA) using a navigator-gated 3D steady state free precession can provide visualization of all three major coronary arteries within a single 3D acquisition. However, the diagnostic accuracy of this method has not been determined in a large number of patients.

Purpose: The purpose of this study was to evaluate the diagnostic accuracy of whole heart coronary MRA for the detection of significant stenoses in the coronary arteries in patients with suspected coronary artery disease.

Methods: Ninety-two patients with suspected coronary artery disease were evaluated in this study. Three dimensional coronary MR images covering the entire heart were obtained with a navigator-gated, steady state free precession sequence with radial k-space sampling (TR/TE = 4.6/2.3 ms, SENSE factor = 2, FOV = 280 × 280 × 120 mm, acquisition matrices = 256 × 256 × 80, reconstruction matrices of 512 × 512 × 160, reconstructed voxel size of 0.55 × 0.55 × 0.75 mm). A subject specific acquisition window in the cardiac cycle was used for 3D MRA acquisition by determining motion of RCA on fast cine MR images. All subjects underwent invasive coronary angiography within two weeks of MR study. All coronary arteries and side branches with a diameter of 1.5 mm or more on coronary angiography were evaluated by two blinded observers, and luminal diameter reduction of 50% or more on quantitative coronary angiography was considered to be significant.

Results: The averaged acquisition time of whole heart coronary MRA was 13.3 ± 4.4 minutes. High quality images (score 3 or 4 on 4-point scale) were observed in all segments of the coronary arteries in 75 (82.0%) of the 92 patients. Without exclusion of distal segments and side branches, the sensitivity, specificity, positive and negative predictive values, and accuracy of the whole heart coronary MRA for detecting patients having at least one coronary arterial stenosis was 85.3%, 90.2%, 87.9%, 88.1% and 88.0%, respectively. The sensitivity and specificity were 93.3% and 95.0% for RCA, 82.4% and 94.8% for LAD, and 84.6% and 93.1% for LCX, respectively.

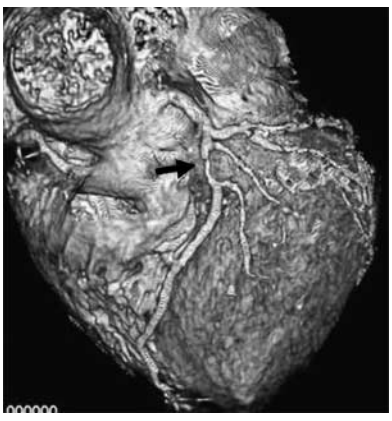

Conclusions: Free breathing whole heart coronary MRA with a navigator-gated steady state sequence can provide noninvasive detection of coronary artery disease with high diagnostic accuracy.

170. Quantification of Coronary Artery Stenoses Using Interventional MRI: Comparison to X-Ray Angiography

Jordin D. Green, MS, Reed A. Omary, MD, MS, Brian E. Schirf, MD, Richard Tang, MD, Biao Lu, MD, James A. Gehl, James C. Carr, MD, J. Jenny Huang, ScD, F. Scott Pereles, MD, Debiao Li, PhD. *Northwestern University, Chicago, IL, USA.*

Introduction: Interventional MRI (iMRI) is an alternative to X-ray fluoroscopy for the detection of coronary artery disease. In the iMRI setting, catheter-directed coronary magnetic resonance angiography (MRA) has been primarily used for vessel delineation (Serfaty et al., 2000) because it uses minimal contrast agent. However, the accuracy of this technique is unknown and imaging time is limited because of rapid perfusion following intra-coronary injection. An alternative approach to improve accuracy would be to use iMRI as a rapid screening method to identify potential stenoses and then obtain MRI cross-sections at these stenoses without additional injections.

Purpose: The purpose of this study was to identify and quantify coronary artery stenoses using a two-step iMRI protocol, consisting of stenosis detection via a quick 3D catheter-directed MRA and then using thin-slice 2D cross-sections to quantify the coronary lumen diameter. We compared iMRI to X-ray angiography for accuracy.

Methods: We conducted studies in 9 swine. We surgically induced a chronic model of coronary artery stenosis by placing ameroid constrictors around the proximal left circumflex coronary artery (LCX). Three weeks later, animals were transported to the X-ray fluoroscopy suite. A 6-F coronary catheter was used to engage the left main coronary artery for X-ray angiography. The catheter was removed and each pig transferred to a 1.5 T Sonata (Siemens, Erlangen, Germany).

We advanced a loopless antenna guidewire coil (Intercept, Surgi-Vision, Inc., Gaithersburg, MD) and the same angiographic catheter into the left coronary ostium under MR. We

then performed MRA using 3D thick-partition magnetization-prepared SSFP with intra-coronary injection of diluted gadolinium. Once the stenosis was localized, we acquired 2D SSFP cross-section images at and proximal to the stenosis without contrast injection.

Typical sequence parameters for 3D contrast-enhanced MRA: TR/TE/flip angle = 3.8 ms/1.5 ms/70°, 2 partitions interpolated to 4, partition thickness = 10 mm, resolution = 1.1 × 0.8 mm^2; for 2D cross-section imaging: TR/TE/flip angle = 3.8 ms/1.7 ms/65°, slice thickness = 2 mm, resolution = 0.8 × 0.8 mm^2, 4 signal averages.

We calculated percent stenosis for each of the three data sets (X-ray angiography, 3D contrast-enhanced MRA, 2D cross-sectional MRI) using full width at half maximum (FWHM) criteria. MRA data sets were used to screen subjects for the presence of CAD. At all sites that MRA detected a stenosis of $\geq$ 30%, we performed subsequent cross-sectional MRI. 30% was chosen because it was assumed that the error for MRA is at least as great as the error for X-ray angiography [up to 20%, (Key et al., 1987] and a 50% stenosis is considered clinically significant. To compare the ability of X-ray fluoroscopy and cross-sectional MRI to quantify CAD, we measured agreement between percent stenosis values using the intra-class correlation coefficient (ICC). Alpha was set to 0.05.

Results: X-ray angiography was successfully performed in 9/9 pigs. Under MR, the coronary ostium was successfully engaged in 8/9 pigs. 3D catheter-directed MRA was performed in the 8 animals where catheterization was successful. A percent stenosis of $\geq$ 30% was detected in 8/8 pigs. This data set was then used to plan MR cross-sections of the LCX (Fig. 1). In the one animal where the coronary ostium was not engaged, the pre-contrast LCX localizer was used to plan the proximal and stenosis cross-sections. Cross-sectional MRI was compared to X-ray fluoroscopy in all surgically prepared animals (Fig. 2). The ICC was 0.955 ($p < 0.05$).

Conclusion: The combination of catheter-directed MRA and cross-sectional MRI successfully identifies and quantifies coronary artery stenoses in swine. This two-step iMRI approach may be useful for future MRI-guided coronary interventions.

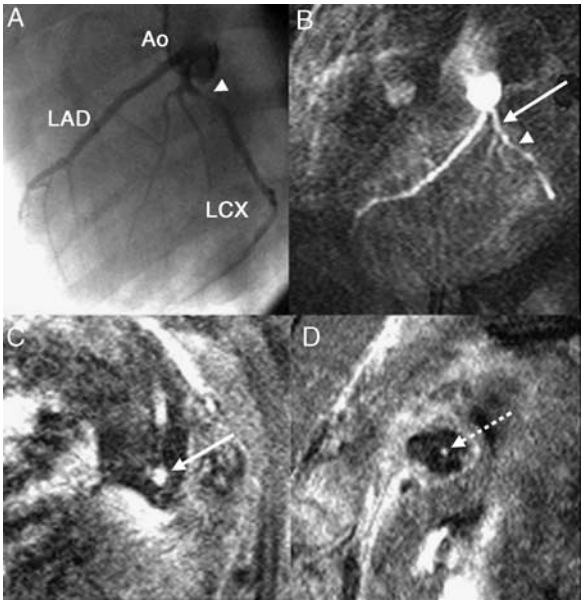

Figure 1. Coronary angiograms with corresponding MRI cross-sections. A) X-ray angiography. Stenosis is present in the proximal LCX (arrowhead). B) MIP of a 3D catheter-directed MRA, used to plan MRI cross sections proximal to the stenosis (arrow, C) and at the stenosis (arrowhead, D).

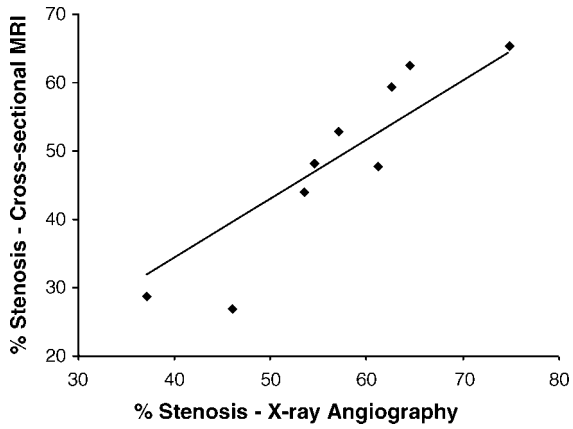

Figure 2. Percent stenosis measured using cross-sectional MRI vs. X-ray. Dark line represents perfect agreement. Correlation between the two methods was outstanding, with ICC = 0.955 ($p < 0.05$).

REFERENCES

Key, H., et al. (1987). *Br. J. Radiol.* 60:. 1083–1088.
Serfaty, J.-M., et al. (2000). *Radiology* 217:. 290–295.

171. Coronary MRA at 3.0 Tesla Compared to 1.5 Tesla: Initial Results in Patients with Suspected Coronary Artery Disease

Matthias Hackenbroch, MD,[1] Carsten Meyer,[1] Alexandra Schmiedel,[1] Jürgen Gieseke,[1] Claus Tiemann,[2] Hans Schild,[1] Torsten Sommer.[1] [1]*Radiology, University of Bonn, Bonn, Germany,* [2]*Cardiology, University of Bonn, Bonn, Germany.*

Introduction: The recent development of 3.0 T MR systems with whole-body volume radio-frequency (RF) coils and dedicated phased array coil technology has led to an increased interest in high-field cardiac imaging, and preliminary experience with cardiac imaging at 3.0 T and higher field strengths has been reported.

Purpose: To evaluate prospectively the feasibility, image quality and accuracy of coronary MRA at 3.0 T in patients with suspected coronary artery disease and to compare

prospectively these results with coronary MRA data acquired at 1.5 T.

Methods: 18 patients (11 men, 7 women, mean age: 63 years, range: 45–76 years) with suspected coronary artery disease, who were scheduled to undergo elective x-ray coronary angiography were included. For coronary MRA at 3.0 T and 1.5 T, a Vector-ECG gated three-dimensional segmented k-space gradient echo imaging sequence was combined with real time respiratory navigator gating and tracking. Signal-to-noise ratios (SNR), contrast-to-noise ratios (CNR), scores of image quality and sensitivity/specificity in the detection of coronary artery stenosis on a segment-to-segment basis were assessed at 3.0 T and 1.5 T. Data were analysed for statistical differences using the Wilcoxon matched pairs test and the McNemar test.

Results: The average increase in SNR at 3.0 T with respect to coronary MRA at 1.5 T was 29.5% for the left coronary artery (LCA) and 31.2% for the right coronary artery (RCA) ($p < 0.001$) and the average increase in CNR was 21.8% for the LCA and 23.5% for the RCA. ($p < 0.001$). Scores of image quality ($p = 0.77$) and diagnostic accuracy in the detection of coronary artery stenoses (sensitivity and specificity: 82% and 89% at 3.0 T vs. 82% and 88% at 1.5 T, respectively; $p > 0.99$) were equal at both field strengths.

Conclusions: Coronary MRA at 3.0 T is feasible in patients with suspected coronary artery disease, providing a significant increase in SNR and CNR although current techniques do not result in significantly improved image quality and diagnostic accuracy in comparison to imaging at 1.5 T.

172. Coronary Angiography In Vivo Employing PASADENA ^{13}C and ^{1}H Magnetic Resonance Imaging

Thao T. Tran, BS,[1] Pratip Bhattacharya, PhD,[1] Alexander P. Lin, BS,[1] Kent Harris, PhD,[1] Daniel Weitekamp, PhD,[2] Brian D. Ross, MD, PhD.[1] [1]*Cardiac MR Unit, Huntington Medical Research Institutes, Pasadena, CA, USA,* [2]*California Institutes of Technology, Pasadena, CA, USA.*

Introduction: Coronary angiography can be performed with proton cardiovascular magnetic resonance imaging (^{1}H cvMRI), with contrast agents such as gadolinium (Gd), but is often difficult to reconstruct and visualize due to underlying proton signal from cardiac tissue. ^{13}C MRI, which will not have background proton signal, may yield a more complete analysis of coronary imaging that can currently be achieved by Gd-enhanced ^{1}H cvMRI. The PASADENA (parahydrogen and synthesis allow dramatically enhanced nuclear alignment) method has been successfully utilized to polarize the ^{1}H and ^{13}C atoms in several molecules (Bhattacharya et al., 2004; Bowers and Weitekamp, 1987; Johansson et al., 2004) providing an increase in signal to several thousand times that of its original state. These PASADENA molecules or agents are likely to be much more versatile than traditional Gd, so that successful ^{13}C MRI could then be adapted to provide high contrast coronary angiography.

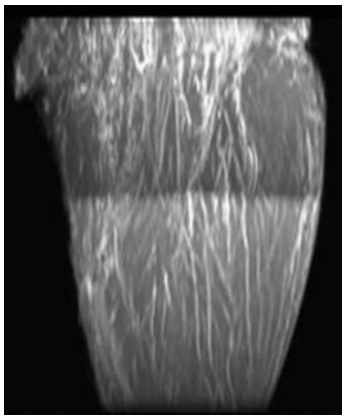

Figure 1. Left ventricle with Gad. enhancement, non-ECG gated.

Aims: The aim of the present work has been to demonstrate the potential of using ^{1}H and ^{13}C cvMRI aiming for real time visualization of the coronary arteries with PASADENA reagents. In order to achieve that, we first aim to determine the feasibility of coronary angiography with PASADENA reagents using ^{1}H cvMRI in vivo. Our second aim was to achieve ^{13}C cvMRI in vivo. Our final aim was to combine the ^{13}C cvMRI and PASADENA reagents in vivo to provide high-contrast ^{13}C coronary angiography.

Methods: Experimental work was performed in pig heart that was harvested and injected with Heparin to prevent coagulation and perfused using the Langendorff technique. All MRI exams were done on a 1.5 T clinical scanner (GE LX) and reagents were injected using a power injector (Medrad). Initial fSPGR ^{1}H scans were used as localizers to

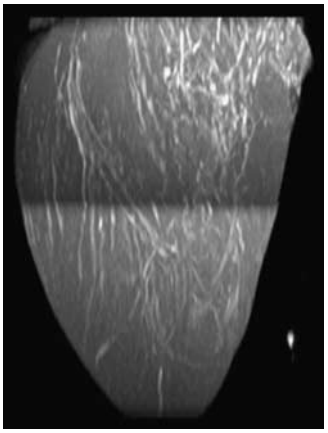

Figure 2. Left ventricle with PASADENA reagent enhancement, non-ECG gated.

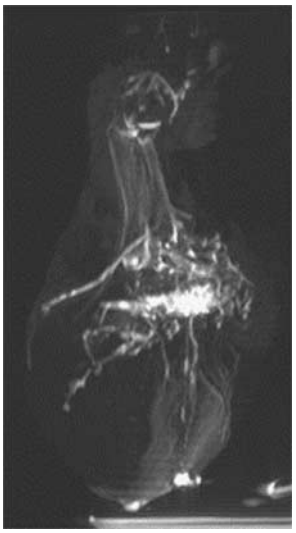

Figure 3. Heart with Gad., imaged using MRA sequence, ECG-gated.

select optimal projection angle for the ^{13}C scans. The heart was then imaged in vivo using three different sequences and two different reagents: 1) standard ^{1}H MRA with Gd (as the current gold standard), ECG-gated 2) standard ^{1}H FIESTA with a) Gd and b) PASADENA reagent to enhance the vessels, non ECG-gated; 3) ^{13}C FIESTA with a) ^{13}C reagent and b) PASADENA reagent, non-ECG gated.

Results: ^{1}H MRI results demonstrated successful imaging of both Gd and PASADENA reagent (Figures 1 and 2). The signal increase due to the PASADENA effect in ^{1}H was expected to be of relatively low yield compared to the 1,000 × magnification in ^{13}C MRI. In addition, the ^{1}H PASADENA cvMRI and ^{1}H MRA scans suffer from the same background signal problem for proton imaging. ^{13}C cvMRI overcomes this problem by imaging solely the ^{13}C signal as demonstrated by successful ^{13}C imaging of ^{13}C reagent. The ^{13}C signal enhancement of PASADENA reagent combined with ^{13}C imaging provided high contrast coronary artery images. These images can then be overlayed over proton images using a contrasting color scheme that allows coronary artery images to be readily distinguished from cardiac tissue and other physiology (Fig. 3).

Conclusion: Our results demonstrate that smart PASADENA contrast agents may be used to visualize coronary arteries during dynamic cardiac MRI to provide greater contrast and better visualization than current ^{1}H MRA techniques. Together with the pioneering in vivo demonstration of parahdyrogen enhanced ^{13}C cardiac MRI by Golman et al. (Johansson et al., 2004), these results indicate the potential for a new generation of CVMR method. Furthermore, the flexibility of PASADENA reagents allows for "smarter" imaging of coronary arteries as well as increased signal.

REFERENCES

Bhattacharya, P., Harris, K., Lin, A., Weitekamp, D. P., Ross, B. D. (2004). ESMRMB Abstract #236.

Bowers, C. R., Weitekamp, D. P. (1987). *J. Am. Chem. Soc.* 109:. 5541–5542.

Johansson, E., Magnusson, P., Chai, C. M., Petersson, J. S., et al. (2004). ESMRMB Abstract #117.

173. Multi-slice Dark-Blood TSE Carotid Imaging at 3T with Regional Saturation and Rapid Extended Coverage—A Feasibility Study

Ioannis Koktzoglou, MS,[1] Yiu-Cho Chung, PhD,[2] Venkatesh Mani, PhD,[3] Timothy J. Carroll, PhD,[1] Gabor Mizsei, MS,[3] Orlando Simonetti, PhD,[2] Zahi A. Fayad, PhD,[3] Debiao Li, PhD.[1] [1]*Departments of Biomedical Engineering and Radiology, Northwestern University, Chicago, IL, USA,* [2]*Siemens Medical Solutions, Chicago, IL, USA,* [3]*Imaging Science Laboratories, Mount Sinai School of Medicine, New York, NY, USA.*

Introduction: Turbo spin-echo (TSE) imaging of the carotid bifurcation at 1.5 T has been used to detect and characterize carotid atherosclerotic plaque. Characterization of carotid plaque, however, requires relatively high resolution imaging which limits attainable signal-to-noise ratio (SNR). MR imaging at 3 T may help improve SNR or allow for higher resolution imaging (Hinton et al., 2003). Nonetheless, high RF power deposition of TSE imaging may limit imaging efficiency and/or coverage. Work is needed to optimize carotid wall imaging protocols at 3 T.

Purpose: This work sought to evaluate the feasibility of dark-blood TSE carotid artery wall imaging at 3.0 T by comparing two rapid multi-slice imaging sequences.

Materials and Methods: Four healthy volunteers (2 males, 2 females, mean age = 41 years) were imaged on a whole body 3.0 T scanner (Magnetom Trio, Siemens Medical Solutions) with a maximum gradient amplitude of 40 mT/m and a maximum slew rate of 200 mT/m/ms. An in-house four

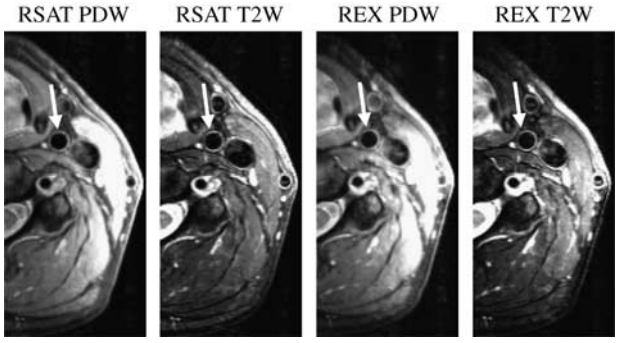

Figure 1. In-vivo PDW and T2W dark blood images of the carotid artery walls (arrows) acquired with the RSAT and REX sequences.

Table 1. Mean SNR and CNR measurements

	RSAT	REX	n	p-Value
PDW SNR	28.9 ± 9.0	29.1 ± 9.2	96	0.75
T2W SNR	18.2 ± 5.8	17.0 ± 6.5	96	0.04
PDW CNR	22.8 ± 8.1	22.7 ± 8.5	96	0.86
T2W CNR	13.8 ± 5.2	12.4 ± 5.9	96	< 0.01

channel phased-array carotid coil (consisting of two left and two right channels) was used for signal reception. In each volunteer, 12 cross-sectional slices through the carotid bifurcation were imaged using TSE. Two magnetization preparation methods were used to suppress the blood signal. The first method applied two regional saturation (RSAT) bands (50 mm) before data acquisition of each slice during each TR, 10 mm above and below the imaging slices. The second method was a rapid extended coverage (REX) sequence in which four double inversion recovery blocks were applied before data acquisition within every TR (Mani et al., 2004). Fat saturated proton density-weighted (PDW) and T2-weighted (T2W) imaging was performed with both sequences with the following imaging parameters: FOV = 12 × 12 cm^2, matrix = 256 × 256, SL = 3 mm, slice gap = 10%, TR = 4 s, TE = 10 ms (PDW), TE = 50 ms (T2W), ETL = 9, bandwidth = 200 Hz/pixel, NEX = 2, imaging time = 3′55″ per scan. Refocusing flip angle was SAR (specific absorption rate) limited, with the RSAT and REX sequences employing an average of 165° and 167°, respectively.

Signal intensities were measured in the left and right carotid artery wall and lumen. A paired samples t-test was used to determine significant differences in wall SNR and wall-lumen CNR between the two acquisitions.

Results: Twelve-slice dark-blood T2W and PDW imaging of the carotid bifurcation was achieved in all volunteers with the RSAT and REX sequences. SAR levels were about the same for the two protocols. Representative images from both imaging techniques are shown in Figure 1. Carotid artery wall was clearly depicted with excellent lumen and fat signal suppression. Mean wall SNR and wall-lumen CNR in all acquired images are given in Table 1. No significant differences in SNR and CNR were found with PDW imaging, however, statistical significance ($p < 0.05$) was achieved in the T2W images.

Conclusion: Despite increased SAR levels at 3.0 T, multislice TSE imaging of the carotid bifurcation was possible. Excellent image quality was achieved with both the RSAT and REX sequences, yielding comparable image appearances, SNR and CNR. Patient studies are needed to assess the utility of the two sequences for carotid plaque detection and characterization at 3 T.

REFERENCES

Hinton, D., et al. (2003). ISMRM 11th Annual Meeting, 176.
Mani, V., et al. (2004). *Radiology* 232:281–288.

174. MR and CT Imaging of Patients with Atherosclerotic Aortic Plaque and Evaluation of New MR Methods

Daisy Chien, PhD, David Fieno, MD, PhD, Rola Saouaf, MD, Damini Dey, PhD, Ling De Yang, MD, Heidi Gransar, MS, Louise Thomson, MD, John Friedman, MD, Daniel Berman, MD. *Cedars-Sinai Medical Center, Los Angeles, CA, USA.*

Introduction: MR has been established as a reliable noninvasive tool to evaluate atherosclerotic plaque. The method of choice has been 2D dark blood techniques which have generated good results but can be time consuming. Our hypothesis is that 3D imaging may improve the ability to evaluate patients with atherosclerosis and to more effectively cover an extended area of interest such as the aorta.

Purpose: To evaluate a new 3D approach based on steady state free precession (SSFP) for plaque imaging, to compare it with the established 2D technique, and to correlate with CT in patients with aortic atherosclerotic plaque.

Methods: We evaluated 12 patients (6 men and 6 women, 55–79 years old) with known atherosclerosis indicated by their CT studies. Standard 2D MR images were acquired with T1, T2, and proton density weighting, each acquired in a single breathhold. Two 3D SSFP methods were assessed. The non-breathhold (3DnBH) method acquired 80 slices in < 5 minutes of scan time. The breathhold (3DBH) acquired 12 slices in a single breathhold. The smallest pixel size was 0.35 mm × 0.5 mm and the slice thickness was 3 mm.

Signal-to-noise measurements of the vessel wall versus the background were made comparing 2D, 3DnBH, and 3DBH. The MR images were examined and graded side by side by 3 expert readers according to: 1) image quality, 2) plaque margin definition, 3) plaque characterization, and 4) the ability to visualize plaque calcification. The CT images were examined at the same level as the MR acquisitions.

Results: Signal-to-noise measured was 4.5 ± 1.5, 8.0 ± 2.0, and 14.0 ± 3.8 for the 2D, 3DBH, and 3DnBH methods respectively. Fig. 1 shows the image acquired using 2D, 3D breathhold, 3D non-breathhold, and EBCT at the same level in a 74 year old patient.

In the category of plaque delineation and plaque characterization, the 3D images had up to 200% improvement in grade when compared with the 2D images ($P < 0.05$). Furthermore, the calcified region was inconspicuous in 88% of the lesions and was missed in 70% of the lesions in the dark blood images. Comparisons with CT showed that 3D bright blood imaging was correct in identifying the calcified region in every lesion.

Conclusion: 3D MR imaging was performed for the first time to evaluate plaque burden in the thoracic aorta. The 3D methods demonstrated significantly improved results in plaque definition, plaque characterization, and visualization of calcification when compared with the established 2D

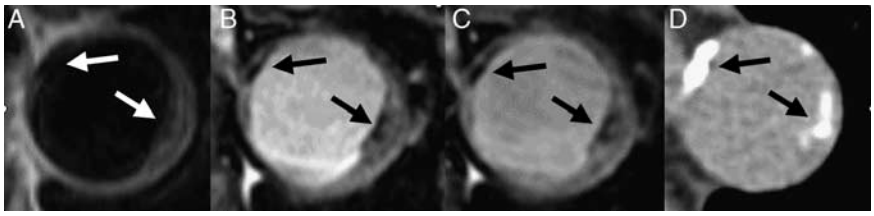

Figure 1. A) Standard 2D, B) breathhold 3D (showing 1 image out of 12 contiguous slices), and C) non-breathhold 3D (showing 1 image out of 80 contiguous slices) acquired in a patient with atypical chest pain. D) The EBCT calcium scan confirms 2 major areas of calcification (areas of low signal intensity) that are clearly seen in the 3D but are less conspicuous in the 2D images.

technique. Furthermore, the 3D non-breathhold technique is time-effective and can cover the complete thoracic aorta with no slice gap in < 5 minutes of scan time.

175. Interactive Real-Time Magnetic Resonance-Guided Atrial Septal Puncture and Atrial Balloon Septostomy Are Feasible in Swine

Amish N. Raval, MD,[1] Parag V. Karmarkar, MSc,[2] Michael A. Guttman, MSc,[3] Cengizhan Ozturk, MD, PhD,[1] Ranil DeSilva, MD, PhD,[1] Ronnier J. Aviles, MD,[1] Elliot R. McVeigh, PhD,[3] Ergin Atalar, PhD,[4] Robert J. Lederman, MD.[1] [1]*Cardiovascular Branch, National Heart Lung and Blood Institute/National Institutes of Health, Bethesda, MD, USA,* [2]*Johns Hopkins University, Baltimore, MD, USA,* [3]*Laboratory of Cardiac Energetics, National Heart Lung and Blood Institute/National Institutes of Health, Bethesda, MD, USA,* [4]*Johns Hopkins University, Baltimore, MD, USA.*

Introduction: Atrial septal puncture (ASP) guided by xray fluoroscopy (XRF) is an initial step in many procedures, including atrial balloon septostomy (ABS). Compared to XRF, interactive real-time magnetic resonance imaging (IR-MRI) using modified interventional devices offers superior tissue imaging without ionizing radiation exposure, which is harmful in children.

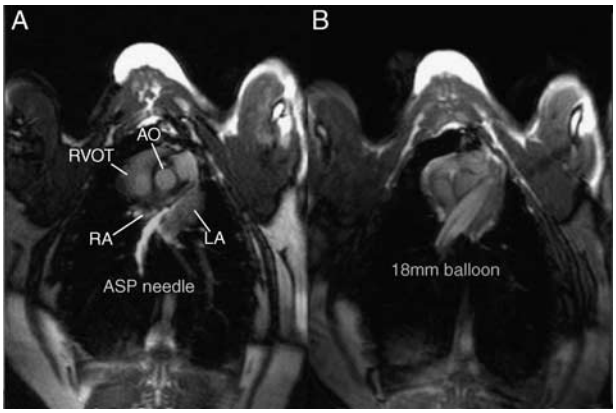

Figure 1.

Purpose: To determine if ASP and ABS are feasible using an IR-MRI platform.

Methods: 10 healthy swine (21–60 kg) underwent IR-MRI guided ASP/ABS. Active ASP needles were inserted into 6F/10F dilator and introducer sheaths with passive tip markers. Incrementally sized 8–18 mm balloon catheters inflated with 5 mM Gd-DTPA were passed over an active wire for ABS after successful ASP. Interactive, simultaneous multi-slice, rapid SSFP image acquisition/reconstruction was performed in the XMR suite at NHLBI.

Results: ASP was successful in 10/10 animals. ABS was successfully achieved in 4/5 animals. In one case, inadvertent contrast staining of the septum caused image distortion and procedure termination. Following ABS, a left to right shunt of 1.5:1 was measured invasively. Figures 1A and 1B demonstrate active needle and balloon/active wire across the inter-atrial septum.

Conclusions: ASP and ABS are feasible using an IR-MRI interventional platform. Further imaging and device development toward future clinical application are warranted.

176. Chronic Total Peripheral Artery Occlusion Recanalization Using Interactive Real-Time Magnetic Resonance Imaging Guidance Is Feasible in a Swine Model

Amish N. Raval, MD,[1] Parag V. Karmarkar, MSc,[2] Cengizhan Ozturk, PhD,[1] Michael A. Guttman, MSc,[3] Minnan Xu,[2] Ranil DeSilva, MD, PhD,[1] Ronnier J. Aviles, MD,[1] Alexander J. Dick, MD,[1] Venkatesh K. Raman, MD,[1] Elliot R. McVeigh, PhD,[3] Ergin Atalar, PhD,[2] Robert J. Lederman, MD.[1] [1]*Cardiovascular Branch, National Heart Lung and Blood Institute/National Institutes of Health, Bethesda, MD, USA,* [2]*Johns Hopkins University, Baltimore, MD, USA,* [3]*Laboratory of Cardiac Energetics, National Heart Lung and Blood Institute/National Institutes of Health, Bethesda, MD, USA.*

Introduction: Conventional x-ray fluoroscopic guided chronic total arterial occlusion (CTO) recanalization requires significant operator experience, prolonged fluoroscopic time,

increased use of potentially nephrotoxic radiocontrast and is associated with a substantial risk of perforation due to poor arterial wall visualization. In comparison, interactive real-time magnetic resonance imaging (IR-MRI) using active receiver antennae and modified passive interventional devices offers superior tissue imaging without requiring ionizing radiation or radiocontrast. In particular, IR-MRI may offer sufficient artery wall visualization despite the absence of flowing blood in the lumen and may permit easier, safer and quicker traversal through the occluded arterial segment.

Purpose: To demonstrate the feasibility of CTO recanalization wholly guided by IR-MRI, using custom-modified MRI visible devices in an experimental swine model.

Methods: An atherogenic diet fed swine underwent percutaneous left carotid artery (LCA) balloon injury using an oversized peripheral interventional balloon (Agiltrac, Guidant) which resulted in intimal dissection and acute thrombosis. The animal was recovered and returned six weeks later for attempted CTO recanalization in an the NHLBI cardiovascular intervention suite consisting of independently operating MRI and XRF systems (Sonata 1.5 T and Axiom Artis FC, Siemens) with smooth intermodality transport (Miyabe, Siemens) through sliding radiofrequency shielded doors. The MRI scanner was connected via Gigabit ethernet to a custom external workstation for real-time, lowlatency image reconstruction. Images were displayed in-lab using shielded LCD projectors. Online 3D rendering was used to display all or selected slices at their respective spatial positions. Custom designed active receive-coil antennae catheters, floppy tipped guide wire, and stiff tipped CTO wire were manufactured with careful attention to imaging profile and mechanical functionality for CTO recanalization. Real-time steady state free precession was used intra-procedurally for with careful attention to imaging vessel wall. Pre and post x-ray digital subtraction angiography (XRA), contrast enhanced MR angiography (MRA) and high resolution T1 weighted imaging was performed.

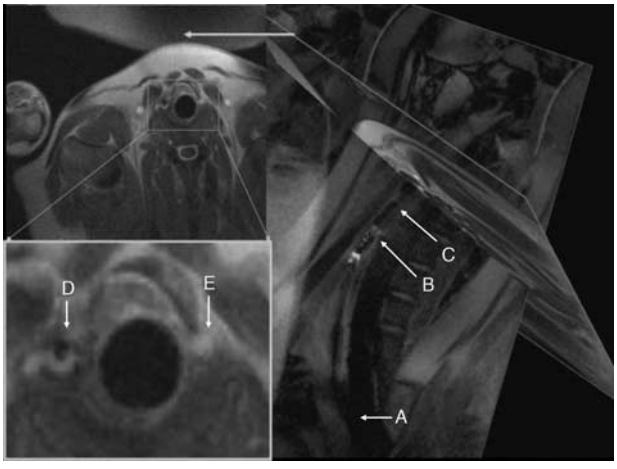

Figure 1. Oblique and axial slice planes demonstrating CTO wire and catheter navigation at a point 3/4 of the way through LCA occlusion A—location of proximal stump, B—active catheter (green), C—active wire (red), D—occluded LCA, E—RCA.

Results: The length of occlusion from the proximal stump to the point of reconstitution was 119 and 115 mm by XRA and MRA respectively. The LCA diameter at a point midway through the obstruction was 5.2 mm and 4.8 mm by T1 weighted MR image and real-time SSFP respectively. The contralateral vessel diameter at this level was 6.2, 6.0, 5.8 and 5.6 mm by T1 weighted MR, real-time SSFP, MRA and XRA respectively. There was a moderate degree of resistance during initial passage of the wire into the obstruction suggesting the similarity of our CTO model to the clinical situation. Eventually, successful wire and catheter navigation, steering and traversal was performed, despite its tortuous course. Following re-entry into the normal distal vessel, catheter was exchanged for a long 5.0×100 mm balloon (Guidant, Agiltrac) and serial inflations were performed using 5 mM Gd-DPTA along the artery length without complication. Post procedural MRA and XRA revealed excellent restoration of flow and residual 40% diameter proximal and distal stenoses. No complications were evident (Fig. 1).

Conclusion: We have demonstrated the first successful CTO recanalization of a peripheral artery in a swine model. Further study is warranted to validate these initial proof-of-concept results.

177. MR-Compatible Coronary Stent: In-Vitro and First Human MR Imaging Experience with an Absorbable Magnesium-Alloy Stent

Peter Hunold, MD,[1] Harald H. Quick, PhD,[1] Holger Eggebrecht, MD,[2] Michaela Jökel, RT,[1] Sandra Massing, RT,[1] Axel Schmermund, MD,[2] Jörg Rodermann, MD,[2] Jörg Barkhausen, MD,[1] Raimund Erbel, MD.[2] [1]*Department of Diagnostic and Interventional Radiology, University Hospital, Essen, Germany,* [2]*West German Heart Center, Department of Cardiology, University Hospital, Essen, Germany.*

Introduction: Bare metal stents are associated with susceptibility artifacts hampering non-invasive follow-up studies by magnetic resonance imaging (MRI). Recently, a novel absorbable metal stent (AMS) has been developed and implanted into human coronary arteries. Due to its composition of a magnesium-based alloy, the stent is not radio-opaque and can, therefore, not be visualized by x-ray or CT. The MRI features of this AMS are still unknown. Artifact-free imaging would allow for non-invasive follow-up of coronary stents as an attractive alternative to coronary cath angiography.

Purpose: To evaluate the MR compatibility of the AMS in-vitro and after implantation in human coronary arteries.

Methods: In an in-vitro study, expanded as well as unexpanded AMS (Biotronik, Berlin, Germany) were examined in a water bath phantom using a 1.5 Tesla MR-scanner (Sonata, Siemens, Erlangen, Germany) with different sequences. A comparison with standard bare metal stents in terms of visibility and artifacts was performed by visual analysis. As part of the first-in-man trial, 5 patients (age: 39–72 yrs, 3 male/2 female) underwent AMS implantation. MR coronary angiography (MRCA) was performed the day before and 3 to 4 days after implantation using two different sequences: a) a segmented steady-state free precession sequence without contrast material (TrueFISP) and b) contrast-enhanced MRCA with a segmented inversion-recovery 3D gradient-echo sequence (FLASH). Both sequences were applied during breath-hold with a navigator-based slice follow option. Images were compared in terms of visibility of the stented coronary artery lumen and artefacts.

Results: In the in-vitro study, the stents could be visualized by MRI. The magnesium-alloy stent did not produce recognizable susceptibility artifacts allowing for unhampered detailed evaluation of the stent lumen in the water bath. Conversely, the bare metal stents showed the typical material-dependent susceptibility artifacts rendering evaluation of the stent lumen impossible. In the patients, all coronary arteries could be delineated before AMS implantation with both described techniques. After AMS implantation the corresponding parts of the stented coronary arteries (2 × RCA, 1 × LAD, 2 × LCX) could also be visualized by MRCA. The artifact-free visualization allowed for evaluation of the stented lumen without image quality loss (Fig. 1).

Conclusions: MR imaging of a novel absorbable magnesium-alloy stent was performed demonstrating artifact-free visualization of the stent in-vitro and after implantation in coronary arteries. MRCA yielded diagnostic images of the stented artery lumen without quality loss. This may provide the basis for non-invasive follow-up studies of coronary stent patency.

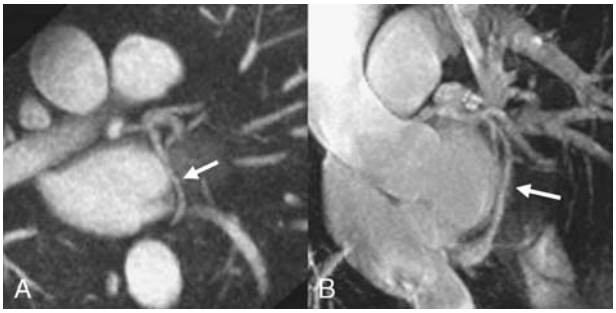

Figure 1. Contrast-enhanced FLASH MRCA of the RCX artery in a male patient. A shows the coronary artery before AMS implantation presenting an intermediate stenosis of the proximal segment (arrow). B After AMS implantation, no artifacts are depictable, the stent lumen can well be visualized and shows a lumen gain compared to the stenosis before.

178. MR Fluoroscopy for Delivery of Non-ionic Dysprosium-DTPA-BMA Into Scarred Myocardium

Maythem Saeed, DVM, PhD,[1] Alastair Martin, PhD,[2] Oliver Weber, PhD,[1] Charles B. Higgins, MD,[1] David Saloner, PhD,[1] Randal Lee, MD, PhD.[3] [1]*Radiology, University of California San Francisco, San Francisco, CA, USA,* [2]*Radiology, Philips Medical Systems, San Francisco, CA, USA,* [3]*Medicine, University of California San Francisco, San Francisco, CA, USA.*

Introduction: Our recent MR study has demonstrated the potential of Vistarem (a blood pool agent) in discriminating acutely infarcted myocardium from scar tissue. The scar tissue appears bright on Dotarem-enhanced MRI, but not Vistarem. The ability of MR to localize and discriminate myocardial status makes it a suitable modality for the administration of drug, gene or stem cell therapies. Since positive enhancement is utilized to delineate infarcted myocardium, we propose that negative enhancement is the appropriate mechanism for monitoring these therapies.

Purpose: To demonstrate the feasibility of MR fluoroscopy in guiding the delivery of nonionic extracellular T2* MR contrast medium Dysprosium-DTPA-BMA in a swine model of chronic myocardial infarction.

Methods: Experiments were performed in 4 pigs subjected to 2 hrs coronary artery occlusion followed by reperfusion. Eight weeks after infarction, the animals were imaged using 1.5 T MR scanner (Philips Medical Systems, Netherlands). Scar tissue was identified by intravenous administration of 0.026 mmol/kg Vistarem (P792; blood pool MR contrast medium) or by 0.1 mmol/kg Dotarem (Gd-DOTA; extracellular MR contrast medium) (Guerbet Group, France) in conjunction with inversion recovery gradient echo MRI.

The guiding catheter and injecting needle (MRI-modified Stiletto 2, Boston Scientific Corporation) were adapted to serve as MRI receiver coils in parallel with surface coils. An additional receiver coil was added to the Stiletto needle tip to generate a high intensity signal on a separate receiver channel (Dick et al., 2003).

The advancement of the endovascular catheter to ascending aorta and then to the LV was monitored using an MR fluoroscopic pulse sequence (bFFE). The imaging parameters for the bFFE were: TE 1.89 ms, TR 3.8 ms, flip angle 60°, slice thickness 5 mm, FOV 200 mm, scan matrix 144 × 144, temporal resolution 500 ms in continuous imaging. Dysprosium-DTPA-BMA (0.4–1.0 ml, 0.5 M, Nycomed Amersham Imaging) was injected into the rim of Dotarem-enhanced region. The injection was monitored using MR fluoroscopy. Gradient echo MRI sequences were used to visualize the myocardial deposition of the Dysprosium-chelate. Blood pressure, heart rate and oxygen saturation were measured during the intervention.

Results: Sequentially administration of Vistarem and Dotarem provided valuable information on the status of

infarcted myocardium. The scar tissue was clearly recognized as bright region on Dotarem, but not Vistarem. The scar tissue defined by Dotarem was used as a target and was evident on bFFE images as a region of modest enhancement relative to the normal myocardium.

LV catheterization via arterial access was feasible under 3D MR fluoroscopy. The tip of the catheter appeared bright on MRI and the catheter could be manipulated within the ventricle to select different targets (Fig. 1). Once appropriately positioned, the injection and consequence of the deposition of Dysprosium-chelate could be monitored on MRI. The procedure of catheterization and intramyocardial injection of Dysprosium took less than 30 min. Successful intramyocardial injection was confirmed by the persistent of myocardial signal loss. The failure of intramyocardial injection was confirmed by the brief signal loss of LV camber blood. Dysprosium-chelate caused signal loss of the Doraterm-enhanced region (Fig. 1). Catheter navigation and intramyocardial injection of Dysprosium-DTPA-BMA caused no significant changes in blood pressure, heart rate or oxygen saturation. Postmortem evaluation showed that there was no evidence of vascular, valvular or endocardial damage.

Conclusion: The procedure of catheterization and intramyocardial injection is safe and without homodynamic side effects. Endocardial delivery of potential low molecular agents is feasible under MR-guidance. Nonionic Dysprosium-DTPA-BMA can be mixed with potential cells during delivery to ensure intramyocardial injection and to eliminate the long-term effects of intracellular iron on stem cells or myoblasts.

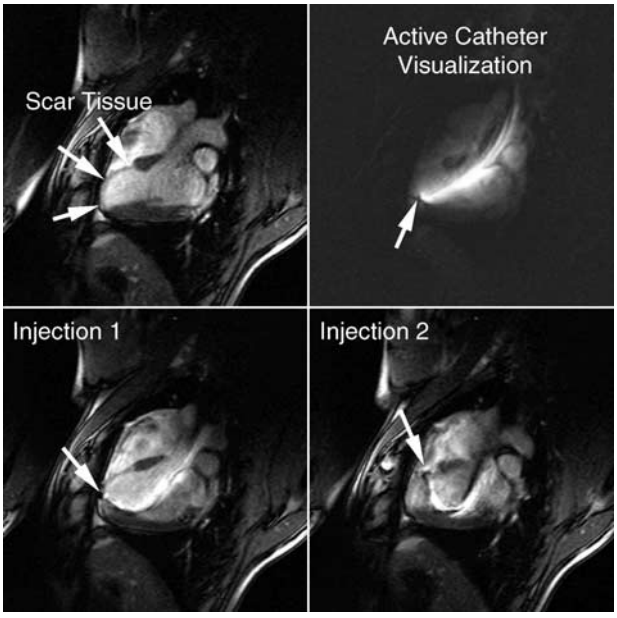

Figure 1.

ACKNOWLEDGMENTS

This study was supported by grants from NIH (RO1HL07295) and Philips Medical System, Best, The Netherlands.

REFERENCE

Dick, A. J., et al. (2003). *Circulation* 108:. 2899–2904.

179. Prevalence of Incidental Non-cardiac Findings Detected by Cardiac MRI

Kai-Uwe Waltering, MD,[1] Thomas Schlosser, MD,[1] Oliver Bruder, MD,[2] Mahnaz Mohammad Sadeghi, MD,[1] Peter Hunold, MD,[1] Jörg Barkhausen, MD.[1] [1]*Department of Diagnostic and Interventional Radiology, University Hospital Essen, Essen, Germany,* [2]*Department of Cardiology and Angiology, Elisabeth Hospital Essen, Essen, Germany.*

Introduction: Vast improvements in MR hard- and software have resulted in a considerable increase in the number of MR exams focussing on the heart. Cardiac MR is now routinely used for the assessment of myocardial function at rest and stress and for detection and characterization of scar tissue in patients with coronary artery disease. However, cardiac exams cover parts of several other organs of the thorax and the upper abdomen and, therefore, incidental findings may well become increasingly apparent.

Purpose: Aim of this study was to evaluate the number of incidental non-cardiac finding during cardiac MR examinations.

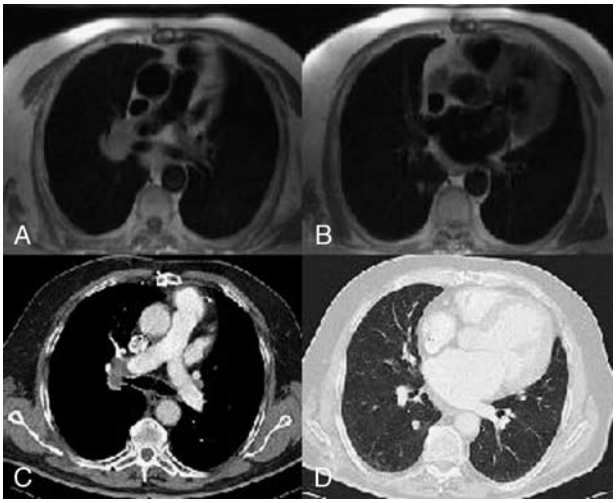

Figure 1. 76 yo male patient referred for Dobutamin stress MR. A right hilar mass (A) and a pulmonary lesion (B) was incidentally detected. Contrast enhanced CT (C, D) confirmed the MR findings.

Methods: From April 2002 to December 2003, 1359 patients underwent cardiac MRI on a 1.5 T MR system for detection of myocardial ischemia n = 638, assessment of myocardial viability n = 479, assessment of cardiac masses or thrombi n = 139 and assessment of myocarditis or cardiomyopathies n = 103. The standard imaging protocol included a proton-density weighted dark-blood prepared half-Fourier single-shot turbo spin-echo (HASTE, TR 2RR, TE 23 ms, FA 160°) sequence in axial orientation covering the entire chest in a single breath-hold, steady-state free precession cine sequences (TR 3 ms, TE 1.5 ms, FA 60°) in standard long and short axes orientations and inversion recovery gradient echo sequences (TR 8 ms, TE 4 ms, TI 180–160 ms, FA 20°) in the same orientation. All relevant non-cardiac findings unknown prior to MR imaging were recorded.

Results: A total of 124 relevant clinical findings were detected in 118 patients. 49 thoracic pathologies were recorded including pulmonary lesions suspected for bronchial carcinoma or metastases n = 23, hilar masses n = 9 (Fig. 1), enlarged mediastinal lymph nodes n = 12 and mediastinal masses n = 5. Additionally, 47 vascular variants or pathologies (dilation or aneurysm of the thoracic aorta n = 37, right aortic arch n = 1, aberrant right subclavian artery n = 4, pulmonary emboli n = 3, persistent left superior vena cava n = 1, vena cava thrombus n = 1) were detected. 28 relevant findings were located in the upper abdomen including non-cystic liver lesions n = 25 (Fig. 2), renal cell carcinoma n = 1, hydronephrosis n = 1 and spinal metastases n = 1. 78 patients were referred to additional diagnostic procedures which confirmed the MR findings in 85% of the cases, whereas 46 patients were referred for follow-up examinations.

Conclusions: Incidental non-cardiac findings can frequently be detected during contrast enhanced cardiac MRI using standard imaging protocols. This suggests that investigators using cardiac MRI have to focus on all visualized organs to make sure that all information provided by the examination is taken into account. Therefore physicians reporting cardiac MR studies have to focus on all visualized organs and should be trained in cross-sectional anatomy and the MR appearance of non-cardiac diseases.

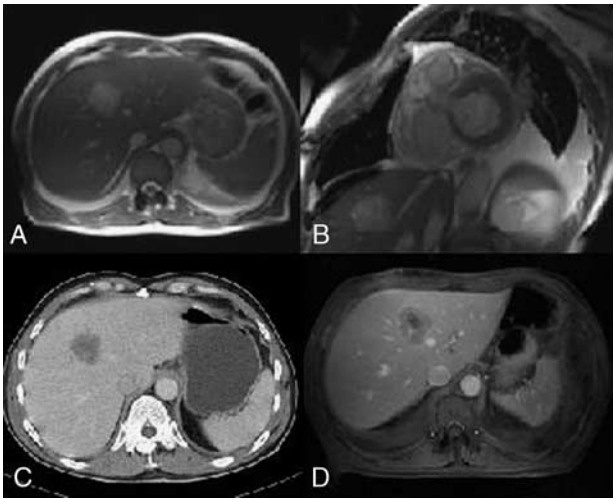

Figure 2. 64 yo male patient referred for the assessment of myocardial viability. A focal liver lesion was incidentally detected (A, B). Contrast enhanced CT (C) and contrast enhanced liver MR (D) confirmed a metastasis of pancreatic cancer.

180. Demonstration and Prediction of the Potential Reversible Nature of Thinned Myocardium by CMR

Olga James, MD,[1] Han W. Kim, MD,[2] Jonathan Weinsaft, MD,[2] Edwin Wu, MD,[3] Michael Elliott, MD,[2] Mark Zenker, MD,[1] Michele A. Parker, MS,[2] Robert O. Bonow, MD,[3] Robert M. Judd, PhD,[2] Raymond J. Kim, MD,[2] Dipan J. Shah, MD.[1] [1]*Nashville Cardiovascular Magnetic Resonance Institute, Brentwood, TN, USA,* [2]*Duke Cardiovascular Magnetic Resonance Center, Durham, NC, USA,* [3]*Northwestern University Feinberg School of Medicine, Chicago, IL, USA.*

Introduction: Clinical dogma states that thinned myocardium lacks viability and cannot improve function after revascularization. In contradiction, a recent study using delayed enhancement (DE) MRI showed substantial viability in some thinned akinetic regions. The prevalence, amount, and clinical and imaging predictors of viability and improvement in thinned myocardium are unknown.

Methods: We prospectively enrolled 1055 consecutive patients with stable coronary artery disease who were referred for viability assessment by CMR at 3 different institutions. All images were reviewed to identify patients with large area of thinned myocardium [> 5% LV with end-diastolic wall thickness (EDWT) $\leq$ 5.5 mm]. In patients with thinned myocardium, cine MRI was quantitatively analyzed to determine the EDWT and systolic wall thickening (SWT) in the thinned region, and the LV ejection fraction (LVEF). The % viability in the thinned region was planimetered from DE-MRI; the presence of Q waves was determined from 12-lead ECG's; and the extent of collaterals and stenosis in the coronary artery supplying the thinned region was determined by review of coronary angiograms. A cohort of patients who underwent revascularization returned for repeat cine MRI to determine if the presence of viability on the initial DE-MRI would be a predictor of improvement.

Results: Of the 1055 patients enrolled, we identified 196 patients (age 64 ± 12, 79% M, LVEF 33 ± 11%) with large regions of akinetic thinned myocardium (35 ± 15% of LV). Substantial viability (> 50% of the region) was found in 36 patients (18%). While the presence of angina, CHF symptoms, CHF duration, NYHA class, extent of angiographic collateral, electrocardiographic Q waves were similar between patients with and without substantial viability; patients with substantial viability had greater severity of coronary stenosis (98 ± 14% vs. 81 ± 32%, p = 0.003) and

EDWT (4.53 ± 0.73 vs. 4.11 ± 0.85 mm, p = 0.006). Follow up imaging was performed in 40 of the 76 patients that underwent revascularization (12 patients with and 28 without substantial viability). After revascularization patients with substantial viability had marked increase in SWT (3.3 ± 13.2% vs. 32.1 ± 16.4%, p < 0.001) and EDWT (4.40 ± 0.59 vs. 7.55 ± 1.08, p < 0.001), whereas those without substantial viability had no significant change in SWT (0.1 ± 8.5% vs. 3.0 ± 6.9%, p = 0.08) and EDWT (4.53 ± 0.64 vs. 4.64 ± 0.74, p = 0.16), see Figure 1. On multivariate analysis the only independent predictors of increase in SWT were % SWT at baseline (p = 0.008) and % viability in the thinned region (p < 0.001). The only independent predictors of increase in EDWT were %LV thinned (p = 0.04) and % viability in the thinned region (p < 0.001).

Conclusion: Up to 18% of patients with thinned akinetic myocardium have substantial viability. Revascularization of these patients results in improvement in systolic wall thickening and reversal of diastolic wall thinning. The % viability in the thinned region based on DE-MRI is the strongest independent predictor of both improvement in function and reversal of wall thinning.

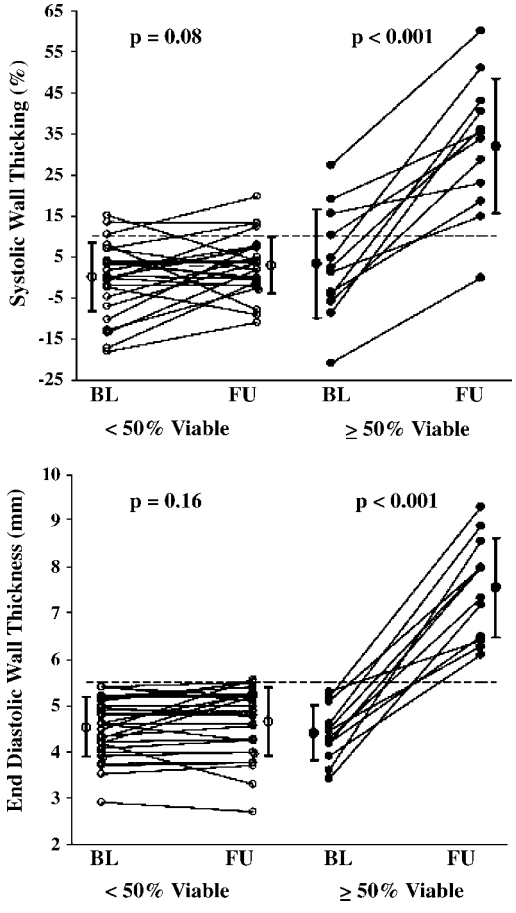

Figure 1.

181. Comparison of Contrast Enhanced Magnetic Resonance Imaging to Positron Emission Tomography with F-18 Fluorodeoxyglucose and Rb-82 for the Detection of Myocardial Viability Using Left Ventricular Bullseye Analysis

Robert Eisner, PhD,[1] Thomas Meyer, MD,[1] Steven Sigman, MD,[1] Susan Eder, ARRT(MR),[1] James Streeter, BS(CNMT),[1] Randolph Patterson, MD,[1] Roderic Pettigrew, MD, PhD.[2]
[1]*Carlyle Fraser Heart Center, Emory Crawford Long Hospital, Atlanta, GA, USA,* [2]*National Institute of Biomedical Imaging and Bioengineering, National Institutes of Health, Bethesda, MD, USA.*

Introduction: Results from previous comparisons of contrast enhanced magnetic resonance imaging (CEMRI) and positron emission tomography with F-18 fluorodeoxyglucose (PET FDG) for detection of viable myocardium have been complicated by methodologies that use segmental analyses applied at a limited number of slice positions. Utilizing a large number of myocardial segments these analyses are made difficult by the inherent differences in spatial and contrast resolution. Acquisition differences related to the lack of respiratory and cardiac gating in PET further complicate comparisons.

Purpose: Present a left ventricular bullseye analysis that takes into consideration coronary arterial territories (CATs) to provide a simplified presentation of CEMRI in a clinically useful manner and to validate CEMRI detection of viability using a similar PET bullseye technique as a reference standard.

Methods: 30 patients had MRI and ungated PET-FDG/rest Rb-82 studies performed within 24 hours.

PET: Rest Rb-82 images were acquired on POSITRON system 180–200 seconds [200 second acquisition] following 40–60 mCi Rb-82 infusion. After 30–60 minutes glucose loading, FDG images were acquired 45 minutes following 10 mCi FDG injection. PET bullseye displays were generated from maximal count circumferential profiles on short axis slices. PET Rb-82 defect region was defined as < 2.5SD from normal and the defect region was mapped to FDG bullseye. PET "scar" (match) and "viable" (mismatch) in defect region were defined as < 50% and > 50% maximum FDG counts, respectively.

MRI: 3D breath hold IR-TFE short axis slice acquisitions at mid-diastole were performed on Philips 1.5 T Intera CV 10–20 minutes following gadolinium injection. CEMRI "scar" wall thickness bullseyes (MRI SCAR in Figure 1) were generated from manual edge drawing encompassing hyperenhanced regions on short axis slices, and CEMRI "viability" wall thickness bullseyes (MRI VIABILITY) were generated from edge drawings that excluded the hyperenhancement regions. To facilitate a clinically relevant comparison, CEMRI "scar" was defined as a region where thickness of subepicardial viable rim < 3 mm (blue region in MRI

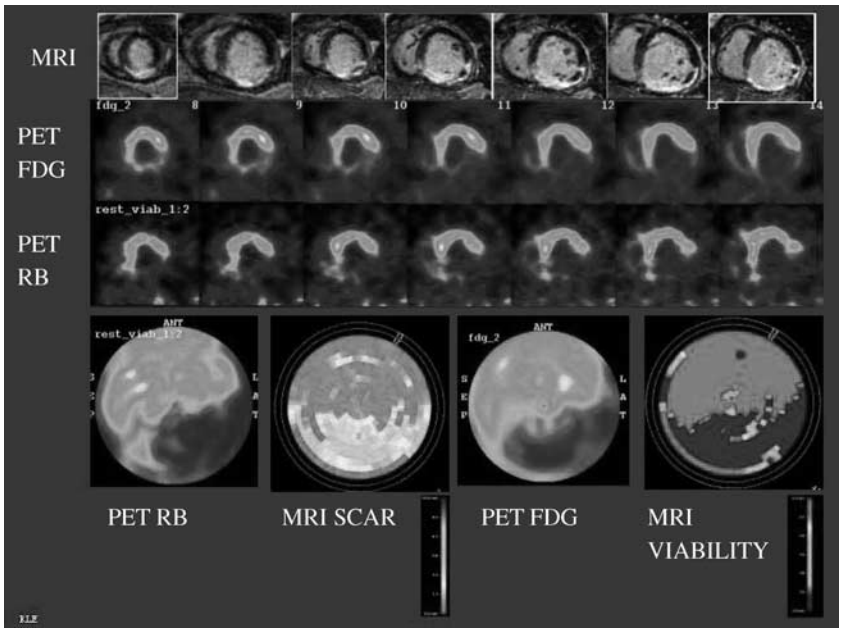

Figure 1.

VIABILITY bullseye) in region of CEMRI hyperenhancement. CEMRI bullseyes were rotated to align with PET bullseyes in standard orientation. In a blinded manner, CEMRI was compared to PET 1) for each patient and 2) using a 17 segment bullseye model which was coalesced into 4 bullseye regions based on CATs.

Results: One PET FDG study could not be evaluated because it had too few counts and another showed an indeterminate FDG uptake pattern. CEMRI identified areas of scar or viability as defined by PET match or mismatch in 27/28 patients. For the CAT analysis, sensitivity for CEMRI to detect PET defined scar was 92% (47/51) and specificity was 98% (60/61). The only patient inconsistency had a matched PET defect with a corresponding 5 mm thick CEMRI hyperhancement but with a 5 mm thick subepicardial rim that was > 3 mm cut-off for CEMRI "scar". There were 4 other discordant regions: 3 were related to small spillover of large non-viable areas into adjacent CATs, and one was a small matched PET defect which was in a slightly different bullseye position than the CEMRI hyperenhancement. 7/10 PET mismatched regions showed no hyperenhancement and 3/10 showed subendocardial hyperenhancement.

Conclusions: 1) Analysis of CEMRI using a bullseye technique provides a clinically useful left ventricular display recognizing coronary arterial territories, and is easily compared to the corresponding PET bullseye images. 2) CEMRI has excellent agreement with clinical PET interpretations for the regional determination of myocardial scar. 3) CEMRI and PET results concur in 27/28 patients with subepicardial viable rim cut-off < 3 mm for MRI "scar" and 28/28 patients with subepicardial viable rim cut-off < 5 mm in hyperenhanced region. 4) CEMRI defines the relative extent of underlying subendocardial scar in PET mismatch regions not resolved by PET.

182. Myocardial Viability Assessment by Contrast-Enhanced MRI Before CABG Surgery—Impact of Late Enhancement Extent in MRI on Coronary Graft Flow

Peter Hunold, MD,[1] Parwis Massoudy, MD,[2] Thomas Schlosser, MD,[1] Claudia Böhm, MD,[2] Jörg Forkel, MD,[2] Sandra Massing, RT,[1] Jörg Barkhausen, MD.[1] [1]*Department of Diagnostic and Interventional Radiology, University Hospital, Essen, Germany,* [2]*West German Heart Center, Department of Thoracic and Cardiovascular Surgery, University Hospital, Essen, Germany.*

Introduction: Contrast-Enhanced cardiac MRI (CE-MRI) has been established for myocardial viability assessment using the late enhancement (LE) concept. It has been proven to reliably detect myocardial scar and predict functional left ventricular (LV) outcome after revascularization in patients with occlusive coronary artery disease (CAD). Coronary artery bypass graft (CABG) flow measured by Doppler sonography during surgery has been shown to predict graft patency. Graft vessels supplying areas of scar with a corresponding lower perfusion are prone to occlusion. CE-MRI might, therefore, predict the probability of functional outcome and, additionally, graft patency after CABG surgery.

Purpose: To determine the relation between myocardial LE in CE-MRI and intraoperative graft flow in CAD

patients with severely impaired LV function undergoing CABG surgery.

Methods: Thirty-three consecutive CAD patients with impaired LV function (mean EF, 29%) underwent CE-MRI using the LE technique before CABG surgery. LE scans were acquired 8–15 min after administration of 0.2 mmol/kg BW of Gd-DTPA (Magnevist™, Schering, Germany) using an inversion-recovery TurboFLASH sequence (TR, 8 ms; TE, 4 ms; FA, 25°; TI, 200–260 ms). The entire LV was covered by long axis and contiguous short axis scans (thickness, 8 mm). Myocardial scar extent was evaluated using a LE score 1–4 (score 1, no LE; 2, LE < 50% of wall thickness; 3, LE > 50%; 4, transmural LE) based on the AHA 17-segment model. A mean score was calculated for each coronary vessel territory (RCA, LAD, LCX). Intraoperative graft flow was determined by Doppler sonography. Flow in grafts supplying vessel territories with a score 1 or 2 (group A) was compared to flow in grafts supplying vessel territories with a score ≥ 3 (group B) which are not expected to improve function after revascularization.

Results: Of the 99 vessel territories, 89 yielded score 1 or 2 (group A), 10 score ≥ 3 (group B). In group A, 68 of 89, and in group B, 9 of 10 territories were grafted using left intrathoracic artery (LITA) or venous grafts. Mean LITA graft flow was 54 ± 6 in group A and 28 ± 11 cc/min in group B ($p < .04$). Mean vein graft flow was 74 ± 6 and 42 ± 8 cc/min in groups A and B, respectively ($p < .05$). After a mean follow-up period of 21 ± 2 months, survival and mean EF were 84% and 36 ± 3% (preop 31 ± 2%) in group A and 88% and 31 ± 3% (preop 28 ± 1%) in group B.

Conclusions: In patients with impaired LV function undergoing CABG, graft flow to vessel territories with no or little scar tissue is higher than flow to vessel territories with more than 50% scar tissue as shown by CE-MRI. Since sufficient flow is a prerequisite for graft patency, the long-term prognosis of those grafts may be better. MRI, therefore, might predict graft patency. However, intermediate-term survival and functional benefit was comparable in both groups.

183. CMR Contrast-Enhanced Study of Dilated Cardiomyopathy

Sandra Pujadas, MD, Francesc Carreras, MD, Antoni Bayes-Genis, MD, Marta Camprecios, MD, Vicenç Brossa, MD, Sonia Mirabet, MD, Ruben Leta, MD, Guillem Pons-Llado, MD. *Cardiology, Hospital de Sant Pau, Barcelona, Spain.*

Introduction and purpose: A unique feature of cardiovascular magnetic resonance (CMR) is that it allows, by means of the delayed contrast-enhancement (DCE) technique, an in vivo detection of myocardial scar due to necrosis and, also, of myocardial focal fibrosis non-ischemic in origin. Several studies have shown different degrees and patterns of myocardial DCE in dilated cardiomyopathy (DCM) thought to be due to focal fibrosis. To further increase the body of information on the subject, the present study was aimed to describe the presence and distribution of focal myocardial fibrosis in a series of patients with idiopathic dilated cardiomyopathy (DCM).

Methods: Thirty consecutive patients (26 males; mean age 50 ± 12) with DCM were studied by CMR using a Philips Intera 1.5 T system. Patients were included only if they had a normal coronary angiogram. Steady-state free-precession cine-MR and DCE images were acquired in short-axis slices from the atrioventricular ring to the apex. All the images were analysed on a dedicated software (MEDIS Mass), where left ventricular end-diastolic (LVEDV) and end-systolic (LVESV) volumes, and ejection fraction (LVEF) were calculated.

Results: 73% (22/30) of patients did not show any kind of DCE. In the remaining 27% (8/30) the following DCE distribution patterns were observed: 1) midwall myocardial striae, in 3 cases (10%); 2) focal in the RV-LV junction, in 2 cases (6%); 3) transmural, in 2 cases (6%). No significant differences were found when comparing the group showing DCE with the one without it, regarding LVEDV (276 ± 75 vs. 247 ± 108 ml, respectively; P = 0.42), LVESV (205 ± 82 vs. 169 ± 112 ml, respectively; P = 0.36) or LVEF (29 ± 11% vs. 35 ± 16%, respectively; P = 0.20).

Conclusions: Most patients (73%) with idiopathic DCM do not show DCE at CMR, while it is present in 27%, presumably due to focal myocardial fibrosis, fairly distinct in location and distribution, in most of the cases, from that seen in patients with a previous myocardial necrosis. Therefore, this technique could be useful as a noninvasive tool for differential diagnosis of idiopathic vs. ischemic DCM. The presence of DCE in patients with DCM does not seem to imply a higher degree of impairment of left ventricular morphological or functional features.

184. Detection of Intraventricular Thrombi by Contrast Enhanced Magnetic Resonance Imaging of the Heart

Okan Ekinci, MD,[1] Thorsten Dill, MD,[2] Alexander Kluge, MD,[2] Anja Deetjen, MD,[2] Jochen Hansel, MD,[2] Christian W. Hamm, MD.[2] [1]*Cardiology, German Clinic of Diagnostic, Wiesbaden, Germany,* [2]*Cardiology, Kerckhoff Heart Center, Bad Nauheim, Germany.*

Introduction: The presence of an intracardiac thrombus denotes an increased risk of both embolism and death. Echocardiography is known to be the gold standard for detecting intracardiac thrombi, but especially if located in the left or right ventricular apex, they might be overseen.

Purpose: We investigated the potential of contrast enhanced MRI (ceMRI) for detecting intraventricular thrombi in comparison to routine transthoracic echocardiography findings.

Methods: 72 patients (pts) (60 ± 11 y) with dilative cardiomyopathy or myocarditis with LV ejection fraction below 35% or history of myocardial infarction, underwent transthoracic echocardiography (TTE) and ceMRI (Siemens Sonata 1.5 T). For ceMRI, bolus tracking was done using 3 mL of Gd-DTPA (Magnevist, Schering) for assessment of the time to peak signal intensity in the LV cavity. An i.v. bolus injection of 1 mmol/kg body weight Gd-DTPA was performed for imaging of the ventricular cavities.

Image acquisition was done by use of an inversion recovery 3D-FLASH sequence (slice thickness 5–6 mm, TI 280–300 ms) covering the left ventricle in 2-chamber view orientation and both ventricles in 4-chamber view orientation during intracavity first-pass.

Imaging was repeated after 1 min for delineation of thrombi from myocardium. Same sequences were used for myocardial viability imaging by detecting areas with *delayed hyperenhancement* 8–15 min after contrast injection.

Results: By echocardiography, 7 out of 72 pts (9.7%) had an intraventricular thrombus located in the apex of the left ventricle. No patients were found having RV thrombi.

By ceMRI, 12 pts (16.7%) could be found having 13 thrombi (R = 0.73) with a mean volume of 7.9 ± 2.9 ccm.

All patients with positive TTE finding had also positive ceMRI. Additional thrombi were found by ceMRI in the right ventricular apex (n = 1), left ventricular apex (n = 3) and as a thin layer along aneurysmatic anterior wall myocardial scar (n = 4). 9 patients had transmural scar. 1 patient had myocarditis and thrombi in both ventricles. 2 pts had severely impaired left ventricular function without regional scar tissue.

The protocol allowed complete delineation of all thrombi against blood pool and myocardium/scar tissue, respectively. Poor image quality due to limited echocardiographic window and technical limitations were the primary reasons for missing thrombi by TTE.

Conclusions: MRI is an accurate tool for detecting intraventricular thrombi, being even superior to transthoracic echocardiography in this patient cohort.

Furthermore, myocardial viability imaging can be done without additional contrast agent application, providing important data regarding the etiology of thrombus formation.

185. Myocardial Scaring and Fibrosis Cause Abnormal Contractile Mechanics in Single Ventricle After Fontan Operation: A New Insight by MRI Studies

Gautam K. Singh, MD,[1] Madelyn Stazzone, MD,[2] Achi Ludomirsky, MD,[1] Sherry Lassa-Claxton,[1] Brian Cupps, PhD,[1] Michael Pasque, MD,[1] Glenn Foster,[1] Joseph J. Billadello, MD,[1] Philip A. Ludbrook, MD,[1] Michael A. Beardslee, MD,[1] Pam Woodard, MD.[1] [1]*Pediatric Cardiology, Washington University School of Medicine, St. Louis, MO, USA,* [2]*Radiology, Washington University School of Medicine, St. Louis, MO, USA.*

Many patients develop long term progressive ventricular failure following Fontan procedure (cavo-pulmonary shunt creation in heart with single ventricle physiology). The exact mechanism for this phenomenon is unclear. Abnormal contractile mechanics can contribute to ventricular dysfunction and failure. The purpose of this study was to assess if myocardial fibrosis/scaring occurs in patients following Fontan and contributes to the abnormal regional and global contractile mechanics in the single ventricle.

Methods: Nine pts with single (left) ventricle (median age 20 yrs, 5 M) > 10 yrs post-Fontan, underwent delayed contrast-enhanced magnetic resonances imaging for quantitative assessment of myocardial scarring. Inversion time was selected to null normal myocardium. Ventricular function was assessed by cine steady-state precession imaging and myocardial strain by myocardial tagging in pts and in 27 normal subjects (median age 29 yrs, 14 M). Eight slices of images were obtained in short axis from ventricular base to apex. Each slice image was divided into 6-segments to assess regions of signal abnormality, abnormal wall motion and strain. Strain was computed using a least squares fitting of measured displacements obtained from tissue-tagged MR images.

Results: Three patterns: diffuse, punctuate and segmental transmural types of scarring were seen in 58/432 segments of 8/9 pts, mostly confined to septal and adjoining segments representing 3 to 10% of LV mass/pt. Compared to normal subjects maximal shortening strains at midventricular level in pts (− 20 ± 3% vs. − 15 ± 5%) were significantly ($p < 0.05$) decreased, more in segments with (− 11 ± 2%) than without (− 16 ± 3%) scar. Twenty-four percent of scar affected segments also showed decreased thickening and abnormal wall motion. Single ventricle EF (median 40%, range 29% to 55%) was decreased as compared to normal population (65 ± 5%).

Conclusions: Segmental and diffuse myocardial fibrosis/scaring occurs at long term in Fontan-palliated single ventricles and contributes to abnormal contractile mechanism resulting in impaired ventricular function. MRI studies of single ventricles can be an important tool in assessing function and predicting the long term outcome in patients after Fontan surgery.

186. Atrial Septal Defect Flow Measured by Cardiac Magnetic Resonance Imaging Predicts Right and Left Ventricular Remodeling After Amplatzer Device Closure

Anna Lisa Crowley, MD, Louise E. J. Thomson, MB ChB, John F. Heitner, MD, N. Raj Subramanian, MD, Peter J. Cawley, MD, Jonathan W. Weinsaft, MD, Robert M. Judd,

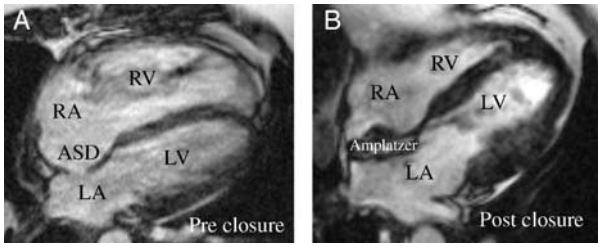

Figure 1. Heart morphology pre (A) and post (B) ASD closure.

PhD, Raymond J. Kim, MD, J. Kevin Harrison, MD. *Cardiology, Duke University, Durham, NC, USA.*

Objective: Whether LV remodeling occurs after atrial septal defect (ASD) closure with the Amplatzer device is unknown. Direct ASD flow measured by cardiac magnetic resonance (CMR) can predict the degree of RV and LV remodeling.

Methods: In 21 patients (age 48 ± 17 yrs, 61%F), CMR (1.5 T Siemens) 1 day prior to and a mean of 5 ± 2.5 months following ASD closure was performed. Contiguous long axis cine images of the heart were obtained. Retrogated velocity encoded CMR was used to measure flow en face through the ASD. Analyses to determine ASD flow, RV and LV volumes were performed with Argus software. We tested whether age, PVR, baseline RVEDV, baseline EF, Amplatzer device size, ASD area, or ASD flow predicted RV and LV remodeling.

Results: A 33% mean reduction in RVEDV ($p < 0.0001$) and a 29% mean reduction in RVESV ($p < 0.0001$) was observed after ASD closure (Figure 1). Baseline RVEDV, ASD flow and ASD area as measured by CMR were the only predictors of the reduction in RVEDV ($r = 0.89$, $p < 0.0001$, $r = 0.8$, $p < 0.0001$ and $r = 0.75$, $p = 0.0003$ respectively). Age, PVR, Amplatzer size, and RVEF did not predict RV remodeling. A 13% mean increase in LVEDV ($p = 0.012$) and a 28% mean increase in LVESV was demonstrated after ASD closure ($p = 0.014$). LVEF did not change. ASD flow was the only predictor of the increase in LVEDV ($r = 0.46$, $p = 0.05$). Age, baseline RVEDV, ASD area, PVR, Amplatzer size and LVEF did not correlate with LV remodeling.

Conclusions: Not only RV, but also LV remodeling occurs after ASD closure. ASD flow as measured by CMR was the only predictor of both RV and LV remodeling, with more remodeling in patients with large intracardiac shunts.

187. Magnetic Resonance Myocardial Delayed Enhancement in Infants with Anomalous Origin of Left Main Coronary Artery from Pulmonary Artery

Carlos E. Rochitte, FlÃ¡vio Luiz Rua Ribeiro, MD, Nana Miura Ikari, MD, Luiz Alberto Bevenuti, MD, Eliza Rumiki Iwahashi, MD, Solange de Sousa Andrade, MD, JosÃ© Rodrigues Parga, MD, Luiz F. Ã!vila, MD, Miguel Lorenzo Barbero Marcial, MD, JosÃ© Antonio Franchini Ramires, MD, Antonio Augusto Barbosa Lopes, MD. *Cardiology, Heart Institute -InCor- University of SÃ£o Paulo Medical School, Sï¿½Ã£o Paulo, Brazil.*

Introduction: Myocardial ischemia in infants with anomalous origin of left main coronary artery from pulmonary artery (AOLM) may lead to variable extent of irreversible injury and severe LV dysfunction. In this condition, severe LV dysfunction associated to very thin LV wall may generate a particular difficult case for the detection of myocardial viability by other methods. The impact of the myocardial viability may direct clinical decision and therapy from coronary re-implant to cardiac transplantation. Myocardial delayed enhancement technique by MRI (MDE) can detect precisely infarct and myocardial fibrosis (MF).

Objectives: To investigate myocardial viability in infants with AOLM by MDE.

Methods: 7 infants (4 females) with AOLM and severe LV dysfunction submitted to corrective surgery between 3–9 month of age, underwent MRI study in a 1.5 T GE scanner using MDE, during the in-hospital period for corrective surgery. We evaluated the LVEF and MF quantitatively by MRI.

Results: Mean LVEF was 17.7 ± 3.5%. MF was detected in all cases. Mean MF was 14.2 ± 8.2% of LV mass. The most affected LV segments were anterior and basal anterolateral. Only 2 cases showed transmural pattern of MF, 5 cases showed mainly subendocardial MF with variable degree of circumferential extent. Late (6–12 month) clinical follow-up of 6 infants showed normalization of LV function. One infant, that had the highest MF (29.7% of LV mass) died during surgical procedure due to cardiogenic shock. On this case, MF by macroscopic pathology matched MF by MRI precisely (Figure 1). Moreover, microscopic staining by Masson's trichrome confirmed massive MF on those segments and revealed islands of MF and diffuse vacuolization (reversible injury) of myocytes on segments with no MDE (Figure 2).

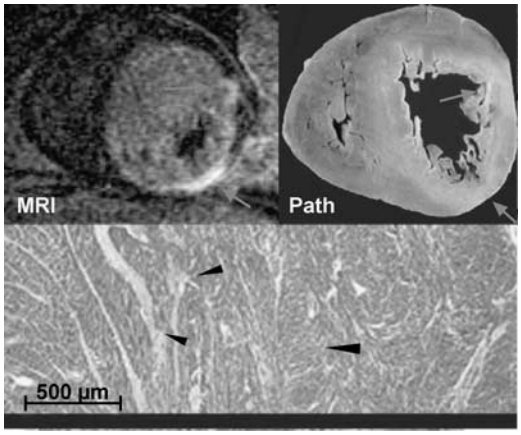

Figure 1.

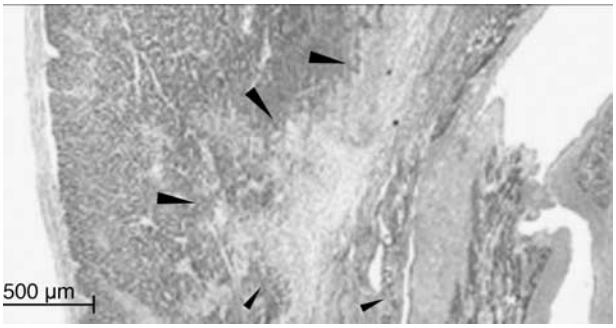

Figure 2.

Conclusion: Myocardial delayed enhancement by MRI can detect myocardial fibrosis in infants with anomalous origin of left main coronary artery from pulmonary artery and provide critical information on myocardial viability to manage therapy (corrective surgery vs. heart transplant).

188. Initial Experience with 3 Tesla Cardiac MRI Studies for Small Infants and Children: The Advantages and Problems

Michael Silberbach, MD,[1] Katherine Hopkins, MD,[2] William J. Woodward, RT,[2] Erwin Schwarz, RT,[2] Michael Jerosch-Herold, PhD,[2] David J. Sahn, MD.[1] [1]*Pediatric Cardiology, Oregon Health & Science University, Portland, OR, USA,* [2]*Diagnostic Radiology, Oregon Health & Science University, Portland, OR, USA.*

Introduction/purpose: While we have expected that the opportunity to study our pediatric patients at 3 Tesla field strength would offer better implementation of a number of pulse sequences and improved diagnostic capability, little experience has been reported at 3 Tesla for pediatric cardiac studies.

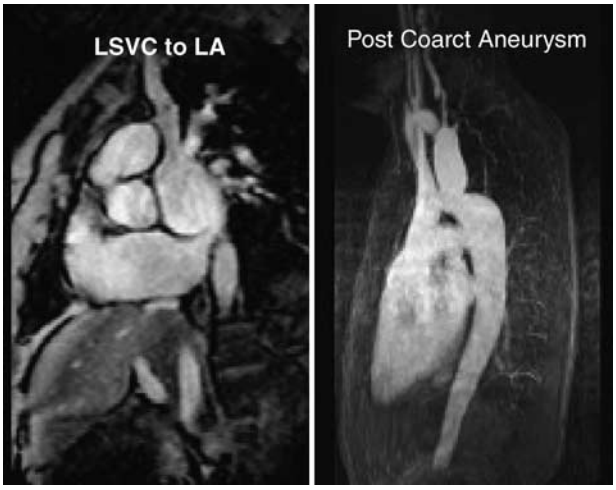

Methods: We studied 35 patients with congenital heart disease (CHD) aged 2 days–19 years, with diagnoses including TOF, VSD, PAPVR aortic area and systemic venous anomalies. We used a 3 Tesla Philips system with a phased-array coil with anterior and posterior elements, allowing parallel image acquisition in older patients and a 2 element flexible surface coil for infants.

Results: Use of fast field echo (FFE) produced artifact-free, high-resolution cine images to evaluate anatomy and function and T1-weighted single-shot survey imaging. S/N ratio for single-shot T1-weighted imaging of contrast enhancement at 3 T was high enough for use of parallel acquisition techniques (SENSE) with acceleration factors of 2; echo times of approx. 1 ms. High quality angio or perfusion images were obtained without appearance of susceptibility artifacts during peak contrast enhancement. 2D and 3D gadolinium angiographic sequences were also shortened with parallel acquisitions. In small infants, MRI tagging with 6 mm tag-line spacing and 2 mm in-plane resolution allowed coverage of the entire cardiac cycle with less tag-line fading than at 1.5 T. FFE with steady state free procession (SSFP) was more prone to flow and chemical shift (fat/water or air/tissue) artifacts than FFE without SSFP. Image susceptibility artifacts with SSFP could only be partially avoided by shimming over the heart, and only standard FFE routinely yielded diagnostic cine images for infants.

Conclusions: Early experience suggests significant advantages for 3 T MRI in children with CHD.

189. Normal Aortic Compliance and Left Ventricular Mass Late After Repair of Aortic Coarctation

Isabelle F. Vonder Muhll, Lorna Swan, Mustafa Kraidly, Michael Gatzoulis, Philip Kilner. *Cardiovascular Magnetic Resonance Unit, Royal Brompton Hospital, London, UK.*

Introduction: After surgical repair, patients with coarctation of the aorta (COA) have been reported to have an increased risk of late atherosclerotic cardiovascular events. The factors mediating this increase in risk are likely multifactorial. Impaired arterial compliance and left ventricular hypertrophy have been implicated, although the degree to which the increased risk can be ascribed to arterial hypertension alone is unclear.

Purpose: We sought to determine if impaired aortic compliance and left ventricular hypertrophy could be demonstrated by cardiac magnetic resonance (CMR) imaging in the absence of arterial hypertension in adult patients late after repair of aortic coarctation.

Methods: Patients with repaired COA who had no residual hemodynamic lesions and without arterial hypertension (n = 23 [9 female], 31 ± 8 years of age) were selected for assessment by CMR (Siemens Sonata whole-body 1.5 T

Table 1.

	CoA	Controls	p
Systolic blood pressure (mmHg)	124 ± 17	114 ± 17	0.04
Diastolic blood pressure (mmHg)	70 ± 12	66 ± 11	0.21
Ascending aortic compliance (μL/mmHg)	16.4 ± 7.5	18.9 ± 7.4	0.27
Left ventricular mass index (g/m sq.)	77 ± 15	72 ± 10	0.14

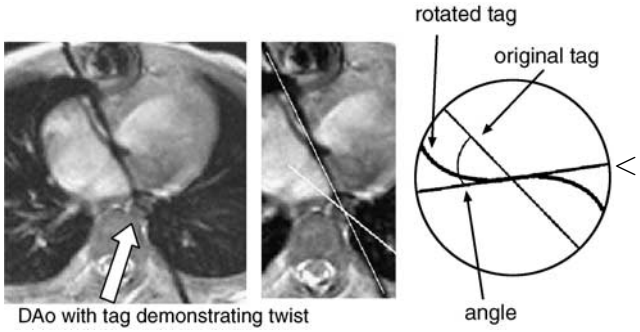

scanner) and compared to age and sex matched normal controls (n = 20 [9 female], 33 ± 7 years of age). High resolution cine imaging was used to estimate regional compliance of the ascending aorta, calculated as the change in volume of the aortic segment over the cardiac cycle, divided by aortic pulse pressure measured non-invasively. Left ventricular mass was determined at end diastole by standard cine imaging of the left ventricle in short axis.

Results: CMR imaging in the COA patients confirmed no residual aortic obstruction at the site of previous coarctation repair. A bicuspid aortic valve was present in 14/23 COA patients, with mild aortic regurgitation in five of these. The remainder of patients and controls had no significant aortic valve disease. Systolic blood pressure was within normal limits in the COA patients, but higher than control subjects (see Table 1). The ascending aortic compliance was not significantly impaired in COA patients (see Table 1). At a median of 22 years (range 5–35) after repair of COA, left ventricular mass indexed to body surface area was not elevated in patients compared to controls (see Table 1).

Conclusions: Patients with repaired COA with no residual hemodynamic lesions and without arterial hypertension have normal aortic pulsatile hemodynamics and do not suffer from left ventricular hypertrophy. These findings suggest that any increase in risk of atherosclerotic complications late after COA repair is more likely to be mediated by hypertension than intrinsic impairment of arterial compliance in the repaired coarcted aorta.

190. Variability in Secondary Flow Patterns in the Aorta of Single Ventricle Patients After Bidirectional Cavo-Pulmonary Connection

Mark A. Fogel, MD, Suzanne Durning, Gil Wernovsky, MD, Avrum Pollock, MD, Nicolson Susan, MD. *Pediatric Cardiology, Children's Hospital of Philadelphia, Philadelphia, PA, USA.*

Introduction: We have previously demonstrated that primary flow profiles in the descending aorta (DAo) skew posteriorly in pts who have undergone an aortic to pulmonary anastomosis and in those who have not. It is not known whether secondary flow profiles are affected by an aortic reconstruction (recon). Flow profiles are important in cardiovascular energetics, organ perfusion and future development of atherosclerosis.

Purpose: To determine secondary flow patterns in patients after bidirectional cavopulmonary connection.

Methods: 10 single ventricle pts (7 recon, 3 no recon) after hemiFontan (age 2.2 ± .5 yrs) underwent MRI blood (bolus) tagging in the DAo. The tag was placed parallel to the direction of blood flow and the twist of the tag was measured relative to stationary structures over the DAo cross-section (see images).

Results: In 2/7 pts with recon, DAo flow twisted counterclockwise and the others twisted clockwise. In single left ventricles with Damus-Kaye-Stansel procedures (N = 2), 1 Dao was clockwise and the other was counterclockwise. In the 3 pts without recon, one pt twisted clockwise while 2 twisted counterclockwise. Maximum twist, whether clockwise and counterclockwise was 43–47 degrees occurring 275 ± 30 milliseconds after the R wave.

Conclusions: Unlike primary flow patterns in the DAo, secondary flow patterns in recon and non-recon aortas are variable, twisting both clockwise and counterclockwise. This information may be useful when planning future modifications of aortic recons.

191. Cardiac Magnetic Resonance Imaging in Congenital Heart Disease Using Free Breathing with Deep Sedation

Emily A. Wessler, MD,[1] Barry A. Love, MD,[1] Karen I. Norton, MD,[2] Frank Macaluso,[2] James C. Nielsen, MD.[1] [1]*Pediatric Cardiology, Mount Sinai Hospital, New York, NY, USA,* [2]*Radiology, Mount Sinai Hospital, New York, NY, USA.*

Background: Cardiac magnetic resonance imaging (CMRI) has become a valuable non-invasive tool for evaluating structure, function, and flow rates in congenital heart disease. General anesthesia is commonly used in infants and small children because of the cooperation required for accurate imaging. An alternative approach utilizing deep sedation and

imaging during free-breathing may be advantageous in some patients. We sought to determine the accuracy of deep sedation free-breathing CMRI data using catheter obtained data as the reference standard.

Methods: From June 2003 until June 2004, 17 deep sedation CMRI were performed using chloral hydrate (80 mg/kg) with no adverse events. There was 1 failed sedation which was repeated with success. Nine patients (mean age 1.2 ± 0.6 years) had cardiac catheterization data available. Indexed pulmonary (Qp) and systemic (Qs) blood flow were measured using a standard segmented *k*-space phase contrast sequence (TR 6.8–7.8 msec, TE 3.2–3.4 msec, VPS 2, NEX 3, FOV 20–26 cm, slice thickness 5–6 mm, matrix 256 × 128, BW 31.3 kHz, flip angle 20). Qp and Qs were determined by the Fick method using invasive oximetry and estimated oxygen consumption. Pearson's correlation coefficient (R) and the Bland-Altman method of agreement were used to evaluate the accuracy of the CMRI data. All data are presented as mean ± SD or as median (range).

Results: Median time between CMRI and catheterization was 27 days (− 3 to 317 days). The mean heart rate during the CMRI and the catheterization were 106 ± 21.4 and 122.5 ± 21.7 beats per minute (bpm), respectively. The mean difference in heart rate was − 16 ± 14.5 bpm. The patients' physiology included cavopulmonary anastomosis (N = 4), no shunting (N = 3), and left-to-right shunting (N = 2) with a range for CMRI Qp/Qs of 0.49–3.3 and for catheter obtained Qp/Qs of 0.46–2.8.

Variable	R	Mean difference	Limits of agreement (mean ± 2SD)
Qp	0.89	− 0.46 L/min/m^2	− 3.0 to 2.1 L/min/m^2
Qs	0.79	− 1.0 L/min/m^2	− 4.1 to 2.1 L/min/m^2
Qp/Qs	0.96	+ 0.2	− 0.48 to 0.89

Conclusion: CMRI using free breathing and deep sedation is safe and reliable, and for flow ratio (Qp/Qs) there is good agreement compared with oximetry. The relatively poor agreement found between CMRI and catheterization data for absolute flow (Qp and Qs) is not surprising given the inherent variability of cardiac output over time, the different physiologic states during data acquisition (deep sedation versus general anesthesia), the known error with assumed oxygen consumption in young subjects, and the non-simultaneous comparison.

192. CMR Assessment of Pulmonary Regurgitation and Right Ventricular Function After Repair of Tetralogy of Fallot

Karen G. Ordovas, MD, Mei-Han Wu, MD, Gautham P. Reddy, MD, M.P.H., Charles B. Higgins, MD. *Radiology, UCSF, San Francisco, CA, USA.*

Introduction: Pulmonary regurgitation is one of the most important sequela after surgical correction of tetralogy of Fallot and is one of the determinants of long term clinical outcome. Several prior studies have used volumetric cine MR and phase-contrast cine MR to evaluate severity of pulmonary regurgitation and right ventricular volumes and function in these patients (1,2). Traditionally, the major parameter used in evaluating right ventricular (RV) function has been ejection fraction. Pulmonary valve replacement has been shown to improve ventricular function in these patients as assessed by CMR (3). Consequently, it is important to determine the need for and timing of valve replacement.

The purpose of this study was to evaluate CMR measurements of RV volumes and function that can indicate diminished RV ventricular function in order to provide an indication for valve replacement.

Patients and Methods: We evaluated 14 patients with surgically corrected tetralogy of Fallot with pulmonary regurgitation who had undergone MRI studies over a two year period. Time since surgical correction varied from 2.5 months to 53 years. Pulmonary regurgitant volume, pulmonary regurgitant fraction , RV end-diastolic volume (RVEDV), RV end-systolic volume (RVESV), RV stroke volume (RVSV) and RV ejection fraction (total RVEF) were calculated from short-axis cine-MR images. Severe tricuspid regurgitation was excluded in all patients throught echocardiography. In the presence of regurgitation, the use of ejection fraction to assess ventricular function is complicated by the fact that much of the stroke volume is related to regurgitant volume. As an alternative, we assessed the effective (forward) RVEF , calculated by dividing the difference between right ventricular stroke volume and pulmonary regurgitant volume by the right ventricular end-diastolic volume (RVSV-pulmonary regurgitant volume/RVEDV). End-diastolic volume and end-systolic volume indexes (EDVi, ESVi) were calculated based on the body surface area. Correlation coeficient was assessed to measure the correlation of pulmonary regurgitant fraction with total RVEF and effective RVEF. ANOVA was use to compare EDVi with effective RVEF and total RVEF. A cut-off of 180 ml/m^2 for RVEDi was used to categorize the sample.

Results: A strong correlation between pulmonary regurgitant fraction and effective RVEF ($r = 0.81$, $p = 0.001$) was identified. There was no significant correlation between pulmonary regurgitant fraction and total RVEF. The mean effective RVEF in the group of patients with REDVi less then 180 ml/m^2 was 30.3% ± 9.8%, while in the patients with REDVi greater than 180 ml/m^2, the mean effective RVEF was 17.2% ± 4.4% ($p = 0.016$). The sample size was not large enought to evaluate any correlation between time since surgical procedure and RV function.

Conclusion: Calculation of total RVEF in patients with pulmonary regurgitation is probably not usefull because of the confounding effect of pulmonary regurgitant volume. Effective (forward) RVEF provides a better indication of RV function in this setting and is inversely related to regurgitant

fraction. RV volumetrics, as reflected by RVEDVi, seems to be predictive of deteriorating RV function.

193. Impaired Left Ventricular Function in Patients with Severe Dilatation of the Right Ventricle Late After Total Repair of Tetralogy of Fallot

Alexander van Straten, MD,[1] Heynric Grotenhuis, MD,[1] Hubert W. Vliegen, MD, PhD,[2] Mark G. Hazekamp, MD, PhD,[3] Albert de Roos, MD, PhD.[1] [1]*Radiology, Leiden University Medical Center and Kennemer Gasthuis in Haarlem, Leiden, The Netherlands,* [2]*Cardiology, Leiden University Medical Center, Leiden, The Netherlands,* [3]*Cardiothoracic Surgery, Leiden University Medical Center, Leiden, The Netherlands.*

Background: In patients late after repair of tetralogy of Fallot (TOF), pulmonary regurgitation (PR) may lead to enlargement of the right ventricle and eventually to arrhythmias and even sudden death. Many studies have focussed on the right ventricular (RV) function in these patients, however, not much is known about the left ventricular (LV) function during follow-up. Therefore, we investigated the influence of RV dilatation on LV function in patients late after repair of TOF.

Methods: Two hundred thirty consecutive magnetic resonance (MR) examinations were performed in our institution between January 1990 and May 2003 in 126 TOF patients. The mean age at total repair was 8.3 ± 10.5 years and the mean follow-up after repair was 16.6 ± 10.1 years. RV and LV volumes were assessed using a standard gradient-echo sequence in the short-axis and ejection fractions were calculated according to the Simpson's method. Furthermore, a phase-contrast cine MR sequence was used to assess flow curves for the pulmonary valve. Bivariate correlation analysis was performed to evaluate correlations between RV and LV function parameters and correlation coefficients were calculated.

Results: Mean PR fraction was 31.1 ± 20.1% and mean RV end-diastolic volume (EDV) was 221.1 ± 90.8 ml. There was a positive correlation between RV-EDV and LV-EDV ($R = 0.64$, $P < 0.05$) (Figure 1). Furthermore, a strong positive correlation was found between the RV-EF and LV-EF ($R = 0.55$, $P < 0.01$). These results indicate that RV dysfunction has a deleterious effect on LV function.

Conclusion: LV function is a strong prognostic factor in all heart diseases. In this study we found that in repaired TOF patients, RV enlargement leads to LV dilatation and decreased systolic function. Furthermore, LV systolic function was diminished in patients with decreased RV-EF. The relationship between right and left ventricular function has not yet been elucidated. Possibly, RV dilatation leads to traction on the ventricular septum and consequently enlargement and dysfunction of the left ventricle. Therefore early replacement of the pulmonary valve for RV dysfunction is desirable to prevent its negative effects on the LV function.

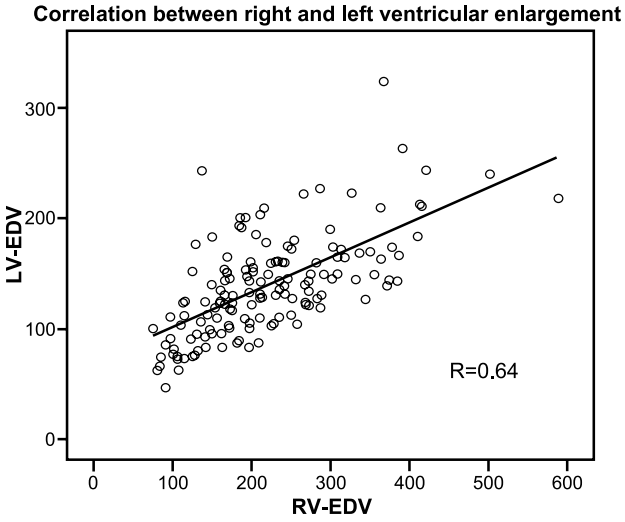

Figure 1. Correlation between right and left ventricular enlargement.

194. STEAM Localization for Short Echo Time Cardiac Proton Spectroscopy at 3.0 Tesla

Michael Schär,[1] Sebastian Kozerke,[1] Robert G. Weiss,[2] Paul A. Bottomley,[2] Peter Boesiger.[1] [1]*Institute for Biomedical Engineering, University and ETH Zurich, Zurich, Switzerland,* [2]*School of Medicine, Johns Hopkins University, Baltimore, MD, USA.*

Introduction: Cardiac proton spectroscopy allows the non-invasive investigation of creatine and lipid metabolism in the human heart. The total creatine content has been shown to be reduced in myocardial infarction (Bottomley et al., 1998) and in heart failure (Nakae et al., 2003). Determination of myocardial lipid content offers a new strategy to study the functional importance of cardiac steatosis (Szczepaniak et al., 2003).

Cardiac and respiratory motion can cause displacements on the order of the localized voxel and difficulties in shimming and water suppression calibration. Therefore, respiratory and cardiac double triggering may be necessary for high spectral quality and reproducibility (Felblinger et al., 1999). Recently, a double triggered technique based on navigator echoes was introduced at 3.0 T (Schär et al., 2004). The higher field strength should improve spectral resolution and signal to noise ratio compared to 1.5 T.

Purpose: Spatially-localized 3.0 T studies on the human heart using PRESS localization (Bottomley et al., 1987)

resulted in longer echo times TE ($\sim$ 40 msec) than earlier work at 1.5 T because of the reduced maximum amplitude ($B1_{max}$) of the radio-frequency excitation pulses and the need for strong crusher gradients. The purpose of this study was to reduce TE by applying a STEAM localization technique (Frahm et al., 1987).

Methods: STEAM localization was implemented allowing short echo times when using the whole body coil for excitation. STEAM (90°-TE/2-90°-TM-90°-TE/2-acquisition; TM the mixing time) has an inherent shorter TE than PRESS as magnetization does not undergo any T2 decay during TM because it is stored in the longitudinal direction. The shorter TE comes at the cost of loosing half of the initially excited magnetization. The use of 90° instead of 180° pulses with the limited $B1_{max}$ leads to shorter excitation pulses reducing TE even further. The shorter pulses allow stronger spatial selective gradients and, therefore, reduce the chemical shift selective artifact.

In-vivo measurements were performed in a healthy volunteer on a 3.0 T Intera whole body MR system (Philips Medical Systems, Best, The Netherlands) using a circular surface coil. Cardiac triggering was performed using a vector-ECG. A mid-ventricular short-axis cine was acquired to determine the trigger delay for least motion in mid-diastole. Second order shimming and frequency determination was based on B_0-mapping. For STEAM volume placing, short-axis and long-axis views were measured using the calculated shim and frequency settings (Figure 1).

For the spectroscopy scan, the navigator echo excitation was applied after the chemical shift-selective water suppression to minimize the time delay between the navigator acquisition and the actual data collection, which led to degraded water suppression. Outer volume suppression was applied in all six directions. The parameters for the spectroscopy measurement were: TE: 20 ms,TM: 20 ms, bandwidth: 2000 Hz, 1024 data points, repetition time: at least 3500 ms, position: supine, and averages: 128 resulting in a scan time of less than 10 minutes assuming a navigator efficiency of 50%.

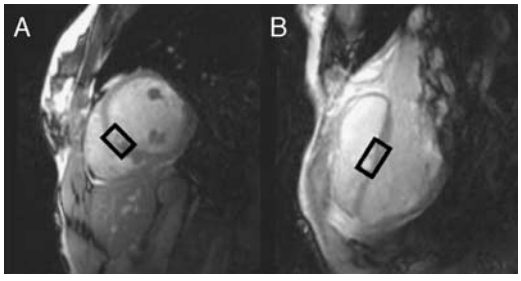

Figure 1. Short-axis (A) and long-axis (B) views at mid-diastole to position the STEAM volume (black box) measured during free-breathing using navigator respiratory motion correction identical to the subsequent spectroscopy measurement.

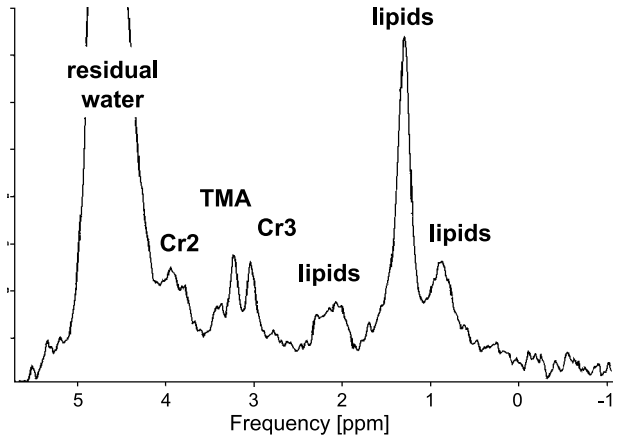

Figure 2. STEAM proton spectrum measured at an echo time of 20 ms from a 10.5 ml volume in the septum of the same healthy volunteer as shown in Figure 1.

The 128 spectra were phased based on the residual water peak, averaged, zero filled to 2048 data points and exponentially filtered with 10 Hz.

Results: Figure 2 shows a spectrum from a 14 × 25 × 30 mm^3 volume in the septum. Peaks from methylene protons (Cr2) of creatine/phosphocreatine (Cr), trimethylammonium compounds (TMA), methyl protons (Cr3) of Cr, and lipids can be observed.

Conclusions: STEAM localization was implemented and combined with the navigator based double triggered cardiac spectroscopy protocol at 3.0 T and allowed reduction of echo times to 20 ms. Initial results show the potential of the technique to acquire high quality spectra from human cardiac muscle in-vivo.

REFERENCES

Bottomley, P. A., et al. (1987). *Ann. N.Y. Acad. Sci.* 508:. 333–348.
Bottomley, P. A., et al. (1998). *Lancet* 351:. 714–718.
Felblinger, J., et al. (1999). *MRM* 42:. 903–910.
Frahm, J., et al. (1987). *JMR* 72:. 502–508.
Nakae, I., et al. (2003). *JACC* 42:. 1587–1593.
Schär, M., et al. (2004). *MRM* 51:. 1091–1095.
Szczepaniak, L. S., et al. (2003). *MRM* 49:. 417–423.

195. In vivo Magnetic Resonance Imaging of Inflammation in Myocardial Infarct Mouse Model

Takayasu Arai,[1] Anthony D. Caffarelli, MD,[2] Joan M. Greve, MS,[3] Paula M. Jacobs, PhD,[4] Robert C. Robbins, MD,[2] Michael V. McConnell, MD,[1] Phillip C. Yang, MD.[1] [1]*Department of Medicine, Division of Cardiovascular Medicine, Stanford University, School of Medicine, Stanford, CA, USA,* [2]*Department of Cardiothoracic Surgery, Stanford*

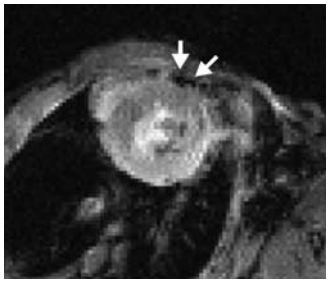

Figure 1. Ferumoxtran-10 signal in the anterior to antero-lateral infarct region as shown by a signal void (white arrows).

University, School of Medicine, Stanford, CA, USA, [3]Department of Radiology, Stanford University, School of Medicine, Stanford, CA, USA, [4]Advanced Magnetics, Cambridge, MD, USA.

Introduction: A reliable method for imaging the inflammatory changes induced by myocardial infarction (MI) has not been established. However, it is well known the presence of inflammatory process in the area of MI. Feasibility of in vivo magnetic resonance (MR) imaging using ultra-small paramagnetic iron oxide (USPIO) agents to detect post-MI inflammatory changes was tested.

Methods: 129Sv/J mice underwent LAD ligation to induce MI (n = 9) or sham operation (n = 3). On post-MI day #6, the USPIO agent ferumoxtran-10 (Combidexâ, Advanced Magnetics, 10 mg Fe/kg) was injected via tail vein. Twenty-four hours following the injection, MR imaging using an EKG-gated and respiratory monitored gradient-echo sequence (TR 20 ms, TE 2.5 ms, FOV 30 mm, matrix 128 × 128, slice thickness 1 mm and flip angle 60°) was performed at 4.7 T using a 15 cm horizontal bore magnet (Oxford Instruments) with GE Techron Gradients (12 G/cm) and a volume coil with an inner diameter of 3.5 cm (Varian Inc.). The explanted hearts were sliced along the short-axis plane at 4-micrometer thickness and then fixed in 10% formalin. The sections were stained with macrophage-specific antigen F4/80 and Prussian blue for iron.

Results: As shown in Figure 1, T2* dephasing effect due to ferumoxtran-10 particles taken up by macrophages homing to the infarct territory was detected by in vivo MR in 7 out of 9 MI animals but not in sham-operated animals. Using a 16-segment analysis (American Society of Echocardiography), a strong anatomical correlation was demonstrated between the MR and histology images of the ferumoxtran-10-laden macrophages in the infarct region ($r = 0.784$, $p < 0.005$). Histologically, iron particles were identified only in the area of infarct using Prussian blue (Figure 2). The area of infarct contains significant number of macrophages stained with F4/80. Significantly fewer macrophages can be noticed in the non-infarct area as shown in Figure 3.

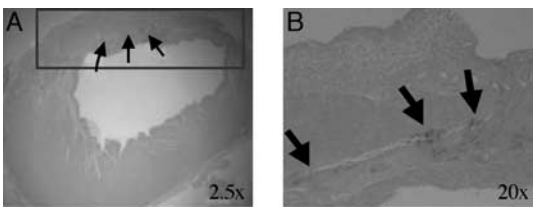

Figure 2. (A) Ferumoxtran-10 in the anterior infarct territory (blue box) shown by Prussian Blue stain (black arrow). (B) High-power (20×) of ferumoxtran-10 in the infarct region (black arrow).

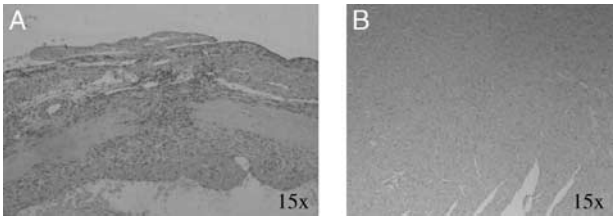

Figure 3. (A) High-power image (15×) of the macrophage-specific stain in the area of infarct. (B) High-power image (15×) of the macrophage-specific stain in the non-infarct territory.

Conclusions: In vivo MR imaging of ferumoxtran-10 particles taken up by macrophages allows accurate assessment of the inflammatory process following myocardial infarction.

196. Selective Cerebral Overexpression of Growth Hormone Alters Cardiac Function, Morphology, Energy Metabolism and Catcholamines in Transgenic Mice

Mohammad Bohlooly, PhD,[1] Entela Bollano, MD, PhD,[2] Reza Mobini, PhD,[2] Bassam Soussi, PhD,[2] Jan Thornell, MD, PhD,[2] Elmir Omerovic, MD, PhD.[2] [1]*AstraZeneca R&D, Molndal, Sweden,* [2]*Sahlgrenska University Hospital, Wallenberg laboratory, Gothenburg, Sweden.*

Introduction: Growth hormone (GH) has important regulatory effects on cardiac morphology and function both during normal development as well as in pathophysiological settings such as myocardial infarction (MI) and congestive heart failure (CHF). energy metabolism.

Purpose: The aims of this study were to evaluate the effects of selective overexpression of GH in the brain on cardiac morphology, function, interaction between GH and sympathetic nervous system (SNS) as well as on cardiac and brain.

Methods: Transgenic mice with selective GH overexpression in the brain under control of the glial fibrillary acidic protein promoter (GFAP-bGH, n = 15) were created and compared to genetically matched non-transgenic littermate controls (C, n = 15). Cardiac morphology and function were evaluated in vivo using transthoracic echocardiography during resting and stress conditions induced pharmacologically by dopamine (D) and isoprtenolol (ISO). Myocardial

and brain energy metabolism were evaluated noninvaseively using in vivo volume-selective phosphorus magnetic resonance spectroscopy (31P MRS). Myocardial content of noradrenaline (NA) was analyzed by means of HPLC.

Results: Compared to the C animals, the bGH mice have show several differences in the cardiac phenotype. Systolic (fractional shortening) and diastolic function (E/A wave ratio) was disturbed in the GFAP-bGH mice ($p < 0.05$). During the dopamine stress, there was chronotropic insufficiency in the bGH group ($p < 0.01$) while no difference was observed in response to isoprotenolol. Left ventricular dimensions were increased in GFAP-bGH mice ($p < 0.05$). There was no difference in body weight, heart weight and brain weight. Myocardial content of noradrenaline was lower in the GFAP-bGH group ($p < 0.05$). PCr/ATP ratio was higher in the brain (2.98 ± 0.14 v. 2.15 ± 0.14, $p < 0.05$) and lower in the heart ($1{,}59 \pm 0{,}07$ v. $1{,}96 \pm 0{,}04$, $p < 0.05$) in the GFAP-bGH mice.

Conclusions: Selective cerebral overexpression of GH results in marked alterations of cardiac function, morphology and metabolism in transgenic mice. Decreased myocardial content of catecholamines in GFAP-bGH mice suggests complex interaction between GH and sympathetic nervous system that my be involved in altered cardiovascular phenotype of the GFAP-bGH mice.

197. Obesity is Associated with Abnormal Myocardial Energetics as Detected by Cardiovascular Magnetic Resonance Spectroscopy

Monique R. Robinson,[1] Michaela Scheuermann-Freestone,[1] Andrew Blamire,[2] David Manners,[3] Kieran Clarke,[4] Stefan Neubauer.[1] [1]*Cardiovascular Medicine, University of Oxford Centre for Clinical Magnetic Resonance Research, Oxfordshire, UK,* [2]*Wolfson Research Centre, Institute for Ageing and Health, Newcastle General Hospital, UK,* [3]*Dipartimento di Medicina Clinica e Biotecnologia Applicata, Universita di Bologna, Italy,* [4]*University of Oxford, University Laboratory of Physiology, Oxfordshire, UK.*

Introduction: Decreased phosphocreatine (PCr)/adenosine triphosphate (ATP) ratios reflect abnormal cardiac metabolism and have been demonstrated in heart failure and diabetes, where they correlate negatively with increased circulating free fatty acid (FFA) concentrations. Obesity predisposes to heart failure.

Purpose: We hypothesized that obese individuals, in the absence of hypertension, diabetes and insulin resistance would show deranged myocardial energetics, and that these energetic changes would be closely associated with the adipokine leptin, and FFA levels.

Methods: Using ^{31}P magnetic resonance spectroscopy (MRS) on a 2 T MR scanner, we measured cardiac energetics (PCr/ATP) in sixteen normotensive asymptomatic obese adults, mean body mass index (BMI) 31.2 kg/m^2, and eleven age- and sex- matched controls. Using a 1.5 T MR scanner, cardiac function was assessed and measurements taken for end diastolic volume (EDV), end systolic volume (ESV), stroke volume (SV), ejection fraction (EF), and left ventricular mass (LVM). LVM was corrected for height and log transformed to better approximate a normal distribution

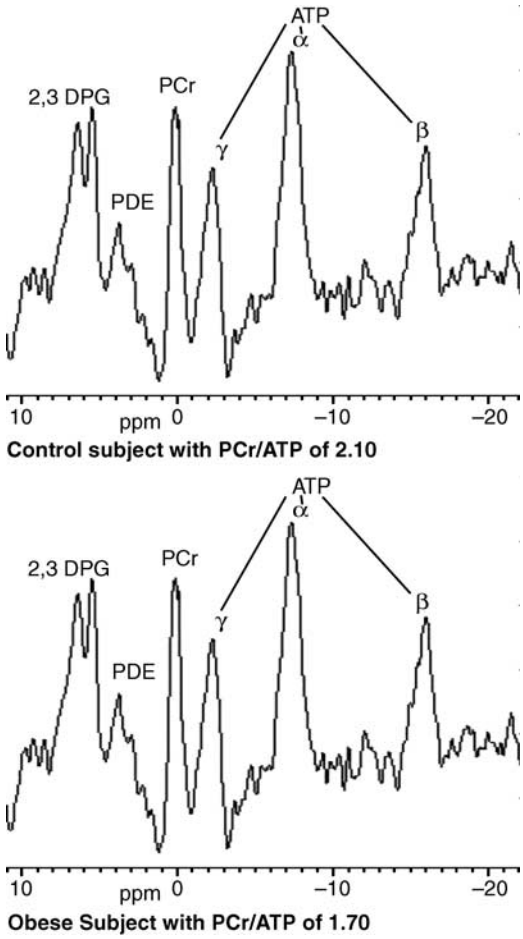

Figure 1. Cardiac ^{13}P MR spectra of lean compared with an obese subject.

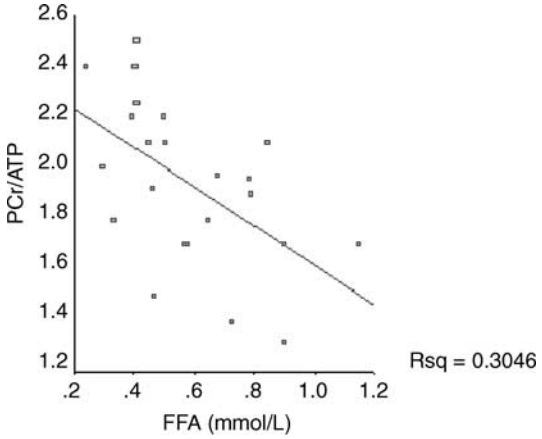

Figure 2. Graph showing correlation of FFA with PCR/ATP.

(LnLVM). Fasting leptin, glucose, insulin, C-reactive protein, lipids and FFA levels were measured. Insulin resistance was assessed by HOMA.

Results: The obese group were insulin sensitive but had significantly higher free fatty acid (0.64 ± 0.06 vs. 0.42 ± 0.05 mmol/L, $p < 0.05$) and leptin (30.5 ± 3.9 vs. 8.0 ± 1.1 ng/ml, $p < 0.001$) levels, compared to the lean group. There was no significant difference for EDV, ESV, SV or EF between the obese and control groups but LnLVM was significantly increased in the obese (144 ± 9.3 vs. 112 ± 11.0 g, $p = 0.04$). PCr/ATP ratios were significantly decreased in the obese group (1.81 ± 0.6 vs. 2.26 ± 0.08, $p < 0.001$). PCr/ATP negatively correlated with BMI ($r = -0.56$, $p < 0.05$), fat mass ($r = -0.58$, $p < 0.05$), leptin ($r = -0.47$, $p < 0.05$) and FFA (-0.55, $p < 0.05$). No correlation was observed between PCr/ATP and other measured metabolites. Multiple linear regression analysis demonstrated that FFA levels were the strongest predictors of cardiac energetics in uncomplicated obesity (Regression coefficients -6.41×10^{-4}, 95% confidence intervals -0.001 to 0.000, $p = 0.018$) (Figures 1 and 2).

Conclusions: In the absence of other cardiovascular risk factors, obesity is associated with deranged myocardial metabolism. The energetics abnormalities in this subpopulation may precede abnormal contractile function and explain the increased risk of the development of heart failure in obesity.

198. Lipid Identification by Image-Guided (^{1}H) Proton Magnetic Resonance Spectroscopy of Human Carotid Atherosclerosis

Frederick L. Ruberg, MD,[1] Jason Viereck, MD, PhD,[2] Ye Qiao,[2] Joseph Loscalzo, MD, PhD,[1] James A. Hamilton, PhD.[2] [1]*Evans Department of Medicine, Section of Cardiology, Whitaker Cardiovascular Institute, Boston University School of Medicine, Boston, MA, USA,* [2]*Department of Physiology and Biophysics, Boston University School of Medicine, Boston, MA, USA.*

Introduction: Commonly employed modalities utilized to image atherosclerosis, such as invasive catheterization, incompletely identify specific plaque components. Magnetic resonance imaging (MRI) offers greatly improved soft tissue resolution and can noninvasively characterize certain plaque morphologic components, however imaging features of plaque lipid remain incompletely defined. Image-guided proton (^{1}H) magnetic resonance spectroscopy (MRS) permits acquisition of high-resolution spectra from discrete volumes of tissue (or voxels) localized by an MR image, and thus may offer a complimentary technique to detect and quantify plaque lipid.

Purpose: As the predominant component of plaque lipid is cholesteryl ester, which is readily identified by MRS, we hypothesized that image-guided proton MRS would confirm the presence of lipid in selected regions of human atherosclerotic plaque thought to contain lipid by MRI.

Methods: Human carotid plaque specimens (n = 4) were obtained following carotid endarterectomy, maintained at 37°C, and imaged by MRI at high-field (11.7 T) utilizing standard T1 and T2 weighted spin-echo protocols. Image quality was sufficient to permit microscopic resolution of plaque components. The generation of a polar map from the ratio of T2/T1 weighted image intensities provided guidance for voxel selection, with lipid-rich regions of plaque defined as those that were T1 intense relative to T2. Proton MRS spectra (TR 500 ms, TE 16 ms, NEX 600) were acquired from 1 mm^3 voxels, localized to plaque regions that

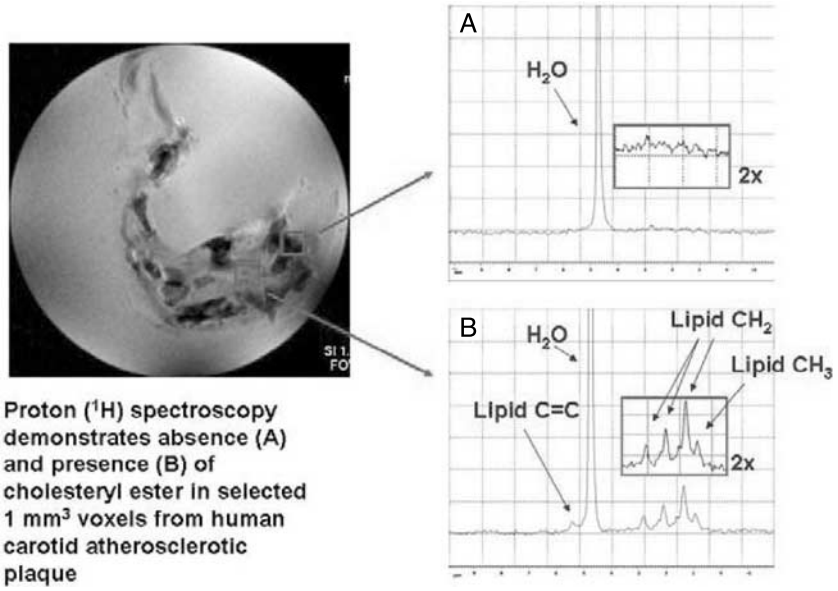

Figure 1.

appeared either lipid-rich (n = 4) or lipid-poor (n = 4) by intensity mapping.

Results: Spectra obtained from a priori identified lipid-rich regions permitted identification of the methyl and methylene resonances of cholesteryl ester, whereas spectra from lipid-poor regions did not demonstrate these resonances (see Figure 1). To permit semi-quantitative comparison of spectral data from different plaque specimens, the integrated intensity of the peak lipid methylene resonance from each spectrum was divided by the integral of the water peak. The calculated lipid: water ratio of lipid-rich regions was 0.49 ± 0.04 vs. 0.13 ± 0.05 for lipid-poor regions ($p = 0.00001$). Histologic analysis, including polarized light-microscopy, confirmed the presence of lipid in the regions identified by both MRI and MRS.

Conclusions: The application of image-guided proton MRS accurately identified lipid in selected regions of atherosclerotic plaque as small as 1 mm^3 at high-field strength (11.7 T). When applied at lower field-strengths, this technique may also permit both detection and quantification of lipid in selected plaque regions noninvasively and thus may be applied to future in vivo studies.

199. Obesity is Associated with Abnormal Skeletal Muscle Energetics—A Magnetic Resonance Spectroscopy Study

Monique R. Robinson,[1] David Manners,[2] Michaela Scheuermann-Freestone,[1] Kieran Clarke,[3] Stefan Neubauer.[1] [1]*Cardiovascular Medicine, University of Oxford Centre for Clinical Magnetic Resonance Research, Oxfordshire, United Kingdom,* [2]*Universita di Bologna, Dipartimento di Medicina Clinica e Biotecnologia Applicata, Bologna, Italy,* [3]*University of Oxford, University Laboratory of Physiology, Oxfordshire, UK.*

Introduction: Obesity is associated with metabolic abnormalities and when complicated by insulin resistance and diabetes, abnormal skeletal muscle energetics. The adipocyte-derived hormone, leptin, is elevated in obesity, and has been associated with deranged skeletal muscle metabolism in cachectic patients.

Purpose: We hypothesised that insulin-sensitive obese patients have abnormal skeletal muscle energetics secondary to hyperleptinaemia.

Methods: Using ^{31}P magnetic resonance spectroscopy (MRS) on a 2 T system, 78 overweight and obese patients (mean body mass index (BMI) 34.2 kg/m^2) and 19 age- and sex-matched controls (mean BMI 23.8 kg/m^2) were examined. Rest, exercise and recovery skeletal muscle energetics profiles of the right gastrocnemius muscle were analysed for concentrations of phosphocreatine (PCr), adenosine triphosphate (ATP) and inorganic phosphate (P_i). Fasting glucose, insulin and leptin were measured and relative insulin resistance (IR) was assessed using HOMA.

Results: Insulin sensitivity was normal in the obese group but leptin was significantly higher in the obese (29.1 ± 2.0 vs. 7.9 ± 0.7 ng/ml, $p < 0.001$). Both groups exercised for similar durations but the phosphorylation potential in the obese (expressed as its inverse for better approximation to a normal distribution (1/pot), a measure of the energy available to the muscle fibres, was half that of the lean group at rest (6.9 ± 0.4 vs. $11.2 \pm 1.2 \times 10^6$, $p < 0.001$). Obese subjects also had significantly slower PCr recovery half times (44.2 ± 1.9 vs. 30.4 ± 2.5 s, $p < 0.001$). V_{max}, an indicator of the maximal rate of mitochondrial ATP synthesis, was also decreased in the obese. 1/pot correlated negatively with leptin ($r = -0.3$, $p < 0.05$), as did the initial rate of PCr formation ($r = -0.3$, $p < 0.05$).

BMI also negatively correlated with 1/pot ($r = -0.3$, $p < 0.001$) and the initial rate of PCr formation ($r = -0.4$, $p < 0.05$).

Further, leptin showed a progressive increase across the BMI categories from overweight to Class III obesity, which was matched by decreasing phosphorylation potential and initial rate of PCr formation and increasing V_{max}, and half time recovery for PCr.

Conclusions: Obesity is a risk factor for abnormal skeletal muscle energetics after exercise, with diminished oxidative phosphorylation capacity. The abnormalities seen were associated with elevated leptin levels. Decreasing fat mass, thereby lowering leptin, might reduce skeletal muscle metabolic derangement early in the pathophysiology of obesity.

200. P31 MRS and Delayed Recovery of Phosphocreatine After Exercise: A New Diagnostic Test for Peripheral Arterial Disease?

David C. Isbell, MD,[1] Stuart S. Berr, PhD,[2] Alicia Toledano, PhD,[3] Frederick H. Epstein, PhD,[2] Craig H. Meyer, PhD,[4] Jennifer Hunter, BSN,[2] Nancy L. Harthun, MD,[5] Walter J. Rogers, PhD,[2] Christopher M. Kramer, MD.[1] [1]*Medicine, University of Virginia, Charlottesville, VA, USA,* [2]*Radiology, University of Virginia, Charlottesville, VA, USA,* [3]*Brown University, Providence, RI, USA,* [4]*Biomedical Engineering, University of Virginia, Charlottesville, VA, USA,* [5]*Surgery, University of Virginia, Charlottesville, VA, USA.*

Introduction: Peripheral arterial disease (PAD) is characterized by inadequate blood flow to the lower extremities as a consequence of atherosclerotic vascular disease. Despite a growing incidence, PAD remains underdiagnosed, undertreated, and understudied. Non-invasive modalities employed for the diagnosis of PAD have a number of limitations, including inaccuracy among patients with aorto-iliac disease, diabetes mellitus, collateralized territories, and heavily calcified vessels. Angiography, long considered the gold standard, is limited to visualizing the vascular lumen and

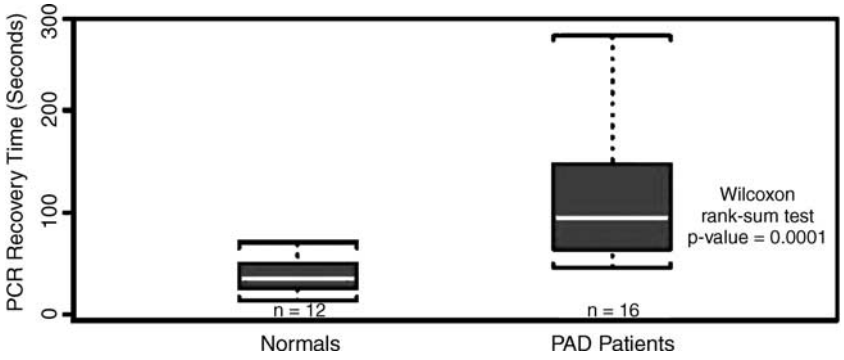

Figure 1.

exposes patients to ionizing radiation and nephrotoxic contrast agents. With each of these techniques, macrovascular abnormalities are interpreted as a surrogate marker of tissue ischemia, largely ignoring adaptations in cellular metabolism and within the microvasculature that develop during the evolution of vascular insufficiency. Clearly, new diagnostic tools that focus on the *end-organ* impact of PAD are needed to enhance our understanding, monitor disease progression, and objectively evaluate response to therapy.

We hypothesized that ^{31}phosphorus (^{31}P) magnetic resonance spectroscopy (MRS) could identify metabolic evidence for ischemia during recovery from exercise in calf muscle. ^{31}P MRS facilitates the exploration of muscle metabolism at a subcellular level. The purpose of this study was to develop and test a technique for determining phosphocreatine (PCr) recovery time in patients with established PAD compared to normal subjects exercising in the MRI environment.

Methods: We studied 12 normal subjects (3 male, age 41 ± 12, mean ± S.D.) and 16 patients with PAD and claudication (10 male, age 66 ± 10, ankle-brachial index 0.62 ± 0.14). Normal subjects and PAD patients exercised one leg to exhaustion while supine in a 1.5 Tesla Siemens Sonata MR scanner using a custom-built plantar flexion exercise ergometer. ^{31}P-spectra were acquired using a single-pulse, surface coil-localized, free induction decay (FID) acquisition localized to the mid-calf. FIDs were multiplied by an exponential with a linewidth of 110 Hz and zero-filled from 1024 to 2048 points prior to Fourier transformation. Twenty five signal averages at a repetition time of 550 ms were acquired over 15 seconds. Two acquisitions over 30 seconds were performed prior to the end of exercise and 18 acquisitions at the end of exercise (270 seconds). All spectra were phase and baseline corrected followed by integration of spectral peaks using a Lorentzian lineshape to estimate relative levels of PCr. The rate of recovery of PCr was calculated by exponential fit of the data beginning at the end of exercise.

Results: Normal subjects exercised on average 4.0 ± 2.0 minutes and PAD 2.5 ± 0.6 minutes ($p < 0.05$). Despite shorter exercise time in PAD patients, the recovery rate of PCr was 38 ± 16 seconds in normal subjects and 133 ± 111 seconds in PAD ($p = 0.0001$, Fig. 1).

Conclusion: MRS of PCr recovery is a sensitive marker of symptomatic PAD, clearly distinguishing patients from normals, and may be a method to quantify response to therapy. Future studies will quantify effect of medical and interventional therapies on PCr recovery.

201. Multi-contrast Delayed Enhancement Imaging for Improved Detection of Subendocardial Infarcts

Peter Kellman, PhD,[1] Yiu-Cho Chung, PhD,[2] Orlando P. Simonetti, PhD,[2] Elliot R. McVeigh, PhD,[1] Andrew E. Arai, MD.[1] [1]*NIH/NHLBI, Bethesda, MD, USA,* [2]*Siemens Medical Solutions, Chicago, IL, USA.*

Introduction: Delayed enhancement imaged using an inversion-recovery sequence exhibits excellent contrast between infarcted and normal myocardium; however, the contrast between the MI and the blood pool is frequently suboptimal. Since a large fraction of infarctions caused by coronary artery disease are subendocardial, it is often difficult to assess the precise size of the infarct or to detect small infarcts. The T2 of blood is significantly longer than either acute or chronic MI. The proposed Multi-COntrast Delayed Enhancement (MCODE) imaging method produces a series of images with both T1 and T2 weightings which provides both excellent contrast between normal and infarcted myocardium, and between blood and MI. This enhances detection of the infarcted region and improves infarct measurement accuracy.

Purpose: To demonstrate that multi-contrast delayed enhancement imaging of myocardial infarction improves contrast between MI and blood pool.

Methods: The MCODE imaging method produces separate images with T1 and T2-weighting. Both images are acquired during the same breath-hold at the same cardiac

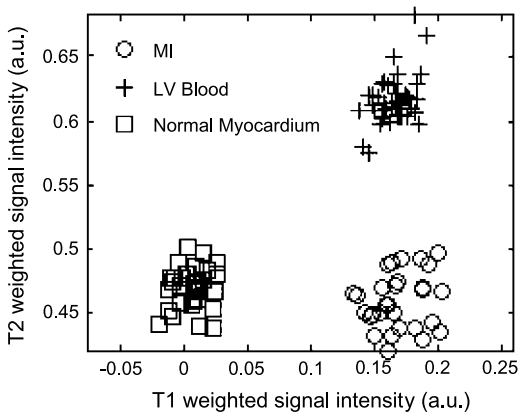

Figure 1. T1 and T2-weighted signal intensities in MI, blood, and normal myocardium regions illustrating the discrimination of the MCODE method.

phase and are therefore registered, which is critical to discriminate subendocardial MI. Both single-shot trueFISP and turboFLASH sequences are being evaluated. For the single-shot trueFISP sequence, T2 weighting is achieved using a large flip angle readout after magnetization recovery, whereas the segmented turboFLASH sequence uses a T2 preparation.

The sequences were implemented on a Siemens Sonata 1.5 T scanner. Results are shown for the single-shot phase-sensitive inversion-recovery (PSIR) trueFISP sequence. The multi-contrast sequence required a single 3 heartbeat acquisition to acquire T1-weighted (IR image), PSIR reference, and T2-weighted images at the same cardiac phase in mid-diastole. A B_1-weighted phased-array combined phase-sensitive reconstruction method was used (Kellman et al., 2002.

N = 6 patients with chronic MI were imaged approximately 20 minutes after administering a double dose of Gd-DTPA. CNR between MI and blood were measured.

Results: A scatter plot of signal intensities for MI, blood, and normal myocardium regions (Fig. 1) shows how T2 may be used to separate blood and MI despite similarity in T1 weighted intensities. The measured MI-to-blood CNR (m ± sd) was better in the T2-weighted image than T1-weighted image (15.7 ± 8.5 vs. 4.4 ± 3.9, N = 6, P = 0.009). Short axis images for a patient with chronic MI are shown in Fig. 2. The MI and normal myocardium are easily discerned in (a) while the MI and blood are easily discerned in (b). Fig. 2(c) displays a ratio image which enhances the MI-to-blood contrast. Alternatively, the endo and epi contours may be traced on (b) and copied to (a) (not shown) as an effective means of visualization and detection. Long axis images from a second patient are shown in Fig. 3 illustrating enhanced detection of a small sub-endocardial MI. The MI indicated by arrow might easily be missed in the T1-weighted image (a) but is easily distinguished from the blood pool by comparison with T2-weighted image (b).

Conclusions: Multi-COntrast Delayed Enhancement (MCODE) imaging provides a significant improvement in the ability to detect subendocardial MI by providing a T2 weighted image with high contrast between blood and MI. MCODE improves both the detection and sizing of MI and has the potential to image edema allowing differentiation of acute vs. chronic MI.

REFERENCE

Kellman, P., et al. (2002).*MRM* 47:. 372–383.

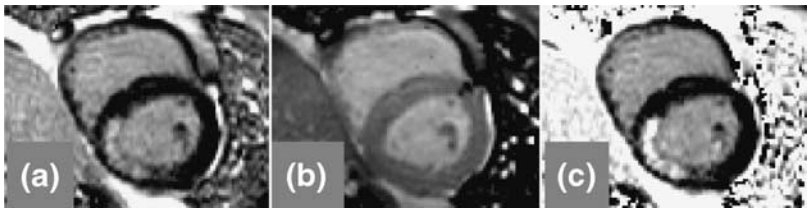

Figure 2. (a) T1-weighted, (b) T2-weighted, and (c) ratio image illustrating improved MI-to-blood contrast.

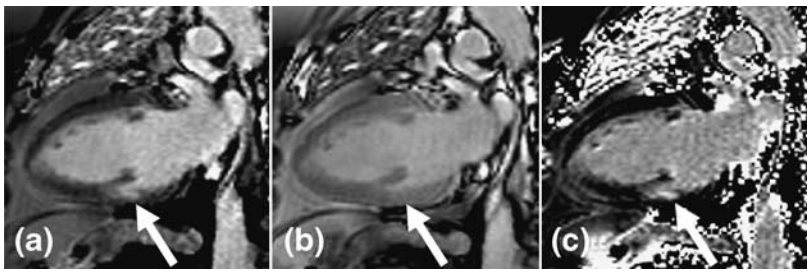

Figure 3. (a) T1-weighted, (b) T2-weighted, and (c) ratio image illustrating improved MI-to-blood contrast.

202. Characterizing Radial Undersampling Artifacts for Cardiac Applications

Dana C. Peters,[1] Pratik Rohatgi,[2] Rene M. Botnar,[1] Susan B. Yeon,[1] Kraig V. Kissinger,[1] Warren J. Manning.[1] [1]*Cardiology, Beth Israel Deaconess Medical Center, Boston, MA, USA,* [2]*Biomedical Engineering Department, University of Michigan-Ann Arbor, Ann Arbor, MI, USA.*

Introduction: Undersampled radial MR imaging has been shown to provide images displaying good visual quality with undersampling factors of 2 to 8. However, exact characterization of the impact of the artifacts on image quality has not been well assessed, since the artifact pattern depends on anatomy.

Purpose: To characterize artifacts patterns, and the artifact signal as a percent of the image signal, for short-axis, long-axis, and right coronary artery (RCA) images.

Methods: 5 healthy subjects were scanned (all female, average age 26 ± 5) on a 1.5 T Gyroscan ACS-NT (Philips Medical Systems, Best, NL). High SNR (> 100) short-axis and long-axis images were obtained, using standard radial protocols (Shankaranarayanan et al., 2001), but acquiring 32 signal averages with navigator-gating (balanced SSFP, 256 × 256 Np, 32 cm FOV, TR/TE/θ = 4.2/2.1/60°, 10 mm slice, 48 views per heart-beat). The protocol for RCA imaging (Leiner, 2004) (36 cm FOV, 368 × 368 Np, TR/TE/θ = 5.5/2.2/110°, T2prep, fat saturation, diastolic window, 48 views per heart-beat) was modified to employ 2D imaging with a 10 mm thick slice, and 32 averages. All magnitude images (Fig. 1A) were subjected to reprojection and then back-projection (using Matlab) at various numbers of projections between 60 and 320 Np. The artifact was isolated by subtracting an image backprojected at fully sampled Np value from undersampled images (Fig. 1B). The artifact signal, in percent, was defined as the square-root of all artifact signal squared, divided by the square-root of all signal squared. Total artifact signal was measured using full and reduced spatial resolution. The artifact power at each undersampling level was averaged among volunteers. Phantom experiments (not shown) demonstrated that this projection/backprojection method is accurate and agreement with true artifact is within 1%. For an individual volunteer, maps of the artifact power in a block regional fashion (32 × 32 pixel blocks) were created to exhibit the artifacts (Fig. 1C).

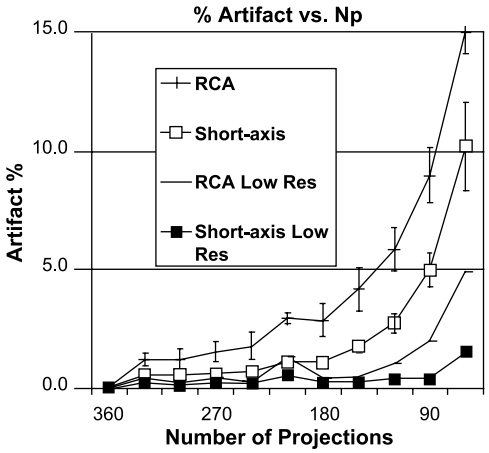

Figure 2. The total artifact signal, in % of the total image signal, from 360 to 60 Np, for short-axis and RCA images, for full and halved resolution images.

In five volunteers, RCA scans were acquired by reducing the number of projections, using Np = 288, 144, 112, 90, but maintaining scan time (and therefore SNR), by increasing partition-encodings. Image quality was scored subjectively by a reader blinded to the undersampling level. The 3D volumes were prepared to mask signal outside of the heart, and contain the same number of slices. The grading was performed by an experienced reader (1.0 = uninterpretable 2.0 = good 3.0 = very good 4.0 = excellent) and total length was measured (Etienne et al., 2002).

Results: Figure 1 shows a short-axis image, the artifact image (60 Np) and the artifact signal map. Figure 2 shows the artifact powers in percent vs. Np, for the RCA and short-axis images, for full and half resolution. Artifacts from long-axis images were similar to the short-axis. Table 1 presents the measurements of visible lengths, and the subjective scorings, for the progressively undersampled RCA images.

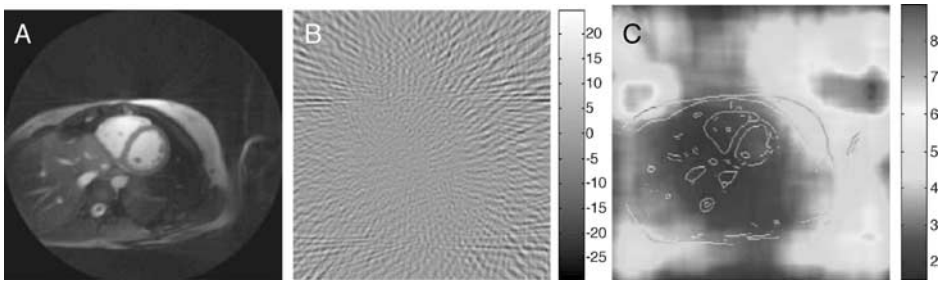

Figure 1. A) Short-axis image. B) Undersampling pattern (Np = 60). C) Color map of artifact signal, with object edges outlined, with a scale from 2 to 8%.

Table 1. Results of grading RCA images in 5 volunteers with different Np values

	Np = 288	Np = 144	Np = 112	Np = 96
R = 368/Np	1.3	2.5	3.3	3.8
Visual score	3.8 ± 0.4	2.9 ± 0.5	2.0 ± 0	1.8 ± 1
RCA length (cm)	10.5 ± 3	10.1 ± 3	10.4 ± 3	9.7 ± 3

Conclusions: The artifact pattern in cardiac applications can be characterized. The small standard deviations in Fig. 2 indicate consistent artifact levels among subjects, that are lower for reduced spatial resolution. Figs. 1B–C show that artifact appears predominantly outside of the heart. The study of the RCA shows that the visible length decreases only for Np = 96, but subjective assessment of quality declines for Np < 144. Further investigation is required to interpret the artifact metric, to determine the maximum acceptable level of undersampling.

REFERENCES

Etienne, A., et al. (2002). *Magn. Reson. Med.* 48(4):658–666.
Leiner, T. (2004). *ISMRM* 705.
Shankaranarayanan, A., et al. (2001). *Radiology* 221(3):827–836.

203. Assessment of Labeled Mesenchymal Stem Cell Biodistribution and Homing in a Canine Model of Myocardial Infarction by MRI and SPECT/CT

Wesley D. Gilson, PhD,[1] Mitsuaki Tatsumi, MD,[1] Thomas G. K. Foo, PhD,[1] Hunter Chen, MS,[1] Danielle Fritzges,[1] Mark F. Pittenger, PhD,[2] Randell G. Young, DVM,[2] Michelle Marcelino, BS,[2] Ben M. Tsui, PhD,[1] Richard L. Wahl, MD,[1] Jeff W. M. Bulte, PhD,[3] Dara L. Kraitchman, DVM, PhD.[1] [1]*Department of Radiology, Johns Hopkins University, Baltimore, MD, USA,* [2]*Osiris Therapeutics, Inc, Baltimore, MD, USA,* [3]*Department of Radiology and Institute for Cell Engineering, Johns Hopkins University, Baltimore, MD, USA.*

Introduction: Bone marrow-derived mesenchymal stem cells (MSC) may be therapeutically beneficial in the context of myocardial infarction (MI) as these cells have been shown to home to sites of injury. Noninvasively tracking the movement of the cells following an intravenous (iv) injection is important in understanding the dynamics of MSC homing and biodistribution. Previous methods have been developed to label MSCs with iron oxide particles (Kraitchman et al., 2003; Hill et al., 2003) and radiotracers such as 111-Indium oxine (Chin et al., 2003; Gao et al., 2001) for noninvasive imaging by MRI and SPECT, respectively.

Purpose: This study aims to assess the temporal biodistribution and homing of labeled MSCs following iv injection in a canine model of acute myocardial infarction (MI) using MRI and SPECT/CT.

Methods: Mongrel dogs (n = 6 MI, n = 1 no MI) underwent a 90-minute closed-chest balloon coronary occlusion followed by reperfusion. Allogeneic MSCs, co-labeled with 111-Indium oxine and ferumoxides-poly-L-lysine, were injected iv at 72 hours post-MI. Serial whole body SPECT/CT (Millenium VH/Hawkeye, GE) and cardiac MRI (1.5 T Signa, GE) scans were performed immediately (d0), 24 hrs (d1), and 4–7 days post-injection (d4–d7). Cardiac MRI scans included short- and long-axis multislice fast gradient echo (FGRE) images, and short-axis T1 and T2 maps. T1 maps were acquired using an inversion recovery fast spin-echo sequence with inversion times from 50 to 500 ms in increments of 50 ms and TR/TE = 7.3/3.2 ms. T2 mapping used a multislice FGRE sequence with TR = 21.5 ms and TE ranging from 2.3 to 18.3 ms. Delayed contrast-enhanced (DCE) MRI was also performed for infarct detection. SPECT emission data were processed using iterative techniques and fused with CT images for visualization and analysis. Infarct size was determined from DCE images. FGRE images were examined for the presence of signal voids from SPIO-labeled cells. T1 and T2 maps were evaluated for focal changes in tissue characteristics. Following

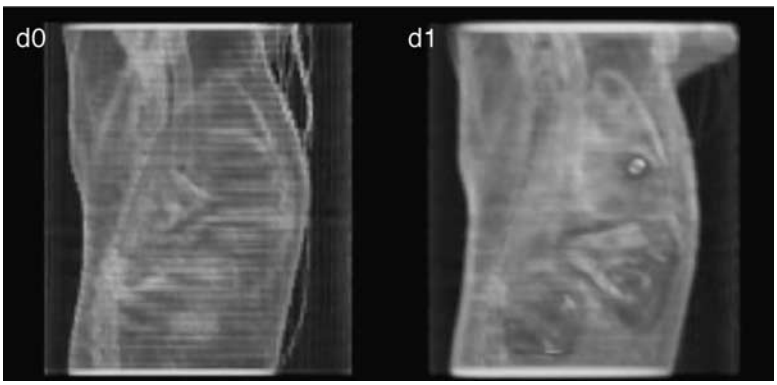

Figure 1.

humane euthanasia, tissue was collected for gamma counting and histology. Histology included co-staining with Prussian Blue (PB) and acid phosphatase (AP) for iron and macrophages, respectively.

Results: Infarct size by DCE MRI was 19 ± 8%. MSC uptake based on d0 SPECT images was greatest in the lungs and redistributed to the liver and spleen by d1 (Figure 1). Significant focal uptake corresponding to the MI occurred in three dogs at d1 with diffuse uptake seen in all MI dogs at d4–d7. Tissue gamma counts in infarcted myocardium were significantly higher than in noninfarcted tissue ($P < 0.01$), while no regional variation in uptake or tissue counts was present in the noninfarcted dog. However, neither T1 maps, T2 maps, or FGRE images were able to detect MSC populations in the heart at any time points. Histology revealed MSCs (positive for PB and negative for AP) in the lungs, liver, spleen, and infarcted tissue. No MSCs were identified in the kidneys or noninfarcted myocardium.

Conclusions: MSCs were initially trapped in the pulmonary bed but redistributed primarily to the liver and spleen within 24 hrs post-injection. MSC localization to injured myocardium following iv injection in a canine model of MI was detectable by noninvasive SPECT/CT but not MRI. Intravascular administration of MSCs may be useful for cardiac cellular therapy.

REFERENCES

Chin, B. B., Nakamoto, Y., Bulte, J. W. M., et al. (2003). *Nucl. Med. Commun.* 24:1149–1154.

Gao, J., Dennis, J. E., Muzic, R. F., et al. (2001). *Cells Tissues Organs* 169:12–20.

Hill, J. M., Dick, A. J., Raman, V. K., et al. (2003). *Circulation* 108:1009–1014.

Kraitchman, D. L., Heldman, A. W., Atalar, E., et al. (2003). *Circulation* 107:2290–2293.

204. Myocardial Strain-Rate Improvements After Transmyocardial Fluoroscopic Delivery of Feridex-Labeled Mesenchymal Stem Cells in Acute Canine Myocardial Infarction

Asif Mahmood,[1] Jeff W. M. Bulte,[2] Izlem Izbudak,[1] Parag Karmarkar,[1] Ray C. Boston,[3] Allen Jeong Keel,[1] Danielle Fritzges,[1] Ana Victoria Soto,[1] Michelle Marcelino,[4] Randell G. Young,[4] Mark F. Pittenger,[4] Dara L. Kraitchman.[1]
[1]*Department of Radiology, Johns Hopkins University, Baltimore, MD, USA,* [2]*Department of Radiology and Institute for Cell Engineering, Johns Hopkins University, Baltimore, MD, USA,* [3]*School of Veterinary Medicine, University of Pennsylvania, Kennett Square, Pennsylvania, PA, USA,* [4]*Osiris Therapeutics, Inc, Baltimore, MD, USA.*

Introduction: Remodeling of the left ventricle after acute myocardial infarction (AMI) leading to heart failure is a major cause of morbidity and mortality. Preventing remodeling and restoring contractile function has been the focus of new cellular therapy including the use of bone marrow-derived mesenchymal stem cells (MSCs).

Purpose: The purpose of this study was to determine the efficacy of targeted MR-labeled MSCs (MR-MSCs) in a canine AMI model as defined by improvements in cardiac contractile function measured serially by MRI.

Methods: Mongrel dogs (25–30 kgs, n = 11) were subjected to a 90-minute closed-chest coronary artery occlusion followed by reperfusion to create an AMI. MSCs were isolated from bone marrow and magnetically labeled with 25 μg Fe/ml Feridex and 375 ng/ml poly-L-lysine for 24 h prior to injection under MR fluoroscopy (1.5 T GE Signa scanner). In five dogs, MR-MSCs ($3–15 \times 10^7$ cells) delivery was performed 72 h post-MI. Infarcted myocardium was identified using delayed contrast-enhanced (DCE) MRI. Using a custom MR-compatible, steerable guide injection catheter, MR-MSCs injections were targeted adjacent to the MI. A real-time imaging sequence with interactive scan plan acquisition was used to guide left ventricular (LV) catheterization as well as MSC injection.

In all dogs, DCE and tagged MRI were serially obtained at 1, 2, 4, and 8-weeks post-injection to evaluate MI size and regional function, respectively. MI size and location was determined using full-width half-maximum (FWHM) thresholding criteria on DCE-MRI. Subendocardial circumferential strain (ECC) was determined in 30 regions of the tagged MR images (i.e., 6 circumferential regions in 5 base to apex slices) in each animal using HARP analysis custom software (Diagnosoft, Inc., Baltimore). The regions were further grouped into three categories according to infarction status based on DCE-MRI [i.e., normal (nl), adjacent (adj) to infarct, or infarcted (inf)].

Systolic strain rate (SSR) was determined by a linear regression of subendocardial ECC versus time during systole. SSR, where more negative strain represents improved contraction, was compared between animals, infarction categories, and imaging sessions. Percent improvement is the ratio of SSR change relative to baseline. The changes in the strain rate over 8 weeks as a response to therapy were determined using a feasible generalized least squares of the cross-sectional time series and compared to control MI dogs that did not receive MR-MSCs. Values are expressed as mean ± SEM; $P < 0.01$ was considered statistically significant (Figs. 1 and 2).

Results: SSR in all three categories of MR-MSC-treated animals improved from 72 hours post-MI to 8 weeks (Nl: -1.3 ± 0.06 vs. $-2.0 \pm .05$*, Adj: $-.92 \pm 0.07$ vs. -1.86 ± 0.05*, Inf: -1.04 ± 0.05 vs. -1.5 ± 0.05*, *$p < 0.001$). By contrast, SSR did not improve in control animals (Nl: -1.14 ± 0.03 vs. -1.13 ± 0.03, Adj: -1.2 ± 0.03 vs. -1.3 ± 0.04, Inf: -0.9 ± 0.03 vs. -1.04 ± 0.03, p = NS). Regression analysis revealed improvement ($p < 0.001$) in all categories over the 8-week

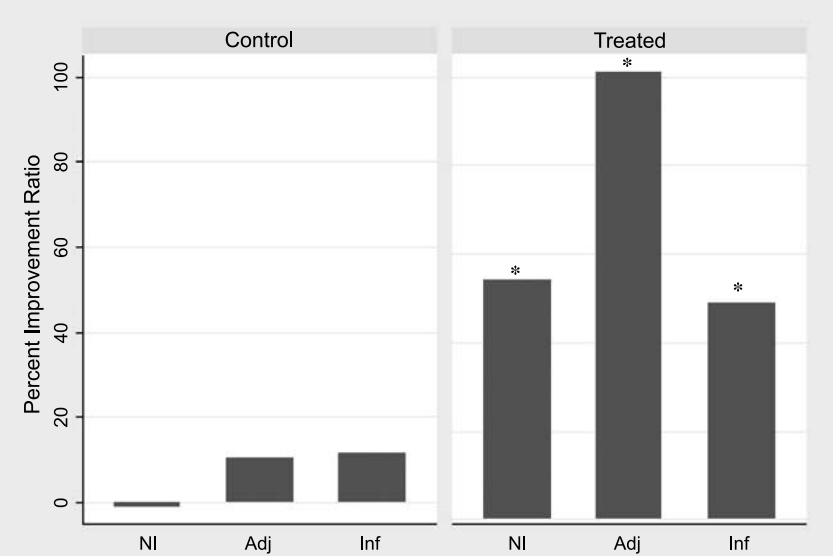

Figure 1. Percent improvement ratio at 8 weeks post-infarction between categories, based on infarction status, in MR-MSC treated and control dogs, (*$p < 0.01$).

period in treated animals compared to controls. MI size (as percent of LV mass) decreased significantly in control (19.3 ± 9% vs. 8.1 ± 2%) and MR-MSC-treated (20.0 ± 5% vs. 8.9 ± 2%) animals but was not different between groups.

Conclusions: Cellular therapy with MSCs early after AMI demonstrated regional improvements in function, regardless of MI size, in normal, peri-infarcted, and infarcted myocardium over 2 months when compared to non-treated animals. These preclinical studies lend promise to the use of direct intramyocardial injections of MSCs as a therapeutic option in future patient trials.

205. Angiotensin II Type 2 Receptor Overexpression Adds to Knockout of the Type 1a Receptor in the Attenuation of Post-Infarction Remodeling, Independent of Blood Pressure

Szilard Voros,[1] Zequan Yang, MD,[2] Joseph DiMaria, BA,[3] Stuart S. Berr, PhD,[3] Frederick H. Epstein, PhD,[3] Brent A. French, PhD,[2] Robert M. Carey, MD,[4] Christopher M. Kramer, MD.[1] [1]*Cardiology, University of Virginia, Charlottesville, VA, USA,* [2]*Biomedical Engineering, University of Virginia, Charlottesville, VA, USA,* [3]*Radiology,*

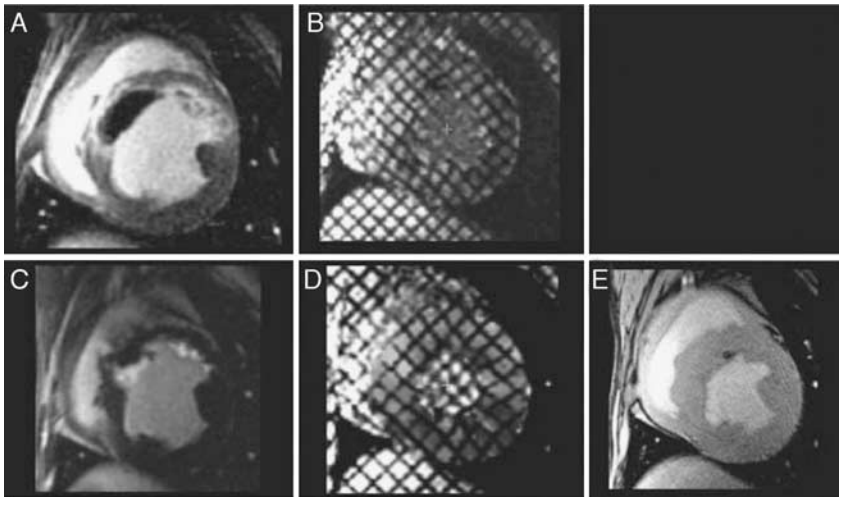

Figure 2. Infarction zone based on DCE MR images (A) shows a larger region of contractile dysfunction in pseudocolor map of ECC(B) at 72 hours. No contraction is shown as green, with myocardial stretching in red, and normal myocardial contraction as blue. Eight weeks post-MI, the infarction size is reduced (C) with improved myocardial function (D). With MR-MSCs (hypointense lesion, E) in an area showing improvements in contractility.

University of Virginia, Charlottesville, VA, USA, [4]*University of Virginia, Charlottesville, VA, USA.*

Introduction: CMR is an important tool in the evaluation of pharmacologic and genetic factors that alter post-MI LV remodeling. Cardiac overexpression of the angiotensin II type 2 receptor (AT_2-R) or knockout of the AT_{1a}-R limits post-infarction remodeling, but their additive value is unknown.

Purpose: The contribution of blood pressure (BP) lowering of AT_{1a}-R knockout in the setting of AT_2-R overexpression is unknown. We sought to determine the role of BP lowering of AT_{1a}-R knockout in the setting of AT_2-R overexpression.

Methods: Two groups of mice on C57Bl/6 background underwent MI by 1 hour occlusion and reperfusion of the LAD; 1) Systemic AT_{1a}-R knockout mice (AT1KO, n = 6) and 2) cardiac overexpression of AT_2-R and systemic AT_{1a}-R knockout (AT2OX-AT1KO, n = 10). Weekly systolic blood pressure (BP) and heart rate were measured. ECG-gated cardiac MRI was performed at baseline and on days 1,7, and 28 post-MI, using a 4.7 T imaging system (Varian 200/400 Inova MRI). Mice were anesthetized with 1% isoflurane and body temperature was maintained at 37°C. An ECG-triggered multi-phase FLASH cine sequence (12–14 phases/cardiac cycle) was performed in the short-axis orientation, covering the heart from base to apex (6–8 contiguous slices) (TR 8 ms [~ 90%of R–R interval], TE 3.1–3.9 ms, flip angle 20° [without contrast; baseline, day 7 and 28] and 60° [with contrast; day 1], slice thickness 1 mm, field of view [FOV] 2.56 cm, matrix 128 × 128). Endo- and epicardial borders were planimetered to determine end-diastolic volume and end-systolic volume indexed to body weight (ESVI, EDVI) and ejection fraction (EF). Twenty minutes after injecting 0.3 mM/kg gadolinium-DTPA, infarct size (IS) was measured on day 1 cine images as the mass of hyperenhanced myocardium, expressed as %LV mass. EDVI , ESVI, and EF were compared by 2-way ANOVA; average BP and infarct size were compared by unpaired t-test between groups.

Table 1. EDVI and ESVI on Days 0 and 28

	Group	Day 0	Day 28
EDVI (μl/g)	AT1KO	1.80 ± 0.12	2.51 ± 0.15
	AT2OX-AT1KO	1.81 ± 0.11	2.14 ± 0.12
ESVI (μl/g)	AT1KO	0.69 ± 0.10	1.36 ± 0.12*
	AT2OX-AT1KO	0.55 ± 0.10	1.02 ± 0.10*,†

*$p < 0.002$ vs. Day 0.
†$p = 0.04$ vs. AT1KO.

Results: Infarct size was similar between groups (34 ± 5% in AT1KO and 38 ± 6% in AT2OX-AT1KO, p = NS). BP averaged over 4 weeks in AT1KO was significantly lower than in AT2OX-AT1KO (88 ± 15 mmHg vs. 99 ± 17 mmHg, p = 0.012). EDVI and ESVI at Day 0 were similar between groups (Table 1). By Day 28, ESVI was significantly lower in AT2OX-AT1KO than in AT1KO despite lower BP in AT1KO (Table 1). EF fell in parallel in the 2 groups (62 ± 3% to 46 ± 4% in AT1KO and 70 ± 3% to 54 ± 3% in AT2OX-AT1KO; p = NS).

Conclusions: AT_2-R overexpression further attenuates post-MI LV remodeling in AT_{1a}-R knockout mice and this is independent of BP lowering. Direct tissue effects of the AT_2-R pathway might partially mediate the benefits of pharmacologic AT_1-R blockade post-MI.